TECHNISCHE UNIVERSITÄT MÜNCHEN

Fakultät für Medizin

Chirurgische Klinik und Poliklinik
des Klinikums rechts der Isar

Epigenetic changes in acinar-to-ductal metaplasia and in $Kras^{G12D}$-mediated pancreatic carcinogenesis

Simone Benitz

Vollständiger Abdruck der von der Fakultät für Medizin der Technischen Universität München zur Erlangung des akademischen Grades eines

Doktors der Naturwissenschaften

genehmigten Dissertation.

Vorsitzender: Prof. Dr. Radu Roland Rad

Prüfende/-r der Dissertation:

1. apl. Prof. Dr. Güralp O. Ceyhan
2. Prof. Dr. Gabriele Multhoff
3. Prof. Dr. Roland Kappler

Die Dissertation wurde am 28.11.2016 bei der Technischen Universität München eingereicht und durch die Fakultät für Medizin am 09.08.2017 angenommen.

Zusammenfassung

Die azinär-duktale Metaplasie (ADM) wird als wichtige Voraussetzung für die Entstehung des duktalen Adenokarzinoms des Pankreas (PDAC) angesehen. Hierbei unterliegen die pankreatischen Azinuszellen einer De- oder Transdifferenzierung und nehmen einen duktalen Charakter ein. Die Eigenschaften der ADM-Zellen sowie die Schlüsselfaktoren, die für die transkriptionelle Reprogrammierung der Zellen verantwortlich sind, sind jedoch kaum beschrieben. In dieser Studie zeigen Genexpressionsanalysen, dass ADM-Zellen eine große Ähnlichkeit zu embryonalen Azinuszellen aufweisen, da zahlreiche embryonale Entwicklungssignalwege in den metaplastischen Zellen hochreguliert sind. Dies suggeriert, dass Azinuszellen bei der ADM eher einer Dedifferenzierung unterliegen, wobei gleichzeitig ein duktaler, progenitor-ähnlicher Phänotyp erlangt wird. Die reaktivierte Expression von Progenitorgenen und die Herunterregulierung von azinären Differenzierungsgenen ist für ADM- und Tumorzellen des Pankreas charakteristisch. Ebenfalls kann in diesen Zellen eine erhöhte Expression von epigenetischen Faktoren, wie der katalytischen Untereinheit Ring1b des Polycomb Repressorkomplexes 1 (PRC1), nachgewiesen werden. Eine signifikante Anreicherung der Ring1b-vermittelten repressiven Histonmodifikation H2AK119ub befindet sich in den Promotorbereichen der azinären Differenzierungsgene *Rbpjl* und *Ptf1a* in Pankreaskrebszellen. Dies belegt, dass PRC1-katalysierte epigenetische Modifikationen zu einer Abschaltung von azinären Differenzierungsgenen im PDAC beitragen (Benitz et al. 2016).

Erhöhte Spiegel der PRC1 Komponenten Bmi1 und Ring1b, als auch von H2AK119ub können sowohl in Pankreatitis-gesteuerten ADM-Zellen in Wildtyp-Mäusen, als auch in pankreatischen Vorläuferläsionen und Tumorzellen eines PDAC Mausmodells detektiert werden (Benitz et al. 2016). Interessanterweise entwickeln Mäuse, welche einen konditionellen Ring1b-Knockout in Azinuszellen aufweisen, bei induzierter akuter Pankreatitis kaum ADM-Strukturen. Darüber hinaus ist die Ausbildung von Tumorvorläuferläsionen in Ring1b-depletierten $Kras^{G12D}$-Mäusen, trotz inflammatorischer Stimuli, erheblich eingeschränkt. Hier bestätigen Genexpressionsanalysen, dass die Etablierung eines progenitor-ähnlichen Transkriptionsprofils in den Ring1b-Knockout-Mäusen reduziert ist. So werden Differenzierungsgene stärker exprimiert und die Aktivierung von Progenitorgenen ist unterdrückt. Dies legt dar, dass ein Verlust von Ring1b die $Kras^{G12D}$-gesteuerte Zelltransformation abschwächt.

Eine komplette transkriptionelle Reprogrammierung von etablierten Pankreaskrebszellen kann über einen CRISPR/Cas9-vermittelten Knockout (KO) von Ring1b allerdings nicht erreicht werden. Jedoch korreliert das veränderte Transkriptionsprofil mit einer erhöhten Expression von Genen, die mit einer epithelialen Zellabstammung assoziiert sind, was auf

eine stärkere Differenzierung der Tumorzellen nach einem Verlust von Ring1b hindeuten kann. Auf funktioneller Ebene zeigen die Ring1b-KO-Zellen eine erhöhte Sensitivität gegenüber Gemcitabin und ein leicht reduziertes Tumorwachstum *in vivo*. Die Anwendung eines PRC1-Inhibitors beeinträchtigt die ADM Bildung *in vitro* und löst ebenfalls eine geringe transkriptionelle Reprogrammierung von Krebszellen des Pankreas aus.

Insgesamt verdeutlicht diese Arbeit, dass eine Reaktivierung des epigenetischen Regulators Ring1b entscheidend für die ADM und die Pankreaskarzinogenese ist. So tragen Ring1b-vermittelte epigenetische Veränderungen zu der Etablierung eines progenitor-ähnlichen Expressionsprofils bei, welches als wichtige Grundvoraussetzung für die Initiation und Progression des PDACs angesehen wird.

Parts of this thesis were previously published:

Benitz, S., I. Regel, T. Reinhard, A. Popp, I. Schaffer, S. Raulefs, B. Kong, I. Esposito, C. W. Michalski, and J. Kleeff. 2016. "Polycomb repressor complex 1 promotes gene silencing through H2AK119 mono-ubiquitination in acinar-to-ductal metaplasia and pancreatic cancer cells." *Oncotarget* 7 (10):11424-33. doi: 10.18632/oncotarget.6717.

Table of contents

List of abbreviations

°C	Degree Celsius
% v/v	Percent volume concentration
% w/v	Percent mass concentration
α-SMA	Alpha-smooth muscle actin
*µ*g	Microgram
*µ*l	Microliter
*µ*M	Micromolar
2D	Two-dimensional
3D	Three-dimensional
3D-ADM	Three-dimensionally cultured ADM
ADM	Acinar-to-ductal metaplasia
AFL	Atypical flat lesion
AP	Acute pancreatitis
APS	Ammonium persulfate
ASR	Age-standardized rate
BCP	1-Bromo-3-chloropropane
BMI1	B lymphoma Mo-MLV insertion region 1
bp	Basepair
BrdU	5-Bromo-2'-deoxyuridine
BSA	Bovine serum albumin
C	Caerulein treatment
$C_{24}H_{39}NaO_4$	Sodium deoxycholate
CA 19-9	Cancer antigen 19-9
$CaCl_2$	Calcium chloride
CBX	Chromobox homolog
CCK	Cholecystokinin
CDK	Cyclin-dependent kinase
CDKN2A	Cyclin-dependent kinase inhibitor 2A
cDNA	complementary DNA
Cela1	Chymotrypsin-like elastase family member 1
ChIP	Chromatin immunoprecipitation
Ck19	Cytokeratin 19
cm	Centimeter
CP	Chronic pancreatitis
CpG	5'-C-phosphate-G-3'
CRISPR/Cas9	Clustered regularly interspaced short palindromic repeats/CRISPR associated protein 9
CSC	Cancer stem cell
C_T	Cycle threshold value
Cxcl	C-X-C motif chemokine ligand
d	Day
DAPI	4′,6-Diamidino-2-phenylindole dihydrochloride
DAVID	Database for Annotation, Visualization and Integrated Discovery
ddH_2O	Double-distilled water
DMEM	Dulbecco’s Modified Eagle’s Medium

DMSO	Dimethyl sulfoxide
DNA	Deoxyribonucleic acid
DNMT	DNA methyltransferase
Dox	Doxycycline
DRS	Dual recombinase system
DTT	Dithiothreitol
E2F	Retinoblastoma-associated protein
E6-AP	E6-associated protein
E-cadherin	Epithelial cadherin
ECL	Enhanced chemiluminescence
ECM	Extracellular matrix
EDTA	Ethylenediaminetetraacetic acid
EED	Embryonic ectoderm development
EGFR	Epidermal growth factor receptor
Ela1	Elastase1
EMT	Epithelial-to-mesenchymal transition
ERK	Extracellular signal-regulated kinase
ES cells	Embryonic stem cells
EZH2	Enhancer of zeste homolog 2
FACS	Fluorescence-activated cell sorting
FAK	Focal adhesion kinase
FOLFIRINOX	Folinic acid, 5-Fluorouracil, Irinotecan and Oxaliplatin
FRT	Flippase recognition target
g	Gravitational force
G_1	Gap 1
GAP	GTPase-activating protein
Gapdh	Glyceraldehyde-3-phosphate dehydrogenase
GDP	Guanosine-5'-diphosphate
Gli3	GLI family zinc finger 3
GEMM	Genetically engineered mouse model
GO	Gene Ontology
Gsta4	Glutathione S-transferase alpha 4
Gstt1	Glutathione S-transferase theta 1
GTP	Guanosine-5'-triphosphate
h	Hour
H&E	Haematoxylin and eosin
H2AK119ub	Mono-ubiquitination of lysine 119 of histone 2A
H3K4me3	Trimethylation of lysine 4 of histone 3
H3K27me3	Trimethylation of lysine 27 of histone 3
HAT	Histone acetyltransferase
HBSS	Hanks' Balanced Salt Solution
HCl	Hydrogen chloride
HCO_{3-}	Bicarbonate ion
HDAC	Histone deacetylase
HDR	Homology directed repair
HEPES	4-(2-Hydroxyethyl)-1-piperazineethanesulfonic acid
Hes1	Hes family BHLH transcription factor 1

Hnf6	One cut homeobox 1
HP	Hereditary pancreatitis
IC_{50}	Half maximal inhibitory concentration
IF	Immunofluorescence
IgG	Immunoglobulin G
IHC	Immunohistochemistry
Ihh	Indian hedgehog
IgG	Immunglobulin G
i.p.	Intraperitoneal
IPMN	Intraductal papillary mucinous neoplasm
JARID2	Jumonji- and ARID-domain-containing protein
KC	$p48^{Cre/+}$;LSL-$Kras^{G12D/+}$
kDa	Kilodalton
Kdm2b	Lysine demethylase 2B
KEGG	Kyoto Encyclopedia of Genes and Genomes
kg	Kilogram
Klf4	Kruppel-like factor 4
KO	Knockout
KPC	$p48^{Cre/+}$;LSL-$Kras^{G12D/+}$;$Trp^{53lox/+}$
KRAS	Kirsten rat sarcoma viral oncogene homolog
$Kras^{G12D}$	Amino acid substitution of glycine to aspartate in codon 12 of the *Kras* gene
$Kras^{G12V}$	Amino acid substitution of glycine to valine in codon 12 of the *Kras* gene
LDH	Lactate dehydrogenase
LiCl	Lithium chloride
log	Logarithm
Lox P	Locus of X-over P1
LSL	Lox-STOP-Lox
LY 294002	PI3K inhibitor
mA	Milliampere
MAPK	Mitogen-activated kinase
MBD	Methyl-CpG binding protein
MCN	Mucinous cystic neoplasm
MCP-1	Monocyte chemoattractant protein-1
MDM2	Mouse double minute 2 homolog
me	methylated
MEF	Mouse embryonic fibroblast
MEK	Mitogen-activated protein kinase kinase 1
mg	Milligram
$MgCl_2$	Magnesium chloride
min	Minute
Mist1	Basic helix-loop-helix family, member A15
ml	Milliliter
mM	Millimolar
MNase	Micrococcal nuclease
mRNA	messenger RNA
MSP	Methylation-specific PCR
M.SssI	CpG methyltransferase

MTT	3-(4,5-Dimethylthiazol-2-yl)-2,5-diphenyl tetrazolium bromide tetrazolium bromide
n	Number
$Na_4P_2O_7$	Sodium pyrophosphate
NaCl	Sodium chloride
NaF	Sodium fluoride
$NaHCO_3$	Sodium bicarbonate
NaOH	Sodium hydroxide
$NaVO_3$	Sodium metavanadate
ng	Nanogram
NHEJ	Non-homologous end joining
nm	Nanometer
nM	Nanomolar
NOD/SCID	Non-obese diabetic/severe combined immunodeficiency disorder
NP-40	Nonident P-40
Nras	Neuroblastoma RAS viral oncogene homolog
P	*P*-value
$P15^{INK4A}$	Cyclin-dependent kinase inhibitor 2B
$P16^{INK4A}$	Cyclin-dependent kinase inhibitor 2A
$P21^{Cip1}$	Cyclin-dependent kinase inhibitor 1A
$P27^{Kip1}$	Cyclin-dependent kinase inhibitor 1B
P53	Tumor protein P53
PAGE	Polyacrylamide gel electrophoresis
PanIN	Pancreatic intraepithelial neoplasia
PBS	Phosphate buffered saline
PBS-T	Phosphate buffered saline with Tween-20
PCA	Principle component analysis
PcG	Polycomb group
PCR	Polymerase chain reaction
PD 98059	MEK inhibitor
PDAC	Pancreatic ductal adenocarcinoma
PDX1	Pancreatic and duodenal homeobox 1
Pen	Penicillin
PFA	Paraformaldehyde
pg	Picogram
PI3K	Phosphoinositol-3 kinase
PIC	RNA polymerase II preinitiation complex
PIPES	1,4-Piperazinediethanesulfonic acid
PJS	Peutz-Jeghers syndrome
PLK1	Polo-like kinase-1
Pnlip	Pancreatic lipase
Ppib	Peptidylprolyl isomerase B
pRB	Phosphorylated retinoblastoma protein
PRC	Polycomb repressor complex
PRSS1	Protease, serine 1
PRT4165	2-Pyridine-3-yl-methylene-indan-1,3-dione
PSC	Pancreatic stellate cell
PTF1a	Pancreas specific transcription factor-1a

qRT-PCR	Quantitative real-time reverse transcription polymerase chain reaction
R1b	Ring1b
RAS	Rat sarcoma
RB	Retinoblastoma protein
RBPJ	Recombination signal binding protein for immunoglobulin kappa J region
RBPJL	Recombination signal binding protein for immunoglobulin kappa J region-like
RING1a	Ring finger protein 1
RING1b	Ring finger protein 2
RNA	Ribonucleic acid
ROS	Reactive oxygen species
RPMI	Roswell Park Memorial Institute Medium
RT	Room temperature
S	Svedberg unit
S phase	Synthesis phase
SDS	Sodium dodecyl sulfate
sec	Second
SEM	Standard error of the mean
Shh	Sonic hedgehog
siRNA	Small interfering RNA
shRNA	Short hairpin RNA
SMAD	Sma- and mad-related protein
SOX9	Sry sex determining region y-box 9
SPION	Superparamagnetic iron oxide nanoparticle
STE	Sodium chloride - Tris - EDTA
STEM	Short time-series expression miner
STK11	Serine/threonine kinase 11
Strep	Streptomycin
SUZ12	Suppressor of zeste homolog 12
TBE	Tris - Borate - EDTA
TE	Tris - EDTA
TEMED	Tetramethylethylenediamine
TGF	Transforming growth factor
T	Tamoxifen
TNF-α	Tumor necrosis factor-alpha
Tris	Tris(hydroxymethyl)aminomethane
TrxG	Trithorax group
unme	Unmethylated
UV	Ultraviolet
V	Volt
W	Watt
WB	Western blot
Wnk2	Lysine-deficient protein kinase 2
WT	Wildtype
ZEB1	Zinc finger E-box binding homeobox 1
Zn^{2+}	Zinc ion

1 Introduction

1.1 Insights into the anatomy, histology and physiology of the pancreas

The pancreas is an accessory gland of the digestive system and is located in the retroperitoneal space. It extends from the C-shaped loop of the duodenum to the hilum of the spleen. The common bile duct traverses the pancreatic head and, together with the main duct of the pancreas converges into the duodenum (Figure 1.1 A) (Pandol 2010). Functionally, the pancreas exhibits both an exocrine and endocrine glandular compartment. The exocrine tissue accounts for 80 % of the organ mass and is responsible for the secretion of an enzyme-rich digestive juice (Hezel et al. 2006). Acinar cells are morphologically clustered into a so-called acinus (Figure 1.1 B) and are the main producers of digestive enzymes, such as amylase (Geron, Schejter, and Shilo 2014). Neurotransmitters and hormones, like the cholecystokinin (CCK), stimulate acinar cells to release the enzyme granula (Jensen et al. 1989). Enzymes are secreted into the lumen of the acinus, which is connected to the ductal system. Through the secretion of water and bicarbonate (HCO_3-) ions, ductal structures ensure transportation of the enzyme-rich digestive juice into the duodenum. The ductal tree involves the terminal intercalated ductal structures as well as intralobular, interlobular ducts and the pancreatic main duct. Ductal cells, which protrude into an acinus are designated as centroacinar cells (Figure 1.1 B) (Reichert and Rustgi 2011).
Besides acinar and ductal cells, a small proportion of pancreatic stellate cells (PSCs) resides in the periacinar, periductal and perivascular space of the exocrine compartment. In physiological conditions PSCs are kept in a quiescent state, but in response to acute pancreatic damage, cells are activated and produce extracellular matrix (ECM) proteins and growth factors to support tissue repair (Omary et al. 2007).

The endocrine compartment is organized in so-called islets of Langerhans (Figure 1.1 C). One islet consists of different types of epithelial cells, producing amongst others the hormones insulin and glucagon, which control blood glucose levels (Bardeesy and DePinho 2002).

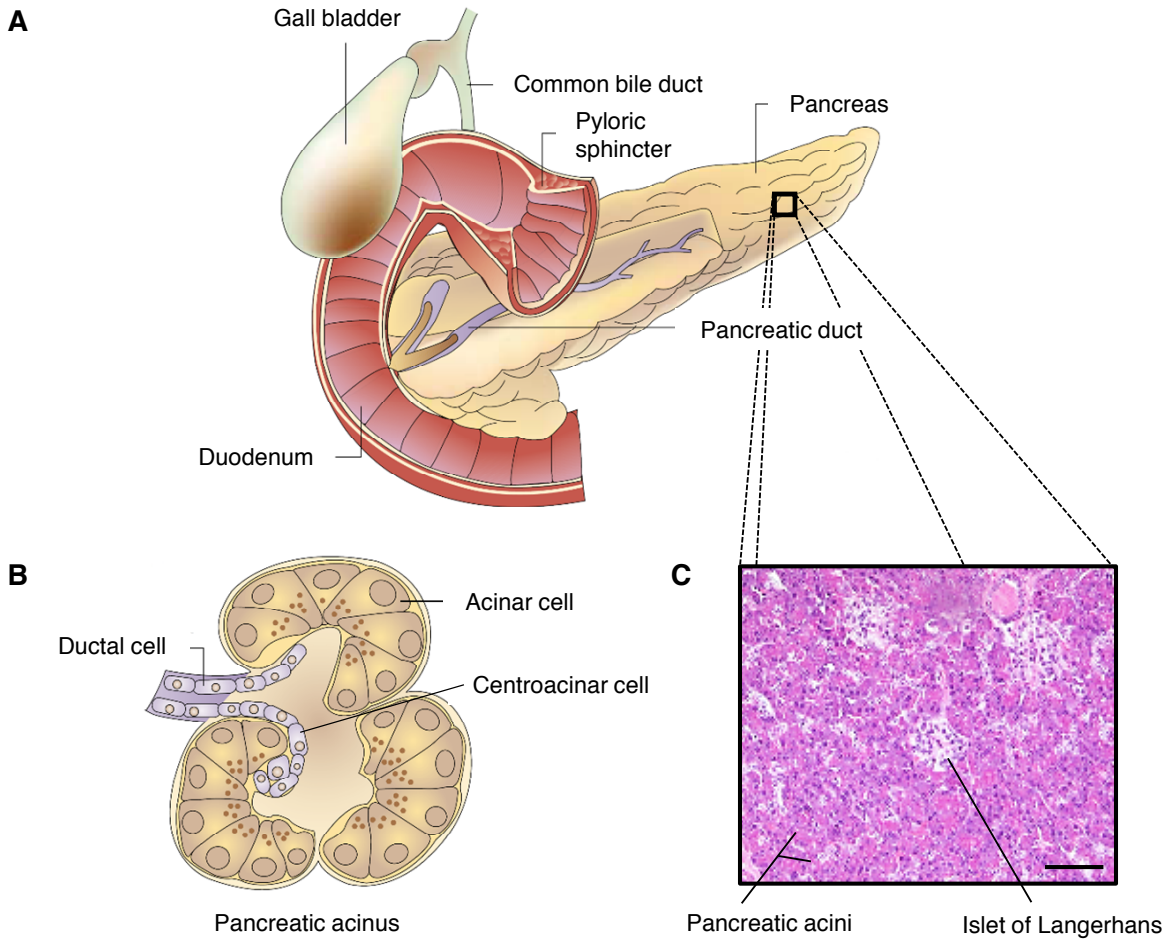

Figure 1.1: Anatomy and histology of the pancreas. (**A**) Gross anatomy of the pancreas. The head of the pancreas is embedded in the duodenal C loop. The common bile duct and the pancreatic main duct cross the pancreas and enter the duodenum (Pandol 2010). Graphic was adapted and modified from (Bardeesy and DePinho 2002). (**B**) Schematic representation of a pancreatic acinus. Apical membranes of clustered acinar cells are orientated towards the acinus lumen, into which digestive enzymes are secreted. Each acinus is connected to an intercalated duct. Cells located at the junction between ductal cells and acinar cells are centroacinar cells (Reichert and Rustgi 2011). Graphic was adapted and modified from (Bardeesy and DePinho 2002). (**C**) Histology of the pancreas. Haematoxylin and eosin (H&E) staining of a human pancreas, illustrating that pancreatic tissue mostly consists of acinar cells. Scale bar, 100 μm.

1.2 Pancreatic development

The first pancreatic progenitor cells derive from the foregut endoderm, forming a ventral and dorsal bud in mice at around E9.5 to E10 (primary transition) (Stanger and Hebrok 2013). Next, the proto-differentiated epithelium establishes micro-lumina, which subsequently merge into a single lumen lined by ductal cells (Villasenor et al. 2010) and macroscopically establish a branching network (Gittes 2009). The so-called 'secondary transition' is initiated around E12 to E14 (Figure 1.2 A), which is accompanied by cell differentiation processes (Benitez, Goodyer, and Kim 2012). At this developmental stage, multipotent cells located at the tips of

the primitive ducts can give rise to nearly all pancreatic cell types, including acinar cells and cells from ductal and endocrine lineages. In contrast, trunk cells are dedicated to serve as progenitors for ductal and endocrine lineages, only. Before birth, residing tip cells mature into acinar cells, trunk cells form ductal branches and endocrine cells escape from the trunks fusing to the islets of Langerhans (Stanger and Hebrok 2013).

Cell fate determination and differentiation is orchestrated by the activity of various signaling pathways and by the interaction of different transcription factors. One master regulator is the transcription factor **Pdx1** (pancreatic and duodenal homeobox 1), which is already expressed in the first arising pancreatic precursors (Figure 1.2 B) (Stanger and Hebrok 2013, Hale et al. 2005). Expression is maintained during the maturation of acinar and islet cells (E14.5), whereas at birth, Pdx1 is exclusively found in islet β-cells (Hale et al. 2005). Pancreatic development is blocked in mice lacking Pdx1 (Jonsson et al. 1994). Pdx1 depletion at E12.5 greatly impairs acinar differentiation (Hale et al. 2005), indicating that the transcription factor is absolutely crucial for pancreatic development and cell fate decisions.

In addition, expression of **Sox9 (**sry sex determining region y-box 9) is regarded as a key regulator governing pancreatic development. It was detected in early Pdx1-positive cells (Seymour et al. 2007) as well as in multipotent progenitors until E18.5 (Kopp et al. 2011). When Sox9 is depleted around E10, pups die shortly after birth suffering from exocrine and endocrine insufficiency (Seymour et al. 2007). In an adult stage, Sox9 expression is restricted to a subset of ductal and centroacinar cells (Seymour et al. 2007).

Establishment and differentiation of acinar cells is greatly regulated by the pancreas-specific transcription factor-1a (**Ptf1a**, also known as p48). Although expression already occurs in early progenitors at E10 (Krapp et al. 1998), it is exclusively maintained in nascent and mature acinar cells (Masui et al. 2007, Krah et al. 2015). At E12.5, Ptf1a interacts with **Rbpj** (recombination signal binding protein for immunoglobulin kappa J region), forming the PTF1-J complex. Subsequently, PTF1-J binds to the promoter of ***Rbpjl*** (recombination signal binding protein for immunoglobulin kappa J region-like) and activates its expression (Masui et al. 2007). Then, Rbpjl replaces Rbpj in the PTF1-J complex and the so-called PTF1-L complex is formed (Figure 1.2 B) (Beres et al. 2006, Masui et al. 2010, Masui et al. 2007). PTF1-L activates transcription of acinar-specific digestive enzymes such as of elastase 1 (Ela1) (Beres et al. 2006), thus, promoting acinar cell differentiation. Rbpjl knockout mice display less pancreatic weight and expression of digestive enzymes is reduced up to 98 % (Masui et al. 2010).

Acinar cell maturation is further supported by the transcription factor **Mist1 (**basic helix-loop-helix family, member A15), which is crucial for acinar cell organization and exocytosis of enzyme granula (Pin et al. 2001).

However, a key marker for early ductal progenitor cells remains elusive. Pierreux et al. revealed that in mice lacking the transcription factor **Hnf6** (one cut homeobox 1), normal duct morphogenesis is defective and mice develop cysts (Pierreux et al. 2006). This indicates that Hnf6 seems to be indispensable for the regulation of duct cell lineages (Figure 1.2 C).

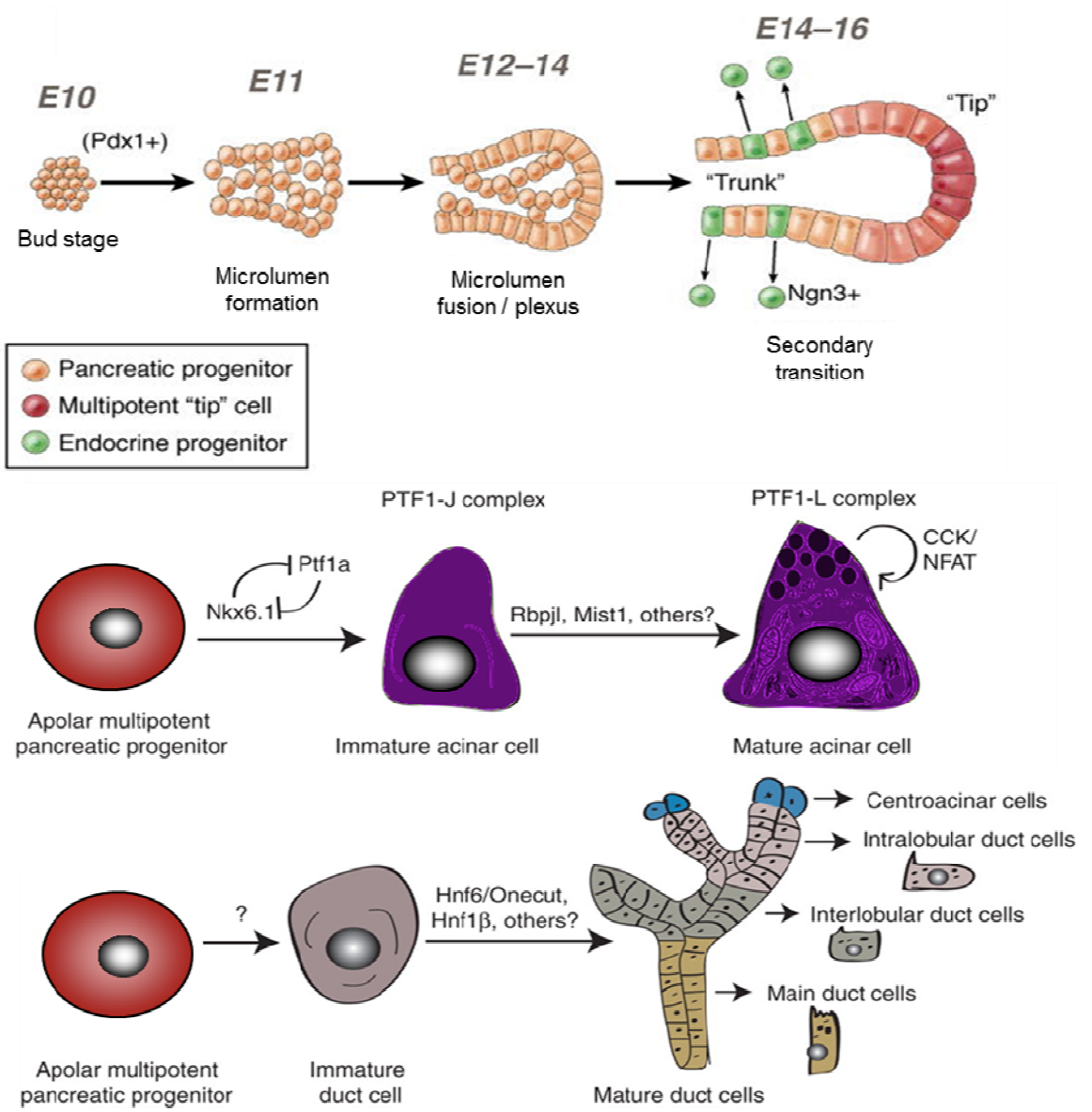

Figure 1.2: Events of pancreatic morphogenesis and cell differentiation.
(**A**) Pancreatic progenitor cells (Pdx1+) arise from the endoderm. During secondary transition, primitive ducts are formed, harboring distinct progenitor populations, which give rise to acinar, ductal and endocrine cells (Stanger and Hebrok 2013). Graphic was adapted and modified from (Stanger and Hebrok 2013). (**B**) Key pancreatic transcription factors, such as Ptf1a, Rbpjl and Mist1 orchestrate acinar cell differentiation and maturation (Benitez, Goodyer, and Kim 2012). Graphic was adapted and modified from (Benitez, Goodyer, and Kim 2012) (**C**) Factors**,** mediating duct cell determination remain largely unknown. However, Hnf6 was identified to induce differentiation of immature duct cells (Benitez, Goodyer, and Kim 2012). Graphic was adapted and modified from (Benitez, Goodyer, and Kim 2012)).

Besides the influence of transcription factors, **Hedgehog** and **Notch signaling** contribute to the tight regulation of pancreatic development. Thus, Notch signaling is important for maintaining pancreatic progenitor cells prior to secondary transition. If an active form of Notch1 is expressed after this stage, exocrine and endocrine cell lineages do not differentiate (Hald et al. 2003). Pancreatic organogenesis is greatly controlled by Hedgehog signaling. Depletion of its ligands sonic hedgehog (Shh) and indian hedgehog (Ihh) causes pancreatic malformation, such as the development of an annular pancreas, increases pancreas size and elevates the proportion of the endocrine cell compartment. Moreover, mice lacking both molecules die early during embryonic development (Hebrok et al. 2000).

1.3 The pancreatic ductal adenocarcinoma (PDAC)

The pancreatic ductal adenocarcinoma (PDAC) is the most common tumor type of the exocrine pancreas, accounting for 95 % of pancreatic cancer cases (Becker et al. 2014). With a five-year survival rate of seven percent (Siegel, Miller, and Jemal 2015), PDAC is graded as a very devastating disease. Latest incidence rates of pancreatic cancer averages 8.6 ASR (age-standardized rate per 100,000), which is almost equal to the described mortality rate of 8.3 ASR (Torre et al. 2015). Most symptoms, such as jaundice and abdominal pain, occur at late stages of the disease, at which curative resection cannot be performed anymore. Thus, more than 80 % of patients, who become clinically apparent, have already developed an advanced metastatic disease (Lowy, Leach, and Philip 2008) and are subjected to palliative chemotherapeutic treatment. However, the five-year survival rate for patients, who underwent surgical resection and received adjuvant chemotherapy, also only represents 21 % due to local recurrence or metastatic disease (Neoptolemos et al. 2004).
Consequently, the identification of early diagnostic tools is of major importance. Current biomarkers, like the cancer antigen 19-9 (CA 19-9) are not sensitive and specific enough to be applied to preventive population screenings (Ballehaninna and Chamberlain 2011). The small size of precursor lesions in early disease stages further complicates early diagnosis.

1.3.1 Risk factors

Due to poor survival rates and limited therapeutic and diagnostic approaches, the identification of risk factors for the development of PDAC is of great importance.

1.3.1.1 Genetic disorders

Genetic abnormalities, such as the Peutz-Jeghers syndrome (PJS), can dramatically increase the risk of developing PDAC (Giardiello et al. 2000). The autosomal dominant

disorder is characterized through mutations in the tumor suppressor gene *STK11* (*serine/threonine kinase 11*) (Jenne et al. 1998).

Genetic mutations affecting the *PRSS1* (*protease, serine 1*) gene were found to be present in patients suffering from **hereditary pancreatitis** (**HP**) (Whitcomb et al. 1996). The *PRSS1* gene encodes a trypsinogen, constituting the precursor of trypsin, which is normally activated in the duodenum. The most frequent point mutation comes along with the substitution of arginine to histidine (R122H), which accelerates the auto-activation of the trypsinogen and favors its intrapancreatic activation (Szabo and Sahin-Toth 2012). This can cause early chronic pancreatitis (CP) (Reznik, Hendifar, and Tuli 2014). Moreover, the cumulative risk for developing pancreatic cancer to an age of 70 years was estimated to represent 40% for patients with HP (Lowenfels et al. 1997).

1.3.1.2 Pancreatitis

Chronic pancreatitis, a persistent inflammatory disease of the pancreas associated with a permanent impairment or even loss of its function (Etemad and Whitcomb 2001), has been described as an independent risk factor for pancreatic cancer (Morris, Wang, and Hebrok 2010). A cohort study revealed that the cumulative risk for patients with CP constitutes four percent for developing PDAC within 20 years (Lowenfels et al. 1993). CP is thought to originate from recurrent episodes of **acute pancreatitis** (**AP**) (Uomo and Rabitti 2000).

Acute pancreatitis is designated as a short-term acute inflammation of the pancreas. Main risk factors comprise gallstones and alcohol. For instance, gallstones cause bile/pancreatic duct obstruction, leading to bile reflux, intra-pancreatic activation of the digestive enzyme trypsin and pancreatic autodigestion (Wang et al. 2009). Halangk et al. found that co-localization of the lysosomal cysteine protease cathepsin B and trypsin is responsible for its premature activation (Halangk et al. 2000). Consequently, injured acinar cells release pro-inflammatory cytokines, such as TNF-α (tumor necrosis factor-alpha) (Gukovskaya et al. 1997) or chemokines, like the monocyte chemoattractant protein-1 (MCP-1), provoking the recruitment and activation of monocytes (Brady et al. 2002). The acute inflammatory phase is associated with a hyper-stimulation of inflammatory cells, edema due to endothelial barrier damage and acinar cell metaplasia (Al Mofleh 2008). Generally, acute pancreatitis can clinically progress in a mild or severe form. In 80 % of patients, the disease is self-limiting (Frossard, Steer, and Pastor 2008). The severe form is characterized by pancreatic necrosis and a mortality rate of 16 % caused by multiple organ failure or secondary infections (Fu et al. 2007). Early diagnosis of acute pancreatitis is supported by the detection of elevated levels of serum amylase and lipase as well as of lactate dehydrogenase (LDH), a widely established marker for tissue damage (Matull, Pereira, and O'Donohue 2006, Al Mofleh 2008).

Depending on the incidence and severity of the alcoholic-related acute pancreatitis events, the disease can progress to **CP** (Ammann and Muellhaupt 1994). For instance, intake of more than five alcoholic drinks a day, increases the risk of developing CP (Yadav et al. 2009). Since CP itself is considered as a significant risk factor for PDAC, this is one explanation as to how **alcohol abuse** contributes to pancreatic cancer. CP patients exhibit irreversibly damaged exocrine and endocrine parenchyma, accompanied by strong tissue fibrosis (Brock et al. 2013). Since PDAC tissue is characterized by the occurrence of large fibrotic areas and desmoplastic tissue reactions (Pandol et al. 2009), chronic inflammation is assumed to significantly link CP and PDAC (Helm et al. 2014). Thus, aspects of pancreatitis are extensively studied in animal models. Common methods that cause pancreatitis involve bile duct ligation or the administration of supra-physiological doses of the CCK analogue caerulein. Caerulein binds to the CCK receptor and stimulates aberrant secretion of digestive enzyme and bicarbonate fluid (Dockray 1972, Niederau, Ferrell, and Grendell 1985). Consequently, enzymes accumulate in the pancreas, leading to a systemic inflammatory response, reflecting the human situation.

1.3.1.3 Smoking

Smoking is regarded as a further major risk factor for PDAC. Approximately a quarter of all pancreatic cancer cases is related to tobacco smoking (Maisonneuve and Lowenfels 2010). Nicotine can mediate premature intra-pancreatic activation of digestive enzymes (Lau et al. 1990) leading to broad pancreatic tissue damage and inflammation. Namely, when rats were exposed to tobacco smoke for twelve weeks, the animals have developed chronically inflamed and fibrotic pancreatic tissue areas (Wittel et al. 2006), suggesting that smoking could reprogram the pancreatic microenvironment towards a tumor promoting setting.

1.3.2 PDAC precursor lesions

Early detection of PDAC allows surgical resection and dramatically increases five-year survival up to 60 % (Shimizu et al. 2005). Thus, improving the identification and characterization of PDAC precursor lesions is of major importance. Carcinogenesis of PDAC is described as a stepwise process from intraepithelial neoplasia to invasive cancer (Brat et al. 1998, Andea, Sarkar, and Adsay 2003). So-called pancreatic intraepithelial neoplasias (PanINs), intraductal papillary mucinous neoplasms (IPMNs), mucinous cystic neoplasms (MCNs) and atypical flat lesions (AFLs) are manifested as morphologically well-defined PDAC precursor lesions (Figure 1.3) (Maitra et al. 2005, Aichler et al. 2012).

1.3.2.1 PanINs

PanIN lesions are very common PDAC precursors and it is assumed that pancreatic cancer progression occurs from low- to high-grade PanINs to PDAC. PanINs appear as ductal structures with a size of less than 0.5 cm and are subdivided into three morphologically distinct groups. PanIN-1 lesions are characterized by the presence of columnar epithelial cells with basal nuclei (Hruban, Maitra, and Goggins 2008). Precisely, flat lesions are considered to be PanIN-1A lesions, whereas PanIN-1B lesions are recognized by their papillary appearance (Distler et al. 2014). Criteria for the classification into PanIN-2 lesions are nuclear changes, such as nuclear crowding, nuclear pleomorphism or nuclear hyperchromasia (Hruban et al. 2001, Hruban, Maitra, and Goggins 2008). High-grade PanIN-3 lesions are greatly dysplastic. They exhibit severe architectural atypia, such as the occurrence of papillary or cribriform patterns as well as great cytological changes, concerning a loss of the nucleic polarity or the presence of oversized nuclei and abnormal mitoses (Figure 1.3) (Hruban, Maitra, and Goggins 2008). The PanIN-based cancer progression model is accompanied by the occurrence of defined genetic mutations. Laser-capture based micro-dissection of PanIN-1 lesions and subsequent pyrosequencing prevalently identified genetic alterations in the oncogene ***KRAS*** (kirsten rat sarcoma viral oncogene homolog) as well as in the tumor-suppressor gene ***CDKN2A*** (cyclin-pependent kinase inhibitor 2A) (Kanda et al. 2012). Mutations in the tumor-suppressor genes ***P53*** (tumor protein P53) and ***SMAD4*** (sma- and mad-related protein 4) occur at later stages of tumor development (Figure 1.3) (Hezel et al. 2006).

1.3.2.2 IPMNs

IPMNs are considered as cystic lesions, exhibiting a pronounced papillary structure and producing mucins (Figure 1.3). Since IPMNs arise from pancreatic ducts, they can be classified into main and branch duct types (Castellano-Megias et al. 2014). Main duct IPMNs frequently are associated with poor prognosis (Tanaka et al. 2006). Early mutations also occur in the *KRAS* gene locus (Distler et al. 2014).

1.3.2.3 MCNs

Like IPMNs, **MCN**s are cystic mucin-producing epithelial neoplasias but uniquely display an ovarian-like stroma (Figure 1.3) (Hezel et al. 2006, Castellano-Megias et al. 2014). These lesions predominantly affect women and can be found in the pancreatic tail and body (Testini et al. 2010). Oncogenic *KRAS* and *P53* mutations were detected in the majority of malignant MCNs (Jimenez et al. 1999).

1.3.2.4 AFLs

The recently described **AFL**s are ductal structures with a flat or cuboidal epithelium, enlarged nuclei and aberrant mitoses. Typically, these tubular structures are surrounded by an α-SMA-expressing (alpha-smooth muscle actin) cellular stroma (Figure 1.3). Particularly, Aichler et al. described murine AFLs as lesions with a high proliferative capacity, loss of Pdx1 and with activated stroma features (Aichler et al. 2012).

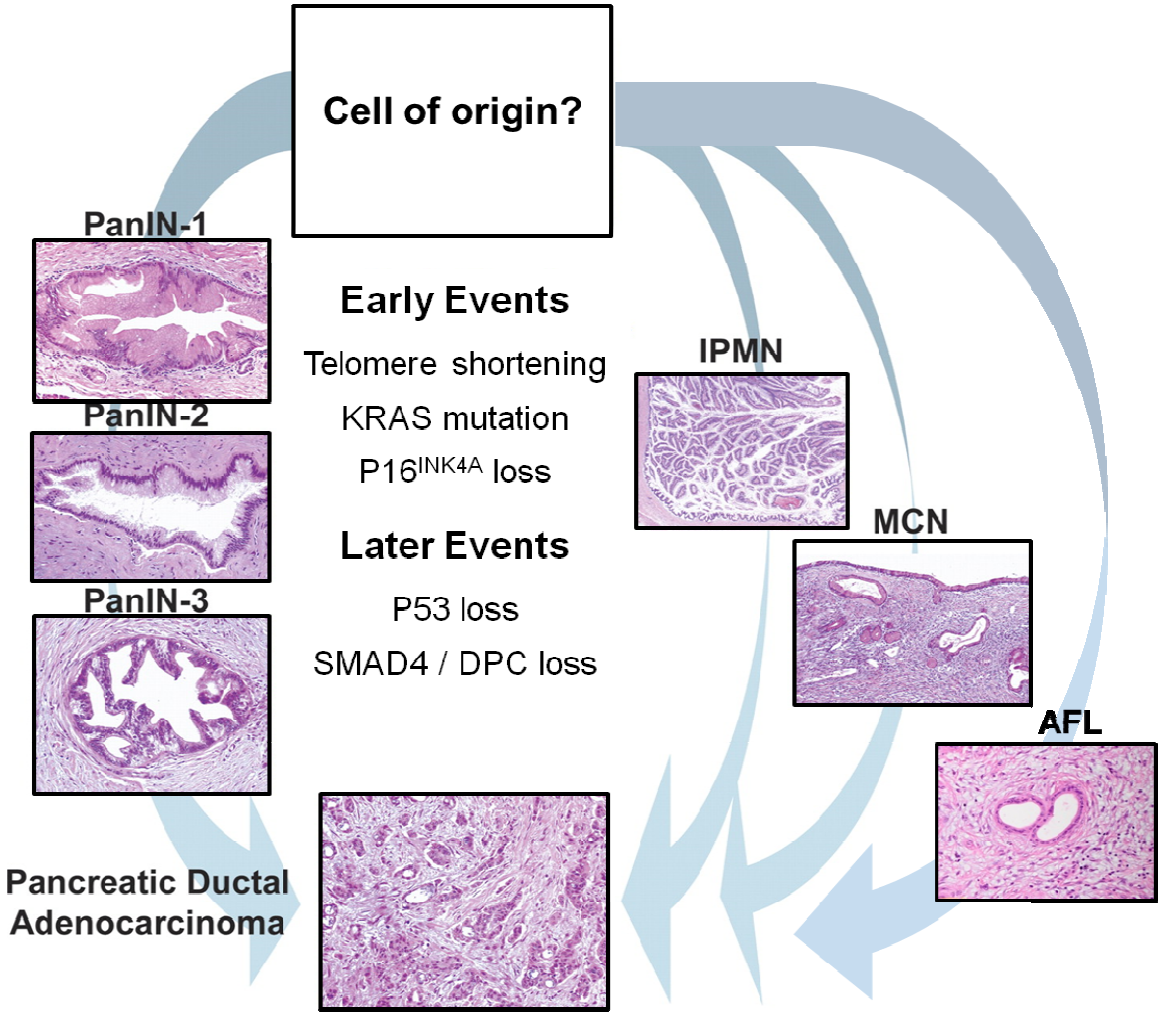

Figure 1.3: PDAC precursor lesions. Histology of PanIN, IPMN, MCN and AFL lesions as well as of PDAC tissue is depicted. PanIN lesions are very common PDAC precursors, progressing from a low-grade to a highly dysplastic form (Hruban, Maitra, and Goggins 2008). Graphic was adapted and modified from (Hezel et al. 2006). H&E staining depicting AFL lesions was adapted from (Esposito et al. 2014).

1.3.3 Morphological appearance of PDAC

In most cases PDAC develops in the head of the pancreas and tumor tissue exhibits cancer cell glands with duct-like structures (Figure 1.3) (Hezel et al. 2006). Benign pancreatic tissue can be distinguished from PDAC by the presence of both ductal and acinar cells, whereas

the PDAC is mainly hallmarked by the existence of a pure population of duct-like cells. Cytological features of carcinoma cells involve nuclear enlargement, abnormal chromatin distribution and numerous mitoses (Field and Zarka 2016). One characteristic hallmark of PDAC is the strong **desmoplastic reaction**, encapsulating cancer cells and shielding them from the immune system or from therapeutic agents. Desmoplasia is composed of immune cells, activated pancreatic stellate cells and ECM components (Pandol et al. 2009), and can account for up to 80 % of the tumor mass (Erkan et al. 2010). Moreover, the vast majority of PDAC is associated with **perineural invasion**, mediating tumor dissemination and pain in cancer patients (Marchesi et al. 2010).

1.3.4 Common genetic mutations in PDAC

PDAC development is hallmarked by the occurrence of key genetic alterations within **oncogenes** and **tumor-suppressor genes**. Oncogenes are characterized by a "gain of function" mainly mediated by activating structural changes (Croce 2008). Consequences are aberrant cell proliferation, cell growth and cell division. In contrast, tumor-suppressor genes go along with a "loss of function" due to their power in controlling cell cycle transitions, induction of apoptosis and DNA repair (Abreu Velez and Howard 2015). Since the vast majority of tumor-suppressor genes is inherited recessively, both alleles have to be inactivated to completely abolish protein function. According to this 'two-hit-hypothesis', inactivation of the first allele can be accomplished through a sporadic or inherited mutation, whereas the second hit is often due to mitotic recombination (Knudson 1971).
Regarding PDAC development, key driver mutations, occurring in oncogenes and tumor-suppressor genes, have already been identified and linked to histopathological precursor lesions and PDAC.

1.3.4.1 The oncogene KRAS

Strikingly, *KRAS* mutations can be detected in more than 90 % of human PDAC cases (Morris, Wang, and Hebrok 2010). Since *KRAS* mutations are already found in the vast majority of the low grade precursor lesions PanIN-1A (Kanda et al. 2012), they are regarded as one of the key genetic drivers for PDAC. Indeed, expression of oncogenic $Kras^{G12D}$ in early progenitor cells of mice leads to the formation of PDAC precursor lesions and PDAC (Hingorani et al. 2003). The question is how a single mutation can have such a great impact on cell homeostasis?
As a monomeric, membrane-coupled G protein, RAS transmits signals from growth factor receptors, like the EGF receptor family, to downstream signaling cascades. Once activated, RAS binds GTP and interacts with its downstream effectors. Subsequently, intrinsic GTPase

activity is induced by GTPase-activating proteins (GAPS), GTP is hydrolyzed to GDP and the G protein converts into an inactive state (Wennerberg, Rossman, and Der 2005). Single point mutations in codon 12 of the *KRAS* gene (98 % of *KRAS* mutations in PDAC) favor amino acid substitutions, such as glycine to aspartate (G12D) or glycine to valine (G12V) (Smit et al. 1988, Eser et al. 2014). These alterations attenuate GAP-mediated GTP hydrolysis and render KRAS in an active state (Scheffzek et al. 1997). Consequently, its downstream effector pathways, such as RAF/MEK/ERK and PI3K/PDK1/AKT are aberrantly stimulated, favoring cell proliferation and malignant transformation (Eser et al. 2014).

1.3.4.2 Tumor suppressor genes

1.3.4.2.1 P53

The tumor suppressor gene *P53* is widely recognized as the "the cellular gatekeeper for growth and division" (Levine 1997). Inactivation of the tetrameric transcription factor can accelerate oncogenic transformation. Under physiological circumstances, p53 protein levels are kept low due to the persistent ubiquitination through mdm2 (mouse double minute 2 homolog) and its subsequent degradation. DNA damage, hypoxia or imbalances in signaling pathways induce phosphorylation of P53, causing its stabilization and binding to promoters of downstream targets, like DNA repair and cell cycle arrest genes or regulators of apoptosis (Weinberg 2007). Since P53-activating signals are aberrantly present in tumor cells, P53 function must be eliminated to ensure cancer cell survival. Thus, mutations in the *P53* gene locus appear in the majority (> 70 %) of PDAC patients (Scarpa et al. 1993). In most cases, P53 inactivation is due to miss-sense mutations (Morton et al. 2010). Endogenous expression of $Trp53^{R172H}$ and $Kras^{G12D}$ in Pdx1-positive pancreatic progenitor cells fully recapitulates human PDAC carcinogenesis. Thus, $Pdx1^{Cre}$;$Kras^{G12D}$;$Trp53^{R172H}$ mice develop PanIN lesions, invasive and metastatic PDAC and it was reported that they exhibit an overall survival of five months (PDAC mouse models are described in section 1.4.4) (Hingorani et al. 2005). Interestingly, a recent study revealed that *p53* mutation rather than *p53* deletion in mice overcomes $Kras^{G12D}$-mediated growth arrest/senescence and promotes metastatic processes (Morton et al. 2010).

1.3.4.2.2 SMAD4/DPC4

Inactivation of the tumor suppressor SMAD4 usually occurs at late stages of PDAC tumor progression (Wilentz et al. 2000) and is associated with a worse prognosis (Singh, Srinivasan, and Wig 2012). As a transcription factor, SMAD4 is an integral component of the TGF-β (transforming growth factor-beta) signaling pathway, which favors cellular growth inhibition and impairs cell cycle progression. Thereby, TGF-β binds to the TGF-β receptor

and its internal serine/threonine kinases subsequently phosphorylate Smad proteins, such as Smad2 and Smad3. Consequently, activated Smad proteins complex with Smad4 and migrate into the nucleus and activate amongst others, the expression of the cell cycle inhibitors $p15^{INK4A}$ (cyclin-dependent kinase inhibitor 2B) and $p21^{CIP1}$ (cyclin-dependent kinase inhibitor 1A) (Weinberg 2007).
Establishment of a $Pdx1^{Cre};Kras^{G12D};Smad4^{lox/lox}$ mouse model indicated, that a loss of Smad4 increases the formation of precursor lesions, especially of IPMNs, and shortenes overall survival (Bardeesy, Cheng, et al. 2006). These data suggest that a Smad4 deficiency enhances tumor cell malignancy and accelerates $Kras^{G12D}$-initiated tumor formation.

1.3.4.2.3 $P16^{INK4A}$

Loss of CDKN2A, also known as $P16^{INK4A}$, can be regarded as one further major hallmark of PDAC. The cell cycle inhibitor was found to be lost in 67 % of PDAC patients (Oshima et al. 2013) and $Pdx1^{Cre};Kras^{G12D};p16^{INK4A-/-}$ mice develop PDAC with a shortened latency (Bardeesy, Aguirre, et al. 2006).
$P16^{INK4A}$ exerts its function through inhibiting the kinase activity of the CDK4-CDK6 complex, which mediates cell cycle progression. Consequently, phosphorylation of the retinoblastoma protein (RB) is imapired and cell cycle transition from the S (synthesis) into the G_1 (Gap 1) phase is interrupted (Serrano, Hannon, and Beach 1993, Rayess, Wang, and Srivatsan 2012). In response to severe cell stress or oncogenic signaling, cells are kept in a $P16^{INK4A}$-mediated cell cycle arrest, a condition called cellular senescence (Collado, Blasco, and Serrano 2007). Senescent cells stay metabolically active but lose their capability to divide (Weinberg 2007, Rodier and Campisi 2011). Obviously, loss of P16 can help to prevent induction of cellular senescence and maintain tumor cells in a highly proliferative state.
In PDAC, inactivation of $P16^{INK4A}$ is achieved through intragenic mutations and homozygous deletions (Schutte et al. 1997). Additionally, Schutte et al. demonstrated that a subset of patients harbor a wild-type *P16^{INK4A}* locus, but had lost $P16^{INK4A}$ expression. In these patients, epigenetic silencing of the *P16^{INK4A}* promoter through DNA methylation was identified (Schutte et al. 1997). These results indicate that apart from genetic mutations, also epigenetic modifications can contribute to PDAC tumorigenesis.

1.3.5 Therapeutic approaches for the management of PDAC

Since pancreatic cancer is estimated to represent the second leading cause for cancer-related deaths in the US by 2030 (Rahib et al. 2014), many efforts have to be taken to improve therapeutic options, such as surgical procedures, neo-adjuvant and adjuvant treatment courses. To date, the only curative approach is provided by surgical resection. Regarding adjuvant options, treatment with the nucleoside analog gemcitabine has been

proven to be the beneficial (Oettle et al. 2007). Patients with advanced cancer, who were treated with the combination therapy FOLFIRINOX (folinic acid, 5-fluorouracil, irinotecan and oxaliplatin) showed a medium overall survival of 11 months in comparison to 6.8 months for those who received gemcitabine alone (Conroy et al. 2011). In addition to chemotherapeutic agents, small molecule inhibitors are increasingly integrated into therapeutic concepts. Since oncogenic Kras has not been successfully druggable so far, other targets had to be identified. It was found that targeting the epidermal growth factor receptor (EGFR) with the small molecule inhibitor erlotinib in combination with gemcitabine treatment, can provide a significant survival benefit for patients with advanced tumors (Moore et al. 2007).
Moreover, future directions will integrate epigenetic drugs. First trials in combining the HDAC (histone deacetylase) inhibitor vorinostat with chemoradiation show promising results (Chan et al. 2016).
Very recently, a study came up with the use of superparamagnetic iron oxide nanoparticles (SPIONs) to specifically deliver anti-tumor agents into cancer cells (Mahajan et al. 2016). In this study, SPIONs were coupled with a siRNA against an important mediator of cell cycle progression, polo-like kinase-1 (PLK1). After introduction into $Pdx1^{Cre}$;$Kras^{G12D}$;$Trp53^{R172H}$ mice, tumor growth was significantly reduced (Mahajan et al. 2016). In principle, the involvement of SPIONs offers the great therapeutic option to selectively target tumor cells and to initiate the gene silencing of specific oncogenes.

1.4 Models reflecting pancreatic carcinogenesis

To comprehend the biological nature of PDAC and to develop new diagnostic and therapeutic approaches, various PDAC models have been extensively studied. To date, studies typically rely on the analysis of primary tumors, cancer cell lines, three-dimensional culture systems, xenografts and genetically engineered mouse models (GEMMs).

1.4.1 Pancreatic cancer cell lines

Of great importance is the study of established cancer cell lines, originally isolated from primary tumor tissues. Generally, cancer cell lines are handled easily, thus, deregulation of genetic, epigenetic and cellular pathways, proliferation, migration and invasion capacities as well as the response to cancer therapeutics can be quickly evaluated. Moreover, cancer cell lines can be genetically manipulated through transfection of expression plamids or application of siRNA (small interfering RNA), shRNA (short hairpin RNA) and the recently described CRISPR/Cas9 (clustered regularly interspaced short palindromic repeats/CRISPR associated protein 9) system to specifically knock down or knock out the gene of interest, respectively. However in general, it has to be taken into account that cell culture conditions

can change the tumor cell behavior. After several passaging rounds, genomic instability and changes in gene expression changes could occur (Muff et al. 2015). Since isolated cancer cell lines represent a highly homogenetic population, the natural heterogeneity of tumors is not considered. Moreover, interactions between various cell types and the tumor microenvironment can barely be studied.

1.4.2 Three-dimensional (3D) culture systems

By embedding cells into extracellular matrix components, such as collagen or matrigel, the cellular microenvironment can be more accurately reflected. In comparison to two-dimensional (2D) cell cultures, 3D culture systems allow the proper analysis of physiological cell-cell and cell-matrix interactions, cell migration and differentiation. Importantly, the process of acinar-to-ductal metaplasia can be mimicked with the aid of the 3D *in vitro* culture system. After embedding acinar epithelial explants into collagen and stimulation with TGF-α (transforming growth factor alpha), acinar cells convert into metaplastic cells, which exhibit a ductal phenotype (Means et al. 2005).

1.4.3 Xenograft models

To predict how a human tumor will respond to a specific therapeutic strategy, the establishment of a human tumor xenograft model on mice is advisable. In principle, human tumor cells or pieces of human primary/metastatic tumors can be implanted subcutaneously or orthotopically into the pancreas. To ensure engraftment, immuno-compromised mouse models, such as the non-obese diabetic/severe combined immunodeficiency disorder (NOD/SCID), can serve as hosts (Hidalgo et al. 2014). Importantly, the experimental setup can be exploited to establish personalized tumorgrafts and used to identify individual treatment courses. Within a pilot study, Hidalgo et al. treated patients corresponding to the data of their personalized avatar mouse models and the great majority of patients achieved partial responses (Hidalgo et al. 2011). However, one must be aware that the generation of avatar mice is time- and cost-consuming and that interactions with the inflammatory tumor microenvironment are not considered.

1.4.4 Genetically engineered mouse models (GEMMs)

With the aid of GEMMs, tumor carcinogenesis, cancer cell - microenvironment interactions or the application of new therapeutic approaches can be extensively analyzed and monitored. Nowadays, a number of powerful tools exist to manipulate gene expression and protein function, allowing a functional characterization of specific target genes. For instance, gene

expression changes can be induced by the site-specific Cre-*Lox* recombinase system. Here, the Cre (causes recombination) recombinase recognizes a 34 bp long sequence called a *Lox P* site, DNA is cut between two *Lox P* sites and recombination occurs (Abremski et al. 1986). GEMMs reflecting PDAC often harbor a *Lox-STOP-Lox* (LSL) cassette in front of a mutant *Kras* allele bearing a G12D or G12V transition. When the Cre recombinase is expressed under the control of a tissue-specific promoter, the STOP cassette is excised and oncogenic Kras is specifically expressed in target cells (Figure 1.4 A) (Guerra and Barbacid 2013). The first conditional $Kras^{G12D}$ mice were introduced by Hingorani et al. in 2003. Here, constitutive Cre expression was driven by the *Pdx1* or *Ptf1a* promoter, both targeting early pancreatic progenitor cells (Figure 1.4 A left). Mice developed PanIN lesions and spontaneously PDAC (Hingorani et al. 2003). Additional endogenous expression of mutant p53, greatly accelerates pancreatic carcinogenesis and causes metastatic and invasive PDAC, thus, reflecting human disease (Hingorani et al. 2005). However, in these mouse models, oncogenic Kras expression was already activated during embryonic development. Now, newly designed inducible GEMMs allow activation of Cre-mediated recombination at distinct developmental stages, also in adulthood. For instance, use of an inducible Tet-Off system, in which resident $Kras^{G12V}$ expression is induced following doxycycline (Dox) removal from the drinking water (Figure 1.4 A right), revealed, that adult acinar cells are resistant towards oncogenic Kras-driven cell transformation. However, in combination with pancreatitis, pancreatic carcinogenesis can be initiated (Guerra et al. 2007). Since it is assumed that human PDAC arises through sporadic mutations in adulthood, the use of temporally controllable Cre lines allows a more realistic recapitulation of the human situation. Thus, further *in vivo* inducible recombination models were designed, such as the tamoxifen-dependent Cre recombinase (Cre^{ERT}) (Figure 1.4 A right, Figure 1.4 B). Cre^{ERT} is a fusion protein, consisting of the Cre recombinase and a modified ligand binding domain of the human estrogen receptor. Upon tamoxifen (T) administration, the hormone binds to the Cre^{ERT} construct and allows the translocation of the Cre-recombinase from the cytosol into the nucleus (Feil et al. 1996). Recombination efficiency can be determined through activation of a fluorescent reporter, such as tdTomato, whose expression is controlled by a LSL cassette (Figure 1.4 B).

Now, next-generation mouse models with an inducible dual recombinase system (DRS) combining the use of the Cre-*LoxP* and the Flippase-*FRT* mediated recombination, have been developed (Schonhuber et al. 2014). Thus, DRS allows sequential introduction of gene mutations into a defined subset of cells, mimicking multi-step carcinogenesis. However, the recombination-based generation and breeding of mice with multiple gene mutations is very time- and cost-consuming. The latest innovation in the creation of GEMMs is not dependent on recombination systems, but uses CRISPR/Cas9-mediated genome editing. Wang et al.

impressively demonstrated that with the CRISPR/Cas9 system they were able to simultaneously delete five genes in mouse embryonic stem cells, enabling a one-step generation of mice (Wang et al. 2013). Moreover, in combination with an inducible Cas9 (Dow et al. 2015), CRISPR/Cas9 represents a flexible, efficient and fast tool to create the next generation of GEMMs to study PDAC.

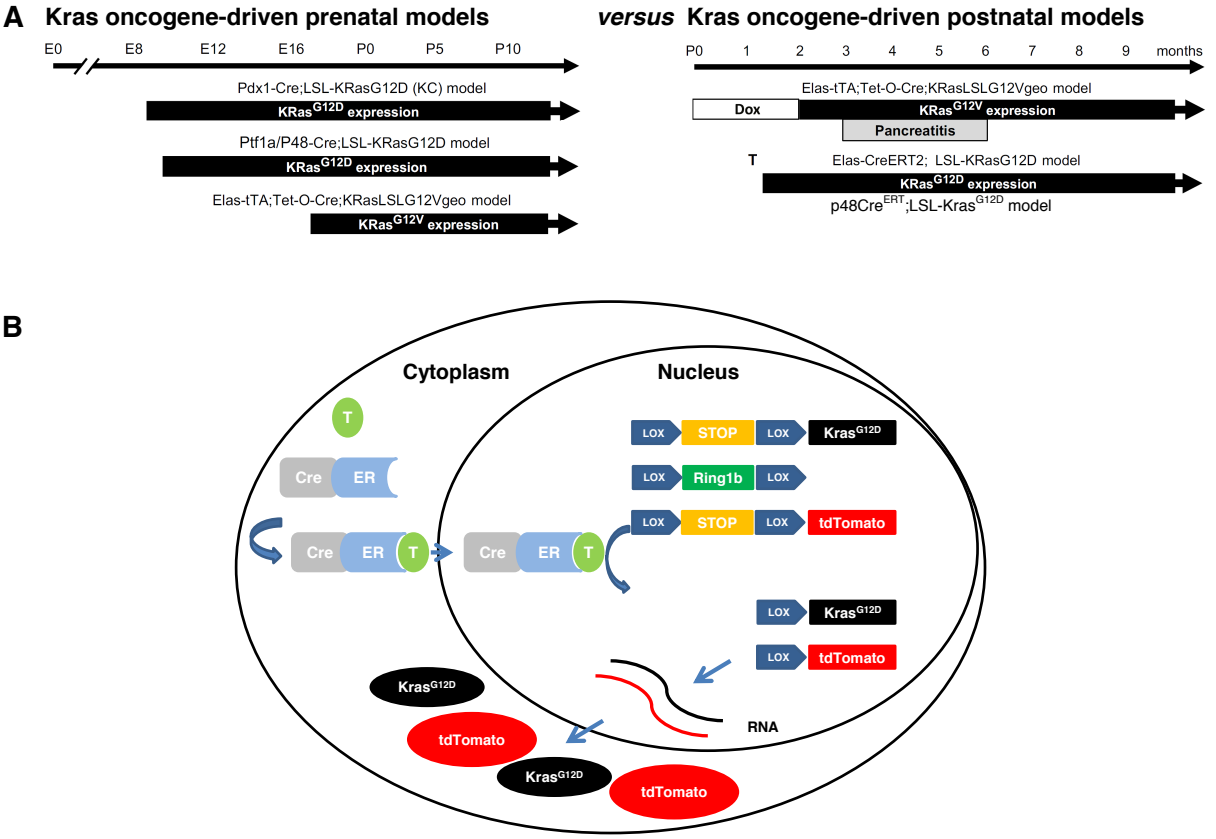

Figure 1.4: Common GEMMs mimicking PDAC carcinogenesis. (**A**) The broad majority of GEMMs of PDAC relies on pancreatic expression of oncogenic *Kras*^{G12D} or *Kras*^{G12V}, which is induced upon Cre-mediated deletion of a *Lox-STOP-Lox* cassette. For this, constitutive (left) or inducible Cre lines, allowing a time-specific recombination (right), can be used (Guerra and Barbacid 2013). Graphic was adapted and modified from (Guerra and Barbacid 2013) (**B**) Upon tamoxifen binding, Cre^{ERT} translocates into the nucleus and recombines floxed DNA sequences (Feil et al. 1996). Recombination efficiency can be validated by the expression of a fluorescent reporter, such as tdTomato.

1.5 Acinar-to-ductal metaplasia is an important prerequisite for the initiation of PDAC

For the identification of the cell of origin for PDAC, various GEMMs have been developed and analyzed. Since pancreatic precursor lesions, such as PanINs, harbor a ductal phenotype, it was initially claimed that ductal cells could be the origin for PDAC. Thus, Brembeck et al. expressed oncogenic Kras under the control of the ductal-specific *Ck19*

(cytokeratin 19) promoter. Mice developed periductal lymphocytic infiltrations and occasional hyperplastic ductal cells were detected, but the model failed to recapitulate the formation of PanINs and PDAC (Brembeck et al. 2003). Moreover, the hypothesis that pancreatic precancerous lesions could arise from normal ductal epithelia was disproven by the use of a $Sox9^{CreER}$;$Kras^{G12D}$ mouse model; after activation of mutant Kras in ductal cells at postnatal day 10, pancreata displayed only rare PanINs and had an almost normal appearance (Kopp et al. 2012).

The first indications, that acinar cells could give rise to ductal structures, came up in 1987. Here, Willemer et al. described that in the setting of a pancreatitis, acinar cells are responsible for the generation of tubular complexes (Willemer et al. 1987). Actually, this assumption was proven by several studies, demonstrating that upon cell damage, acinar cells undergo the so-called **acinar-to-ductal metaplasia** (**ADM**) and de-/transdifferentiate into cells with a ductal appearance (Figure 1.5) (Strobel et al. 2007, Habbe et al. 2008, Guerra et al. 2007, Jensen et al. 2005). ADM formation can be induced through the expression of oncogenic Kras (Guerra et al. 2007), over-expression of TGF-α (Wagner et al. 1998, Means et al. 2005) or through inflammatory processes (Strobel et al. 2007).

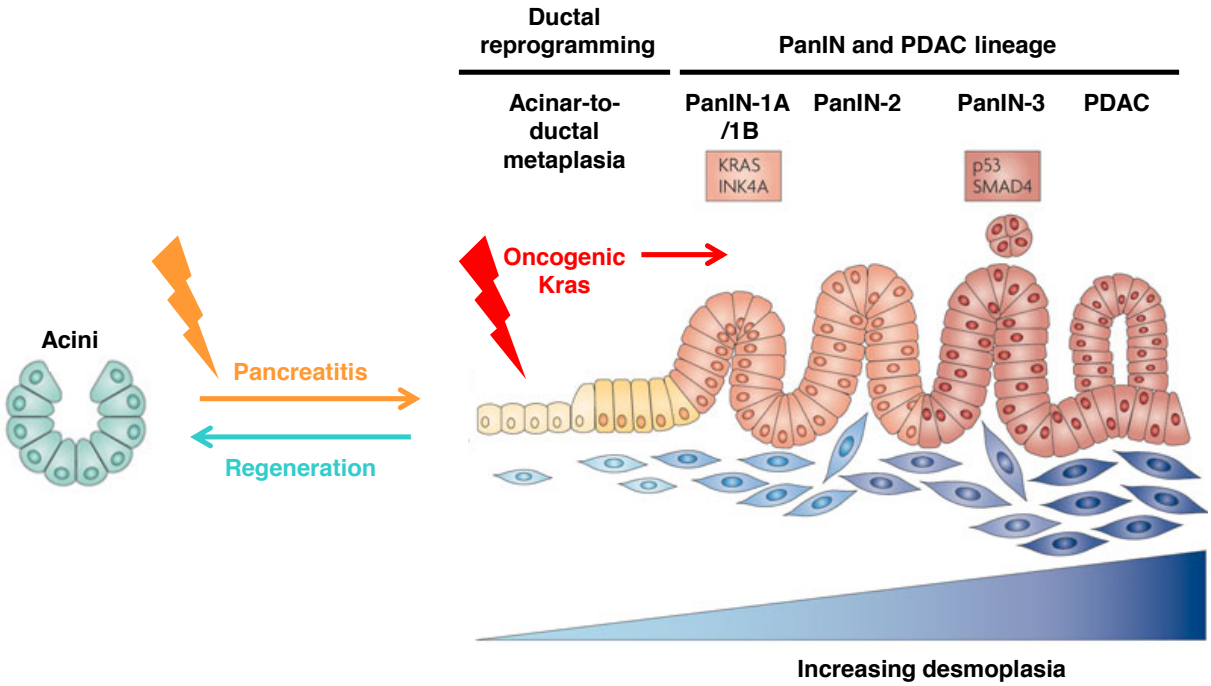

Figure 1.5: Acinar-to-ductal metaplasia initiates PDAC development. Conversion of acinar cells into metaplastic ductal cells can be induced in the setting of pancreatitis. In principle, ADM is a reversible process, cells can regenerate (Kong et al. 2016). However, oncogenic Kras expression in inflammation-triggered ADM cells is supposed to initiate the formation of PDAC precursor lesions and PDAC (Guerra et al. 2007). Graphic was adapted and modified from (Morris, Wang, and Hebrok 2010).

Upon the induction of a caerulein-mediated acute pancreatitis, transient ADM formation can be observed. During pancreatic regeneration, tubular complexes are replaced by normal pancreatic parenchyma, suggesting that ADM is a reversible process (Figure 1.5) (Kong et al. 2016). When oncogenic $Kras^{G12V}$ is expressed in embryonic acinar cells (inducible *Elastase*-Cre mouse model), mice develop ADMs between an age of one to three months, at later stages PanINs (three-month-old mice) and PDAC (twelve-month-old mice) (Guerra et al. 2007). Due to the fact that ADM seems to precede PanIN development, it is believed that ADM poses the precursor state for manifested pancreatic precursor lesions or PDAC. Moreover, since pancreatitis together with the concomitant expression of mutant Kras is required to initiate PDAC development in an adult stage, it is supposed that inflammation-induced ADM is essential to commence oncogenic transformation by oncogenic Kras (Figure 1.5) (Guerra et al. 2007).

1.5.1 ADM cells, PDAC precursor lesions and pancreatic tumor cells acquire a progenitor-like cell character

Since differentiated acinar cells are refractory to oncogenic Kras-driven cell transformation, but not embryonic acinar and ADM cells (Guerra et al. 2007), expression of pancreatic cell fate genes and the activation status of signaling pathways could be remodeled in metaplastic structures. Importantly, caerulein-induced acinar dedifferentiation is hallmarked by a re-expression of the transcription factors Pdx1 and Hes1 (hes family BHLH transcription factor 1), which are characteristically expressed in pancreatic progenitor cells (Jensen et al. 2005). Up-regulation of nestin, a filament marker for exocrine progenitor cells can be also detected in metaplastic ductal lesions (Fendrich et al. 2008). According to Prevot et al., ADM cells highly express the transcription factor Hnf6, which stimulates expression of the ductal marker Sox9 (Prevot et al. 2012). Over-expression of Sox9 in $Kras^{G12D}$-expressing mice aggravates ADM and PanIN formation, whereas Sox9 deletion leads to a significant decrease of precursor lesions (Kopp et al. 2012). Moreover, 100 % of PanIN and 89 % of PDAC samples were found to be positive for SOX9 (Shroff et al. 2014), whereas PDX1 was detected in more than 40 % of human PDAC cases (Liu et al. 2007). Besides the reactivated expression of transcription factors, important in pancreatic development, a silencing of acinar-specific genes appears in pancreatitis-induced ADM and pancreatic carcinogenesis. Thus, expression of amylase is greatly reduced in acute pancreatitis, one day after caerulein administration in wildtype mice (Jensen et al. 2005) and expression of the enzyme is inhibited in PDAC cell lines (Torres et al. 2013). Moreover, expression of the acinar differentiation transcription factor Ptf1a is greatly lost in PanIN lesions (Krah et al. 2015). Levels of MIST1 were found to be largely decreased in human CP and PDAC tissue (Johnson et al. 2012). Depletion of these factors in oncogenic Kras-expressing mice

accelerates PDAC development (Shi et al. 2009, Krah et al. 2015), suggesting that a repression of a acinar differentiation genes promotes PDAC.
In early pancreas development, expression of the progenitor genes PDX1 and SOX9 is positively stimulated through epigenetic histone remodeling (Xie et al. 2013). Hence, epigenetic modifications could contribute to the transcriptional reprogramming, occurring in pancreatic carcinogenesis.

1.6 Epigenetic modifications

The term **epigenetics** refers to heritable changes in gene expression, which are not caused by alterations in the DNA sequence (Goldberg, Allis, and Bernstein 2007). So far, DNA methylation, histone modification and microRNA-induced regulation of gene expression have been described as epigenetic mechanisms (McCleary-Wheeler et al. 2013).

1.6.1 DNA methylation

Regulation of DNA methylation at promoter regions serves as an important tool to influence gene expression. Thus, DNA methylation plays a pivotal role in X chromosome inactivation, genomic imprinting, embryonic development and differentiation processes (Bird 2002). However, deregulation of DNA methylation drives tumor development and progression. On the one hand, tumor cell genomes posses hypomethylated areas, which are also apparent at oncogenes (Feinberg and Vogelstein 1983), while on the other hand focal DNA hypermethylation can be frequently detected at gene loci of tumor suppressor genes, like $P16^{INK4A}$ (Herman et al. 1995, Schutte et al. 1997). DNA methylation occurs at cytosine residues of so-called CpG (5'-C-phosphate-G-3') nucleotides, which are frequently accumulated in CpG islands (Larsen et al. 1992). Two distinct groups of DNA methyltransferases catalyze DNA methylation. DNA methyltransferase 1 (DNMT1) maintains and copies methyl group patterns from the parental to the newly synthesized daughter strand during replication (Song et al. 2012). DNMT3a and DNMT3b are designated as de novo methyltransferases and set up methylation patterns during embryonic development (Robertson et al. 1999). Generally, DNA methylation can prohibit the binding of core transcription factors and therefore impedes gene transcription (Choy et al. 2010). Moreover, methyl-CpG binding proteins (MBDs), such as MeCP2, recognize methylated DNA (Hendrich and Bird 1998) and serve as docking sites for repressive histone modifying complexes, helping to strengthen chromatin compaction and induce a more persistent gene silencing. For instance, MeCP2 can interact with HDACs (Nan et al. 1998) or histone methyltransferases (Fuks et al. 2003).

Expression of DNMT1, DNMT3a and DNMT3b is elevated in PanIN lesions and PDAC, and high levels correlate with low survival (Zhang et al. 2012). Immunoprecipitation of highly methylated DNA from PDAC patients and normal tissue identified promoter hypermethylation of the tumor-suppressor gene *Wnk2* (Lysine-Deficient Protein Kinase 2), a negative regulator of the ERK/MAPK pathway, in PDAC. Expression of this gene is indeed decreased in PDAC, demonstrating that DNA methylation-induced gene silencing contributes to oncogenic cell transformation (Dutruel et al. 2014).

1.6.2 Histone modifications

Recently, several studies indicated that DNA methylation acts in concert with further epigenetic mechanisms like histone modifications (Nan et al. 1998, Fuks et al. 2003). Histones are positively charged protein components of the eukaryotic chromatin, responsible for packaging of DNA into so-called nucleosomes. The histone family comprises histone H2A, H2B, H3, H4 and H1. Precisely, nucleosomes are assembled as octamers, consisting of two H2A-H2B histone dimers and one H3-H4 tetramer, bound by 146 bp of DNA (Luger et al. 1997, Marino-Ramirez et al. 2005). Histone H1 dynamically binds to the nucleosomes, stabilizes the wrapped and adjacent linker DNA and is therefore described as linker histone (Bustin, Catez, and Lim 2005).

Importantly, histones can be modified post-translational within their N-terminal tails or core globular domains (Figure 1.6 A) (Tropberger and Schneider 2013). Histone tail amino acids, such as serine, threonine or tyrosine, are commonly phosphorylated, whereas lysine and arginine residues can undergo methylation, acetylation, ubiquitination or sumoylation (Strahl and Allis 2000). Assessing the "histone code" of a specific gene can predict if gene transcription is in an active or repressed state (Figure 1.6 B).

A

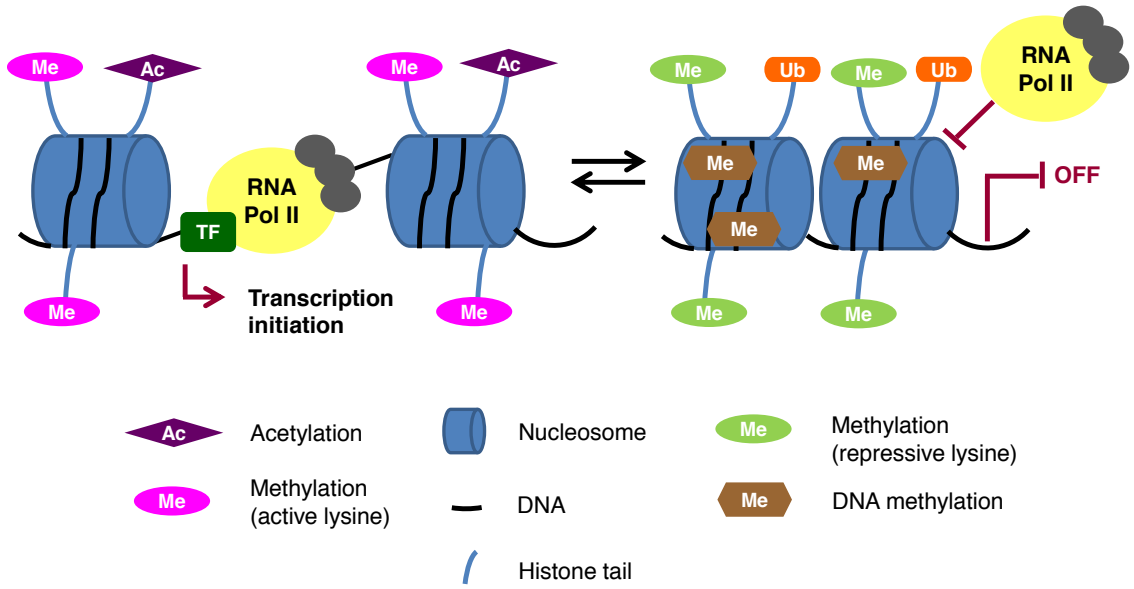

B

	Histone modification		
	H3K4me3	**H3K27me3**	**H2AK119ub**
Nature	Activating	Repressive	Repressive
Location	TSS (Koch et al. 2007)	TSS gene body (Young et al. 2011)	TSS gene body (Jin et al. 2012)
Modified by	TrxG proteins	PRC2	PRC1

Figure 1.6: Epigenetic mechanisms control gene expression. (**A**) Open chromatin conformation is guaranteed by histone acetylation and activating histone methylation, such as H3K4me3 (Legube and Trouche 2003, Zhang, Wen, and Shi 2012). In contrast, DNA methylation, histone ubiquitination or repressive histone methylation, like H3K27me3, favor chromatin compaction (Zhang, Wen, and Shi 2012). Consequently, RNA transcription machinery can no longer access DNA and gene expression is repressed (Niessen, Demmers, and Voncken 2009) (**B**) Overview of relevant histone modifications.

1.6.2.1 Activating histone modifications

Activation of gene expression is triggered, amongst others, by histone acetylation, which is catalyzed by histone acetyltransferases (HATs) (Legube and Trouche 2003). Lysine acetylation can stimulate gene expression in distinct ways. First, upon acetylation, neutralization of positively charged histones occurs, leading to weakened histone-DNA interactions and to a more open chromatin conformation (Hong et al. 1993) (Legube and Trouche 2003). Second, recent studies implicated that histone acetylation is recognized by small proteins, called bromodomains, which coordinate the binding of further chromatin remodelers, transcription factors or the transcription machinery. For instance, p300 harbors a bromodomain, which allows the docking to acetylated lysines. Consequently, p300's intrinsic

HAT module enriches histone acetylation and transcriptional activation is achieved (Chen, Ghazawi, and Li 2010).

In contrast, histone deacetylation by histone deacetylases (HDACs) induces gene silencing. Under normal circumstances, the activity of HATs and HDACs is tightly coordinated to ensure dynamic gene transcription (Legube and Trouche 2003). However, in PDAC, HDAC1 and 2 are highly expressed (Schneider et al. 2011) and are involved in the ZEB1-mediated (zinc finger E-box binding homeobox 1) repression of *E-Cadherin* (Aghdassi et al. 2012). Loss of E-cadherin favors epithelial-to-mesenchymal transition (EMT) and cancer cell metastasis (Kalluri and Weinberg 2009).

Unlike activating histone acetylation, histone methylation can either serve as a positive or a repressive mark. For instance, methylation on lysine 4 of histone H3 (H3K4) is associated with transcriptional activation, whereas di- and trimethylation on lysine 27 of histone H3 (H3K27) is linked to transcriptional repression (Zhang, Wen, and Shi 2012). The level of tri-methylated H3K4 (H3K4me3) peaks at transcriptional start sites (TSS) of actively expressed genes (Koch et al. 2007). Tri-methylation of H3K4 is catalyzed by a heterogeneous group of Trithorax group (TrxG) proteins. Depending on their function, TrxG proteins are either designated as histone-modifying or ATP-dependent chromatin remodeling complexes (Schuettengruber et al. 2007).

1.6.2.2 Repressive histone modifications - Polycomb group (PcG) proteins

By causing transcriptional repression, the so-called Polycomb group proteins behave antagonistically to the TrxG proteins. PcG proteins are arranged in complexes, such as the the Polycomb repressor complexes 1 and 2 (PRC1, PRC2). First, PRC2 mediates the trimethylation of H3K27, which is then recognized by PRC1 (Cao et al. 2002). Subsequently, PRC1 catalyzes the mono-ubiquitination of lysine 119 of histone H2A (H2AK119ub), leading to chromatin compaction and gene repression (de Napoles et al. 2004, Niessen, Demmers, and Voncken 2009). PRC2 and PRC1 are assembled as multiprotein complexes, composed of catalytic subunits, co-activators, complex stabilizers and chromatin binding domains (Figure 1.7).

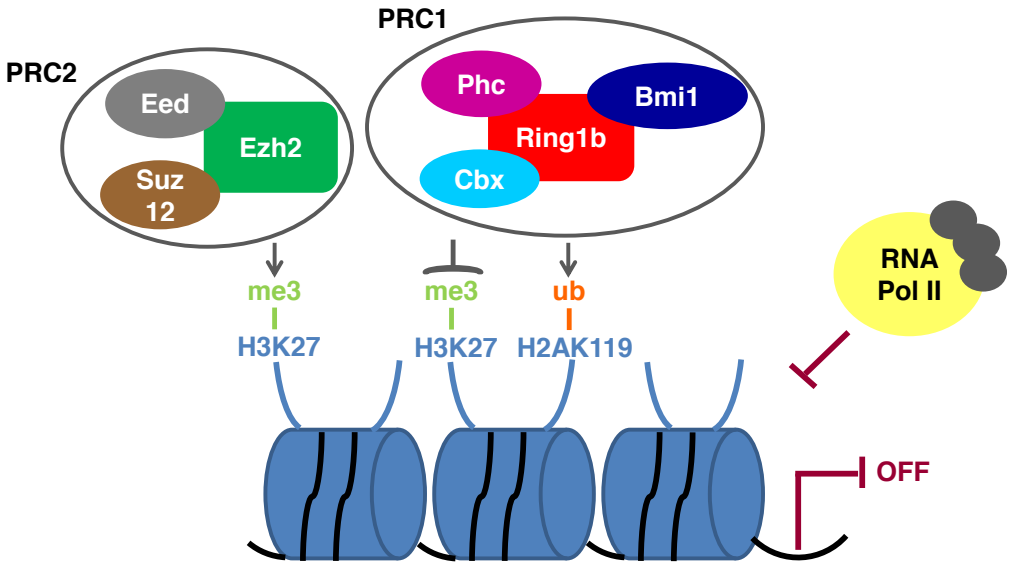

Figure 1.7: Epigenetic gene silencing mediated by the Polycomb repressor complexes 2 and 1. PRC2 catalyzes the tri-methylation of H3K27. Sequentially, H3K27me3 recruits PRC1 and its catalytic subunit mono-ubiquitinates H2AK119. Both histone marks cause compaction of chromatin and gene repression (Niessen, Demmers, and Voncken 2009).

1.6.3 Structure of PRC2

Core **PRC2** consists of three proteins, **EZH2** (enhancer of zeste homolog 2), **SUZ12** (suppressor of zeste homolog 12) and **EED** (embryonic ectoderm development) (Montgomery et al. 2005). Trimethylation of H3K27 is catalyzed by the histone-lysine N-methyltransferase EZH2 (Cao et al. 2002). EED, as well as SUZ12 are required for enzymatic activity of PRC2 (Cao and Zhang 2004, Kim et al. 2013). It was suggested that SUZ12 mediates the interaction between EZH2 and the nucleosomes (Cao and Zhang 2004) and that EED is required to stabilize functional PRC2 (Montgomery et al. 2005). Moreover, EED is believed to coordinate recruitment of PRC1 to H3K27me3 and can enhance the activity of the complex (Cao et al. 2014).

1.6.4 Structure of PRC1

In particular, mammalian core PRC1 is built up of **RING1a** (ring finger protein 1) and **RING1b** (ring finger protein 2), **BMI1** (B lymphoma Mo-MLV insertion region 1), **CBX** (chromobox homolog) and the **PH** (Polyhomeotic homologue) proteins (Simon and Kingston 2009, Margueron and Reinberg 2011).

Successive H2AK119ub modification is carried out by the E3 ubiquitin ligases RING1a and RING1b (Cao, Tsukada, and Zhang 2005, de Napoles et al. 2004). As their names suggest, they exhibit a ring finger domain, which is highly related to the zinc finger motif found in transcription factors (Lovering et al. 1993, Choi and Kang 2011). In mammalian cells,

RING1b seems to be of higher importance than RING1a, because its depletion in embryonic stem (ES) or HeLa cells caused a dramatic decrease of global H2AK119ub levels (de Napoles et al. 2004, Wang et al. 2004, van der Stoop et al. 2008). Moreover, global *Ring1b* null embryos turned out to be lethal due to gastrulation defects (Voncken et al. 2003), whereas Ring1a-deficient mice are viable, but exhibit skeletal abnormalities (del Mar Lorente et al. 2000).

Importantly, RING1b function and stabilization is dependent on BMI1. Buchwald et al. revealed that RING1b-mediated H2A ubiquitination is greatly stimulated by the addition of BMI1 *in vitro*. Importantly, BMI1 itself has no intrinsic ubiquitin ligase activity (Buchwald et al. 2006), but helps to adjust nucleosomes for H2A ubiquitination (Li et al. 2006).

Moreover, CBX family proteins are believed to mediate binding of PRC1 to chromatin (Vincenz and Kerppola 2008). For instance, Cbx7 shows a strong affinity for H3K27me3 (Bernstein, Duncan, et al. 2006).

The function of the PH proteins is not entirely clear, but there is evidence that they are necessary for the extension of PcG complexes (Kim et al. 2002).

1.6.5 Mechanisms of PcG-mediated transcriptional repression

It remains largely elusive how PcG proteins actually repress gene transcription. Tiwari et al. suggested that PcG proteins can modulate chromatin organization by inducing the formation of "pre-repressive chromatin hubs", which impedes the binding of the transcriptional machinery (Tiwari et al. 2008). Another study highlights that PRC1 prohibits the assembly of the RNA polymerase II preinitiation complex (PIC) (Lehmann et al. 2012). Moreover, it was proposed that presence of H2AK119ub helps to retain RNA polymerase II in a poised state, characterized by phoshorylation of its carboxy-terminal domain at serine 5 (Stock et al. 2007). Besides retention of the transcriptional machinery, studies revealed that PcG proteins communicate with other epigenetic silencing systems. Thus, the PRC2 subunit EED can interact with HDAC proteins (van der Vlag and Otte 1999) and EZH2 can recruit DNA methyltransferases, which enforce gene silencing. Upon depletion of EZH2, binding of DNMT1, DNMT3a and DNMT3b to EZH2 target genes is reduced, CpG island methylation decreased and gene expression de-repressed (Vire et al. 2006).

In summary, PRC-mediated gene silencing encompasses chromatin organization, interference with the transcriptional machinery and recruitment of other epigenetic modifiers.

1.6.6 PcG target genes

Initially, PcG proteins were discovered in Drosophila melanogaster, supporting proper body segmentation during embryonic development (Schuettengruber et al. 2007). For the large-

scale identification of PcG target genes, chromatin immunoprecipitation experiments (ChIP), such as ChIP-on-Chip or ChIP-sequencing, were performed. In ES cells, PRC2 and PRC1 were found to target genes associated with developmental processes, cell-fate commitment and differentiation (Boyer et al. 2006, Lee et al. 2006, van der Stoop et al. 2008). Here, the majority of repressed genes comprises key developmental regulators, like the *HOX* gene family, suggesting that PcG-mediated gene silencing helps to stably maintain ES cells in an undifferentiated state (Lee et al. 2006). In ES cells, genes of central developmental regulators are strongly associated with bivalent histone marks; gene regions, which simultaneously harbor H3K4me3 and H3K27me3 modifications. Bivalent domains primarily keep genes in an inactivated state, but remain them poised for activation However, in differentiated cells, bivalent domains resolve and genes finally harbor either repressive or activating histone methylation marks, (Bernstein, Mikkelsen, et al. 2006, Mikkelsen et al. 2007). Besides high levels of H3K27me3, the transcriptionally silent state of genes associated with bivalent domains is additionally dependent on the presence of H2AK119ub. Upon depletion of Ring1b, H2AK119ub levels at bivalent domains decrease, the poised form of the RNA polymerase II (phosphorylated on serine 5) is released and genes are actively expressed (Stock et al. 2007).

1.6.7 Regulation of PcG proteins

Differentiation processes are tightly regulated by a dynamic expression of PcG proteins. Thus, Ring1b expression can be detected until E14.5 in pancreatic branch tips, where multipotent pancreatic progenitor cells are located (Martinez-Romero et al. 2009, Stanger and Hebrok 2013). However, when multipotent progenitor cells start to differentiate into immature acinar cells around E15.5-16, Ring1b expression is decreased and nearly completely lost in adult acinar cells (Martinez-Romero et al. 2009). In embryonic epidermal precursor cells, EZH2 can be found, but not in differentiated cell lineages (Ezhkova et al. 2009).

Signaling pathways and associated transcription factors, which control PcG expression, remain largely unkown. However, phosphorylated retinoblastoma protein (pRB) and retinoblastoma-associated protein (E2F), which coordinate cell cycle progression, were identified to positively regulate expression of *EZH2* and *EED* (Bracken et al. 2003).

In human prostate tumors, over-expression of BMI1 correlates with an aberrant activation of the PI3K/Akt signaling pathway. Nacerddine et al. revealed that Akt (protein kinase B) directly phoshorylates BMI1, which in turn stimulates RING1b-mediated histone H2A ubiquitination (Nacerddine et al. 2012). Moreover, posttranslational modifications of RING1b, such as its self-ubiquitination, are required for proper H2A ubiquitin ligase activity (Ben-Saadon et al. 2006). In contrast, ubiquitination of RING1b by exogenous ubiquitin ligases,

such as E6-AP (E6-associated protein), causes proteasomal degradation (Zaaroor-Regev et al. 2010).
In summary, the regulation of PcG protein levels and their activity involves changes in gene expression and posttranslational modifications, respectively.

1.6.8 Recruitment of PcG proteins to their target genes

To date, it is not clear which signals or mechanisms induce recruitment of PcG proteins to their specific target genes. Mendenhall et al. proposed that GC-rich DNA elements, without the presence of activating transcription factor binding sites, can recruit EZH2 to induce heterochromatin formation (Mendenhall et al. 2010). Several studies suggest that transcription factors themselves guide PcG proteins to their target gene promoters. Thus, the transcriptional repressor JARID2 (jumonji- and ARID-domain-containing protein) was identified to recruit PRC2 (Pasini et al. 2010). Göke et al. reported that gene loci bound by ELK1 (ETS transcription factor), but not by ERK2 (mitogen-activated protein kinase 1), are co-occupied by EZH2 and RING1b and repressed, whereas genes associated with both ELK1 and ERK2 are actively expressed (Goke et al. 2013).
Besides transcription factors, chromatin remodelers were also identified to be involved in the recruitment of PcGs. For instance, in ES cells the histone demethylase Kdm2b (lysine demethylase 2B) helps to recruit Ring1b to its target genes. In absence of Kdm2b, binding of Ring1b and H2AK119 ubiquitination is reduced (Wu, Johansen, and Helin 2013).

1.6.9 Role of PRC2 in cancer

Deregulated expression or modified function of PcG proteins highly contribute to cancer initiation and progression. Over-expression of EZH2 was amongst others identified in prostate, breast or non-small lung cancer and is correlated with cellular transformation, cancer aggressiveness, poor prognosis and survival (Varambally et al. 2002, Kleer et al. 2003, Behrens et al. 2013). Regarding pancreatic cancer, EZH2 accumulation was found in 68 % of human PDAC cases and almost always occurrs in poorly differentiated tissue (Ougolkov, Bilim, and Billadeau 2008). Loss of EZH2 in pancreatic cancer cells causes re-expression of the cell cycle inhibitors $P27^{Kip1}$ (cyclin-dependent kinase inhibitor 1B) and $P21^{Cip1}$ (cyclin-dependent kinase inhibitor 1A), causing reduced cell proliferation (Ougolkov, Bilim, and Billadeau 2008, Batchu et al. 2013). Ezh2-mediated suppression of $p16^{INK4A}$ during caerulein-induced pancreatitis was shown to promote cell proliferation in terms of tissue regeneration (Mallen-St Clair et al. 2012).

Importantly, elevated levels of EZH2 are a prerequisite for pancreatic and breast cancer stem cells. Knockdown of EZH2 decreases the frequency of cancer stem cells (CSCs) and is associated with an increased expression of differentiation genes (van Vlerken et al. 2013).

1.6.10 Role of PRC1 in cancer

Besides elevated levels of EZH2, several studies implicated that CSCs from prostate cancer, hepatocellular carcinoma or pancreatic cancer are characterized by high levels of BMI1 (Chiba et al. 2008, Lukacs et al. 2010, Proctor et al. 2013). In pancreatic CSCs, BMI1 knockdown constrains tumor sphere formation and self-renewal capacities (Proctor et al. 2013). Broad over-expression of BMI1 was not only found in CSCs, but also in PanIN lesions, PDAC tissue and human pancreatic cancer cell lines (Proctor et al. 2013, Martinez-Romero et al. 2009). Moreover, in the setting of a caerulein-induced acute and chronic pancreatitis, up-regulation of Bmi1 was observed in damaged acinar cells, as well as in ADM lesions (Martinez-Romero et al. 2009). Strikingly, when both alleles of Bmi1 are depleted in $Pdx1^{Cre}$;$Kras^{G12D}$ mice, formation of PanIN lesions is greatly abolished, claiming that Bmi1 is crucial for pancreatic carcinogenesis (Bednar et al. 2015).

In addition to Bmi1, deregulations of Ring1b also mediate cancer development and progression. RING1b was found to be over-expressed in ductal breast carcinoma, prostate cancer and PDAC (Bosch et al. 2014, van Leenders et al. 2007, Chen, Chen, et al. 2014, Martinez-Romero et al. 2009). To prove that Ring1b expression is a prerequisite for oncogenic transformation, Ring1b was depleted in mouse embryonic fibroblasts (MEFs) prior to or after mutant Kras expression. Interestingly, *in vivo* tumor growth is significantly reduced in both cases, suggesting that Ring1b could be regarded as a relevant oncogene (Piunti et al. 2014). In ductal breast carcinoma, RING1b expression is mostly enhanced in stroma-invading tumor cells. By inhibiting P63 (tumor protein p63) through histone ubiquitination, RING1b indirectly induces expression of the focal adhesion kinase (FAK), which is an important mediator of cell migration and cell invasion (Bosch et al. 2014).

Regarding pancreatic cancer, RING1b expression was found to be up-regulated in PanIN lesions as well as in PDAC (Martinez-Romero et al. 2009). PDAC specimens that display high levels of H2AK119ub correlate with a larger tumor size, poorer differentiation, lymph node metastasis and a shorter survival rate (Chen, Chen, et al. 2014). When RING1b-depleted pancreatic tumor cells were subcutaneously transplanted into nude mice, tumor volume was significantly smaller in comparison to transplanted control cells (Chen, Chen, et al. 2014). A recent study proposed, that Snail, an important mediator of EMT, recruits Ring1b to the *E-cadherin* promoter, contributing to its gene repression and oncogenic cell transformation (Chen, Xu, et al. 2014). However, only few mechanistic studies are available and Ring1b target genes remain largely elusive.

2 Aim of the study

Nowadays, it has been widely accepted that acinar-to-ductal metaplasia is an important prerequisite for the formation of PanIN lesions and PDAC (Zhu et al. 2007, Guerra et al. 2007). However, initial de-/trans-differentiation of acinar cells has not been precisely defined, yet. Thus, in this study, an *in vitro* ADM model shall be established, to allow the isolation and analysis of metaplastic cells.

Pancreatic carcinogenesis is characterized by a loss of acinar differentiation (Krah et al. 2015, Shi et al. 2009) and a concomitant recapitulation of developmental pathways and cellular processes (Morris, Wang, and Hebrok 2010, Liu et al. 2007). mRNA expression profiling will allow the large-scale identification of differentially expressed genes in an *in vitro* multi-step model consisting of embryonic and differentiated acinar cells, ADM and pancreatic cancer cells. In addition, expression data shall be used to characterize the nature of ADM cells.

Since PDAC initiation and progression is hallmarked by broad changes in the transcriptome, the role of epigenetic alterations will be assessed in this study. In ES cells, epigenetic modifications catalyzed by PcG proteins, such as RING1b, mediate repression of differentiation genes and consequently contribute to the maintenance of ES cells (van der Stoop et al. 2008, Ku et al. 2008, Endoh et al. 2008). RING1b is barely expressed in mature acinar cells, but expression has been found to be reactivated in PDAC precursor lesions and PDAC tissue (Martinez-Romero et al. 2009). Thus, it shall be determined if Ring1b-mediated gene silencing contributes to the establishment of a progenitor-like profile in pancreatic cancer. Moreover, to assess the functional role of the epigenetic repressor in inflammatory acinar-to-ductal metaplasia and $Kras^{G12D}$-mediated pancreatic carcinogenesis, conditional Ring1b knockout mice will be investigated. In pancreatic cancer, over-expression of Ring1b correlates with poor survival (Chen, Chen, et al. 2014). Hence, to demonstrate its function in full blown pancreatic cancer cells, CRISPR/Cas9-mediated gene knockout will be performed. Moreover, the application of a PRC1 inhibitor, shall reveal if the epigenetic remodeling complex is suited as a therapeutic target.

3 Materials and Methods

3.1 Materials

Standard chemicals and reagents, which are not listed in the following, were ordered with the purity degree 'pro analysi' from Sigma-Aldrich (St. Louis, USA), Carl Roth GmbH (Karlsruhe) and the on-site dispensary.

3.1.1 Specific chemicals and reagents

Table 3.1: Specific chemicals and reagents

Reagent	Manufacturer
Acrylamide-bisacrylamide solution, Rotiphorese® Gel 30	Carl Roth GmbH, Karlsruhe
Agarose broad range	Carl Roth GmbH, Karlsruhe
Albumine fraction V, Bovine serum albumin (BSA)	Carl Roth GmbH, Karlsruhe
Ammonium persulfate (APS)	Sigma-Aldrich, St. Louis, USA
BCP (1-Bromo-3-chloropropane)	Sigma-Aldrich, St. Louis, USA
BrdU (5-Bromo-2'-deoxyuridine)	Sigma-Aldrich, St. Louis, USA
Caerulein	Sigma-Aldrich, St. Louis, USA
Collagen Type I, rat tail	Corning, Bedford, USA
DAPI (4′,6-Diamidino-2-phenylindole dihydrochloride)	Sigma-Aldrich, St. Louis, USA
DAPI mounting medium	Dianova, Hamburg
Dexamethasone, water-soluble	Sigma-Aldrich, St. Louis, USA
Dimethyl sulfoxide (DMSO)	Sigma-Aldrich, St. Louis, USA
DNA ladder 1 kb Plus, GeneRuler	Thermo Fisher Scientific, Waltham, USA
DNA ladder 100 bp, HyperLadder	Bioline, London, GB
DNA loading dye (6X)	Thermo Fisher Scientific, Waltham, USA
Dulbecco's Modified Eagle's Medium (DMEM), high glucose (4500 mg/l glucose)	Sigma-Aldrich, St. Louis, USA
Ethidium bromide	Sigma-Aldrich, St. Louis, USA
Fetal bovine serum (FBS)	Sigma-Aldrich, St. Louis, USA
Hank's Balanced Salt Solution (HBSS) (1X)	Merck Millipore, Billerica, USA
Heparin-Sodium-25000-ratiopharm®	Ratiopharm, Ulm
HEPES (*4-(2-hydroxyethyl)-1-piperazine-ethanesulfonic acid*) buffer solution (1 M)	Thermo Fisher Scientific, Waltham, USA
Isoflurane CP®	CP-Pharma, Burgdorf

Liquid DAP + substrate chromogen system	Dako, Hamburg
Mayer's hemalum solution	Merck Millipore, Billerica, USA
Mounting medium, VectaMount	Vector Laboratories, Burlingame, USA
MTT (3-(4,5-Dimethylthiazol-2-yl)-2,5-diphenyl tetrazolium bromide)	Sigma-Aldrich, St. Louis, USA
Nonident P-40 (NP-40) (IPEGAL® CA-630)	Sigma-Aldrich, St. Louis, USA
PCR reaction mix, Jumpstart™ REDTaq	Sigma-Aldrich, St. Louis, USA
Phosphate-buffered saline (1X) (PBS)	Sigma-Aldrich, St. Louis, USA
PIPES (1,4-Piperazinediethanesulfonic acid)	Sigma-Aldrich, St. Louis, USA
Plasmid transfection medium	Santa Cruz, Dallas, TX, USA
Protein A agarose/salmon sperm DNA	Merck Millipore, Billerica, USA
Protein G agarose/salmon sperm DNA	Merck Millipore, Billerica, USA
Protein ladder, PageRuler™ (10 to 180 kDa)	Thermo Fisher Scientific, Waltham, USA
Protein loading buffer, NuPAGE® (4X)	Thermo Fisher Scientific, Waltham, USA
qRT-PCR reaction mix, KAPA SYBR FAST LightCycler 480	Kapa Biosystems, Wilmington, USA
Red blood cell lysing buffer	Sigma-Aldrich, St. Louis, USA
RPMI-1640 (Roswell Park Memorial Institute Medium 1640)	Sigma-Aldrich, St. Louis, USA
Serum, goat	Abcam, Cambridge, UK
Sodium deoxycholate	Sigma-Aldrich, St. Louis, USA
Sodium dodecyl sulfate (SDS), ultrapure	Sigma-Aldrich, St. Louis, USA
Tamoxifen	Sigma-Aldrich, St. Louis, USA
TEMED (Tetramethylethylenediamine)	Carl Roth GmbH, Karlsruhe
TGF-α, human recombinant protein	Thermo Fisher Scientific, Waltham, USA
TRI-reagent	Sigma-Aldrich, St. Louis, USA
Triton X-100	Sigma-Aldrich, St. Louis, USA
Trypan blue stain, 0.4 %	Thermo Fisher Scientific, Waltham, USA
Trypsin-EDTA solution	Sigma-Aldrich, St. Louis, USA
Tween® 20	Carl Roth GmbH, Karlsruhe
UltraCruz® transfection reagent	Santa Cruz, Dallas, USA

3.1.2 Kits

Table 3.2: Kits

Kit	Manufacturer
Amersham™ ECL™ Western Blot Detection Kit	GE Healthcare, Little Chalfont, UK
EpiTect® Bisulfite Kit	Qiagen, Hilden

NE-PER® Nuclear and Cytoplasmic Extraction Kit	Thermo Fisher Scientific, Waltham, UK
Pierce BCA Protein Assay Kit	Thermo Fisher Scientific, Waltham, USA
Qiaquick® PCR Purification Kit	Qiagen, Hilden
QIAamp® DNA Mini Kit	Qiagen, Hilden
RNeasy® Plus Mini Kit	Qiagen, Hilden
Verso cDNA synthesis Kit	Thermo Fisher Scientific, Waltham, USA

3.1.3 Inhibitors

Table 3.3: Inhibitors

Inhibitor	Manufacturer
Bmi1-Ring1A E3 ligase inhibitor, PRT4165	Merck Millipore, Billerica, USA
MEK inhibitor, PD 98059	Tocris, Bristol, UK
Phosphatase inhibitor, PhosSTOP, EASYpack	Roche, Basel, Switzerland
PI3K inhibitor, LY 294002 hydrochloride	Tocris, Bristol, UK
Protease inhibitor cocktail, cOmplete Mini	Roche, Basel, Switzerland

3.1.4 Enzymes

Table 3.4: Enzymes

Enzyme	Manufacturer
Collagenase, Type VIII	Sigma-Aldrich, St. Louis, USA
Collagenase P	Roche, Basel, Switzerland
CpG Methyltransferase (M. SssI)	New England Biolabs, Ipswich, USA
DNase, RNase-free DNase set	Qiagen, Hilden
Micrococcal Nuclease (MNase), 100 units/μl	Thermo Fisher Scientific, Waltham, USA
Proteinase K	Peqlab Biotechnologie GmbH, Erlangen
RNase A	Qiagen, Hilden

3.1.5 Plasmids

Table 3.5: Plasmids

Plasmid	Manufacturer / Reference
Control CRISPR/Cas9 plasmid	Santa Cruz, Dallas, USA / sc-418922
Ring1b CRISPR/Cas9 KO plasmid	Santa Cruz, Dallas, USA / sc-422688
Ring1b HDR plasmid	Santa Cruz, Dallas, USA / sc-422688-HDR

3.1.6 Antibodies

3.1.6.1 Primary antibodies

Table 3.6: Primary antibodies

Antibody	Host	Application / Dilution	Manufacturer / Reference
Anti-α-Tubulin	mouse	WB 1:1000	Abcam, Cambridge, UK / ab11304
Anti-β-Tubulin	rabbit	WB 1:1000	Abcam, Cambridge, UK / ab6046
Anti-Akt	rabbit	WB 1:1000	Cell Signaling, Danvers, USA / #9272
Anti-Amylase	mouse	IF 1:100 WB 1:5000	Santa Cruz, Dallas, USA / sc-46657
Anti-Bmi1	mouse	IHC 1:100 WB 1:500	Merck Millipore, Billerica, USA / 05-673
Anti-BrdU	rat	IF 1:100	Santa Cruz, Dallas, USA / sc-56258
Anti-Cytokeratin 19 (Troma III)	rat	IF 1:20 IHC 1:100 - 1:20 WB 1:1000	Developmental Studies, Hybridoma Bank, University of Iowa, USA
Anti-Dnmt3a	rabbit	WB 1:1000	Santa Cruz, Dallas, USA / sc-20703
Anti-Erk	rabbit	WB 1:3000	Cell Signaling, Danvers, USA / #9102
Anti-Gapdh	rabbit	WB 1:2000	Santa Cruz, Dallas, USA / sc-25778
Anti-H2AK119ub	rabbit	ChIP 9 µg IHC 1:1000 IF 1:400 WB 1:40000	Cell Signaling, Danvers, USA / #8240
Anti-H3	rabbit	WB 1:2000	Cell Signaling, Danvers, USA / #9715
Anti-H3K4me3	rabbit	ChIP 4 µg WB 1:1000	Cell Signaling, Danvers, USA / #9751
Anti-H3K27me3	rabbit	ChIP 6 µg WB 1:2000	Merck Millipore, Billerica, USA / #07-449
Anti-H3K27me3	rabbit	ChIP 10 µg	Abcam, Cambridge, UK / ab6002
Anti-*phospho*-Akt	rabbit	WB 1:1000	Cell Signaling, Danvers, USA / #4060
Anti-*phospho*-Erk	rabbit	WB 1:1000	Cell Signaling, Danvers, USA / #9101
Anti-Ring1b	rabbit	WB 1:500	Cell Signaling, Danvers, USA / #5694

Anti-Ring1b	rabbit	IHC 1:400	Novus Biologicals, Littleton, USA / NBP1-49966
Anti-Ring1b	rabbit	IHC 1:200	Epigentek, Farmingdale, USA / A-2720
Anti-tdTomato	mouse	IF 1:200	OriGene, Rockville, USA / TA 180009

IHC = Immunohistochemistry

IF = Immunofluorescence

WB= Western blot

ChIP = Chromatin immunoprecipitation

FACS = Fluorescence activated cell sorting

3.1.6.2 Secondary antibodies

Table 3.7: Secondary antibodies

Antibody	Host	Conjugate	Application / Dilution	Manufacturer / Reference
Anti-mouse IgG	goat	Alexa Fluor® 568	IF 1:200	Thermo Fisher Scientific, Waltham, USA / A11004
Anti-mouse IgG	goat	Horseradish peroxidase	WB 1:2000	Promega, Madison, USA / W4021
Anti-mouse IgG EnVision+ System	goat	Horseradish peroxidase	IHC ready to use	Dako, Hamburg / K4001
Anti-rabbit IgG	goat	Alexa Fluor® 488	IF 1:200	Thermo Fisher Scientific, Waltham, USA / A11034
Anti-rabbit IgG	goat	APC	IF 1:200	Thermo Fisher Scientific, Waltham, USA / A10931
Anti-rabbit IgG	goat	Horseradish peroxidase	WB 1:2000	Promega, Madison, USA / W4011
Anti-rabbit IgG EnVision+ System	goat	Horseradish peroxidase	IHC ready to use	Dako, Hamburg / K4003
Anti-rat IgG	goat	Alexa Fluor® 488	IF 1:200	Thermo Fisher Scientific, Waltham, USA / A11006
Anti-rat IgG	rabbit	Horseradish peroxidase	IHC 1:100	Dako, Hamburg / P0450
Anti-rat IgG	goat	Horseradish peroxidase	WB 1:2000	Santa Cruz, Dallas, USA / sc-2006

3.1.7 Oligonucleotides (Primer)

All primers were designed with a melting temperature of 60 °C and were ordered (25 N, desalted) from Thermo Fisher Scientific (Waltham, USA).

3.1.7.1 Gene expression primer (for qRT-PCR)

Table 3.8: Gene expression primer

Primer	Sequence forward (5' ⟶3')	Sequence reverse (5'⟶ 3')
Amylase (1)*	TCCACCTGTTTGAGTGGCGCTGGGT	TGGGTGGAGAGACCTGCACACCTC
Amylase (2)	TTCGTTCTGCTGCTTTCCCT	ATCGCTCACATTCCTTGGCA
*Bmi1**	GGCTCCAATGAAGACCGAGG	ATCATTCACCTCTTCCTTAGGCT
Dnmt3a	GCTGCTGTGTGACCAAGGAAGGCCG TG	TCGGCCCCGGGAGCCCTCCATT
*Hes1**	AAAATTCCTCCTCCCCGGTG	TTTGGTTTGTCCGGTGTCG
*Mist1**	TCCCCAGTTGGAAGGGCCTCA	TCCTGCATGGGTGTTCGGCG
Pdx1	TGCCACCATGAACAGTGAGG	GGAATGCGCACGGGTC
*Ppib**	GGAGCGCAATATGAAGGTGC	CTTATCGTTGGCCACGGAGG
Ptf1a	CTTGCAGGGCACTCTCTTTC	CGATGTGAGCTGTCTCAGGA
*Rbpj**	GAGGGCGCGTCCCAAAACCC	AAACTTCCCCGCCGATGGAGC
*Rbpjl**	GTATCGAAGTCAGTGGCGGT	GCAGGCTCAGGTGAGTCAAA
Ring1a	GGTGGAGAGATTGAGCTTGTGT	TTCACGTACCGAGTCTGGCA
Ring1b (1)*	GTTGATTCTCGAGTCTCGCTC	TGAGACATTTCGGCTCCTGC
Ring1b (2)	CGGTGCCAGTGAGATTGAGT	CCTCACAGCCAGATACTTGGA

* Primer sequences were published in (Benitz et al. 2016).

3.1.7.2 ChIP primer (for qRT-PCR)

Table 3.9: ChIP primer

Primer	Sequence forward (5'⟶3')	Sequence reverse (5'⟶ 3')
*Bmi1 P1**	CGGTGACTGTACGTTAGCCT	TCAGCTCATCCCACAGCAAA
*Bmi1 P2**	TGTGGTGGCAGTTCAAGCTA	CTCCCTAGTGTACTTAGGACCCA
*Bmi1 P3**	GCCCTTTGGTGGGAACTTGA	TGAAACCACAGGCTCTTTCCT
*Ptf1a**	GGACCAGATCCGACCCTACT	CCGCTCCTACGTTCTTTGGT
*Rbpj**	CCCAACCTCGGCACTCAATG	ATGCCACTGATTCCCTACTGG
*Rbpjl** (1)	GTCGACACCGAATGAACCCA	GATTCGGGCTTCATCCCTCC
Rbpjl (2)	GGGCTTAGATGTGTGAACGGT	AGGGACCTAGTTAGGCTACACA

* Primer sequences were published in (Benitz et al. 2016).

3.1.7.3 Methylation-specific PCR (MSP) primer (for PCR)

Table 3.10: MSP primer

Primer	Sequence forward (5'⟶3')	Sequence reverse (5'⟶3')
p16^{INK4A} unmodified	ACTGAATCTCCGCGAGGAAAGCG	GCACACGGCCCTGGGCCGCCG
p16^{INK4A} methylated	CGATTGGGCGGGTATTGAATTTT CGC	CACGTCATACACACACACGACCCTAA ACCG
p16^{INK4A} unmethylated	GTGATTGGGTGGGTATTGAATTTTTG TG	CACACATCATACACACAACCCTAAAC CA

MSP primer sequences were adapted from (Sharpless et al. 2001).

3.1.7.4 Genotyping primer (for PCR)

Table 3.11: Genotyping primer

Primer	Sequence forward (5'⟶3')	Sequence reverse (5'⟶3')
Kras^{G12D} (1) (2)	CACCAGCTTCGGCTTCCTATT AGCTAATGGCTCTCAAAGGAATGTA	CCATGGCTTGAGTAAGTCTGC
tdTomato (1) (2)	AAGGGAGCTGCAGTGGAGTA GGCATTAAAGCAGCGTATCC	CCGAAAATCTGTGGGAAGTC CTGTTCCTGTACGGCATGG
p48^{ERT}	GAAGGCATTTGTGTAGGGTCA	GGCTGAGTGAGGGTTGTGAG
Ring1b$^{fl/fl}$	GGAAATGCAATGGTATCAATGTATAT G	GCTAGCGATGTGGCTATG

3.1.8 Mouse strains

Table 3.12: Mouse strains

Internal name (Official name)	**Background**	**Origin**	**Reference**
WT (Wildtype)	C57Bl6/J	Janvier Labs, Saint-Berthevin Cedex, France	
p48^{ERT} (p48$^{CreERT/+}$; LSL-tdTomato$^{flox/flox}$)	C57Bl6/J	This mouse line was generated through crossbreeding of p48$^{CreERT/+}$ (B6.129S6(Cg)-*Ptf1a$^{tm2(cre/ESR1)Cvw/J}$, #*019378, Jackson Laboratory, Bar Harbor, USA) and LSL-tdTomato$^{flox/flox}$ mice (B6.Cg *Gt(ROSA) 26Sor$^{tm14(CAG-tdTomato)Hze/}$*J, #007914, Jackson Laboratory, Bar Harbor, USA).	p48$^{CreERT/+}$ (Kopinke et al. 2012) LSL-td Tomato$^{flox/flox}$ (Madisen et al. 2010)

p48^{ERT};R1b$^{fl/+}$ (p48$^{CreERT/+}$; Ring1b$^{flox/+}$; LSL-tdTomato$^{flox/flox}$) **p48^{ERT};R1b$^{fl/fl}$** (p48$^{CreERT/+}$; Ring1b$^{flox/flox}$; LSL-tdTomato$^{flox/flox}$)	C57Bl6/J / FVB/NJ In particular, black mice were used for experiments. Overtime, mice were backcrossed to C57-Bl6/J.	The p48$^{CreERT/+}$;LSL-tdTomato$^{flox/flox}$ mouse model was intercrossed with the Ring1b$^{flox/flox}$ mouse strain. Ring1b$^{flox/flox}$ mice were kindly provided by Miguel Vidal (Centro de Investigaciones Biológicas, Madrid, Spain) and Prof. Dr. Magdalena Götz (Helmholtz Zentrum München, Neuherberg).	Ring1b$^{flox/flox}$ (Cales et al. 2008)
p48^{ERT};K (p48$^{CreERT/+}$; LSL-Kras$^{G12D/+}$; LSL-tdTomato$^{flox/flox}$)	C57Bl6/J	p48$^{CreERT/+}$;LSL-tdTomato$^{flox/flox}$ mice were intercrossed with LSL-Kras$^{G12D/+}$ mice (B6.129S4*Kras^{tm4Tyj}*/J #008179, Jackson Laboratory, Bar Harbor, USA).	LSL-Kras$^{G12D/+}$ (Jackson et al. 2001)
p48^{ERT};K;R1b$^{fl/+}$ (p48$^{CreERT/+}$; LSL-Kras$^{G12D/+}$; Ring1b$^{flox/+}$; LSL-tdTomato$^{flox/flox}$) **p48^{ERT};K;R1b$^{fl/fl}$** (p48$^{CreERT/+}$; LSL-Kras$^{G12D/+}$; Ring1b$^{flox/flox}$; LSL-tdTomato$^{flox/flox}$)	C57Bl6/J / FVB/NJ In particular, black mice were used for experiments. Overtime, mice were backcrossed to C57-Bl6/J.	p48$^{CreERT/+}$;LSL-Kras$^{G12D/+}$; LSL-tdTomato$^{flox/flox}$ were bred with Ring1b$^{flox/flox}$ mice.	-
KC (p48$^{Cre/+}$; LSL-Kras$^{G12D/+}$)	C57Bl6/J	p48$^{Cre/+}$ mice (C57BL/6J;StockPtf1a tm1.1(Cre)Cvw) were kindly provided by Prof. Dr. Roland M. Schmid (Klinikum rechts der Isar, TU München). Mice were crossed with LSL-Kras$^{G12D/+}$ mice.	p48$^{Cre/+}$ (Kawaguchi et al. 2002)
KPC (p48$^{Cre/+}$; LSL-Kras$^{G12D/+}$; LSL-Trp53$^{lox/+}$)	C57Bl6/J	p48$^{Cre/+}$;LSL-Kras$^{G12D/+}$ mice were bred with LSL-Trp53$^{R172H/+}$ animals (B6.129P2-Trp53tm1Brn/J, #008462, Jackson Laboratory, Bar Harbor, USA).	LSL-Trp53$^{R172H/+}$ (Marino et al. 2000)

3.1.9 Cell lines

Table 3.13: Cell lines

Cell line	Characteristics
KC-428	Tumor cell line, isolated from a KC mouse *
KC-921	Tumor cell line, isolated from a KC mouse *
KPC-1050	Tumor cell line, isolated from a KPC mouse *

* The cell lines were already established in the lab.

3.1.10 Consumption materials

Table 3.14: Consumption materials

Consumption materials	Manufacturer
96-well plate (qRT-PCR), white	STARLAB, Hamburg
Cell culture flasks (75 cm^2, 175 cm^2)	Greiner Bio-One, Kremsmünster, Austria
Cell culture plates (6-well, 12-well, 96-well)	Greiner Bio-One, Kremsmünster, Austria
Cell culture plates, TC dish (60 mm, 100 mm)	Sarstedt, Nürnbrecht
Cell scraper (25 cm)	Sarstedt, Nürnbrecht
Cell strainer (100 μm nylon)	BD Biosciences, Franklin Lakes, USA
Chamber slide (8-well)	Thermo Fisher Scientific, Waltham, USA
Chromatography paper	GE Healthcare, Little Chalfont, UK
Cover slip (24 x 50 mm)	Thermo Fisher Scientific, Waltham, USA
Cryo Tube®	Thermo Fisher Scientific, Waltham, USA
Embedding cassette, Rotilabo®	Carl Roth GmbH, Karlsruhe
Insulin syringe (1 ml)	BD Biosciences, Franklin Lakes, USA
Microscope slide, Superfrost® Plus	Thermo Fisher Scientific, Waltham, USA
Microtome blade, R35	Feather, Osaka, Japan
Neubauer chamber	Paul Marienfeld GmbH & Co. KG, Lauda-Königshofen
Nitrocellulose blotting membrane	GE Healthcare, Little Chalfont, UK
Parafilm 'M'	Bemis, Neenah, USA
PCR reaction tube	Sarstedt, Nürnbrecht
Pipette tips (10 μl, 100 μl, 1000 μl)	STARLAB, Hamburg
Pipette filter tips (10 μl, 100 μl, 1000 μl)	STARLAB, Hamburg
Reaction tubes (1,5 ml, 2 ml)	Sarstedt, Nürnbrecht
Reaction tubes, CELLSTAR® TUBES (15 ml, 50 ml)	Greiner Bio-One, Kremsmünster, Austria
Safety IV catheter with injection port, Vasofix®	B. Braun, Melsungen
Scalpel, Feather disposable scalpel	Feather, Osaka, Japan
Serological pipettes, sterile (5 ml, 10 ml, 25 ml, 50 ml)	Greiner Bio-One, Kremsmünster, Austria
Stericup filter unit (250 ml)	Sarstedt, Nürnbrecht
Syringe, Omnifix®-F (1 ml)	B. Braun, Melsungen
Syringe filcon (30 μm) for FACS analysis	BD Bioscience, Franklin Lakes, USA
Syringe filter, Nalgene 0.2 μm	Thermo Fisher Scientific, Waltham, USA
X-ray film, Amersham Hyperfilm™ ECL	GE Healthcare, Little Chalfont, UK

3.1.11 Equipment

Table 3.15: Equipment

Equipment	Manufacturer
Biological safety cabinet, HeraSafe™	Thermo Fisher Scientific, Waltham, USA
Centrifuge, 5415R	Eppendorf, Hamburg
Centrifuge, 5424	Eppendorf, Hamburg
Centrifuge, Heraeus Multifuge 3SR+	Thermo Fisher Scientific, Waltham, USA
Dehydration machine, LEICA ASP 2005	Leica, Wetzlar
Gel documentation system, GenoSmart	VWR International GmbH, Darmstadt
Heating block, TS1 ThermoShaker	Biometra GmbH, Göttingen
Incubator, Hera Cell 150	Thermo Fisher Scientific, Waltham, USA
Micro scale	Sartorius AG, Göttingen
Microscope, Axiovert 40 CFL	Carl Zeiss AG, Oberkochen
Microscope, Imager.M2	Carl Zeiss AG, Oberkochen
Microtome, LEICA-RM2255	Leica, Wetzlar
Paraffin embedding machine, LEICA EG 1160	Leica, Wetzlar
PCR cycler, Doppio VWRI732-1210	VWR International GmbH, Darmstadt
pH meter, peqMETER 1.14	Peqlab Biotechnologie GmbH, Erlangen
Pipetboy acu	Integra Biosciences, Erembodegem, Belgium
Pipettes (0,5 µl - 10 µl, 10 µl - 100 µl, 100 µl - 1000 µl)	Eppendorf, Hamburg
Platform shaker, SHAKER DRS-12	neoLab Migge GmbH, Heidelberg
Real-Time PCR cycler, LightCycler®480	Roche, Basel, Switzerland
Scale, HT-500	A&D Company, Tokyo, Japan
Slide scanner, Aperio ScanScope®	Leica, Wetzlar
Spectrophotometer, Glomax Multi+ Detection System	Promega, Madison, USA
Spectrophotometer, MULTISKAN EX	Thermo Fisher Scientific, Waltham, USA
Spectrophotometer, NanoDrop 2000	Thermo Fisher Scientific, Waltham, USA
Tissue lyser	Qiagen, Hilden
Ultrasonic processor, UP 100H	Hielscher Ultrasonics GmbH, Teltow
Vortex mixer	neoLab Migge GmbH, Heidelberg
Water bath, AQUALINE AL18	Lauda, Lauda-Königshofen
Western blot chamber, Mini-Protean Tetra Cell	Bio-Rad, Hercules, USA
X-ray film processor, OPTIMAX	PROTEC GmbH & Co. KG, Oberstenfeld

3.1.12 Computer applications

Table 3.16: Computer applications

Program	Producer
Affymetrix® Expression Console™ Software	Affymetrix, Santa Clara, USA
Axiovision SE64 Rel.4.9	Carl Zeiss AG, Oberkochen
EndNote X7	Thomson Reuters, New York City, USA
FlowingSoftware_2	By Perttu Terho, Turku Centre for Biotechnology, Finland
GNU image manipulation program 2 (GIMP2)	Open-source
GraphPad Prism 5	GraphPad Software, Inc., La Jolla, USA
ImageJ	By Wayne Rasband, NIH, Bethseda, USA
ImageScope Software	Leica, Wetzlar
Microsoft Office	Microsoft, Redmond, USA
Short time-series expression miner (STEM)	(Ernst and Bar-Joseph 2006)

3.2 Methods

3.2.1 Cell-biological methods

3.2.1.1 Cell culture conditions

Cell culture medium DMEM high glucose,
1 % Penicillin/Streptomycin (Pen/Strep) (v/v), 10 % FBS (v/v)

All cell culture experiments were performed under sterile conditions in a biological safety cabinet. Cell lines were cultivated within cell culture medium in a 37 °C incubator, which maintained a saturated atmosphere with 5 % CO_2.

3.2.1.2 Passaging of cells

When cells reached a confluence of 70 %, they were passaged. Herein, medium was aspirated, cells were washed with PBS (1X) and incubated within Trypsin (1X) / PBS (1X) solution for 15 minutes at 37 °C. Trypsin activity was stopped through the addition of cell culture medium. The cell suspension was centrifuged (5 min, 215 g, RT) and the cell pellet was resuspended in fresh culture medium. Cells were splitted in a ratio of 1:20 to 1:100.

3.2.1.3 Cryopreservation of cells

Freezing medium 80 % FBS (v/v), 20 % DMSO (v/v)

To cryopreserve cells, they were trypsinized, centrifuged (5 min, 215 g, RT) and the pellet was resuspended in 1 ml cell culture medium and transferred to a cryo tube. Additionally, the same volume of freezing medium was added dropwise. Cells were stored at -80 °C and for long-time storage subjected to liquid nitrogen.

3.2.1.4 Revitalization of cells

Cryo tubes with frozen cells were transferred to the 37°C water bath until the freezing medium was nearly thawed. Then, cell suspension was poured to a new falcon tube and 6 ml cell culture medium was added dropwise. To get rid of freezing medium ingredients, cells were pelletized (5 min, 215 g, RT), washed once in PBS (1X) and resuspended in fresh cell culture medium.

3.2.1.5 MTT cell proliferation assay

MTT cell lysis buffer 10 % SDS (w/v), 0.01 N HCl

The MTT assay is based on the reduction of the yellow 3-(4,5-Dimethylthiazol-2-yl)-2,5-diphenyltetrazolium bromide (MTT) reagent to purple formazan by cellular oxidoreductases. Conversion rate is dependent on the number of viable cells and absorbance can be determined with a spectrophotometer.
To analyze cell proliferation, 1 000 - 5 000 cells (KC-428, KC-921, KPC-1050) were seeded in a well of a 96-well plate. Proliferation rates were assessed after 0, 24, 48, 72 and 96 hours. At every time point, MTT reagent (0.5 μg/μl) was added to each single well and incubated for three hours. Then, cells were lysed through the addition of 100 μl MTT cell lysis buffer and MTT reduction was measured with a spectrophotometer (560 nm) after 24 hours. Moreover, MTT assay was used to establish IC_{50} values for the inhibitors LY 294002, PD 98059 and PRT4165.

3.2.1.6 Treatment of cells with inhibitors

Acinar suspension cells were treated with 50 μM of PD 98059 and 30 μM of LY 294002. Inhibitor concentrations used were equal to the IC_{50} (half of the maximal inhibitory concentration), established for the cancer cell line KC-921. During treatment cells were cultured in 2D medium (Table 3.18). After 120 hours, cells were harvested for protein isolation. Since PD 98059 and LY 294002 are soluble in DMSO, equal amounts of the solvent were applied to control cells.

Tumor cell lines KC-921 and KPC-1050 were treated with 70 μM/100 μM of the PRC1 inhibitor PRT4165. Concentrations were established as IC_{50} values. Here, 200 000 cells were seeded into the wells of a 6-well plate, cultured in normal cell culture medium and harvested after 0, 2, 4, 6, 12 and 24 hours of treatment for RNA and protein isolation. Since PRT4165 is soluble in DMSO, control cells were treated with the equal volume of the solvent.

3.2.1.7 Gene editing in tumor cells by using the CRISPR/Cas9 system

By applying the CRISPR/Cas9 (Clustered Regularly Interspaced Short Palindromic Repeats/CRISPR-associated protein 9) system, the target gene *Ring1b* was specifically knocked out in the cancer cell line KPC-1050.

In general, the system involves the prokaryotic nuclease Cas9, which recognizes so-called crRNAs, short noncoding CRISPR RNAs, and their complementary regions on the DNA. Here, the enzyme introduces DNA double strand breaks and DNA is consequently repaired either through non-homologous end joining (NHEJ) or homology directed repair (HDR) (Ma, Zhang, and Huang 2014). Naturally occurring NHEJ can cause reading frame mutations at the target gene loci, but does not offer great efficiency for artificial genome editing. With the aid of a cleavage site-specific template, repair is mainly committed through the HDR mechanism and precise mutations can be introduced at the cleaved target side (Ma, Zhang, and Huang 2014). Additionally, incorporation of selection markers, such as the puromycin resistance gene, allows a stable selection of positively manipulated cells.

For the transfection of the cancer cell line 1050, 200 000 cells were seeded into wells of a 6-well plate and cells were kept within antibiotic-free cell culture medium for 24 hours. Next, 2 μg of plasmid DNA were diluted into plasmid transfection medium. For the generation of Ring1b KO clones, the Ring1b CRISPR/Cas9 KO plasmid was used together with the Ring1b HDR plasmid. However, for the propagation of control clones, the control CRISPR/Cas9 plasmid in combination with the Ring1b HDR plasmid was applied. In parallel, UltraCruz® transfection reagent (10 μl per 2 μg of plasmid DNA) was mixed with plasmid transfection medium. Transfection was performed according to the manufacturer's protocol.

When the cells reached a confluence of 80 %, they were passaged and 5 000 - 10 000 cells were seeded onto new 10 cm dishes. For selection of positively transfected clones, puromycin (4 μg/ml) was added to the cell culture medium on the next day. Single Ring1b KO cell clones were picked after one week of selection, whereas control clones were isolated after 48 hours, because here the puromycin resistance gene was not incorporated into the host DNA. To confirm biallelic *Ring1b* knockout, exon sequencing, Western Blot and qRT-PCR analysis were performed. Possible off-target sites were found using the following website *http://www.sanger.ac.uk/htgt/wge/find_off_targets_by_seq*. Expression of off-targets was verified via qRT-PCR.

3.2.1.8 Isolation of primary acinar cells for RNA/protein, ChIP and FACS analysis

Pancreatic acinar cells can be dissociated from the pancreatic extracellular matrix through collagenase digestion. Moreover, based on their size, acinar cells can be selectively purified from other cell types, such as fibroblasts or ductal cells, through several centrifugation steps.
Murine pancreata were either eviscerated from mouse embryos at E18.5 or from adult eight-week-old mice. After removal, pancreatic tissue was immediately placed in 10 ml of ice-cold PBS (1X).
Pancreatic tissue provided for ChIP analysis was subsequently fixed with paraformaldehyde (PFA) to avoid isolation-caused changes in the cellular histone profile. For this, pancreatic tissue was minced into small pieces and incubated in 1 % PFA (v/v) in PBS (1X) for 10 min on a shaking platform. Then, 125 mM glycine was added for 5 min to quench remaining PFA and small tissue pieces were washed twice in PBS (1X).
Native or fixed pancreatic tissue pieces were subjected to 5 ml of a collagenase/RPMI solution (1.5 mg/ml **Collagenase VIII**, Sigma-Aldrich, St. Louis, USA). Collagenase solution was injected with an insulin syringe into pancreatic tissue and samples were transferred into the 37°C incubator. Collagenase digestion times were adapted to the tissue character (see table 3.17).

Table 3.17: Collagenase VIII incubation times

Tissue	Incubation time at 37 °C
Adult native pancreatic tissue	10 min
Embryonic native pancreatic tissue	5 min
Adult fixed pancreatic tissue	20 min
Embryonic fixed pancreatic tissue	10 min

Afterwards, tissue was washed with 10 ml RPMI containing 5 % FBS (v/v) (washing solution), centrifuged (5 min, 19 g, RT) and subjected to a second collagenase digestion step. Again, the enzyme reaction was stopped through the addition of 10 ml washing solution. Then, digested pancreatic tissue was pressed through a cell strainer (100 μm), causing a physical separation of the various cell types and the connective tissue. The filtrate was centrifuged (5 min, 19 g, RT) and due to their big size, acinar cells were pelletized, whereas all other cell types and cellular debris remained in the supernatant, which was carefully aspirated. Acinar cells were washed again with 20 ml washing solution and finally centrifuged (5 min, 19 g, RT). Purity of the isolated cell population was assessed via mRNA expression analysis.

3.2.1.9 Isolation of primary acinar cells for cultivation in suspension and in 3D

For the cultivation of acinar suspension cells and for setting up 3D cultures, primary acinar cells were isolated according to a more gentle protocol. Here, native pancreatic bulk tissue from adult mice was cut into small pieces and digested with **Collagenase P** (0,5 mg/ml) in RPMI medium for 15 min at 37 °C. Then, the tissue was washed with 10 ml of washing solution (section 3.2.1.8), centrifuged (5 min, 19 g, RT), the supernatant was aspirated, pancreatic tissue pieces were resuspended in 10 ml washing solution and pressed through the 100 μm nylon cell strainer. Isolated cells were washed twice with the washing solution and centrifuged (5 min, 19 g, RT). After these purification steps, the obtained acinar cell pellet was washed with Hank's Balanced Salt Solution (HBSS) (centrifugation 5 min, 54 g, RT) for another three times. Finally, the pellet was resuspended in 2D culture medium (Table 3.18) and transferred onto a 10 cm culture dish.

3.2.1.10 Establishment of 3D cell cultures

Table 3.18: Formulation of culture media for the establishment of 3D cell cultures

2D culture medium	3D culture medium
Waymouth's MB 752/1 culture medium	Waymouth's MB 752/1 culture medium
10 % FBS (v/v)	20 % FBS (v/v)
1 % Penicillin / Streptomycin (v/v)	2 % Penicillin / Streptomycin (v/v)
0,1 mg/ml Trypsin inhibitor	0,2 mg/ml Trypsin inhibitor
0,005 mM Dexamethasone	0,01 mM Dexamethasone
5 mM HEPES	10 mM HEPES
0,13 % $NaHCO_3$ (w/v)	0,26 % $NaHCO_3$ (w/v)

Setting up 3D cell cultures is a valuable tool to recapitulate the ADM process *in vitro*. Herein, acinar cells were embedded into the extracellular matrix component collagen (Figure 3.1).

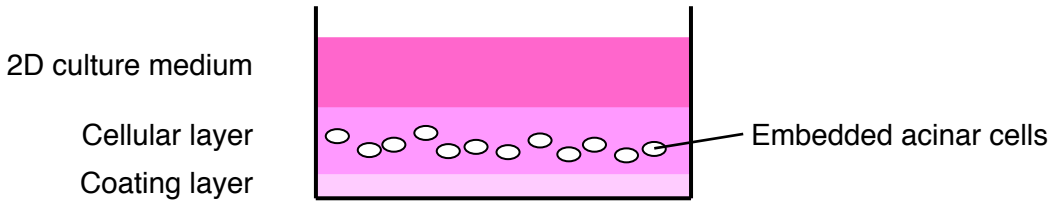

Figure 3.1: Schematic presentation of an *in vitro* 3D cell culture system. First, culture plates were coated with a thin collagen layer. Second, acinar cells were embedded on top of the coating layer (cellular layer). Finally, 2D culture medium was added onto the cellular layer to prevent dehydration of the gel.

For the preparation of 3D cell cultures, purified acinar cells (see chapter 3.2.1.9) were resuspended in 10 ml of 2D culture medium. Caerulein (0.3 pg/ml) was added to stimulate the cells and were kept overnight in the cell incubator. On the next day, the wells of a 12-well plate were coated with 400 µl of the coating (1 mg/ml) layer (Figure 3.1). After incubation for 30 minutes at 37 °C, the first collagen layer was solidified and the cellular collagen layer was prepared (Figure 3.2). For this, purified acinar cells were washed twice with HBSS and centrifuged (54 g, 5 min, RT). Cell pellet was resuspended in 3D medium and carefully added to the already prepared collagen (1.5 mg/ml) - PBS (10X) - NaOH mixture. After the addition of $NaHCO_3$, the composition was carefully stirred and 1.5 ml were placed on top of the first collagen layer (Figure 3.1). After solidification at 37 °C for one hour, 1 ml of 2D culture medium as well as 50 ng/ml TGF-α was added onto the cellular layer.

Preparation of collagen layers

1) *Collagen I rat tail*
Volume of collagen = (Final volume * final collagen conc.) / initial collagen conc.
2) *PBS (10X)*
Volume of PBS (10X) = Final volume / 10
3) *1 M NaOH*
Volume of NaOH (1 M) = Volume collagen * 0.023
4) *3D medium*
Volume 3D medium = Final volume - (volume (collagen + PBS (10X) + NaOH))
5) *$NaHCO_3$*
Volume $NaHCO_3$ = Final volume 1 / 60

Figure 3.2: Scheme for the preparation of 3D culture collagen layers.

Explants were cultured for six days at 37 °C. To assess the proliferation rate of the cultured cells, 10 µM BrdU was added on the fifth day. If it was intended to perform immunofluorescence stainings, collagen gels were harvested and incubated in 4 % PFA (v/v) in PBS (1X) overnight at 4 °C, washed three times in PBS (1X), afterwards stored in 70% ethanol (v/v), dehydrated and embedded into paraffin.

3.2.1.11 Purification of 3D *in vitro* cultured cells

For extracting RNA/proteins or performing ChIP analysis from 3D *in vitro* cultured cells, these had to be purified from the collagen layer. Therefore, the cellular collagen layers were subjected to the same volume of collagenase/RPMI (1 mg/ml, **Collagenase VIII**, Sigma Aldrich) solution and incubated for 20 min on a shaker at 37 °C until the extracellular matrix

was degraded. Then, the double volume of RPMI containing 5 % FBS (v/v) was added to stop the digestion. Cells were centrifuged (215 g, 5 min, 4 °C) and washed again. Finally, cells were washed once with PBS (1X) and pelletized.

3.2.1.12 Isolation of circulating epithelial cells from blood

To determine the number of epithelial tumor cells, which detach from solid tumors and intravasate into the peripheral blood circulation, they have to be recovered from blood. A mouse blood sample was taken from the vena cava and immediately transferred to 100 µl heparin to inhibit blood coagulation. Afterwards, 8 ml of red blood cell lysis buffer (Sigma-Aldrich, St. Louis, USA) was added, the tube was inverted several times and incubated at RT for 10 min. Then, the suspension was mixed with 20 ml PBS (1X) containing 3 % FBS (v/v) and 3 % Pen/Strep (v/v), centrifuged (5 min, 309 g, RT) and the resulting cell pellet was further washed twice. Finally, the pellet was resuspended in cell culture medium and transferred onto wells of a 24-well plate. Medium was changed after three days and cells were cultivated for six days. To quantify the attached cells, they were fixed in ice-cold methanol for five minutes, stained with 10 % crystal violet (w/v) in ethanol (absolute) for 20 minutes, washed with ddH_2O and visualized under the microscope. Five pictures (10x magnification) were taken per well.

3.2.2 Molecular-biological methods

3.2.2.1 RNA Isolation

3.2.2.1.1 RNA isolation from cells

RNA from cell lines was isolated with the RNeasy® Plus Mini Kit according to the manufacturer's protocol.

3.2.2.1.2 RNA isolation from tissue

For RNA extraction from mouse pancreatic tissue, 1 ml TRI-reagent, a metal bead and a small piece of fresh or frozen tissue were provided and subjected to the tissue lyser (3 min, 50 oscillations/s). Lysed tissue was incubated for 5 min (RT) and mixed gently with 1-Bromo-3-chloropropane (BCP) for protein/DNA and RNA phase separation. After incubation for 5 min (RT), the sample was centrifuged (12 000 g, 15 min, 4 °C), the upper colorless RNA-containing phase was withdrawn and mixed with an equal volume of 70 % ethanol (v/v). Then, the whole sample was transferred to a RNeasy® Spin Column from the RNeasy® Plus Mini Kit and RNA isolation was carried out according to the manufacturer's protocol. To gain

a pure RNA fraction, the DNA digestion step (application of DNase, 15 min) was included and performed according to the manufacturer's instructions.

3.2.2.1.3 Determination of RNA-concentration and -integrity

RNA concentration was quantified with the spectrophotometer NanoDrop 2000. For the measurement, 1 µl of RNA was applied and absorption at 260 nm was determined. Samples, characterized by an absorption ratio A_{260}/A_{280} of 2.1 - 2.0, were regarded as free of solvent residues, DNA and protein contaminations. To further assess RNA integrity, 1 µg of RNA was mixed with 4 µl formamide and loading dye (5X). The sample was incubated at 60 °C for 10 min and then loaded onto a denaturing agarose gel (0.8 %, (w/v)) containing 0.37 % formaldehyde and 0.005 % ethidium bromide (v/v). Electrophoresis was performed at 150 V for 40 min. RNA was classified as intact by the presence of the 28S and the 18S rRNA band, whereas degraded RNA had a smeared appearance.

3.2.2.2 cDNA synthesis

To transcribe RNA into cDNA, the Verso cDNA synthesis Kit was utilized according to the manufacturer's protocol. For reverse transcription 1 µg of RNA and random hexamer oligos were used.

3.2.2.3 DNA isolation from mouse biopsies

STE buffer	50 mM Tris-HCl pH 8, 100 mM NaCl, 1 % SDS (w/v), 1 mM EDTA

To extract DNA from mouse biopsies, samples were subjected to 500 µl of STE (Sodium chloride - Tris - EDTA) buffer containing 0.5 mg/ml proteinase K. Samples were incubated overnight at 55 °C for degradation of the extracellular matrix and for cell lysis. Then, DNA was precipitated through the addition of 400 µl isopropanol (incubation 10 min, RT). DNA was pelletized (centrifugation 10 min, 13 400 g, RT) and washed twice with 70 % ethanol (v/v). Finally, DNA was desiccated at 37 °C for 15 min and resuspended in 100 µl ddH_2O.

3.2.2.4 Polymerase chain reaction (PCR)

The polymerase chain reaction (PCR) allows the *in vitro* amplification of specific DNA regions and therefore, genotyping of transgenic mice was performed with the help of this method. Herein, primers for initiation of DNA elongation at selected DNA/gene sites, deoxynucleotide triphosphates (dNTPs) and DNA polymerase were added to the DNA sample.

Pipetting scheme per 25 µl reaction:

Jumpstart™ REDTaq Ready PCR Reaction Mix (2X)	12.5 µl
ddH_2O	10.5 µl
Forward and reverse primer (10 µM)	1 µl
DNA from mouse biopsies	1 µl
	25 µl

The PCR reaction was performed in a PCR cycler. Depending on the annealing temperature of specific primer sets, various PCR programs were set up.

Table 3.19: Genotyping PCR programs

	Step		Number of cycles	Temperature [°C]	Time [sec]
PCR conditions for *Kras^{G12D}*, *p48^{Cre}*, Trp53^{R172H} genotyping	Initial denaturation		1	94	120
	Amplification cycles	Denaturation	40	94	30
		Annealing		58	30
		Elongation		72	60
	Final elongation		1	72	600
	Storage		1	4	∞
PCR conditions for *Ring1b^{fl}* genotyping	Initial denaturation		1	94	120
	Amplification cycles	Denaturation	36	94	20
		Annealing		60	20
		Elongation		72	60
	Final elongation		1	72	30
	Storage		1	4	∞
PCR conditions for *p48^{ERT} and tdTomato* genotyping	Initial denaturation		1	94	120
	Amplification cycles	Denaturation	40	94	30
		Annealing		61	30
		Elongation		72	60
	Final elongation		1	72	600
	Storage		1	4	∞

3.2.2.4.1 Verification of mycoplasma contamination via PCR

After two passaging rounds, all cell lines were analyzed for contamination with mycoplasma. For this, cell culture medium was aspirated and subjected to PCR. Use of specific primers allowed amplification of mycoplasma DNA.

Pipetting scheme per 25 µl reaction:

KAPA2G PCR ReadyMix with dye (2X)	12.5 µl
ddH_2O	8.5 µl
Forward and reverse primer 500 (10 µM)	1 µl
Forward and reverse primer 280 (10 µM)	1 µl
Cell culture medium	2 µl
	25 µl

Table 3.20: Mycoplasma PCR program

Step		Number of cycles	Temperature [°C]	Time [sec]
Initial denaturation		1	94	120
Amplification cycles	Denaturation	35	94	30
	Annealing		55	30
	Elongation		72	120
Final elongation		1	72	120
Storage		1	4	∞

3.2.2.5 Quantitative real-time RT-PCR (qRT-PCR)

3.2.2.5.1 Gene expression analysis

To quantitatively determine gene transcript levels, qRT-PCR (quantitative real-time reverse transcription PCR) was performed. In principle, target gene cDNA is amplified via conventional PCR, but through specific binding of the fluorescent dye SYBR Green to double stranded DNA, the amount of amplified PCR products can be monitored in real-time. Quantification is output as the so-called cycle threshold value (C_T), which is characterized as the point in which the fluorescent intensity of the sample outnumbers those of the background. As an endogenous control, amplification of the housekeeper transcript *Ppib* (*Peptidyl-prolyl cis-trans isomerase*) was included.

Pipetting scheme per 20 µl reaction:

SYBR Green Mastermix (2X)	10 µl
Primer forward (10 µM)	1 µl
Primer reverse (10 µM)	1 µl
cDNA (20 ng/µl)	2 µl
ddH_2O	6 µl
	20 µl

Each sample was transferred into a well of a 96-well plate and applied as duplicate. The PCR reaction was performed in the LightCycler480. Program conditions were chosen as described in Table 3.21.

Table 3.21: qRT-PCR program

Step		Number of cycles	Temperature [°C]	Time [sec]
Initial denaturation		1	95	300
Amplification Cycles	Denaturation	45	95	15
	Annealing		55	15
	Elongation		72	15
Melting Curve	Denaturation	1	95	1
	Hybridization		65	20
	Melting	5 Acquisitions/sec	98	continuous 0.11 °C/sec
Cooling		1	37	∞

For calculating relative expression levels, the 2(-Delta Delta C(T)) method was applied (Livak and Schmittgen 2001). First, the difference between the C_T value of the sample and the housekeeper was calculated (see formula 3.1 (1)). Then, C_T values of distinct experimental groups (e.g. control group versus knockout group) were normalized (see formula 3.1 (2)).

Formula 3.1: Calculation of relative expression levels

$$\Delta C_T = C_T^{\text{Sample}} - C_T^{\text{Housekeeper (Ppib)}} \quad (1)$$

$$2^{(-\Delta\Delta C_T)} = 2^{\,(-\Delta C_T^{\text{Knockout group}} - \Delta C_T^{\text{Control group}})} \quad (2)$$

3.2.2.5.2 Quantification of immunoprecipitated DNA by qRT-PCR

To quantify immunoprecipitated DNA, originating from ChIP experiments (chapter 3.2.3.1), 2 μl of DNA, were subjected to qRT-PCR analysis (similar pipetting scheme as described in section 3.2.5.1). Samples were applied as duplicates. The PCR program involved 50 amplifications cycles, whereas the other program settings remained unchanged (program conditions see paragraph 3.2.5.1).

Here, C_T values were normalized according to the fold enrichment method (Haring et al. 2007). First, the difference between the C_T value of the sample and the background (IgG control sample, see section 4.3.1) was assessed (Formula 3.2 (1)). Then fold enrichment was calculated ((Formula 3.2 (2)).

Formula 3.2: Calculation of fold enrichment, ChIP analysis

$$\Delta C_T = C_T^{\text{Sample}} - C_T^{\text{Background (IgG)}} \quad (1)$$

$$\text{Fold enrichment} = 2^{(-\Delta C_T)} \quad (2)$$

3.2.2.6 Agarose gel electrophoresis

TBE buffer (1X)	99 mM Tris-HCl, 89 mM boric acid, 0.03 mM EDTA

PCR products were analyzed by agarose gel electrophoresis. With this method, DNA fragments can be separated by their length. For this, samples were subjected to an agarose gel (1 % (w/v) in TBE (Tris - Borate - EDTA) (1X)) containing 0.005% (v/v) of the DNA-intercalator ethidiumbromide. In addition, a DNA standard (100 bp DNA ladder) was administered to compare the lengths of the separated DNA fragments. For separation, 150 V was applied for 20 minutes and the separated DNA was visualized under UV light exposure in a gel documentation station.

3.2.3 Epigenetic methods

3.2.3.1 Chromatin immunoprecipitation (ChIP)

Cell lysis buffer	5 mM PIPES, 85 mM KCl, 0.5 % NP-40 (v/v)
MNase digestion buffer	50 mM Tris-HCl (pH 8.1), 5 mM $CaCl_2$
Nuclei lysis buffer	50 mM Tris-HCl (pH 8.1), 10 mM EDTA, 1 % SDS (w/v)
ChIP dilution buffer	0.01 % SDS (w/v), 1.1 % Triton X-100 (v/v), 1.2 mM EDTA, 16.7 mM Tris-HCl pH 8.1, 167 mM NaCl

Low salt wash buffer	0.1 % SDS (w/v), 1 % Triton X-100 (v/v), 2 mM EDTA, 20 mM Tris-HCl (pH 8.1), 150 mM NaCl
High salt wash buffer	0.1 % SDS (w/v), 1 % Triton X-100 (v/v), 2 mM EDTA, 20 mM Tris-HCl (pH 8.1), 500 mM NaCl
Lithiumchloride wash buffer	250 mM LiCl, 1 % NP-40 (v/v), 1 % Na-deoxycholate (w/v), 1 mM EDTA, 10 mM Tris-HCl (pH 8.1)
TE wash buffer	10 mM Tris-HCl (pH 8.1), 1 mM EDTA
Elution buffer	1 % SDS (w/v), 0.1 M $NaHCO_3$

With the aid of ChIP, interactions of transcription factors with distinct DNA regions or the occurrence of histone modifications at specific gene loci can be analyzed. First, DNA associated proteins are crosslinked to DNA. Then, DNA is fragmented and protein-DNA complexes are immunoprecipitated through the addition of specific antibodies. After reverse crosslinking and protein degradation, the DNA is purified and subjected to qRT-PCR analysis or sequencing (Figure 3.3). To perform ChIP, pancreatic bulk tissue, isolated 3D-cultured cells or adherent tumor cells were fixed with 1 % PFA (v/v) in PBS (1X) for 10 min (RT) on a shaker. Through the addition of glycine (125 mM) for 5 minutes, excessive PFA was quenched. Then, the cells were placed on ice and washed twice with PBS (1X). Pancreatic bulk tissue pieces (embryonic and adult stage) were subjected to collagenase/RPMI solution and acinar cells were isolated as described in section 3.2.1.8.

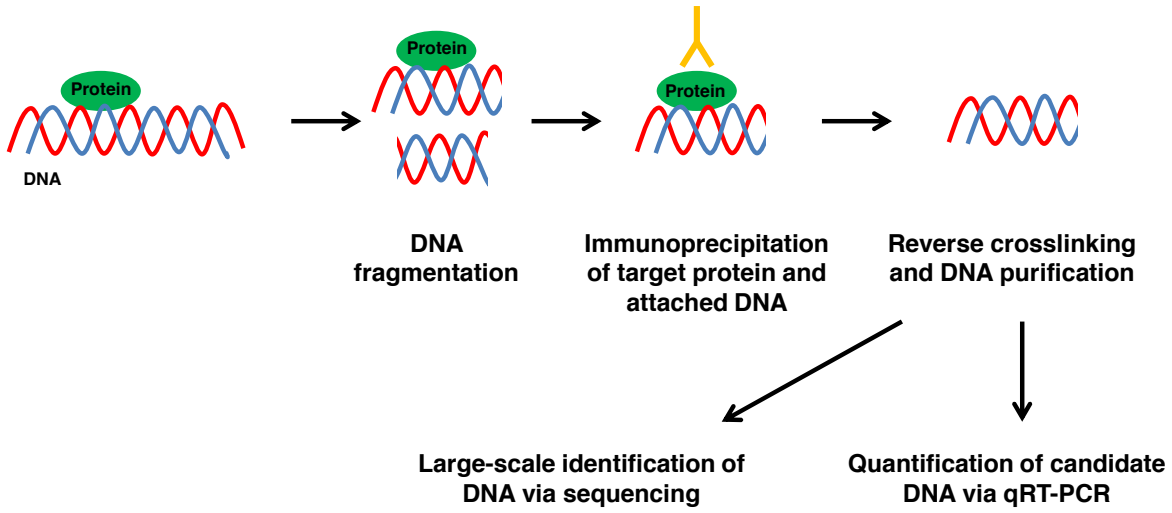

Figure 3.3: Schematic presentation of the ChIP procedure. Experimental setup involves crosslinking of protein-DNA complexes, shearing of DNA into smaller fragments, immunoprecipitation and finally purification, as well as identification and quantification, of isolated DNA.

Isolated acinar and 3D-cultured cells were directly resuspended in 1 ml cell lysis buffer (supplemented with protease and phosphatase inhibitor (1X)) and incubated for 10 minutes on ice. In contrast, adherent tumor cells were directly scraped from cell culture dishes within the cell lysis buffer (per analysis 10 cm culture dishes (3x) were used). The hypotonic cell lysis buffer destroys cell membranes, but leaves cell nuclei intact. Cell nuclei were obtained through centrifugation (10 min, 200 g, 4 °C) and were resuspended in MNase digestion buffer. The addition of the randomly cutting endo-exonuclease MNase caused fragmentation of the DNA to an average fragment size of 200 - 800 bp. The amount of the enzyme and incubation times were validated and adapted to the different cell types. The MNase enzyme reaction was stopped through the addition of 50 mM EDTA. After centrifugation (10 min, 200 g, 4 °C), the collected cell nuclei were lysed in 1 ml nuclei lysis buffer (supplemented with protease inhibitor (1X)) and kept on ice for 10 minutes.

Table 3.22: MNase digestion conditions

Starting material	Amount of enzyme [U]	Incubation time, RT [min]
Adult & embryonic acinar cells, 3D cultured cells	30	5
Cell lines 428, 921, 1050	100	7

To ensure bursting of the nucleic membranes, the solution was sonicated for five cycles for 30 seconds each. Cellular debris was separated from fragmented DNA through centrifugation (10 min, 10 000 g, 4 °C) and the supernatant was transferred to a new tube. Length of the DNA fragments was validated with agarose gel electrophoresis. Depending on the number of antibodies used, the supernatant was divided into several tubes. Here, 1 % of the volume was saved as input control. ChIP dilution buffer (up to the volume of 1 ml) and 50 µl protein A agarose beads were added and the samples were incubated on a rotator for one hour at 4 °C. After this pre-clearing step, the beads were removed through centrifugation (1 min, 4 000 g, 4 °C), immunoprecipitating antibodies were applied (H3K4me3 4 µg, H3K27me3 6 µg/10 µg, H2AK119ub 9 µg, control IgG 4 µg) and the samples were incubated on a rotator overnight at 4 °C. Antibody-protein complexes were isolated through the addition of protein A agarose beads (60 µl). Protein A selectively binds to the F_c fragment of the antibodies, allowing their isolation. To get rid of unspecific binding, antibody - protein - bead complexes were consecutively washed with low salt, high salt, LiCl (lithium chloride) and twice with TE (Tris - EDTA) washing buffers (centrifugation 1 min, 4 000 g, 4 °C). Then, protein - antibody complexes were eluted from the beads through the addition of 200 µl elution buffer. The input sample was also resuspended in 200 µl elution buffer. Reverse crosslinking was performed through the addition of NaCl to a final concentration of

200 mM and incubation at 65 °C overnight. After RNA (addition of RNase A (10 µg), 30 min, 37 °C) and protein degradation (addition of proteinase K (10 µg), EDTA (to a final concentration of 10 mM), Tris-HCl (to a final concentration of 40 mM), 2 h, 45 °C), the DNA was purified with the Qiaquick® PCR Purification Kit according to the manufacturer's protocol. The amount of precipitated and input DNA was quantified via qRT-PCR.

3.2.3.2 DNA methylation analysis

To characterize the DNA methylation status, DNA is treated with sodium bisulfite. This results in the conversion of an unmethylated cytosine to uracil, whereas a methylated cytosine residue remains unaffected. The use of different sets of primer pairs, which are able to distinguish between converted and unconverted cytosines, allows methylation-specific PCR (MSP) amplification. PCR products can be visualized and quantified by agarose gel electrophoresis (Figure 3.4).

DNA was isolated with the QIAamp® DNA Mini Kit according to the manufacturer's protocol. Since cell pellets were used as starting material, proteinase K digestion was performed for one hour. For bisulfite conversion, the EpiTect® Bisulfite Kit was deployed according to the manufacturer's protocol and 2 µg of DNA were utilized per reaction. Converted DNA was amplified in two distinct PCR reactions; using primers against unconverted (methylated (me)) and converted (unmethylated (unme)) DNA (Sharpless et al. 2001). PCR reactions were prepared as described in section 3.2.2.4.

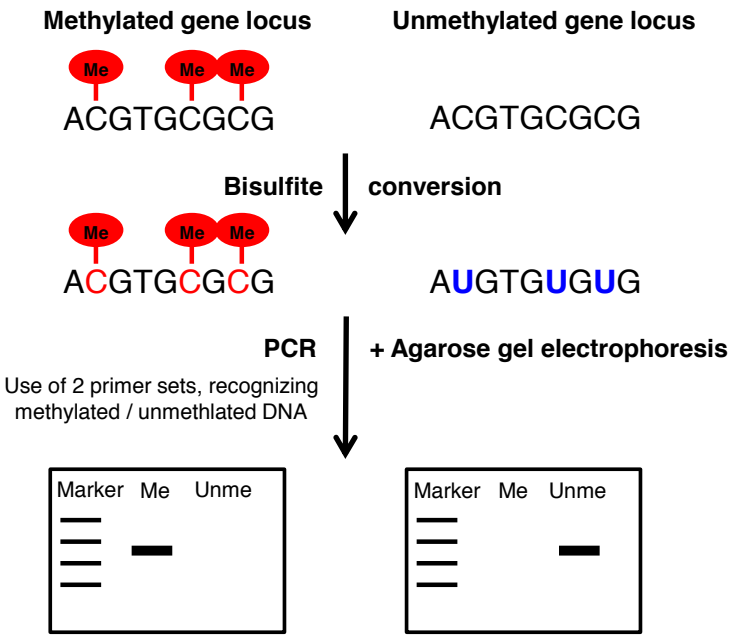

Figure 3.4: Experimental setup of the bisulfite-dependent DNA methylation analysis. Bisulfite treatment leads to conversion of an unmethylated cytosine into uracil. Sequence changes can be analyzed via PCR and agarose gel electrophoresis.

Specific PCR programs were set up for analyzing DNA methylation at the *p16*^{INK4A} promoter. As a positive control, DNA was artificially methylated by the CpG methyltransferase M. SssI according to the manufacturer's instructions. After methylation, DNA was purified with the Qiaquick® PCR Purification Kit and subjected to bisulfite conversion and PCR.

Table 3.23: *p16*^{INK4A} MSP programs

	Step		Number of cycles	Temperature [°C]	Time [sec]
PCR conditions for methylated and unconverted *p16*^{INK4A} *promoter*	Initial denaturation		1	94	60
	Amplification cycles	Denaturation	40	94	30
		Annealing		63	30
		Elongation		72	60
	Final elongation		1	72	600
	Storage		1	4	∞
PCR conditions for unmethylated *p16*^{INK4A} *promoter*	Initial denaturation		1	94	60
	Amplification cycles	Denaturation	40	94	30
		Annealing		61	30
		Elongation		72	60
	Final elongation		1	72	600
	Storage		1	4	∞

3.2.4 Biochemical methods

3.2.4.1 Protein extraction

Cell lysis buffer	50 mM Tris-HCl (pH 8), 2 % SDS (v/v)
Tissue lysis buffer	50 mM Tris-HCl (pH 8), 150 mM NaCl, 2 mM EDTA, 1 % NP-40 (v/v), 0.5 % SDS (v/v), 1 % Na-deoxycholate (w/v), 30 mM NaF, 20 mM $Na_4P_2O_7$, 1 mM $NaVO_3$, 1 mM DTT

Cells from cell lines were resuspended in cell lysis buffer (200 µl) supplemented with protease and phosphatase inhibitors (1X) and incubated on ice for 10 minutes. Through centrifugation (10 min, 16 100 g, 4 °C) proteins (supernatant) were separated from cell debris (pellet).

To harvest proteins from pancreatic bulk tissue, a small piece was added to tissue lysis buffer (300 µl) and a small metal bead. Tissue was homogenized in a tissue lyser (3 min, 50 oscillations/s). Afterwards, samples were centrifuged (20 min, 16 100 g, 4 °C) and the supernatant was transferred into a new tube.

3.2.4.2 Determination of protein concentration

Protein concentrations were determined with the aid of the Pierce BCA (bicinchoninic acid) Protein Assay Kit. Here, 10 µl of a cell lysate was added to the kit reagent A and reagent B (ratio 1/50, 200 µl). The mix was prepared in a well of a 96-well plate and incubated for 30 minutes at 37 °C. In dependence of the protein amount, colour of the solution changes to a purple hue. Absorbance was measured by a spectrophotometer (570 nm). For calculating the protein concentration, a calibrator row of BSA (0.25 µg/µl, 0.5 µg/µl, 1 µg/µl, 2 µg/µl) was included. Thus, protein concentrations were calculated according to Formula 3.3.

Formula 3.3: Calculation of protein concentration

y (protein concentration [µg/µl]) = m (gradient) * x (absorbance [nm]) + b (y axis intercept).

3.2.4.3 SDS polyacrylamide gel electrophoresis (SDS-PAGE)

Running buffer (1X) 192 mM glycine, 25 mM Tris, 0.1 % SDS (w/v)

By means of the SDS polyacrylamide gel electrophoresis, proteins can be separated by their molecular weight.

Table 3.24: SDS-PAGE gel preparation

Reagent	Separating gel*			Stacking gel*
	7.5 %	10 %	12.5 %	4 %
ddH_2O	4.9 ml	4.1 ml	3.2 ml	3 ml
Acrylamide-bisacrylamide solution	2.5 ml	3.3 ml	4.2 ml	750 µl
1.5 M Tris-HCl pH 8.8	2.6 ml	2.6 ml	2.6 ml	-
1 M Tris-HCl pH 6.8	-	-	-	1.3 ml
SDS, 10 % (w/v)	100 µl	100 µl	100 µl	50 µl
APS, 10 % (w/v)	50 µl	50 µl	50 µl	25 µl
TEMED	15 µl	15 µl	15 µl	10 µl

*The stated amounts were sufficient for the preparation of 2 gels.

For this, 15 to 20 μg of protein lysates were mixed with protein loading dye (4X) and denatured at 70 °C (10 min). Then, the protein samples and a standard protein marker were loaded onto the stacking gel. Depending on the size of the protein to be detected, 12.5 % separating gels were prepared for proteins < 40 kDa, 10 % for proteins < 70 kDa and 7.5 % for proteins > 70 kDa. Gel chambers were filled with running buffer (1X) and protein separation was carried out through the application of an electric field (30 mA).

3.2.4.4 Western blot

Blotting buffer (1X)	192 mM glycine, 25 mM Tris, 10 % methanol (v/v)
PBS-T (1X)	PBS (1X), 1 % Tween (v/v)

After separation of the proteins with SDS-PAGE, they were blotted onto a nitrocellulose membrane. Located on such a membrane, target proteins are fixed and easily detected through specific antibodies. For blotting, the nitrocellulose membrane was placed on top of the separation gel. Both sides were embedded with chromatography papers and sponges. This arrangement was placed into the blotting chamber, containing blotting buffer (1X). The transfer of proteins was carried out electrophoretically by applying 100 V for 1 hour.
To avoid unspecific antibody binding, the membrane was first blocked within 5 % milk powder (w/v) or 5 % BSA (w/v) in PBS-T (1X) and incubated on a roller (2 h, RT). Then, the primary antibody was added to the blocking solution (incubation on a roller, overnight, 4 °C). Unspecifically bound antibody was removed through washing with PBS-T (1X) (3x, 10 min). Next, the membrane was incubated in presence of a suitable horseradish peroxidase (HRP)-linked secondary antibody in 1 % milk powder / BSA (w/v) in PBS-T (1X) (1 h, RT). After three washing steps with PBS-T (10 min, each), immunodetection with the Amersham™ ECL™ Western Blot Detection Kit was carried out. For this, the membrane was incubated in 1 ml of ECL (enhanced chemiluminescence) reagent (reagent A/reagent B in the ratio 1/1) and chemiluminescence was detected through the application and development of an X-ray film.

3.2.5 Biophysical methods

3.2.5.1 Fluorescence-activated cell sorting (FACS)

FACS buffer	PBS (1X), 1 % FBS (v/v), 2 mM EDTA

FACS analysis is used to divide a heterogeneous cell sample into distinct cell populations. Separation is based on the cell volume (forward scatter), cell granularity (side scatter) and

cell fluorescence. Distinct cell populations can be labelled with fluorescent antibodies, recognizing specific cell surface markers. In principle, cells are exposed to a laser, the emitted cellular fluorescence is detected and based on different emission spectra the cells are separated.

To estimate the recombination efficiency of $p48^{ERT}$ mice, the number of tdTomato positive acinar cells was assessed. Hereby, acinar cells were isolated according to section 3.2.1.8 and stained with 1 % DAPI (v/v). After washing the cells for three times with FACS buffer, cells were fixed within 1 % PFA (v/v) in PBS (1X) for 10 minutes (on a shaker, RT). Cells were washed again and subjected to the FACS analysis.

For collecting tdTomato positive cells, designated for ChIP analysis, whole cell populations were isolated. Here, cell isolation was performed as described in section 3.2.1.7, but centrifugation steps were performed at 309 g to maintain all cell populations.

FACS analysis as well as cell sorting was performed with the BD FACSAria™ III cell sorter. Adjustment and analysis was performed by Markus Utzt from the deutsche Konsortium für translationale Krebsforschung (DKTK) core facility.

3.2.6 Treatment of mice

All mouse experiments were conducted according to standard protocols and authorized by the government of Bavaria (TVA 55.2-1-54-2532-119-2015).

3.2.6.1 Removal of organs and blood

For organ resection, mice were anesthetized with isoflurane and killed through cervical dislocation. The pancreas and spleen were eviscerated from all mice. Blood was taken with a 30-gauge needle from the vena cava and plasma was subsequently isolated. For this, blood was immediately transferred into EDTA-coated tubes, samples were centrifuged (10 min, 3 000 g, 4 °C), supernatant was aspirated and centrifuged for a second time (10 min, 16 000 g, 4 °C). The supernatant (blood plasma) was isolated and stored at -80° C.

For re-genotyping a tail biopsy was taken from each mouse.

3.2.6.2 Tamoxifen administration

For the induction of the $p48^{ERT}$ recombinase, 5.5- to 6-week-old mice were treated with tamoxifen. Here, 4 mg of tamoxifen was bloated in 200 µl of water (20 mg/ml) and the suspension was administered per oral gavage. For this, a soft plastic needle was used (Safety IV catheter). Tamoxifen was commonly given on Mondays, Wednesdays and Fridays. Continuing experiments were performed one week after the last administration to ensure tamoxifen wash out.

3.2.6.3 Caerulein application

To analyze pancreatitis-mediated tissue damage, ADM and tumor formation, eight-week-old mice obtained eight hourly intraperitoneal (i.p.) injections of caerulein (100 μg/kg body weight caerulein, dissolved in 0,9 % (w/v) saline) on two consecutive days (induction of an acute pancreatitis). Control mice received injections of 0,9 % (w/v) saline. Half an hour before the first and after the last caerulein injection, animals received the analgesic Temgesic (100 μg/kg body weight Temgesic dissolved 0,9 % NaCl (w/v)) through subcutaneous administration into the neck. In the further course, pain medication was renewed every twelve hours and maintained for a total of 72 hours. $p48^{ERT}$, $p48^{ERT}$;$R1b^{fl/+}$ and $p48^{ERT}$;$R1b^{fl/fl}$ mice were sacrificed after six, 24 or 48 hours and seven days. In contrast, mice, which additionally expressed oncogenic $Kras^{G12D}$, were sacrificed after 21 days or six months.

3.2.6.4 Orthotopic injection of tumor cells

$1x10^6$ pancreatic tumor cells (KPC-1050) were resuspended in 50 μl PBS (1X) and injected with a 30-gauge needle into the pancreatic tail of WT mice. The operation was executed by Tao Cheng. Half an hour before the operation and nine hours after the anesthetic induction, the analgesic Temgesic (100 μg/kg body weight Temgesic in 50 µl 0,9 % NaCl (w/v)) was administered. Pain medication was renewed every twelve hours and maintained for a total of 48 hours. Mice were sacrificed after 19 days.

3.2.7 Histological analyses of pancreatic tissue

3.2.7.1 Hematoxylin and eosin stain (H&E stain)

Eosin staining solution:	7.7 mM Eosin Y in 96 % ethanol (v/v), plus 6 drops of glacial acetic acid to a final volume of 300 ml

For histological analyses, tissue sections were stained with hematoxylin in combination with eosin. Hematoxylin stains basophilic structures, such as nuclei, in blue, whereas acidophilic and eosinophilic cell components, like plasma proteins, collagen or mitochondria are stained in red through application of eosin. Formalin-fixed, paraffin-embedded sections were deparaffinized and rehydrated through consecutive incubation in roticlear (3x, 10 min each), 100 % ethanol (v/v) (3x, 2 min each), 96 % ethanol (v/v) (2 min), 70 % ethanol (v/v) (2 min), 50 % ethanol (v/v) (2 min) and ddH_2O (2min). Thereafter, sections were colored in hematoxylin for 30 seconds. Excessive hematoxylin was washed off by incubating the slides for 10 min under running tap water. This was followed by the eosin staining (5 sec) and a

short rinsing in ddH_2O. Next, tissue sections were dehydrated in 70 % ethanol (v/v) (5 sec), 96% ethanol (v/v) (30 sec), 100 % ethanol (v/v) (3x, 2 min each) and roticlear (3x, 10 min each). Finally, the slides were mounted with mounting medium.

3.2.7.2 Immunohistochemistry

Citric acid buffer (1X)	20 mM citric acid monohydrate, pH 6 adjusted with 5 M NaOH

Tissue sections were deparaffinized and rehydrated as described in paragraph 3.2.7.1. Due to the crosslinking of proteins during PFA fixation, heat mediated antigen retrieval was performed. For this, slides were placed in a vessel containing sodium citrate buffer (1X) (pH 6.0). The solution was boiled for 10 min in a microwave (600 W). After cooling (30 min, RT), slides were washed in PBS (1X) (3x, 5 min), subjected to 3 % H_2O_2 (v/v) / PBS (1X) for 10 min to block endogenous peroxidase activity and rinsed in PBS (1X) (3x, 5 min). To prohibit unspecific antibody binding, sections were commonly blocked in PBS (1X) with 5 % goat serum (v/v) and 1 % BSA (w/v) (1 h, RT). Then, the primary antibody was applied to the blocking solution and incubated overnight at 4 °C. Excessive antibody was removed through washing with PBS (1X) (3x, 5 min), secondary HRP-conjugated antibody was applied in PBS (1X) with 1 % BSA and incubated for one hour at room temperature. After three more rinses in PBS (1X), specific protein-antibody binding was visualized through the addition of the chromogen DAB. Moreover, sections were counterstained with hematoxylin (6 sec), rinsed in running tap water for five minutes and consecutively dehydrated and mounted as described in section 3.2.7.1.

3.2.7.3 Immunofluorescence

Sections were subjected to deparaffinization, rehydration and antigen retrieval as described in section 3.2.7.2. After antigen retrieval, slides were rinsed in ddH_2O (3x, 5 min each) and once in PBS (1X) (5 min). Blocking, primary antibody application was performed as presented in section 3.2.7.3. Fluorescent-labeled secondary antibodies were diluted in PBS (1X) and applied for one hour (RT). After washing with PBS (1X), sections were mounted with DAPI mounting medium.

3.2.7.4 Quantification of IHC stainings

To quantify Ck19 IHC staining intensity and distribution, stained tissue slides were scanned (40x magnification) with the slide scanner Aperio ScanScope® and positive pixels were

calculated with the Aperio ImageScope software. Positive pixels were specified in relation to the tissue size (1/mm^2).

3.2.8 Evaluation of mRNA microarray data

3.2.8.1 Pre-processing of the data

mRNA microarray preparation was perfomed at the BMFZ of the Heinrich-Heine-Universität Düsseldorf and at the Helmholtz-Zentrum München GmbH in Neuherberg. Affymetrix GeneChip® Mouse Gene 2.0 ST Arrays were used. Data were provided as CEL files.
To analyze mRNA expression profiles of the *in vitro* carcinogenesis model, data normalization, background correction and quality control was performed with the Affymetrix® Expression Console™. PCA analysis was executed in R. Data was also normalized, corrected, selected (50 % of the genes with the lowest variance were rejected) and annotated in R by the bioinformatician Dr. Phillip Bruns. All continuing analyses were conducted with this gene list. Pre-processing of the mRNA microarray data from the CRISPR/Cas9 experiments was performed by Dr. Ivonne Regel. Generally, values were output as $\log_2$ values.

3.2.8.2 Identification of differentially expressed genes

To identify differentially expressed target genes within the *in vitro* carcinogenesis model, the mean of the $\log_2$ values from each sample group was calculated (n=3). Genes, which showed average $\log_2$ values > 5 in at least one sample group were selected. Next, fold changes of the sample groups were calculated in proportion to the sample acinar cells for each gene (Fold change = 2 ^ (Mean($\log_2$)$_{\text{Group}}$ - Mean($\log_2$)$_{\text{Acinar cells}}$)). Additionally, *t*-test (unpaired, two-tailed) was calculated. Analyses were performed in Microsoft Excel 2013. For GO term analysis, genes with a fold change of > 2 and *P*-value < 0.05 were selected. GO enrichment was conducted with the tool DAVID 6.7 (Database for Annotation, Visualization and Integrated Discovery) (*https://david.ncifcrf.gov/*). GO terms with a *P*-value < 0.05 and at least five genes were considered. Gene expression changes in all four experimental groups were visualized with the Short time-series expression miner (STEM) (Ernst and Bar-Joseph 2006). As input, genes with a $\log_2$ value > 5 in at least one sample group were used. Log fold changes related to embryonic acinar cells (time point 0) were uploaded to STEM. In STEM, genes were clustered to expression profiles (Ernst, Nau, and Bar-Joseph 2005) and associated GO terms were displayed. Gene clusters with a *P*-value < 0.05 were considered.
Fold changes from single CRISPR/Cas9-mediated Ring1b KO clones were calculated in relation to the mean ($\log_2$ values) of the three control clones (Fold change = 2 ^ (Mean($\log_2$)$_{\text{Ring1bKOclone}}$ - Mean($\log_2$)$_{\text{Controlclones}}$)). Functional annotation was performed for

genes, which were up-/down-regulated with a fold change of > 1.5 in at least two Ring1b KO clones. GO terms and KEGG pathways were generated with DAVID and those with a *P*-value < 0.05 and at least five genes were considered.

3.2.9 Statistical analysis

Statistical testing was executed with the GraphPad Prism 5 software and statistical significance was determined by the performance of a two-tailed *t*-test. Depending on the experiments, an unpaired or paired *t*-test was performed.

4 Results

4.1 Acinar-to-ductal metaplasia resembles a cellular dedifferentiation

4.1.1 Establishment of an *in vitro* carcinogenesis model, reflecting different stages of PDAC

Several studies indicate that pancreatic carcinogenesis is initiated by a neoplastic transformation of acinar cells into cells with a ductal phenotype (Strobel et al. 2007, Habbe et al. 2008, Kopp et al. 2012, Zhu et al. 2007). Moreover, in the process of acinar-to-ductal metaplasia (ADM) and further pancreatic tumorigenesis, expression of differentiation genes is repressed and progenitor-like transcriptional programs are reactivated (Jensen et al. 2005, Prevot et al. 2012, Shroff et al. 2014).

To characterize the transcriptional reprogramming during PDAC development more precisely, an *in vitro* cell culture system, mimicking sequential steps of pancreatic carcinogenesis, was established. This model consisted of adult acinar cells (isolated from eight-week-old mice), three-dimensionally-cultured ADM (3D-ADM) cells and pancreatic cancer cell lines (KC-921 and KC-428), originating from $p48^{Cre/+}$;LSL-$Kras^{G12D/+}$ mice (Figure 4.1 A).

To validate, that collagen-embedded acinar cells in 3D culture undergo the process of ADM, cells were stained for the acinar differentiation marker α-amylase (here always designated as amylase) (red) and the ductal-specific protein cytokeratin 19 (Ck19) (green). Indeed, as indicated by the immunofluorescence staining, ADM structures are strongly positive for Ck19, but not for the acinar cell marker, amylase (Figure 4.1 B). In addition, qRT-PCR analysis confirms that in comparison to acinar cells, Ck19 is highly and amylase is barely expressed in 3D-ADM and tumor cells (Figure 4.1 C) (Benitz et al. 2016).

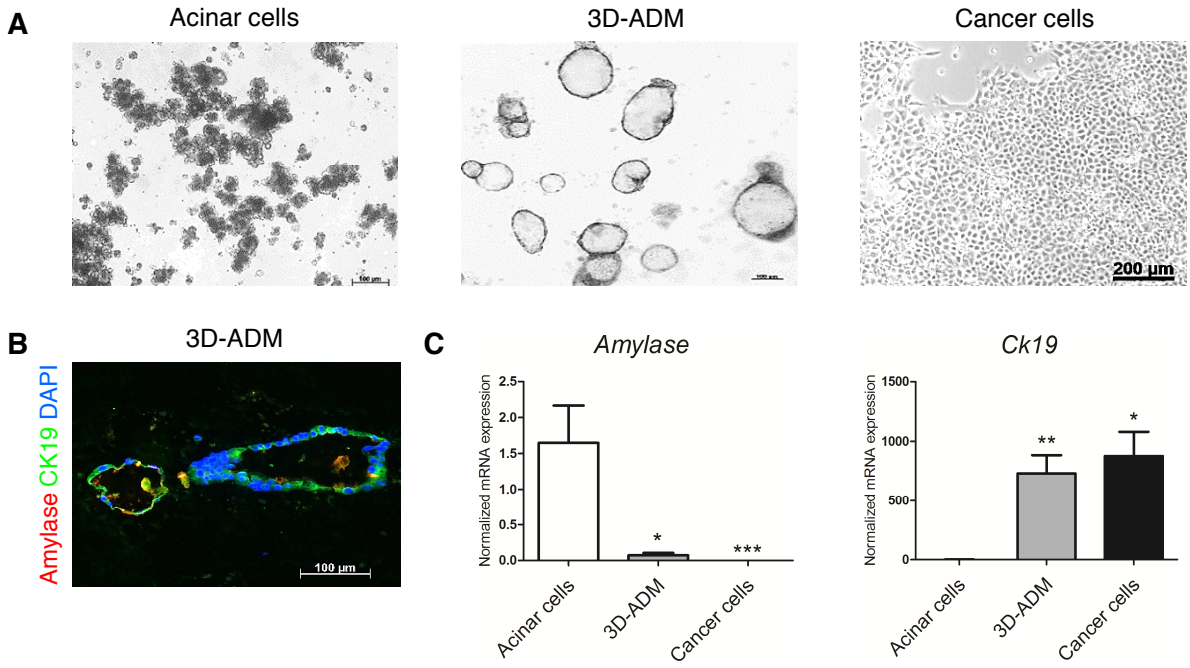

Figure 4.1: *In vitro* multi-step pancreatic carcinogenesis model. (**A**) Representative images of the *in vitro* cell culture system, showing freshly isolated acinar cells, 3D-cultured ADM and adherent cancer cells (cell line KC-921). For the 3D culture, acinar cells were embedded into collagen, stimulated with TGF-α and cultivated for six days. Scale bars, 100 µm/200 µm. (**B**) Representative immunofluorescence picture of amylase (red) and Ck19 (green) of 3D-ADMs. Nuclei were counterstained with DAPI (blue). Scale bar, 100 µm. (**C**) mRNA expression levels of *amylase* and *Ck19* in the *in vitro* carcinogenesis model were assessed by qRT-PCR. Data were normalized to acinar cells and are represented as mean ± SEM (n=3). * $P < 0.05$, ** $P < 0.01$, *** $P < 0.001$ (two-tailed, unpaired *t*-test in relation to acinar cells). Parts from Figure 4.1 C were adapted and modified from (Benitz et al. 2016).

Next, to validate further changes in cell differentiation, the expression of pancreatic transcription factors, important in determining acinar cell fate, was analyzed (Figure 4.2). Here, expression of the embryonic transcription factors, *Pdx1*, *Hes1* and *Rbpj* was found to be reactivated in 3D-ADM and cancer cells, whereas these genes are barely expressed in differentiated acinar cells (Figure 4.2 A) (Benitz et al. 2016).

In contrast, expression of differentiation markers, such as *Ptf1a*, *Mist1* and *Rbpjl* is restrained in 3D-ADM and pancreatic tumor cells (Figure 4.2 B). These results suggest, that fundamental changes in gene expression, affecting cell differentiation, can already be detected in metaplastic cells and seem to be persistent in pancreatic cancer cells (Benitz et al. 2016).

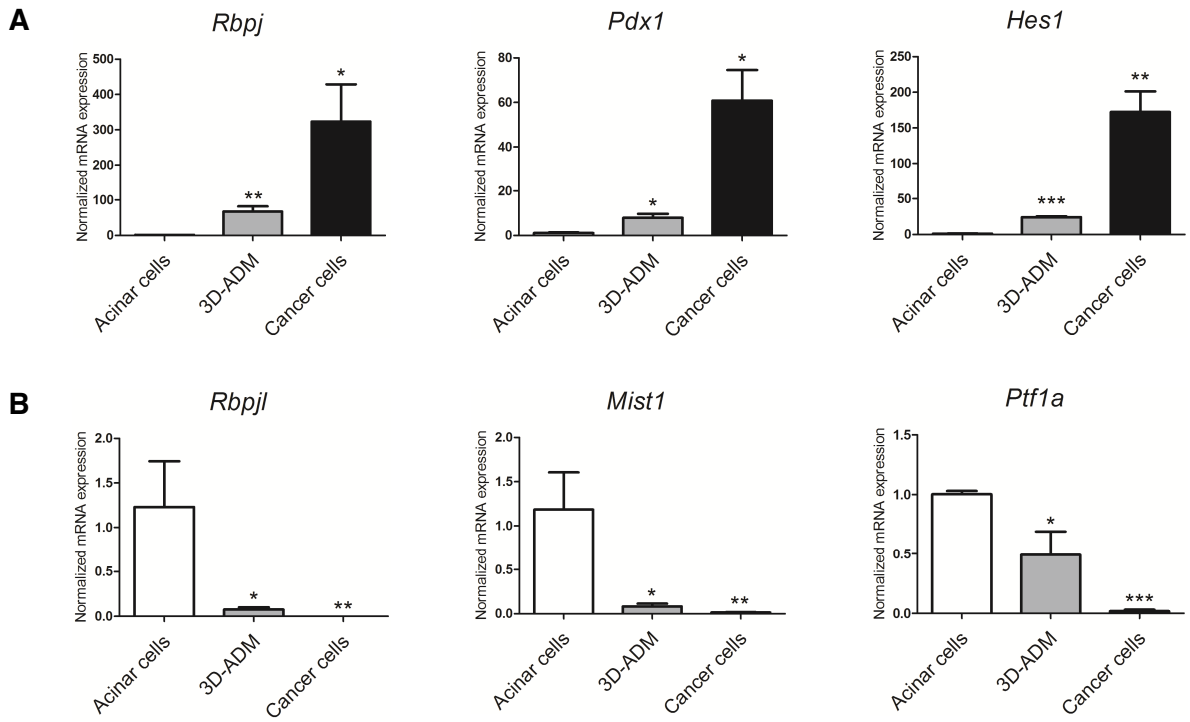

Figure 4.2: Acinar-to-ductal metaplasia and pancreatic carcinogenesis is accompanied by a down-regulation of acinar-specific differentiation genes and by an elevated expression of pancreatic progenitor genes. (**A**, **B**) mRNA expression analysis of the *in vitro* carcinogenesis model was performed by qRT-PCR. Results show expression levels of selected pancreatic progenitor markers (**A**) and of acinar differentiation genes (**B**). Values were normalized to acinar cells and are represented as mean ± SEM (n=2-4). * $P < 0.05$, ** $P < 0.01$, *** $P < 0.001$ (two-tailed, unpaired *t*-test in relation to acinar cells). Figure 4.2 B and parts from Figure 4.2 A were adapted and modified from (Benitz et al. 2016).

4.1.2 Large-scale identification of differentially expressed genes in the *in vitro* PDAC model

Since 3D-cultured ADM cells express embryonic progenitor markers, as well as the ductal-specific gene *Ck19*, it has to be clarified if the process of ADM is rather characterized as a cellular de- or transdifferentiation. Moreover, for the identification of regulators, which could contribute to the set-up of a progenitor-like expression program in ADM and cancer cells, the gene expression profiles of mature acinar cells, 3D-ADM and cancer cells (*in vitro* carcinogenesis model) were compared to the profile of progenitor acinar cells (E18.5). For this, mRNA microarray analyses were performed.

4.1.2.1 3D-ADM cells recapitulate a progenitor-like transcriptional program

After normalization of the mRNA microarray data, expression profiles of the four groups were correlated and visualized within a three-dimensional principle component analysis (PCA) (Figure 4.3 A). Importantly, the graphic illustrates that the transcriptional program of 3D-ADM

cells (green) is close to that of embryonic acinar cells (grey) (Figure 4.3 A). Moreover, the expression profile of differentiated acinar cells (black) shows great variations to that of 3D-ADM and cancer cells (red) (Figure 4.3 A).

To identify genes, which are differentially expressed in progenitor acinar cells, 3D-ADM and cancer cells and in comparison to adult acinar cells, fold changes and statistical significances were calculated. Genes with a fold change of more than 2 and a *P*-value of less than 0.05, were considered as statistically significantly up-regulated candidates. Distribution of up-regulated genes is plotted in Figure 4.3 B, demonstrating that the majority of up-regulated genes (n=925) can be found in all three conditions.

Next, identified up-regulated candidate genes were functionally annotated through gene ontology (GO) terms. Here, GO terms for biological processes were considered. Thus, GO term analysis reveals, that genes which are up-regulated in embryonic acinar and 3D-ADM cells only, are mostly related to developmental and morphogenesis pathways, making up 26 % and 21 % of all GO terms, respectively (Figure 4.3 C). For instance, up-regulated expression of *Hoxa5* or *Gli3,* an important downstream effector of the Sonic Hedgehog pathway, or of *Ring1b* (synonym *Rnf2*) was identified. These factors play a pivotal role during early embryogenesis (Figure 4.3 C) (Jeannotte et al. 1993, Bai, Stephen, and Joyner 2004, Voncken et al. 2003).

The majority of genes up-regulated in progenitor acinar cells, 3D-ADM and cancer cells are involved in cell cycle processes (Figure 4.3 D). Amongst others, expression of *Cdk1* (cyclin-dependent kinase 1), a positive regulator of cell cycle transitions was found to be induced. Interestingly, a GO term for chromatin modification was generated. Thus, mRNA levels of chromatin modifiers, such as the Polycomb group protein *Ezh2* or of the DNA methyltransferase *Dnmt1*, are elevated in progenitor acinar cells, 3D-ADM and cancer cells in comparison to the differentiated acinar cells.

In summary, 3D-ADM cells, originating from differentiated acinar cells, strongly re-express genes associated with developmental and morphogenesis pathways, which are also apparent in embryonic acinar cells (E18.5). Genes, which are also increased in cancer cells, were mainly grouped into cell cycle processes and DNA organization. Here, the term chromatin modification was found, giving a hint that broad variations in the expression profiles of the three groups in comparison to acinar cells could be greatly influenced by changes in the epigenome.

A

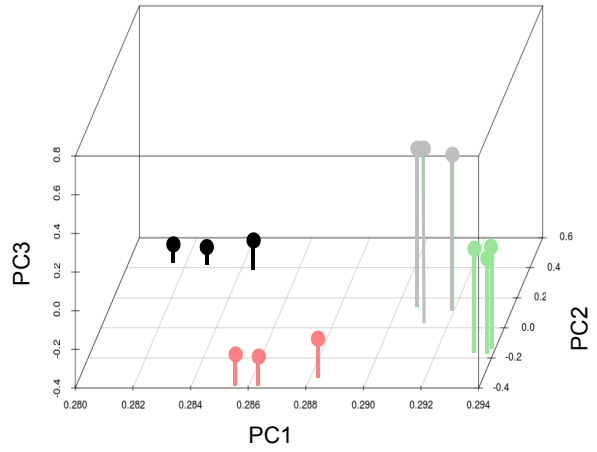

B

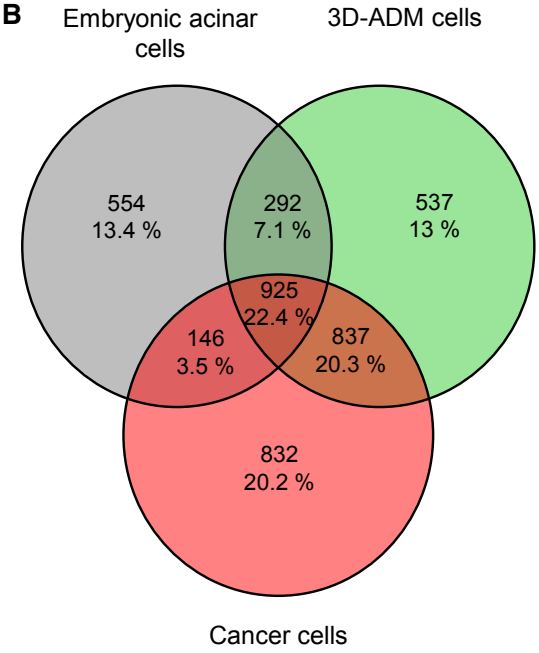

C GO terms up-regulated in embryonic acinar and 3D-ADM cells

GO term	P-Value	Genes
Negative regulation of cell differentiation	5.7E-04	*KLK8, LDB1, SEMA3F, BEX1, RCAN1, TGFB1I1,* ***GLI3****, TCF7L2,* ***KLF4****, EPHB2, THY1*
Embryonic morphogenesis	4.2E-03	*TGFBR1, LDB1, EDN1,* ***PRRX1****, PTK7, HSPG2,* ***GLI3****, TCF7L2, VEGFC, HHEX,* ***HOXA5****, RSPO3,* ***RNF2****, TGFB1I1*
Tube development	2.3E-02	*ATP7A, HHEX, PDPN,* ***HOXA5****, EDN1, PTK7, PDGFRA, LOX,* ***GLI3****, ENG*

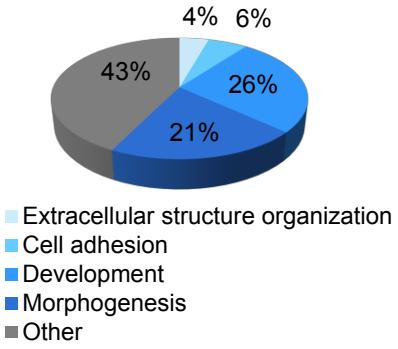

D GO terms up-regulated in embryonic acinar cells, 3D-ADM and cancer cells

GO term	P-Value	Genes
Regulation of cell cycle	2,45E-04	***TRP53****,* ***CDK1****, XPO1, FAM175A, CEP192, ROCK2, MSH2, DBF4, GMNN, TIPIN, SKP2, NUSAP1, CENPF, CDC23, BIRC5, CENPE, CDK4, TACC3, CCNG2, BAK1, CCND1, PLK4, CASP3, MAD2L1*
Chromatin modification	4.15E-04	*SETDB1, TBL1XR1, RBBP4, FAM175A, MTA2, NASP, RBL1,* ***EZH2****, CBX3, HAT1, WHSC1, RBBP7, KDM1A, EPC2, HDAC1, SMARCB1, PRMT5, SMARCC1,* ***DNMT1****, H2AFY, RUVBL2, ASF1B, KDM5A, HELLS, BRD8*

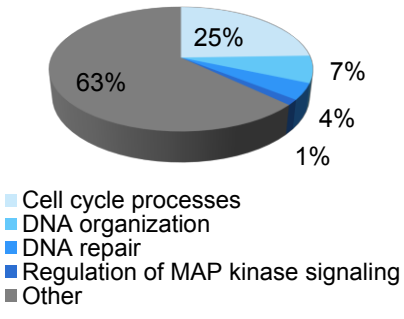

Figure 4.3: Transcriptional program of 3D-ADM and cancer cells overlaps with that of embryonic acinar cells. (**A**) To analyze group variation of embryonic and adult acinar cells, 3D-ADM and cancer cells, principle component analysis (PCA) of normalized mRNA microarray data was calculated in R. Each data set is represented as a colored line (n=3). (**B**) Pie chart revealing the percentage of genes, which are commonly as well as differentially up-regulated in embryonic acinar cells, 3D-ADM and cancer cells. For this, genes with a fold change of > 2 compared to acinar cells and $P < 0.05$, were uploaded to Venny2.1. (**C, D**) GO terms were generated for genes, which are up-

regulated in embryonic acinar cells and 3D-ADM (**C**) and commonly elevated in embryonic acinar cells, 3D-ADM and cancer cells (**D**). GO terms were generated with DAVID 6.7. In addition, GO terms were categorized into functional groups and the percentage distribution is represented in the pie charts (**C**, **D**).

4.1.2.2 GO terms associated with cancer cell characteristics, are already assigned to the expression profile of 3D-ADM cells

Annotation of genes, of which the expression is solely increased in 3D-ADM cells, illustrates that they mainly concern developmental and morphogenesis pathways (14 % and 9 % of all GO terms, respectively). In addition, genes regulating cell death and activation of the MAP kinase cascade, important features of oncogenic cell transformation, were uncovered in metaplastic 3D-ADM cells (Figure 4.4 A).

A GO terms up-regulated in 3D-ADM cells

GO term	P-Value	Genes
Negative regulation of cell death	1.13E-04	*FGFR1, CLN3, PGAP2, ROCK1, ERBB3, CLU, SPHK1, BTC, TGFB3, HSPA1A, ITSN1, YWHAH, PLCG2, CHST11, BCL6, MKL1, RASA1, NGF, ANGPTL4*
Positive regulation of MAPKKK cascade	0.002	*FGFR1, IGF1R, MYD88, RIPK2, EDA2R, IL11, CTNNB1*

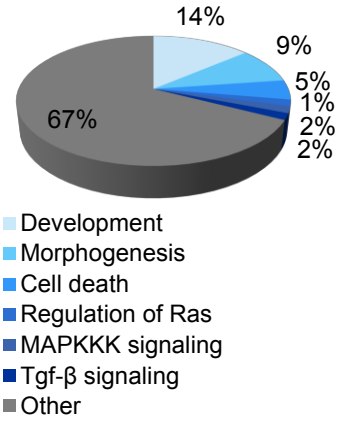

B GO terms up-regulated in 3D-ADM and cancer cells

GO term	P-Value	Genes
Regulation of cell proliferation	0.01	*FOSL2, PDGFB, PTGS2, PPARG, TLR4, PMAIP1, BCL2L1, ITGB1, TGFB1,* ***STAT6****, LIF, CD9,* ***KRAS****, MORC3, SERPINE1,* ***TGFA****, TFF1, ETV4, TES, MAFG, PRKCA, EGFR, KLF5, KLF10, CD276, SMAD3, CTNNA1,* ***NRAS****,* ***CDKN1A****, EREG, LAMA5, BAX, TGIF1, HBEGF, JAK2, KCTD11*
Epithelium development	0.02	*EGFR, BCL10, F11R, PLXNA1, MAP2K1, PTGS2, HTT, PPARG, CTNND1, SMAD3, TGFB1, SRC, SUFU, RDH10, NCOA3, LAMA5, PPL, CFL1, TGIF1, AREG, ETV4*

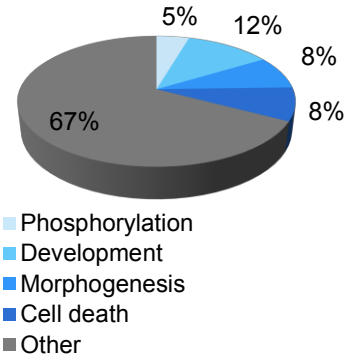

Figure 4.4: GO terms up-regulated in 3D-ADM and cancer cells. Genes, which are up-regulated in comparison to acinar cells (fold change of > 2 and $P < 0.05$), were considered for GO term analysis. GO terms for genes solely elevated in 3D-ADM cells (**A**) and 3D-ADM and cancer cells (**B**) were generated with DAVID 6.7. (**A**, **B**) Single GO terms were selected and overall percentage distribution is represented in associated pie charts.

GO terms, increased in 3D-ADM and cancer cells, involve amongst others the "regulation of cell proliferation". Here, the genes *Kras*, *Nras* (neuroblastoma RAS viral oncogene homolog) or *Tgf-α* were annotated (Figure 4.4 B), which encode cell proliferation-promoting factors. Furthermore, developmental mediators were assigned as well, constituting 12 % of all GO terms (Figure 4.4 B). Amongst others, the term "epithelium development" is attributed (Figure 4.4 B). This reveals, that reactivation of developmental pathways occurs in metaplastic cells, but also persists in cancer cells. Besides the reactivation of progenitor-like transcriptional programs, metaplastic cells are already characterized by an activation of cancer cell characteristics, such as proliferation-promoting pathways. These results suggest that 3D-ADM cells undergo a process of cellular dedifferentiation.

4.1.2.3 Genes down-regulated in 3D-ADM and cancer cells, mainly concern acinar differentiation genes

In a further approach, genes, which are down-regulated in embryonic acinar cells, 3D-ADM and cancer cells in comparison to mature acinar cells, were determined (Figure 4.5 A). Here, candidate genes were mainly grouped into catabolic, metabolic and biosynthetic processes (Figure 4.5 B). Expression of characteristic pancreatic enzymes, such as *Pnlip* (pancreatic lipase) or *Cela1* (chymotrypsin-like elastase family member 1), is decreased in 3D-ADM and cancer cells (Figure 4.5 C). Since embryonic acinar cells were isolated shortly before birth at E18.5, expression of these enzymes was probably already activated. Altogether, these results indicate that 3D-ADM and cancer cells shut down the expression of acinar differentiation genes.
In general, the mRNA microarray data emphasize that the transcriptional program of 3D-ADM and cancer cells has similarities to that of progenitor acinar cells. Precisely, developmental and cell cycle processes are commonly up-regulated, whereas metabolic and catabolic pathways are decreased in comparison to acinar cells. Then, the question was addressed as to what kind of mechanisms could be responsible for changing the transcriptional program of 3D-ADM and cancer cells towards a progenitor-like transcriptome. One possible answer was found in the microarray data. Here, it was detected that expression of epigenetic chromatin remodelers is commonly elevated in embryonic acinar cells, 3D-ADM and cancer cells. Since expression patterns can be rapidly changed through epigenetic alterations, such as DNA methylation or histone modification, it appeared reasonable to investigate if the re-activation of epigenetic modifiers could be important for restoring the expression of progenitor genes and the concomitant down-regulation of acinar differentiation genes in 3D-ADM and cancer cells.

A

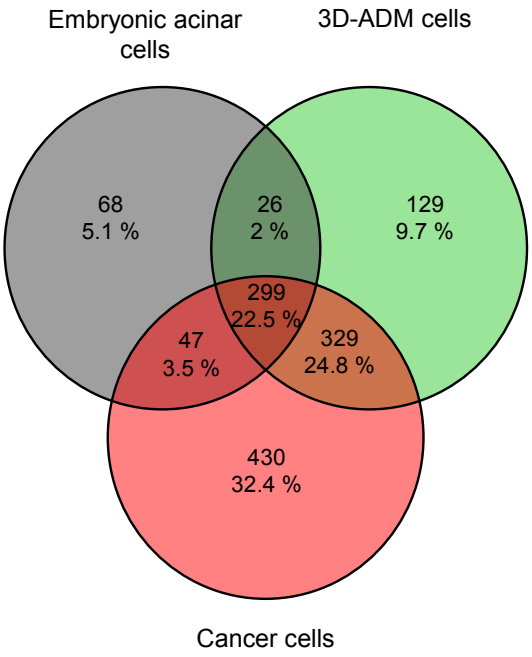

B

GO terms down-regulated in embryonic acinar cells, 3D-ADM and cancer cells

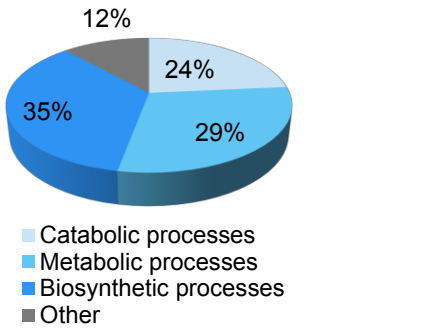

C

GO terms down-regulated in 3D-ADM and cancer cells

GO term	P-Value	Genes
Lipid catabolic process	0.01	***PNLIP***, ***CEL***, *PLA2G12A, PLA2G1B, PLCB1, PHYH, IAH1*
Proteolysis	0.02	*PSMB10, KLK1B8, CELA3B, UFSP2, SEC11C, QPCTL, USP2,* ***PRSS1***, *ANPEP, CUZD1, TRY4, UBA5,* ***CELA1***, *ATG3, FBXO16, UFM1, PRSS2, CTRC, SPCS3,* ***CPA2***, *2210010C04RIK, GM5409, HABP2, CTRL*

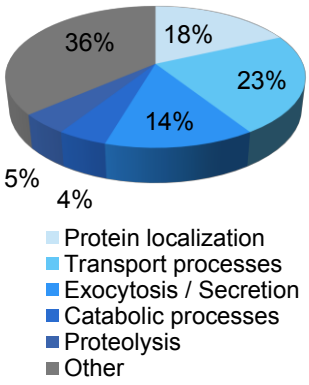

Figure 4.5: Down-regulated expression patterns in embryonic acinar cells, 3D-ADM and cancer cells. (**A**) Genes from mRNA microarray data, which were expressed to a lesser extent in embryonic acinar cells, 3D-ADM and cancer cells in comparison to acinar cells (fold change of < 0.5 and $P < 0.05$) were inserted into Venny2.1.0 and grouped as represented in the pie chart. (**B**) GO terms were generated for genes commonly down-regulated in embryonic acinar cells, 3D-ADM and cancer cells and percentage distribution is visualized in the pie charts. (**C**) Selected GO terms down-regulated in 3D-ADM and cancer cells. Overall distribution was quantified in percent and is represented in the pie chart.

4.1.2.4 Epigenetic remodelers are greatly expressed in 3D-ADM and cancer cells

In a further approach, expression profiles of chromatin modifiers were visualized with the short time-series expression miner (STEM) software (Figure 4.6). GO terms associated with chromatin modification were solely assigned to the temporal courses, delineated in the Figures 4.6 A, 4.6 B and 4.6 C. The graphics illustrate that the expression of chromatin remodelers is commonly up-regulated in embryonic acinar cells (first point from the left), 3D-ADM cells (third point) and cancer cells (fourth point) compared to differentiated acinar cells (second point) (Figure 4.6 A, 4.6 B, 4.6 C). For instance, the *Rnf2* gene, also known as *Ring1b*, which encodes a repressive histone modifier, seems to be similarly expressed in progenitor cells, 3D-ADM and pancreatic tumor cells (Figure 4.6 A), whereas expression of the DNA methyltransferase *Dnmt1* or the histone-acetyltransferase *Hat1* is even more apparent in cancer cells (Figure 4.6 B).

Particularly, expression profiles of chromatin remodelers seem to correlate with those of transcription factors, such as *Rbpj*, which is a well-described pancreatic progenitor marker (Figure 4.6 A). Moreover, inverse correlation between the expression of repressive chromatin modifiers, such as *Ring1b* or *Dnmt1*, and acinar differentiation genes, such as *Ptf1a*, can be observed (Figure 4.6 D).

A

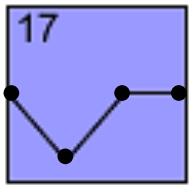

GO term	P-Value	Genes
Chromatin modification	0.017	*EPC2, RBBP4, HDAC1, SMARCB1, NASP,* ***RNF2****, HMG20A, KDM3A, SETD2, KDM5A*
Transcription	1.04E-4	*ELF2, ELF4, TAF1D, REST, ZFP84, MED20, CNOT6, EPC2, CASP8AP2, HSF2, MIER1, ZFP507, KDM5A, KHDRBS1, ATF7IP, RBBP4, ZFP426, ZFP326, ARID5B, SNAPC3, GMEB1, ADNP, CCNL1, HMG20A, ZFP26, MCM6, SARNP, HHEX, RFC1, ZFP821, VGLL4, ZFP516, ZFP512, ZFP397, ZFP113, NR2C2, SMARCB1, ZFP410, GATAD2B, KDM3A, EWSR1, TAF2, ZFP148, TEAD3, MED31, NOTCH2,* ***HDAC1****, SFPQ,* ***RNF2****, PSPC1, PAPOLG*

B

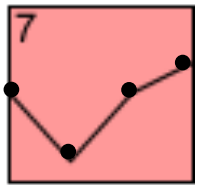

GO term	P-Value	Genes
Chromatin modification	6.8E-06	*SETDB1, TAF1, YEATS4, SETDB2, FAM175A, RBL1,* ***EZH2****,* ***MECP2****, CBX3,* ***HAT1****, WHSC1, KAT5, VPS72,* ***HDAC2****, SMARCE1, PRMT5, SMARCD1, RTF1,* ***DNMT1****, RUVBL2, CARM1, TCF3, HELLS,* ***HDAC7****, BRD8*
Transcription	3.2E-05	*CBX3, MAF1, PNN, PRIM1, GTF2E1, ZFP472, TAF5L, SIN3A, ZFP90, TARDBP, PRIM2, PSIP1, TGS1, TBPL1, PHRF1, TADA2A, RBL1,* ***MECP2****, MED12, MED11, UHRF1, ZFP81, PTRF, ZFP280D, CDCA7L, DNTTIP2, CRTC3, C330013J21RIK, TADA1, ELK3, XAB2, VPS72, TCERG1, TCF3, HELLS, TFDP1, SETDB1, TAF1, YEATS4, ATAD2, WHSC1, PMF1, KAT5, SREBF2,* ***HDAC2****,* ***DNMT1****,* ***RBPJ****, CHAF1A, CHAF1B,* ***HDAC7****, KLF3, TAF1B,* ***EZH2****, FUBP1, MCM7, PRMT5, RTF1, BRD8, ELP2, KHDRBS3, GMEB2, ZFP429, GTF2H4, TLE3, NCOA7, POLR1C, CDK7, MCM2, MCM3, MCM4, GTF2H2, MCM5, MED6, MED4, RUVBL2, CARM1, THOC1, POLR2F, GLIS2, NFYA, POLR2D, TSC22D1, POU2F1, NPAT, GTF3C6, RQCD1, BRMS1L, SSRP1, ERF, TRIM28, ILF3, ADNP2, ILF2, SRFBP1, PPP1R8, IFT57, TCEB1, ZFP189*

C

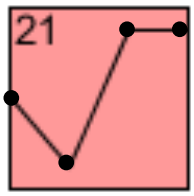

GO term	P-Value	Genes
Chromatin modification	0.015	*UTP3, TBL1XR1, MTA2, HIRA, INO80, TRRAP, HLTF,* ***HDAC3****, EP300, 2210018M11RIK, SMARCC1, SMARCA5,* ***EED****, H2AFY, CHD1, TLK2, SMARCA4*

D

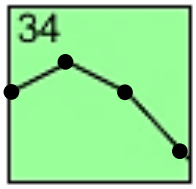

GO term	P-Value	Genes
Lipid catabolic process	3.9E-04	***PNLIP****, PLD3,* ***CEL****, LPL, PNLIPRP2, SMPDL3A, EHHADH, PHYH*
Pancreas development	0.05	*XBP1,* ***PTF1A****, PDE3B*

Figure 4.6: Expression courses of delineated GO terms in the *in vitro* carcinogenesis model. To visualize gene expression changes, selected genes from the mRNA microarray data (genes, with a $\log_2$ value > 5 in at least one sample group, but without fold change analysis and statistical significance determination) were uploaded to STEM. Here, temporal expression profiles were generated and clustered genes were functionally annotated to GO terms with DAVID. Expression profiles of chromatin modifiers (**A**, **B, C)**, transcription factors (**A, B**) and of acinar differentiation genes (**D**) are represented. Datasets are plotted as follows: embryonic acinar cells (first data point), acinar cells (second data point), 3D-ADM (third data point) and cancer cells (fourth data point) (from left to right).

Furthermore, relative expression levels of selected epigenetic remodelers, progenitor and acinar differentiation genes were visualized within a heatmap (Figure 4.7). The graphic illustrates that expression of repressive epigenetic remodelers, like *Ring1b* (*Rnf2*) or *Ezh2*, is elevated in 3D-ADM and cancer cells and correlates with a decrease of acinar-specific differentiation markers, such as *Ptf1a* and *Rbpjl* (Figure 4.7).

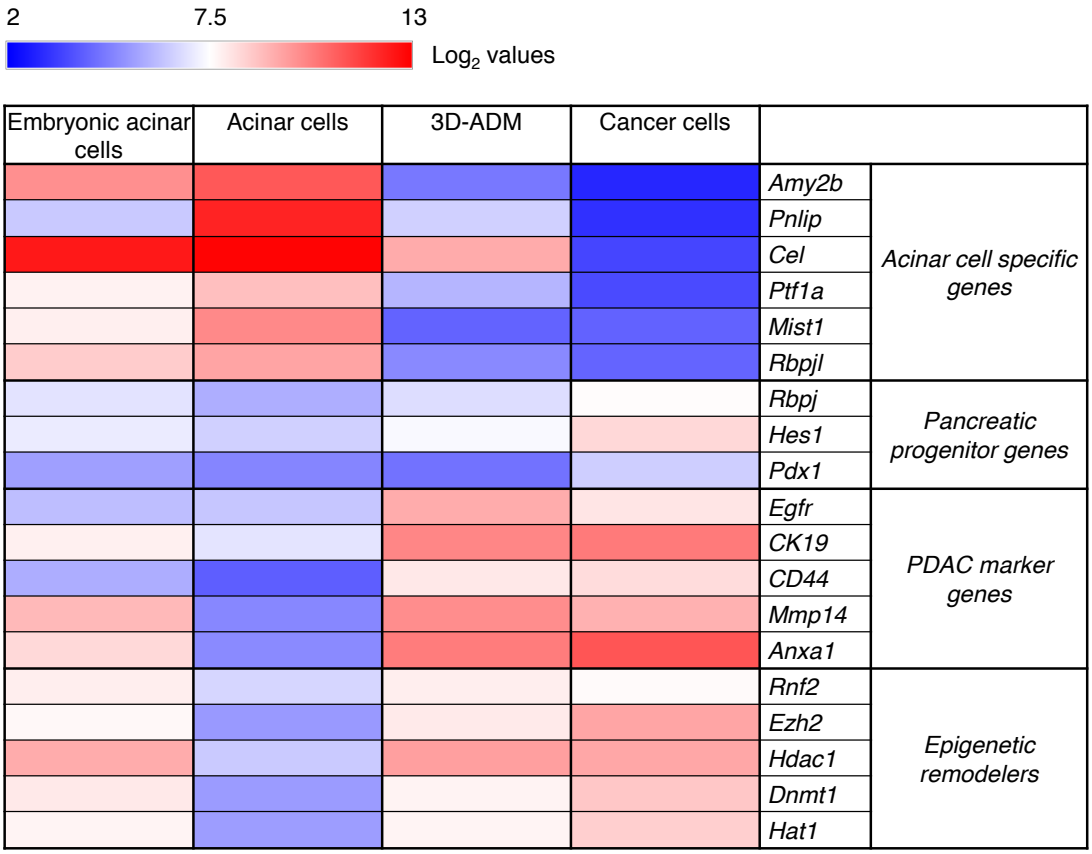

Figure 4.7: Heat Map, illustrating expression profiles of candidate genes in the *in vitro* carcinogenesis model. Target genes were selected from mRNA microarray data and relative log_2 values are represented in a heat map, which was generated in Excel 2007.

4.2 Epigenetic repressors are reactivated in pancreatic carcinogenesis

The analysis of the mRNA microarray data clearly demonstrates, that epigenetic modifiers, important for gene repression, such as DNA methyltransferases or the Polycomb group proteins *Ezh2* and *Ring1b*, are significantly up-regulated in 3D-ADM and pancreatic cancer cells.

Next, expression of these epigenetic remodelers within the *in vitro* carcinogenesis model was validated via qRT-PCR (Figure 4.8 A, Figure 4.9 A).

4.2.1 DNA methyltransferases are over-expressed in 3D-ADM and cancer cells

As indicated by Figure 4.8 A, expression of the maintenance DNA methyltransferase *Dnmt1* and the de novo enzyme *Dnmt3a,* is strongly increased in 3D-ADM and cancer cells. Since loss of the cell cycle inhibitor $P16^{INK4A}$ during PDAC progression is associated with DNA hyper-methylation (Schutte et al. 1997), it was assessed if DNA methylation of the $p16^{INK4A}$ promoter can already occur in metaplastic ADM cells. Here, methylation-specific PCR of bisulfite converted DNA reveals that the $p16^{INK4A}$ promoter of 3D-ADM cells is already methylated (Figure 4.8 B). However, in cancer cells wildtype $p16^{INK4A}$ locus cannot be detected (unconverted $p16^{INK4A}$), suggesting that the locus underwent homozygous deletion (Figure 4.8 B).

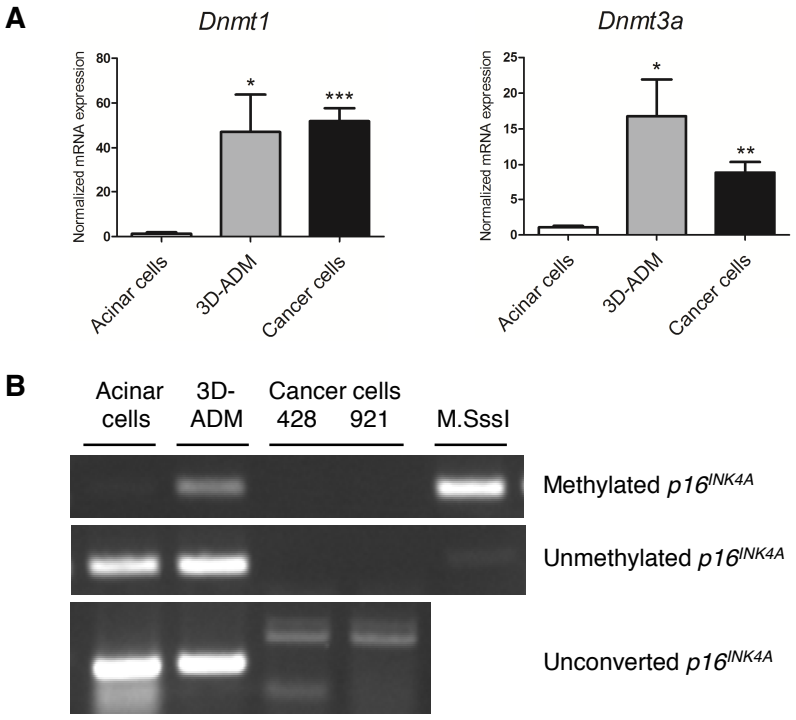

Figure 4.8: Pancreatic carcinogenesis is hallmarked by a reactivation of DNA methyltransferases. (**A**) qRT-PCR analysis of DNA methyltransferases *Dnmt1* and *Dnmt3a* with mRNA from acinar cells, 3D-ADM and cancer cells. Data were normalized to acinar cells and are represented as mean ± SEM (n=2-4). * $P < 0.05$, ** $P < 0.01$, *** $P < 0.001$ (two-tailed, unpaired *t*-test, comparison to acinar cells). (**B**) Methylation-specific PCR analysis of bisulfite-converted DNA from acinar cells, 3D-ADM and cancer cells. As positive control, artficially methylated DNA from acinar cells (through use of M.SssI) was included. Through the employment of distinct primer pairs (methylated and unmethylated), methylation status of the $p16^{INK4A}$ promoter is predicted. Amplification of unconverted $p16^{INK4A}$ promoter was included.

4.2.2 PcG proteins are reactivated in the sequence of pancreatic carcinogenesis

Importantly, a previous study implicated that H3K27me3, catalyzed by PRC2, can serve as mark for the recruitment of DNA methyltransferases in cancer cells (Schlesinger et al. 2007). This suggests that in the course of cancer development, Polycomb-mediated histone modifications could bookmark potential genes for persistent gene silencing. To study if PRC-mediated histone modifications are essential for acinar cell dedifferentiation in pancreatic carcinogenesis, the *in vitro* model was analyzed.

In general, Polycomb-mediated gene repression is induced by PRC2-catalyzed trimethylation of lysine 27 of histone 3 (H3K27me3). This histone modification is recognized by PRC1 and its catalytic subunit, Ring1b, mono-ubiquitinates lysine 119 of histone H2A (Niessen, Demmers, and Voncken 2009). Hence, expression of *Ezh2*, the catalytic subunit of PRC2, as well as of the PRC1 members *Ring1b* and *Bmi1* was validated by qRT-PCR (Figure 4.9 A). In accordance to the microarray data, mRNA expression is reactivated in 3D-ADM and cancer cells. Western blot analyses demonstrate increased amounts of Bmi1 in both 3D-ADM and cancer cells and a clear enrichment of Ring1b in cancer cells (Figure 4.9 B) (Benitz et al. 2016).

Levels of H3K27me3, mediated by Ezh2, do not show great variations in the sequence of the *in vitro* carcinogenesis model. In contrast, a strong increase of the histone modification H2AK119ub, catalyzed by Ring1b, can be detected in 3D-ADM (Figure 4.9 B, 4.9 C) and cancer cells (Figure 4.9 B). This reveals, that PRC1 must already be catalytically active in metaplastic cells, mediating de novo ubiquitination of histone H2A (Figure 4.9 A, 4.9 B). In addition, an immunofluorescence staining of 3D-ADM cells visualizes that acinar cells, which underwent ADM, are positive for H2AK119ub, whereas untransformed cells are largely not stained (Figure 4.9 C) (Benitz et al. 2016).

Elevated Ring1b expression was previously detected in PDAC or ductal breast carcinoma (Martinez-Romero et al. 2009, Bosch et al. 2014), but direct target genes have remained largely elusive. However, few studies indicated that in ES cells, Ring1b helps to repress genes which favor ES cell differentiation (van der Stoop et al. 2008, Endoh et al. 2008). Thus, it can be speculated if the indicated epigenetic remodelers are reactivated in ADM and pancreatic tumor cells (Figure 4.9 A, 4.9 B) to mediate the repression of acinar differentiation genes and to establish a progenitor-like profile (Benitz et al. 2016).

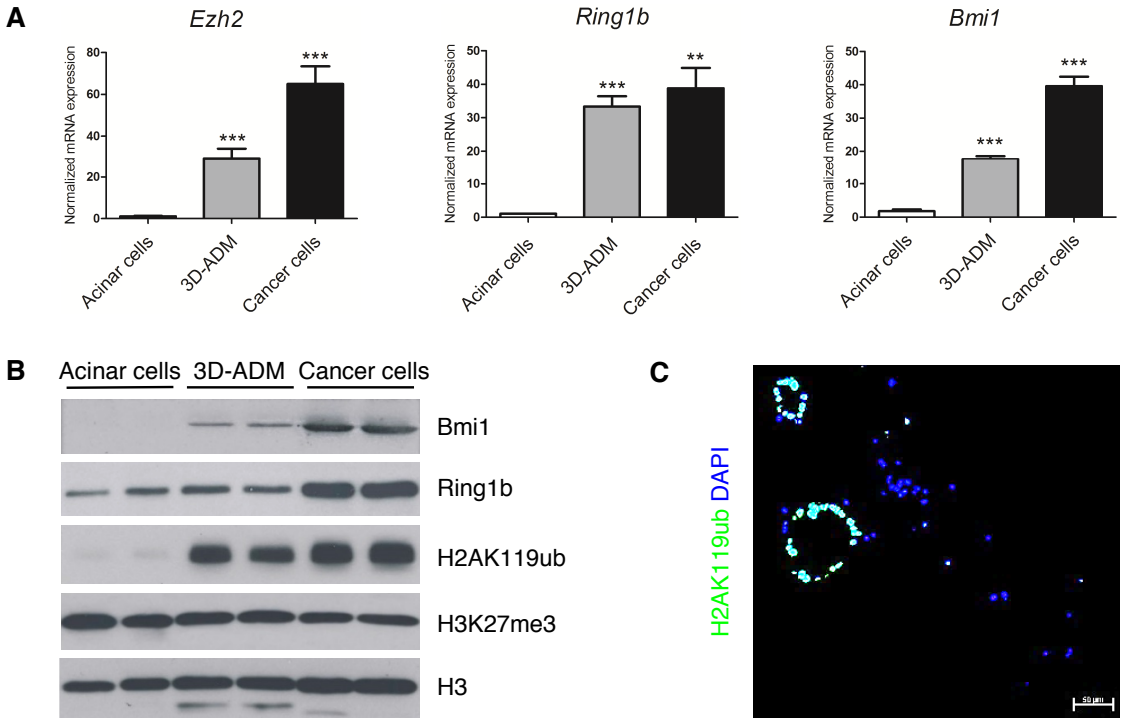

Figure 4.9: Expression of Polycomb repressor complex components is reactivated in 3D-ADM and pancreatic cancer cells. (**A**) qRT-PCR expression analysis of the catalytic subunit of PRC2, *Ezh2*, and the PRC1 components, *Bmi1* and *Ring1b* in acinar cells, 3D-ADM and cancer cells. mRNA expression data were normalized to acinar cells and are represented as mean ± SEM (n=4). ** $P < 0.01$, *** $P < 0.001$ (two-tailed, unpaired *t*-test in relation to acinar cells). (**B**) Western blot analysis of acinar cell, 3D-ADM and cancer cell protein lysates with antibodies against Ring1b, Bmi1, H2AK119ub and H3K27me3. (**C**) Representative image of immunofluorescence staining for the histone modification H2AK119ub (green). Nuclei were labeled with DAPI (blue). Scale bar, 50 μm. Figure 4.9 B and parts of Figure 4.9 A and were adapted and modified from (Benitz et al. 2016).

4.2.3 H2AK119ub is enriched at promoter sites of differentiation genes in pancreatic cancer cells

To analyze if PRC1 is involved in the transcriptional regulation of acinar cell fate genes during pancreatic carcinogenesis, presence of H2AK119ub was determined at the promoter sites of *Rbpj*, *Rbpjl* and *Ptf1a* through chromatin immunoprecipitation (ChIP). In addition, levels of PRC2-induced H3K27me3 and of the activating histone mark H3K4me3 were determined (Benitz et al. 2016).

In acinar cells, high levels of H3K4me3 can be detected at the promoter sites of the actively expressed differentiation genes *Ptf1a* and *Rbpjl*. In contrast, at the *Rbpj* promoter, the repressive modification H3K27me3 was found to be slightly enriched. In comparison to acinar cells, histone profiles of 3D-ADM and cancer cells are greatly distinct. Thus, 3D-ADM

cells harbor bivalent domains, whereas in pancreatic cancer cells, the presence of the repressive H3K27me3 is enriched and levels of H3K4me3 are decreased at the acinar cell fate genes *Rbpjl* and *Ptf1a* (Figure 4.10 A). This correlates with the expression data (Figure 4.2 B). Additionally, cancer cells exhibit a slight accumulation of H3K4me3 at the *Rbpj* promoter (Figure 4.10 A) supporting the expression analysis, which indicates that the gene is actively expressed (Figure 4.2) (Benitz et al. 2016).

A great enrichment of the repressive histone mark H2AK119ub is present at the promoter sites of *Rbpjl* and *Ptf1a* in cancer cells, which could ensure persistent gene silencing (Benitz et al. 2016). However, in 3D-ADM cells only a small accumulation of H2AK119ub is detectable at the *Ptf1a* promoter. No great variations in H2AK119ub are apparent at the promoter site of the progenitor marker *Rbpj* (Figure 4.10 B) (Benitz et al. 2016).

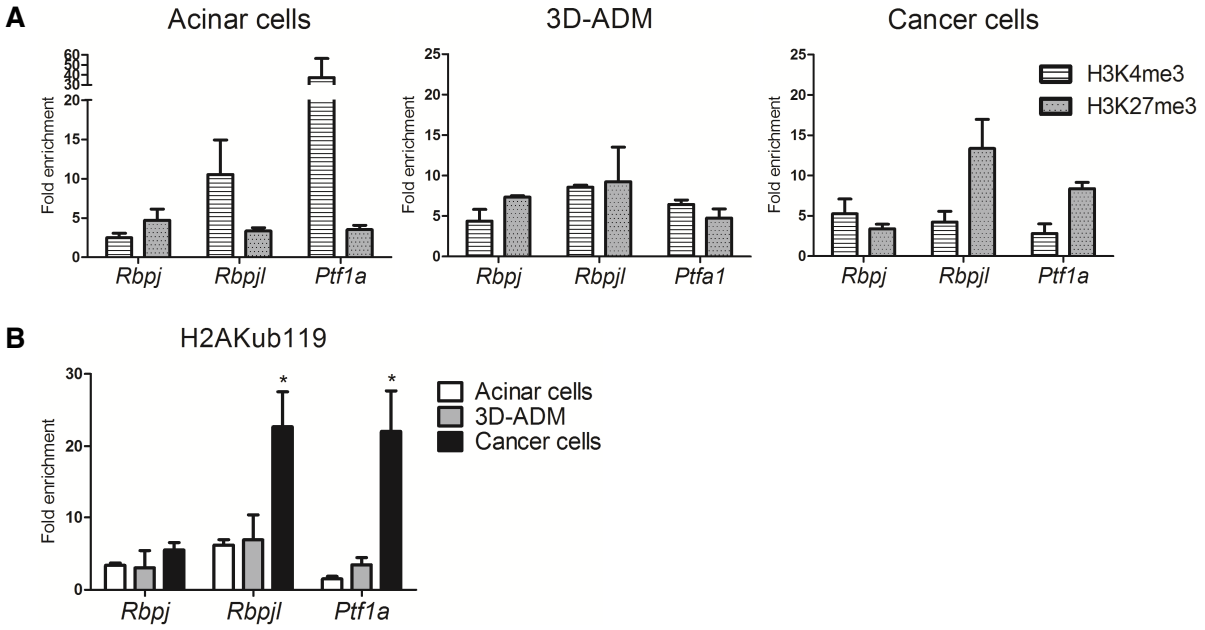

Figure 4.10: Histone modifications, such as H2AK119ub, are remodeled in pancreatic carcinogenesis. Chromatin immunoprecipitation (ChIP) analysis of H3K4me3, H3K27me3 (**A**) and H2AK119ub (**B**) at promoter sites of the progenitor marker *Rbpj* and the acinar cell fate genes *Rbpjl* and *Ptf1a* in acinar cells, 3D-ADM and cancer cells. Immunoprecipitated DNA was amplified by qRT-PCR and data were plotted as fold enrichment over IgG control. Data are represented as mean ± SEM (n=2-6). * $P < 0.05$, (two-tailed, unpaired *t*-test to acinar cells). Figures were adapted and modified from (Benitz et al. 2016).

Overall, these data show that the repressive histone modifications H3K27me3 and H2AK119ub are strongly enriched at the promoter sites of the differentiation genes *Rbpjl* and *Ptf1a* in pancreatic cancer cells. This could contribute to a permanent silencing of these genes (Benitz et al. 2016).

4.2.4 Expression of Bmi1 is epigenetically regulated in pancreatic carcinogenesis

Besides reactivated expression of *Ring1b*, its co-activator *Bmi1* is also increasingly expressed in 3D-ADM and cancer cells (Figure 4.9 A). To investigate, if this reactivation could be due to epigenetic changes, levels of H3K4me3, H3K27me3 and H2AK119ub were assessed at three different *Bmi1* promoter sites (P1, P2, P3, from 5'-3'). ChIP analysis reveals that the *Bmi1* promoter of acinar cells harbors higher levels of the repressive histone mark H3K27me3 than of the activating H3K4me3. In 3D-ADM cells, H3K27me3 is slightly decreased, whereas a massive loss can be detected in cancer cells. Hence, the activating histone mark H3K4me3 is dominantly present at the *Bmi1* promoter in tumor cells (Figure 4.11 A) (Benitz et al. 2016).

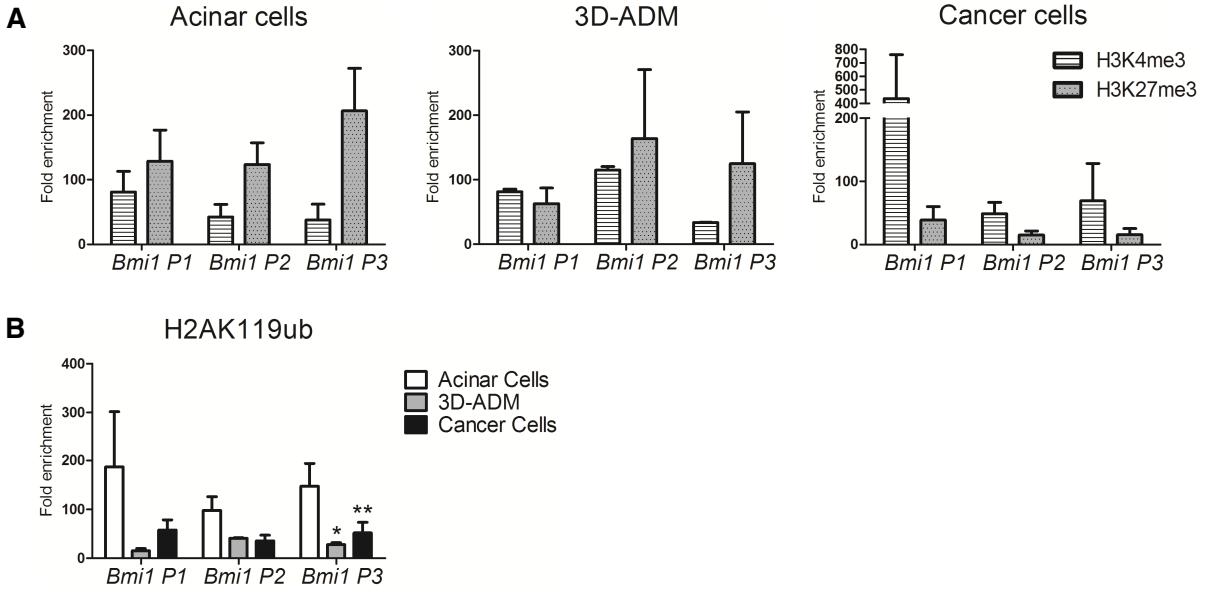

Figure 4.11: *Bmi1* expression in the *in vitro* carcinogenesis model correlates with modifications in the histone profile. Chromatin immunoprecipitation analysis, quantified by qRT-PCR, of H3K4me3, H3K27me3 (**A**) and H2AK119ub (**B**) at the *Bmi1* promoter in the *in vitro* carcinogenesis model. Data are displayed as fold enrichment over the IgG control and are represented as mean ± SEM (n=2-4). * $P < 0.05$, ** $P < 0.01$ (two-tailed, unpaired *t*-test). Figure was adapted and modified from (Benitz et al. 2016).

Notably, H2AK119ub is accumulated at the *Bmi1* promoter in acinar cells, but significantly lost in 3D-ADM and cancer cells (Figure 4.11 B). Altogether, presence of the indicated histone modifications perfectly matches the expression patterns (Figure 4.9 A, 4.9 B), allowing a reactivated expression of *Bmi1* in 3D-ADM and tumor cells. Here, the loss of H2AK119ub in 3D-ADM cells could be responsible for the transient expression of *Bmi1*, whereas an additional depletion of H3K27me3 could guarantee permanent gene expression in cancer cells (Benitz et al. 2016).

4.2.5 Expression of PRC1 components is reactivated in pancreatitis and PDAC development *in vivo*

In vitro data indicates that H2AK119ub is enriched in 3D-ADM and cancer cells (Figure 4.9 B). Moreover, a strong accumulation of the repressive histone modification is present at the promoter sites of the differentiation genes *Ptf1a* and *Rbpjl* (Figure 4.10 B). Now, to investigate if PRC1 is implicated in caerulein-mediated pancreatitis and in PDAC development *in vivo*, appropriate mouse models were studied (Benitz et al. 2016).

4.2.3.1 Elevated expression of PRC1 members in a setting of inflammatory acinar-to-ductal metaplasia

In vivo, transient ADM formation occurs in the setting of pancreatitis. Here, damaged acinar cells undergo dedifferentiation to compensate tissue damage (Jensen et al. 2005).
To identify if PRC1 is reactivated in the context of inflammatory acinar-to-ductal metaplasia, acute pancreatitis was induced in eight-week-old wildtype mice through the application of the choleocystokinin-analogue caerulein. Precisely, eight hourly intraperitoneal injections (100 µg/kg body weight) were administered (Figure 4.12 A). With this model, exocrine cell damage and acinar cell plasticity can be properly recapitulated. Precisely, during acute pancreatitis, acinar cells undergo ADM (24 hours to 48 hours after the last treatment) but regenerate at later time points. To assess if expression of PRC1 components is modulated during pancreatitis, immunohistochemical staining of Bmi1 and Ring1b as well as of the histone modification H2AK119ub was performed on tissue of caerulein-treated (in this study commonly abbreviated as C) wildtype mice, sacrificed after 48 hours and 7 days and on tissue of NaCl-treated WT mice (control). In control tissue, weak staining of Bmi1 and Ring1b is solely apparent in centroacinar, ductal and islet cells. However, H2AK119ub is also slightly stained in single acinar cells. Extensive exocrine tissue damage and ADM is identifiable 48 hours after the last caerulein application. Here, the great majority of ADM cells is positive for Bmi1, Ring1b and H2AK119ub (Figure 4.12 B). In contrast, in recovered acinar cells, apparent seven days after the last caerulein injection, expression of Ring1b and Bmi1 is greatly diminished, whereas the histone modification H2AK119ub can be detected in few acinar cells (Figure 4.12 B). These observations, together with the quantification of the positively stained nuclei (Figure 4.12 C), indicate that expression of Bmi1 and Ring1b, as well as the presence of H2AK119ub are extensively increased during acute pancreatitis and can be dominantly found in ADM cells (Figure 4.12 B). During organ recovery, apparent after seven days after the caerulein administration, Bmi1 and Ring1b as well as H2AK119ub levels nearly come down to the values of the control tissue (Figure 4.12 B, 4.12 C) (Benitz et al. 2016).

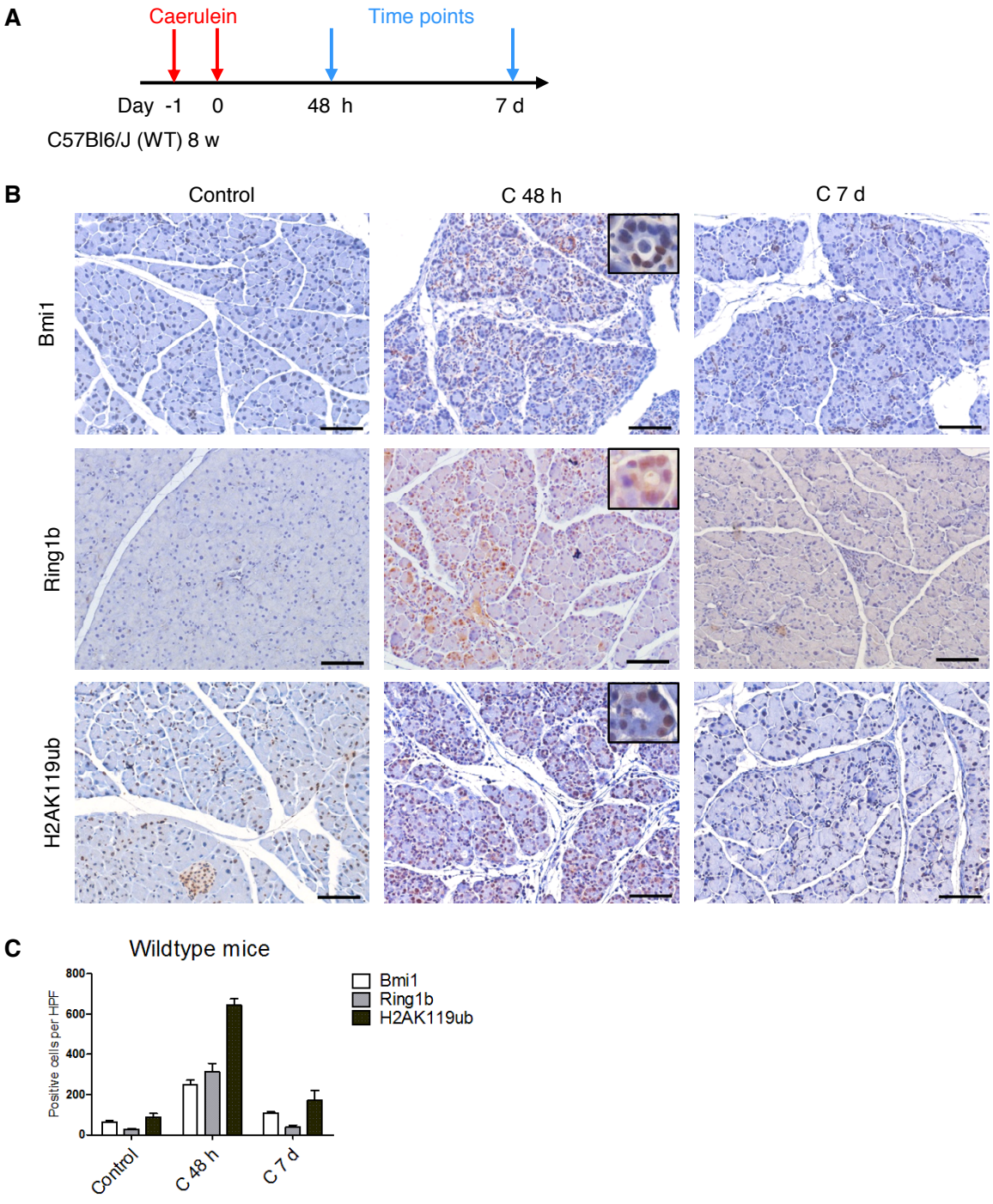

Figure 4.12: Levels of Bmi1, Ring1b and H2AK119ub are increased upon caerulein-induced pancreatitis in wildtype mice. (**A**) Schematic representation of the caerulein administration protocol. Wildtype mice received eight hourly injections (i.p.) of caerulein (100 μg/kg body weight caerulein) on two consecutive days. Mice were sacrificed after 48 hours and 7 days after the last treatment. (**B**) Immunohistochemistry for Bmi1, Ring1b and the histone modification H2AK119ub on tissue of WT mice. Representative pictures show expression patterns in control and caerulein-treated (abbreviated as C) tissue. Mice, injected with caerulein were sacrificed after 48 hours and 7 days. Scale bars, 100 μm. (**C**) Quantification of positively stained nuclei per high power field (HPF). Per animal three pictures were considered. Data are represented as mean ± SEM (n=5). Figures 4.12 B and 4.12 C were adapted and modified from (Benitz et al. 2016).

4.2.3.2 PRC1 components are expressed throughout cancer development in a PDAC mouse model

Since ADM is considered as the first neoplastic cell transformation in the sequence of PDAC development (Zhu et al. 2007, Kopp et al. 2012), expression of PRC1 was moreover determined in consecutive cancer development (Figure 4.13).

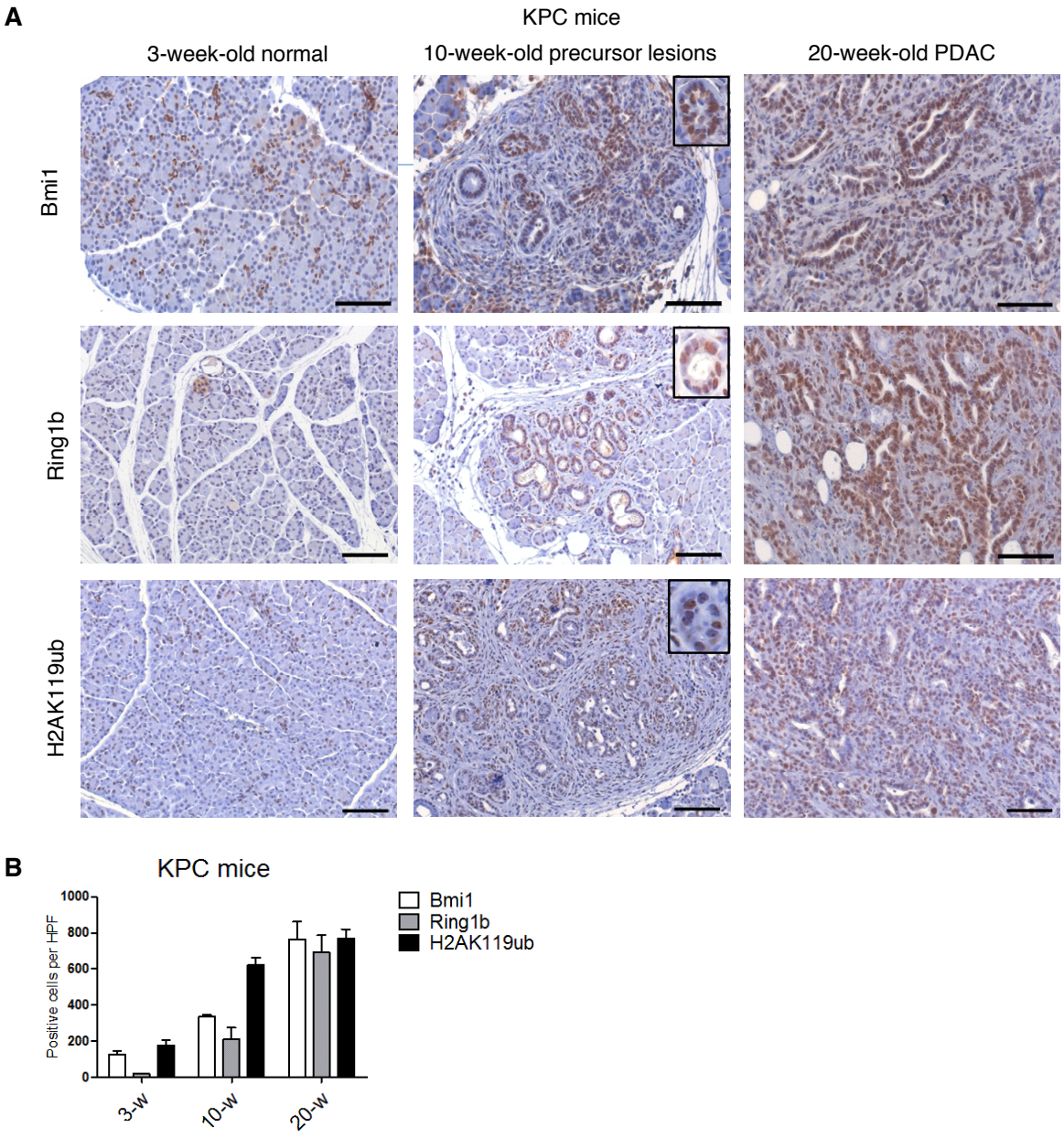

Figure 4.13: PRC1 components are over-expressed in pancreatic cancer.
(**A**) Immunohistochemical analysis of Bmi1, Ring1b and H2AK119ub on pancreatic tissue of 3-, 10-, and 20-week-old KPC mice (n=5). Tissues represent morphologically normal tissue, precancerous lesions and PDAC, respectively. High resolution pictures (10-week-old KPC mice) show positively stained nuclei in ADM lesions. Scale bar, 100 μm. (**B**) Quantification of positive cells per high power field. For this, three pictures per animal were evaluated. Data are represented as mean ± SEM (n=5). Figures were adapted and modified from (Benitz et al. 2016).

For this, p48$^{Cre/+}$;LSL-Kras$^{G12D/+}$;Trp$^{53lox/+}$ (KPC) mice were analyzed, because they develop PDAC within a short period of time (Hingorani et al. 2005). At the age of three weeks, pancreatic tissue morphology is similar to that of wildtype mice, but many acinar cells are already slightly positive for Bmi1, Ring1b and H2AK119ub (Figure 4.13 A). At an age of ten weeks, the mice have already developed precancerous lesions, such as low-grade PanINs or AFLs (Figure 4.13 A). Importantly, the broad majority of these lesions exhibit Bmi1-, Ring1b- and H2AK119ub-positive nuclei. In contrast, surrounding fibroblasts, stellate or immune cells are mostly not stained (Figure 4.13 A). PDAC can be detected in 20-week-old KPC mice. Here, it is evident that tumor cells also greatly express Bmi1 and Ring1b and that H2AK119ub is specifically accumulated (Figure 4.13 A). Overall, the quantification of positively stained nuclei reveals that levels of Bmi1, Ring1b and H2AK119ub are increased during pancreatic carcinogenesis (Figure 4.13 B) (Benitz et al. 2016).

4.3 Ring1b is required for acinar-to-ductal metaplasia and pancreatic carcinogenesis

4.3.1 Establishment of a conditional Ring1b knockout mouse model

So far, the generated results indicate that the epigenetic modifier Ring1b is over-expressed in caerulein-mediated acinar-to-ductal reprogramming during acute pancreatitis and in the sequence of PDAC development and progression (Figure 4.12, 4.13). To identify whether Ring1b is critical for the formation of metaplastic, progenitor-like ADM cells and PDAC, a conditional Ring1b knockout mouse model was established. Herein, Cre^{ERT} expression is driven by the acinar cell-specific p48 promoter, and translocation of the recombinase into the nucleus is induced by the administration of tamoxifen at an adult stage (5.5 - 6-week-old mice).

Since all mice were crossed with a Rosa26-LSL-tdTomato reporter strain, recombination efficiency can be evaluated through measuring the expression of tdTomato. Thus, pancreata of mice with a tamoxifen-induced, activated Cre^{ERT} appear bright pink (Figure 4.14 A). Immunofluorescence staining of tdTomato confirms that the reporter is exclusively expressed in acinar cells, whereas ductal, centroacinar and immune cells remain unstained (Figure 4.14 B). Moreover, the staining illustrates that recombination must have occurred in the majority of acinar cells. To assess the recombination rate more precisely, acinar cells were isolated from 8-week-old wildtype mice and the percentage of tdTomato positive cells was determined by fluorescence-activated cell sorting (FACS) (Figure 4.14 C). On average, a recombination rate of ~ 60 % was observed (Figure 4.14 C).

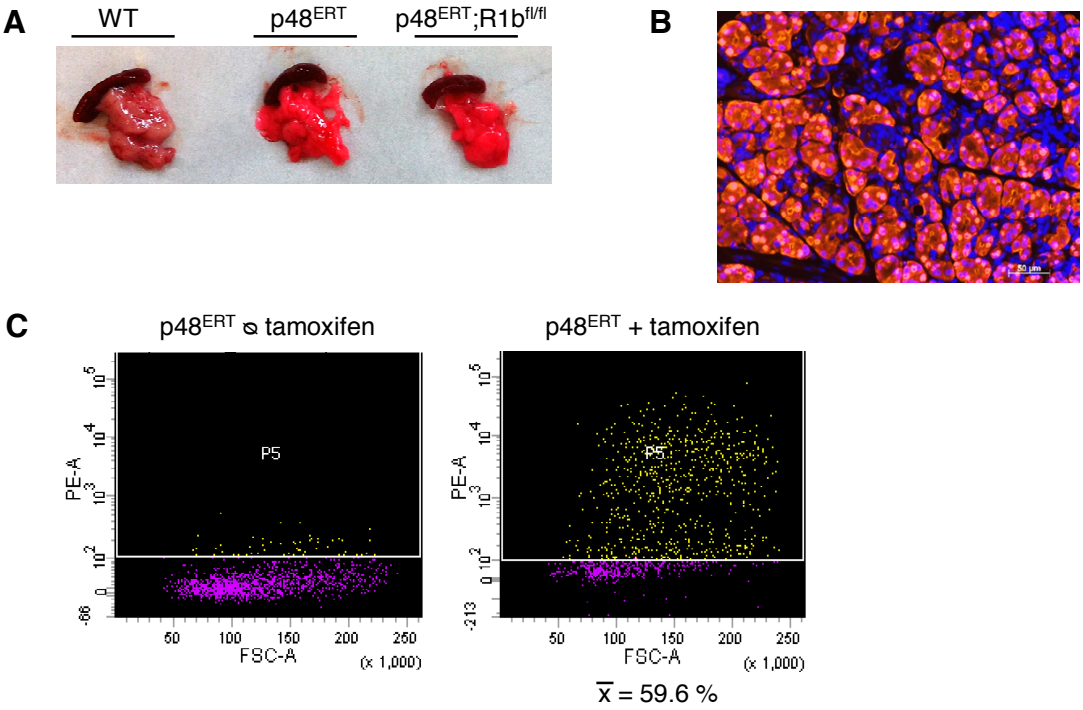

Figure 4.14: Evaluation of the recombination efficiency in the inducible p48^{ERT} mouse model. (**A**) Representative image of pancreata and spleen of wildtype, p48^{ERT} and p48^{ERT};R1b$^{fl/fl}$ mice. Tamoxifen was administered at an age of ~ 6 weeks. Upon p48^{ERT}-mediated recombination, the fluorescent reporter tdTomato is expressed. Animals were sacrificed at an age of 8 weeks. (**B**) Representative picture of a tdTomato immunofluorescence staining (red) of pancreatic tissue of an induced p48^{ERT} mouse. Cell nuclei were counterstained with DAPI. Scale bar, 50 μm. (**C**) Representative dot blot of FACS analysis, illustrating tdTomato positive acinar cells (yellow, P5, right dot blot). Gate was adjusted to unstained control cells (left dot blot, p48^{ERT} Ø tamoxifen). Analysis was performed in the DKTK sort facility. The percentage of positive cells was assessed from p48^{ERT} mice (n=5) and mean was calculated.

As indicated by the H&E staining pancreatic histology is not distinct in p48^{ERT}, p48^{ERT};R1b$^{fl/+}$ and p48^{ERT};R1b$^{fl/fl}$ mice (Figure 4.15 A). Moreover, no variations in the pancreas-to-body weight ratio have been identified (Figure 4.15 B). This met the expectations, because it was demonstrated that Ring1b is barely expressed in adult differentiated acinar cells (Figure 4.9 A, Figure 4.12 A). Therefore, a knockout of Ring1b under physiological conditions should have no effect.

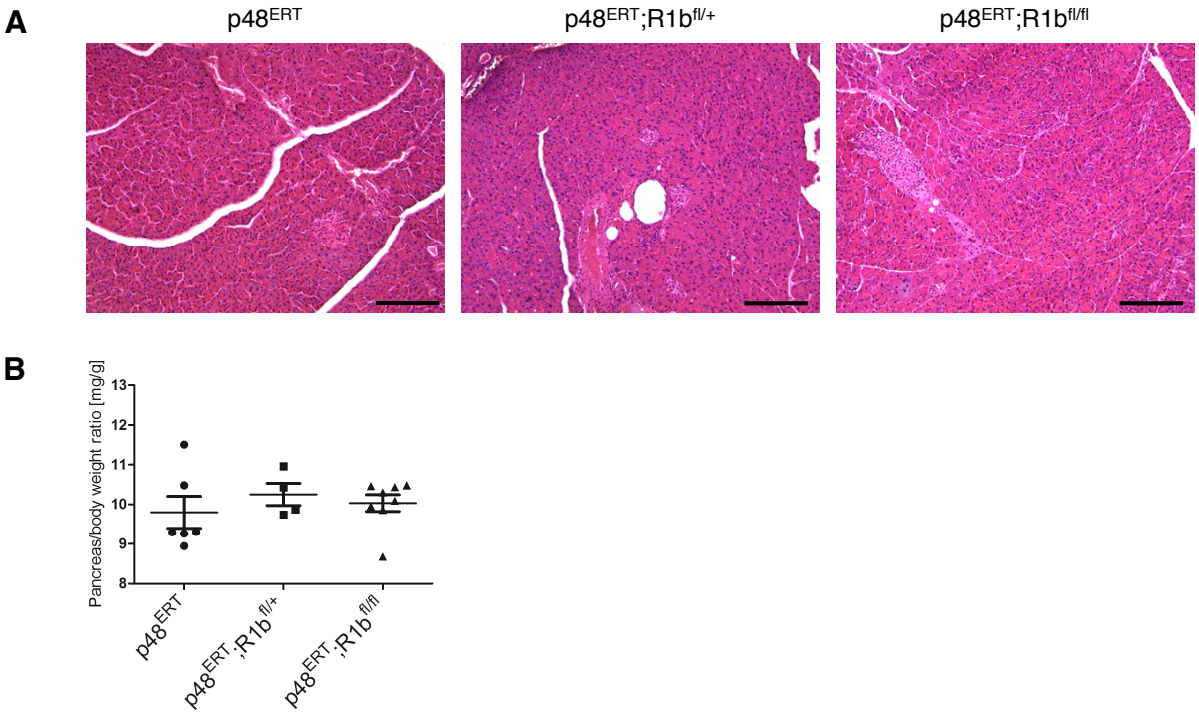

Figure 4.15: Pancreatic morphology is not distinct in p48^{ERT} , p48^{ERT};R1b$^{fl/+}$ and p48^{ERT};R1b$^{fl/fl}$ mice under physiological conditions. (**A**) H&E staining of pancreata of 8-week-old p48^{ERT}, p48^{ERT};R1b$^{fl/+}$ and p48^{ERT};R1b$^{fl/fl}$ mice. Scale bars, 200 μm.
(**B**) Pancreas-to-body weight ratio of 8-week-old p48^{ERT}, p48^{ERT};R1b$^{fl/+}$ and p48^{ERT};R1b$^{fl/fl}$ mice. Data are represented as mean ± SEM (n=4-6).

4.3.2 Ring1b expression is elevated in p48^{ERT} mice during acute pancreatitis, supported by the activation of Akt and Erk

Immunohistochemistry of Ring1b and Bmi1 on tissue of caerulein-treated wildtype mice implicates that their expression is reactivated in the setting of inflammatory ADM formation (Figure 4.12 B) (Benitz et al. 2016). To investigate the effects of a Ring1b loss, mice were administered with tamoxifen and caerulein (Figure 4.16).

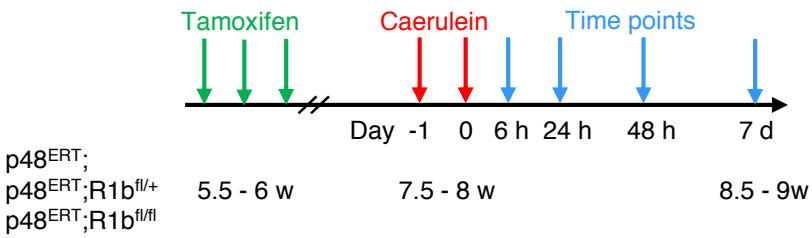

Figure 4.16: Administration of tamoxifen and caerulein to the p48^{ERT} mouse model. At an age of ~ 6 weeks, mice were treated with tamoxifen for three times (every other day). After one week of tamoxifen wash out, eight hourly injections of caerulein (100 µg/kg body weight) were injected on two consecutive days. Mice were sacrificed after six, 24 and 48 hours or seven days after the last caerulein administration.

At first, the time point of elevated Ring1b expression was again verified in caerulein-treated p48^{ERT} mice. In accordance with the immunohistochemical stainings of the caerulein-induced pancreatitis model in wildtype mice (Figure 4.12 B), Western blot analyses of treated p48^{ERT} mice reveal an up-regulation of Ring1b during the acute inflammatory phase (24 h, 48 h) and a decrease during organ regeneration (7 d). Similarly, H2AK119ub is enriched at 24 and 48 hours (Figure 4.17 A, 4.17 B). This also applies to the levels of H3K4me3 and to a lesser extent to H3K27me3 (Figure 4.17 A). Remarkably, caerulein-induced pancreatitis is accompanied by an increased activation of the protein kinase Akt, a downstream effector of the PI3 kinase, and of the mitogen-activated protein kinase Erk, as determined by the presence of their phosphorylated forms (Figure 4.17 A, 4.17 C). Besides the assumption, that activation of the PI3K and the Mek/Erk signaling pathway could promote cell proliferation to overcome pancreatitis-driven tissue damage, it was speculated if they could induce the expression of Ring1b.

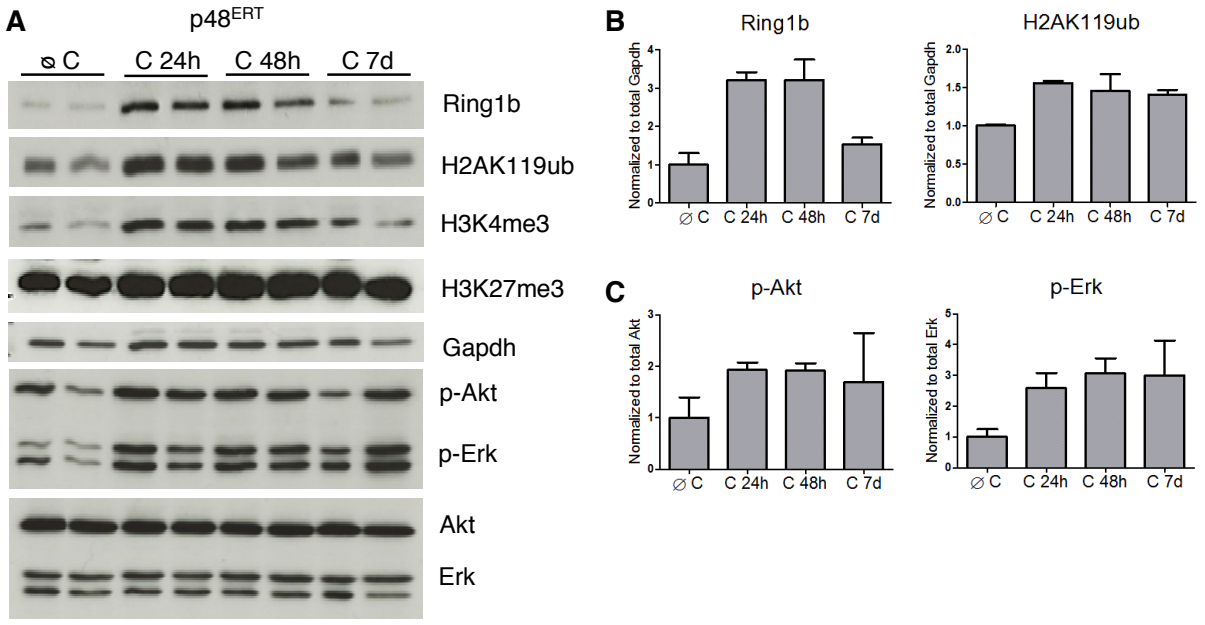

Figure 4.17: Ring1b expression and activation of Akt and Erk are increased during pancreatitis. (**A**) Western blot analyses of bulk tissue protein lysates from untreated (Ø C) and caerulein-treated p48^{ERT} (C) mice, which were sacrificed after 24 and 48 hours and 7 days. Indicated antibodies were used. Immunoblot intensity of Ring1b, H2AK119ub (**B**) and p-Akt and p-Erk (**C**) was quantified with ImageJ and normalized to total Gapdh, Akt, Erk, respectively. Data are represented as mean ± SEM (n=2).

To analyze if reactivation of Ring1b is dependent on the PI3K/Akt or Mek/Erk signaling, the acinar cell suspension model was taken advantage of. When isolated acinar cells from 8-week-old mice are kept in suspension for at least 24 hours, they express progenitor-like expression programs (Pinho et al. 2011). As indicated by Western blot analysis, Ring1b is reactivated and can be detected in acinar suspension cells, which were cultured for 120 hours. However, upon treatment with LY 294002 or PD 98509, potent inhibitors of the

PI3K/Akt and the Mek/Erk pathway respectively, protein levels of Ring1b are greatly reduced. Compared to the controls, levels of H2AK119ub are decreased as well (Figure 4.18 A, 4.18 B).

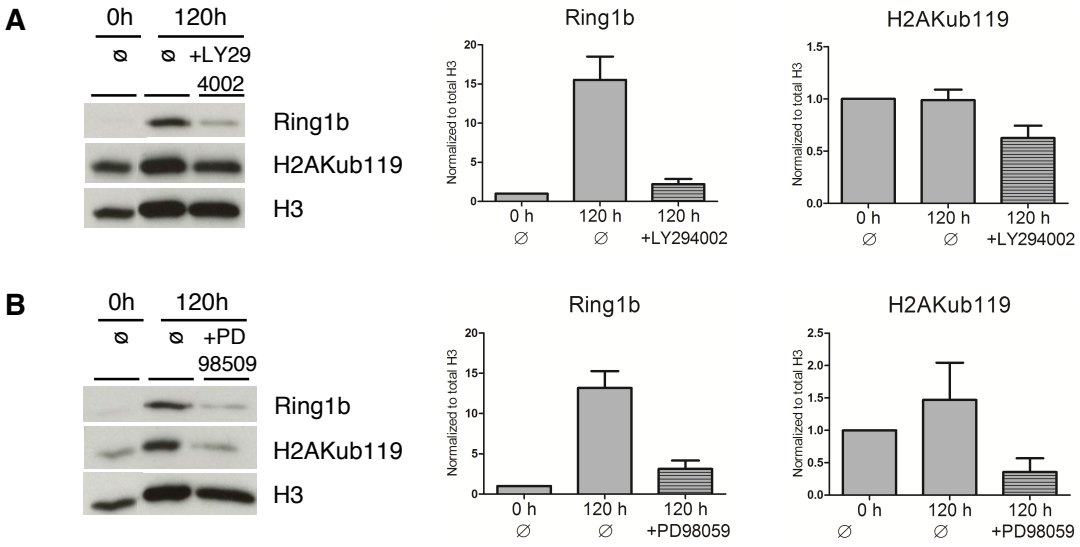

Figure 4.18: Inhibition of PI3K/Akt and Mek/Erk signaling results in an impaired reactivation of Ring1b in acinar suspension cells. Immunoblots with antibodies against Ring1b, H2AK119ub and the housekeeper H3. Herein, protein lysates from freshly isolated WT acinar cells and cultured WT acinar suspension cells (120 h) were applied. Acinar suspension cells were treated with the PI3K inhibitor LY 294002 (30 μM) (**A**) and the Mek inhibitor PD 98059 (50 μM) (**B**). Band intensities were measured with ImageJ and normalized to total H3. Data are represented as mean ± SEM from two independent experiments (n=2).

These results suggest, that in case of the acinar suspension cell model, a re-expression of Ring1b relies on the activation status of PI3K and Mek/Erk signaling pathway. However, it needs to be further elucidated if these pathways directly influence expression or post-translational stabilization of Ring1b or if the reactivation is caused by any indirect effects.

4.3.3 ADM is impaired in the setting of pancreatitis in Ring1b-deficient mice

Now, to investigate the role of Ring1b in pancreatitis-driven ADM, tamoxifen-induced $p48^{ERT}$, $p48^{ERT}$;$R1b^{fl/+}$ and $p48^{ERT}$;$R1b^{fl/fl}$ mice were injected with caerulein according to the model depicted in Figure 4.16. Remarkably, H&E staining shows large variations between the three groups. In comparison to $p48^{ERT}$;$R1b^{fl/+}$ and $p48^{ERT}$;$R1b^{fl/fl}$ mice, more tubular complexes and immune cell infiltrations are apparent in $p48^{ERT}$ animals, 24 hours after the last caerulein injection (Figure 4.19). 48 hours after the last caerulein administration, $p48^{ERT}$ mice have developed complete ADM structures, surrounded by immune cell infiltrations and edema. In

striking contrast, pancreatic tissue of p48^{ERT};R1b$^{fl/fl}$ mice is partially regenerated with only few tubular complexes and less inflammation. However, in p48^{ERT};R1b$^{fl/+}$ mice, ADM and immune cells can be identified, but to a smaller extent than in p48^{ERT} animals. At day seven, p48^{ERT};R1b$^{fl/+}$ and p48^{ERT};R1b$^{fl/fl}$ mice have undergone almost complete regeneration, whereas in the tissue of control mice some small regions with metaplastic cells can still be detected (Figure 4.19).

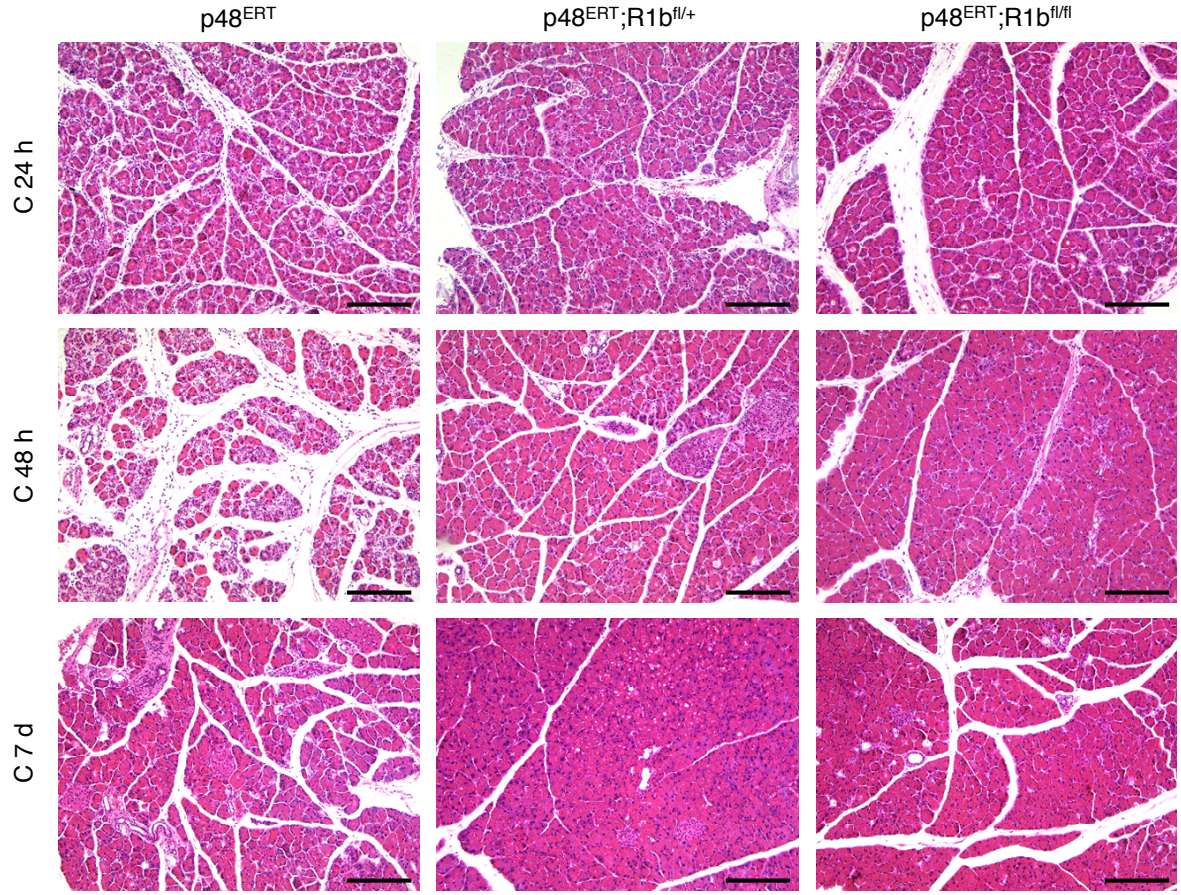

Figure 4.19: Loss of Ring1b leads to reduced ADM formation during acute pancreatitis. (**A**) Representative images of H&E staining of caerulein-treated p48^{ERT}, p48^{ERT};R1b$^{fl/+}$ and p48^{ERT};R1b$^{fl/fl}$ mice. Mice were sacrificed after 24 (C 24 h) and 48 hours (C 48 h) or seven days (C 7 d) (n=5-6). Scale bars, 200 μm.

Overall, these results suggest, that in p48^{ERT};R1b$^{fl/fl}$ mice, the process and persistence of ADM is impaired during caerulein-induced pancreatitis. Moreover, the appearance of acinar cell damage, edema and immune cell infiltrations is reduced.

Blood analyses reveal that amylase and lipase activity is similar in caerulein-treated p48^{ERT} and p48^{ERT};R1b$^{fl/fl}$ mice, sacrificed after six hours after the last caerulein administration. This suggests that caerulein is also effective in Ring1b-depleted mice, leading to stimulation of acinar cells (Figure 4.20).

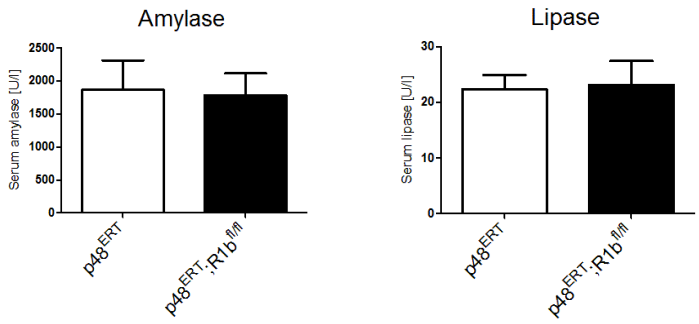

Figure 4.20: Blood amylase and lipase levels do not differ in caerulein-treated p48^{ERT} and p48^{ERT};R1b$^{fl/fl}$ mice . Blood plasma was analyzed for amylase and lipase activity from caerulein-treated mice, which were sacrificed six hours after the last caerulein administration (C 6 h). Data are represented as mean ± SEM (n=3-4).

H&E staining clearly demonstrates, that in p48^{ERT};R1b$^{fl/fl}$ mice the formation of ADM lesions is greatly compromised (Figure 4.19). Next, loss of Ring1b was validated by immunohistochemistry, 48 hours after the last caerulein application. Immunohistochemical detection of Ring1b indicates that ADM cells and atrophic acinar cells from control mice are strongly stained. In contrast, in tissue of p48^{ERT};R1b$^{fl/fl}$ mice most acinar cells have a morphologically normal appearance and do not express Ring1b. Interestingly, the few ADMs present in Ring1b knockout mice are also positive for Ring1b (Figure 4.21 A), suggesting that these cells were not successfully recombined.

Moreover, to verify that Ring1b is essential for ADM, acinar cells from p48^{ERT} and p48^{ERT};R1b$^{fl/fl}$ mice were cultured in the 3D *in vitro* model. While acinar cells from p48^{ERT} mice form massive ductal structures, acinar de-differentiation is largely blocked in Ring1b-deficient cells (Figure 4.21 B). Overall, it can be concluded that expression of Ring1b seems to be a prerequisite for ADM formation.

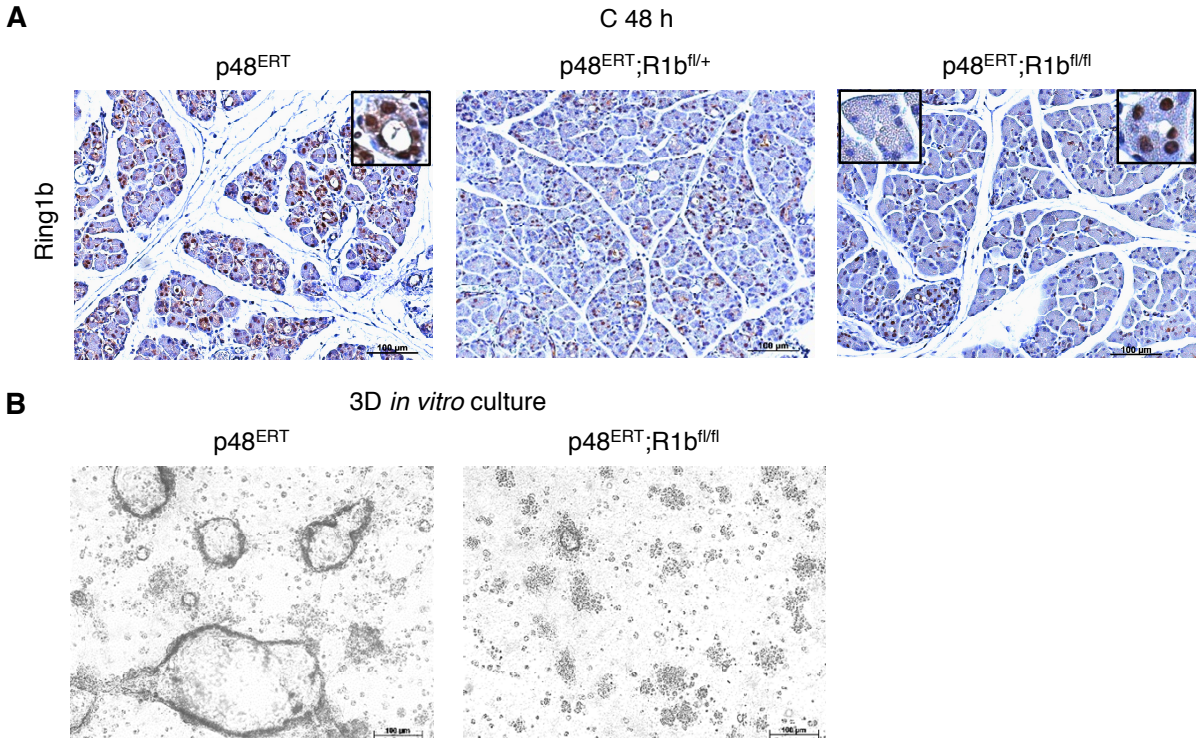

Figure 4.21: Ring1b is required for acinar-to-ductal metaplasia. (**A**) Representative images of Ring1b immunohistochemistry in caerulein-treated p48^{ERT}, p48^{ERT};R1b$^{fl/+}$ and p48^{ERT};R1b$^{fl/fl}$ mice (n=3). Mice were sacrificed after 48 hours after the last caerulein administration. High resolution pictures show ADMs/acini. Scale bars, 100 μm. (**B**) 3D culture of isolated acinar cells from p48^{ERT} and p48^{ERT};R1b$^{fl/fl}$ mice (n=3-4). Representative pictures were taken at day five. Scale bars, 100 μm.

4.3.3.1 Loss of Ring1b in acute pancreatitis impedes the establishment of a progenitor-like expression profile

From the mRNA microarray analysis, it became evident that ADM cells are characterized by a reactivation of progenitor like expression patterns (Figure 4.3, 4.4). To assess if the acquirement of such a profile is compromised in Ring1b-depleted cells, expression of progenitor and differentiation markers was evaluated in tissue of p48^{ERT}, p48^{ERT};R1b$^{fl/+}$ and p48^{ERT};R1b$^{fl/fl}$ mice, sacrificed 48 hours after the last caerulein administration. First, expression of Ring1b was determined by qRT-PCR and Western blot analyses. As expected, expression of Ring1b and presence of H2AK119ub is diminished in p48^{ERT};R1b$^{fl/+}$ and p48^{ERT};R1b$^{fl/fl}$ mice (Figure 4.22 A, 4.22 B). In contrast, levels of H3K4me3 and H3K27me3 remain nearly unchanged within the three groups (Figure 4.22 B).

Importantly, mRNA expression of the acinar-specific progenitor markers *Rbpj* and *Sox9* is significantly decreased in caerulein-treated p48^{ERT};R1b$^{fl/fl}$ mice compared to p48^{ERT} animals. Precisely, the expression values of caerulein-injected p48^{ERT};R1b$^{fl/fl}$ mice are similar to those of NaCl-treated p48^{ERT} animals (p48^{ERT} Ø) (Figure 4.22 C). In regard to the expression of differentiation genes, no great variations can be observed within the three caerulein-treated

groups. This can be explained by the fact that expression of *Rbpjl*, *Mist1* and *Ptf1a* is not repressed at that time point, indicated by the same levels as in the untreated controls (p48^{ERT} Ø) (Figure 4.22 D).

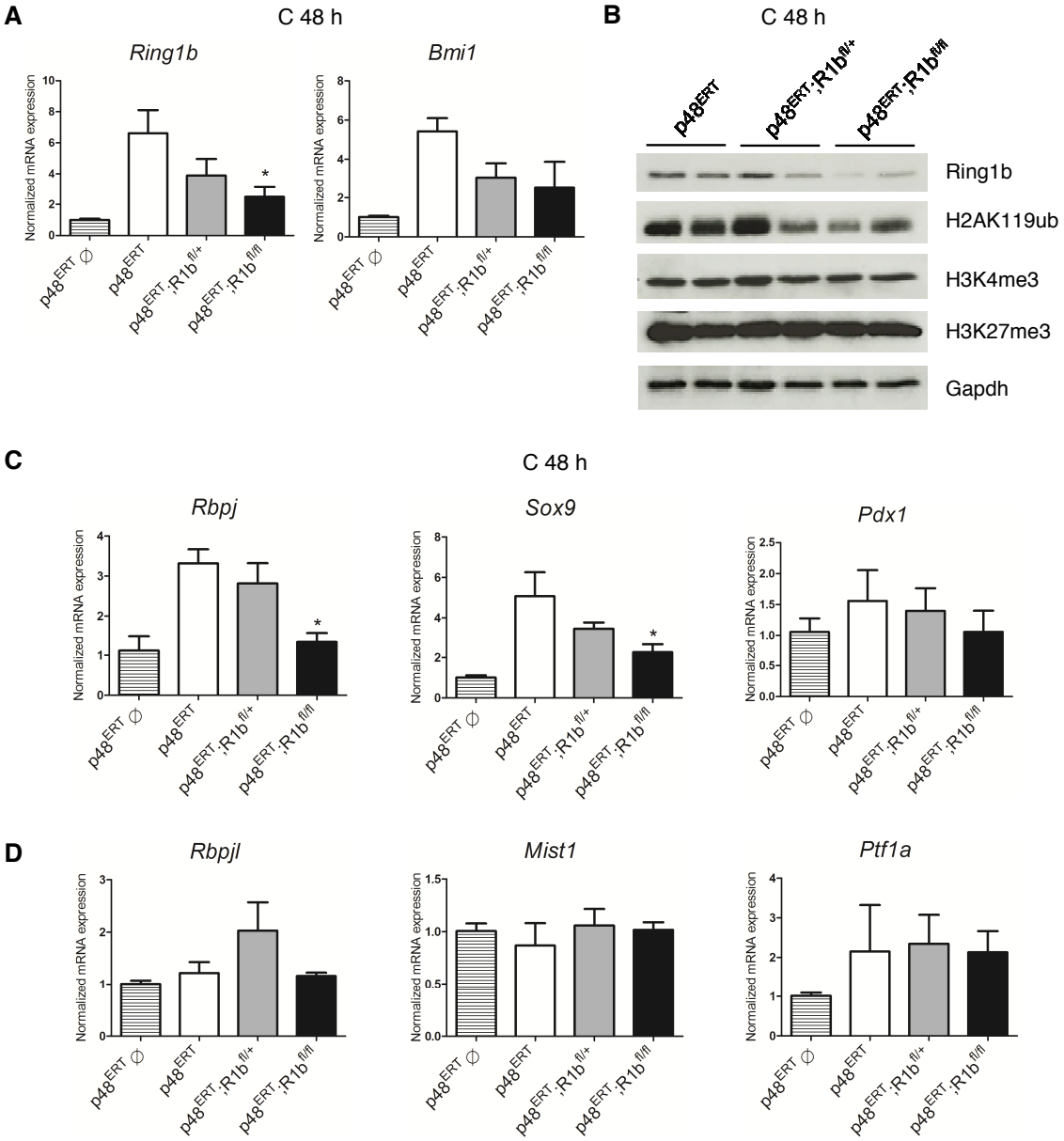

Figure 4.22: Loss of Ring1b constrains the acquirement of a progenitor-like profile during pancreatitis. (**A**) mRNA expression of *Ring1b* and *Bmi1* in bulk tissue of p48^{ERT}, p48^{ERT};R1b$^{fl/+}$ and p48^{ERT};R1b$^{fl/fl}$ mice was validated by qRT-PCR. Mice were sacrificed after 48 hours after the last caerulein or NaCl (p48^{ERT} Ø) treatment. Data are represented as mean ± SEM (n=5). * $P < 0.05$ (two-tailed, unpaired *t*-test, in relation to p48^{ERT} mice). (**B**) Protein levels of Ring1b, H2AK119ub, H3K4me3 and H3K27me3 from bulk tissue lysates of caerulein-treated p48^{ERT}, p48^{ERT};R1b$^{fl/+}$ and p48^{ERT};R1b$^{fl/fl}$ mice (C 48 h) were determined by Western blot. Gapdh serves as the loading control. (**C**) qRT-PCR analysis of indicated progenitor and differentiation genes from bulk tissue of NaCl-treated (p48^{ERT} Ø) p48^{ERT} and caerulein-injected p48^{ERT}, p48^{ERT};R1b$^{fl/+}$ and p48^{ERT};R1b$^{fl/fl}$ mice (C 48 h). Data are represented as mean ± SEM (n=5). * $P < 0.05$ (two-tailed, unpaired *t*-test, comparison to p48^{ERT} mice).

In addition, expression of amylase and Ck19 was analyzed at the 48-hour time point. Here, slightly higher levels of amylase and lower expression of *Ck19* can be detected in p48^{ERT};R1b$^{fl/fl}$ mice. Opposed to the results of the progenitor genes, however, expression levels are not similar to those of untreated mice (Figure 4.23).

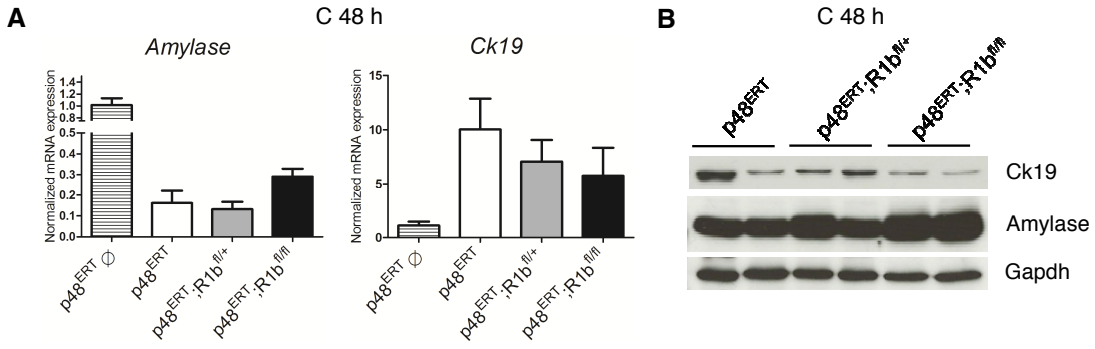

Figure 4.23: Slight differences in acinar and ductal specific markers. (**A**) qRT-PCR analysis to determine mRNA levels of *amylase* and *Ck19* in bulk tissue of NaCl-treated (p48^{ERT} Ø) p48^{ERT} and caerulein-injected p48^{ERT}, p48^{ERT};R1b$^{fl/+}$ and p48^{ERT};R1b$^{fl/fl}$ mice (C 48 h). Data are represented as mean ± SEM (n=5). (**B**) Western blot analysis of indicated proteins from bulk tissue of caerulein-treated p48^{ERT}, p48^{ERT};R1b$^{fl/+}$ and p48^{ERT};R1b$^{fl/fl}$ mice (C 48 h). As a loading control, Gapdh was used.

In summary, results indicate that in the setting of pancreatitis, transient ADM formation is impaired in the Ring1b knockout mouse model. Here, expression analyses show that the expression of progenitor genes is greatly decreased compared to p48^{ERT} mice (Figure 4.22 C). However, at the 48-hour time point, no differences in the expression of differentiation genes, also not in comparison to the untreated controls, are apparent (Figure 4.22 D). According to the study of Kong et al., persistent silencing of differentiation genes occurs in the setting of oncogenic Kras^{G12D}-induced carcinogenesis (Kong et al. 2016). Thus effects of Ring1b-depletion were analyzed in Kras^{G12D}-expressing mice.

4.3.4 Loss of Ring1b attenuates oncogenic Kras^{G12D}-mediated PDAC development

To investigate the influence of Ring1b on persistent ADM formation and PDAC development, oncogenic Kras^{G12D} was additionally expressed in the previously described p48^{ERT} mouse model. Through the administration of tamoxifen, expression of mutant Kras^{G12D} is activated in acinar cells. However, this set-up fails to induce the formation of pancreatic precursor lesions in p48^{ERT};K mice (Figure 4.24). These observations are in line with the study of Guerra et al., which indicated that adult acinar cells are resistant towards neoplastic transformation by oncogenic Kras (Guerra et al. 2007). In addition, no morphological differences were observed in pancreata of p48^{ERT};K, p48^{ERT};K;R1b$^{fl/+}$ and p48^{ERT};K;R1b$^{fl/fl}$ mice (Figure 4.24).

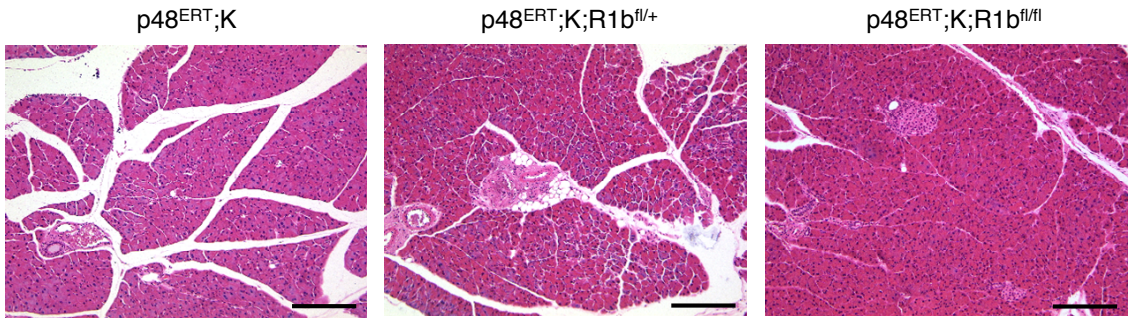

Figure 4.24: Oncogenic Kras^{G12D} expression in an adult stage does not induce the formation of pancreatic precursor lesions. (**A**) Representative H&E stainings of tamoxifen-induced p48^{ERT};K, p48^{ERT};K;R1b$^{fl/+}$ and p48^{ERT};K;R1b$^{fl/fl}$ mice (n=4). Mice were sacrificed at an age of eight weeks. Scale bars, 200 μm.

To induce pancreatic tumor development at an adult stage, oncogenic Kras^{G12D} expression has to be driven in combination with caerulein-induced tissue damage (Guerra et al. 2007). Therefore, in this study, tamoxifen was administered to 5.5- to 6-week-old mice and with an age of 7.5 to 8 weeks, mice were treated with eight hourly injections of caerulein on two consecutive days (Figure 4.16). p48^{ERT};K, p48^{ERT};K;R1b$^{fl/+}$ and p48^{ERT};K;R1b$^{fl/fl}$ animals were sacrificed after 21 days and six months.

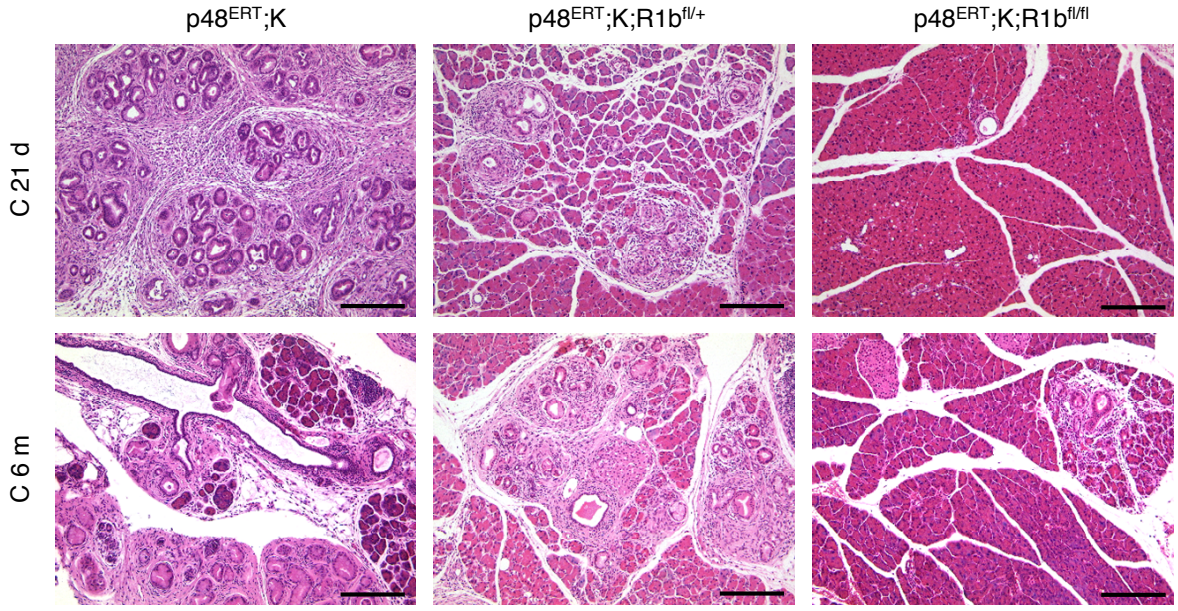

Figure 4.25: Loss of Ring1b impairs mutant Kras^{G12D}-driven development of PDAC precursor lesions. Representative images of an H&E staining of p48^{ERT};K, p48^{ERT};K;R1b$^{fl/+}$ and p48^{ERT};K;R1b$^{fl/fl}$ mice (n=5-6). Tamoxifen was administered at an age of ~ 6 weeks and caerulein was injected according to Figure 4.16. Mice were sacrificed after 21 days or six months. Scale bars, 200 μm.

21 days after the last caerulein injection, great histological differences are evident in p48^{ERT};K compared to p48^{ERT};K;R1b$^{fl/+}$ and p48^{ERT};K;R1b$^{fl/fl}$ mice. p48^{ERT};K mice have

developed ADM and low-grade PanIN lesions and exhibit fibrotic areas and immune cell infiltrations. In contrast, the pancreata of p48^{ERT};K;R1b$^{fl/fl}$ mice barely display any metaplastic transformations or tissue restructurations. In tissue of p48^{ERT};K;R1b$^{fl/+}$ animals scattered lesions, surrounded by immune cells can be found (Figure 4.25).
Six months after the caerulein administration, p48^{ERT};K mice exhibit focal areas with diffuse low-grade, but also high-grade PanIN lesions and minor extents of PDAC. Malignant tissue transformation is also present in p48^{ERT};K;R1b$^{fl/+}$ animals. Here, foci harboring multiple PanINs and stromal reaction can be detected. Notably, in p48^{ERT};K;R1b$^{fl/fl}$ mice, presence and malignancy of PDAC precursor lesions is decreased (Figure 4.25).

4.3.4.1 Presence of PDAC precursor lesions is diminished in p48^{ERT};K;R1b$^{fl/fl}$ mice

To validate whether recombination of the *Kras^{G12D}* and *Ring1b$^{fl/fl}$* locus succeeded, pancreatic tissue of mice, treated with caerulein and sacrificed after 21 days, was analyzed. Here, immunohistochemical stainings show that especially ADM and PanIN lesions of p48^{ERT};K mice are positive for Ring1b. Single precancerous lesions, occurring in p48^{ERT};K;R1b$^{fl/+}$ animals are also positively stained for Ring1b, whereas untransformed acinar cells mainly appear to be negative. This is also the case for the acinar compartment in p48^{ERT};K;R1b$^{fl/fl}$ mice. However, rare ADMs detected in these mice are mostly positive for Ring1b (Figure 4.26 A). This suggests that single recombination of Kras^{G12D} but not of the Ring1b locus could have randomly happened in single cells.
Finally, to verify that Cre-mediated recombination also occurred in p48^{ERT};K;R1b$^{fl/+}$ and in p48^{ERT};K;R1b$^{fl/fl}$ mice**,** immunofluorescence staining of the reporter tdTomato was performed. Indeed, in the majority of acinar cells of p48^{ERT};K;R1b$^{fl/+}$ and p48^{ERT};K;R1b$^{fl/fl}$ mice, tdTomato can be detected, proving that recombination was successful. Remarkably, metaplastic ductal lesions of p48^{ERT};K mice express the fluorescent reporter, validating that acinar cells must give rise to the precancerous ductal structures. As expected, normal ductal epithelium, immune and mesenchymal cells were not stained (Figure 4.26 B).
Moreover, Ring1b knockdown in p48^{ERT};K;R1b$^{fl/+}$ and knockout in p48^{ERT};K;R1b$^{fl/fl}$ mice (C 21 d) was verified by qRT-PCR and Western blot analyses. Compared to p48^{ERT};K mice, a stepwise decrease of Ring1b mRNA and protein levels are apparent in p48^{ERT};K;R1b$^{fl/+}$ and in p48^{ERT};K;R1b$^{fl/fl}$ animals (Figure 4.26 C, 4.26 D). Like in the regeneration model, *Bmi1* expression is also not induced in Ring1b-deficient mice (Figure 4.26 C). In addition, Western blots reveals that presence of the histone modification H2AKub119 is greatly, whereas that of H3K27me3 and H3K4me, is slightly diminished in p48^{ERT};K;R1b$^{fl/+}$ and in p48^{ERT};K;R1b$^{fl/fl}$ mice in comparison to the controls (Figure 4.26 D).

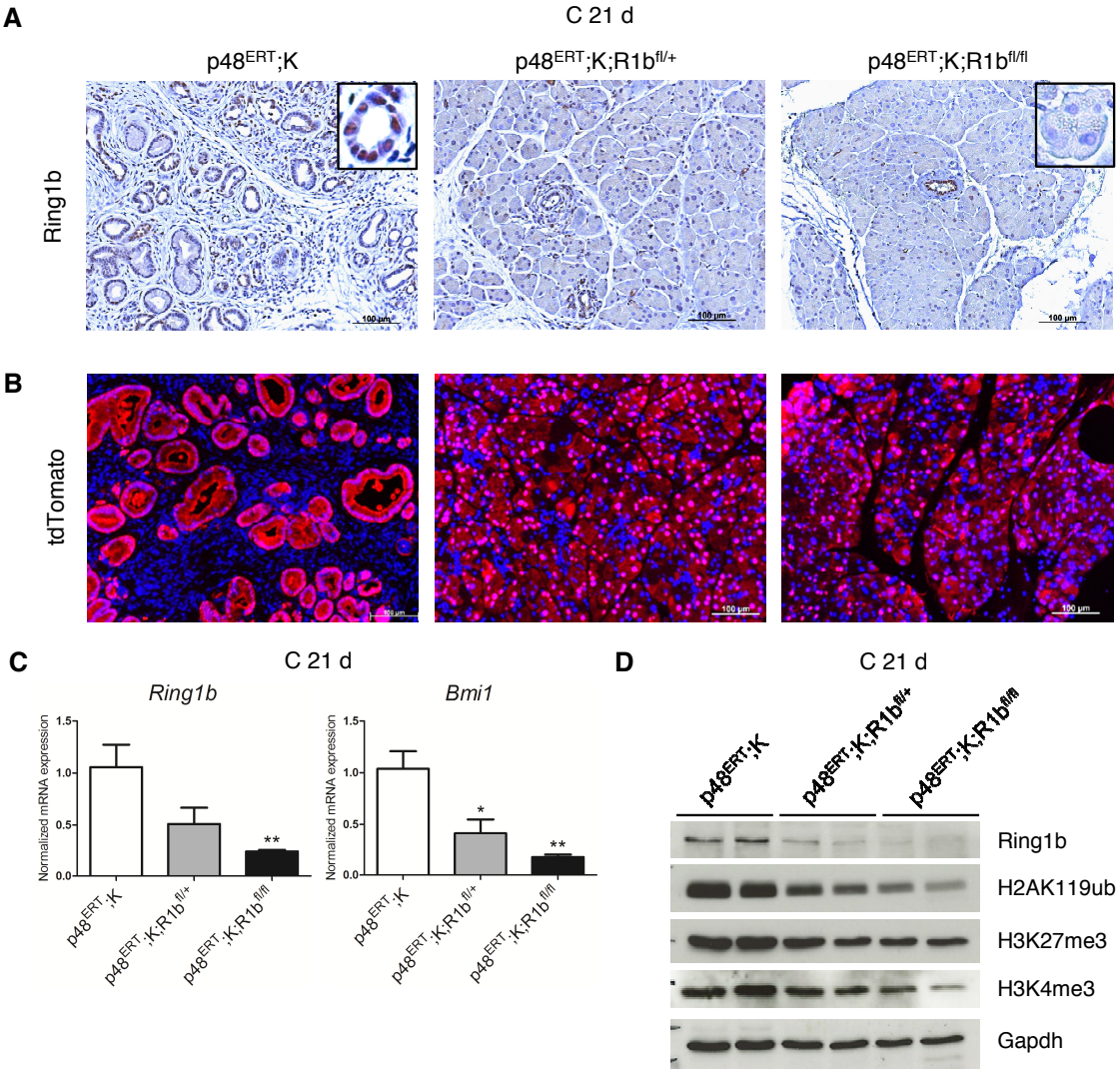

Figure 4.26: Validation of the p48^{ERT};K;R1b$^{fl/fl}$ mouse model. (**A**) Immunohistochemistry staining of Ring1b in caerulein-treated p48^{ERT};K, p48^{ERT};K;R1b$^{fl/+}$ and p48^{ERT};K;R1b$^{fl/fl}$ mice, 21 days after the last caerulein application (C 21 d). Scale bars, 100 μm. (**B**) Representative pictures of tdTomato immunofluorescence staining from p48^{ERT};K, p48^{ERT};K;R1b$^{fl/+}$ and p48^{ERT};K;R1b$^{fl/fl}$ mice (C 21 d). Cell nuclei were counterstained with DAPI. Scale bars, 100 μm. (**C**) mRNA expression of *Ring1b* and *Bmi1* was assessed with qRT-PCR (C 21 d). Data were normalized to p48^{ERT};K mice and are represented as mean ± SEM (n=4). * $P < 0.05$, ** $P < 0.01$ (two-tailed, unpaired *t*-test in relation to p48^{ERT};K mice). (**D**) Immunoblot analysis of bulk tissue protein lysates from caerulein-treated p48^{ERT};K, p48^{ERT};K;R1b$^{fl/+}$ and p48^{ERT};K;R1b$^{fl/fl}$ mice (C 21 d) with indicated antibodies. Gapdh was used as loading control.

Immunofluorescence staining of amylase and Ck19 demonstrate that metaplastic lesions, apparent in caerulein-treated p48^{ERT};K mice (C 21 d), greatly express Ck19 and are nearly negative for amylase, indicating that they have undergone the process of ADM. In contrast, tissue of p48^{ERT};K;R1b$^{fl/+}$ and p48^{ERT};K;R1b$^{fl/fl}$ mice (C 21 d) was barely transformed, marked by a broad amylase staining (Fig 4.27 A). Additionally, overall amounts of Ck19 were quantified. For this, whole tissue specimens were subjected to Ck19 immunohistochemistry, scanned and positive areas were counted with the Aperio ImageScope software. As

expected, in comparison to Ring1b-deficient mice, p48^{ERT};K mice exhibit a higher ratio of positive pixels per area (Figure 4.27 B).

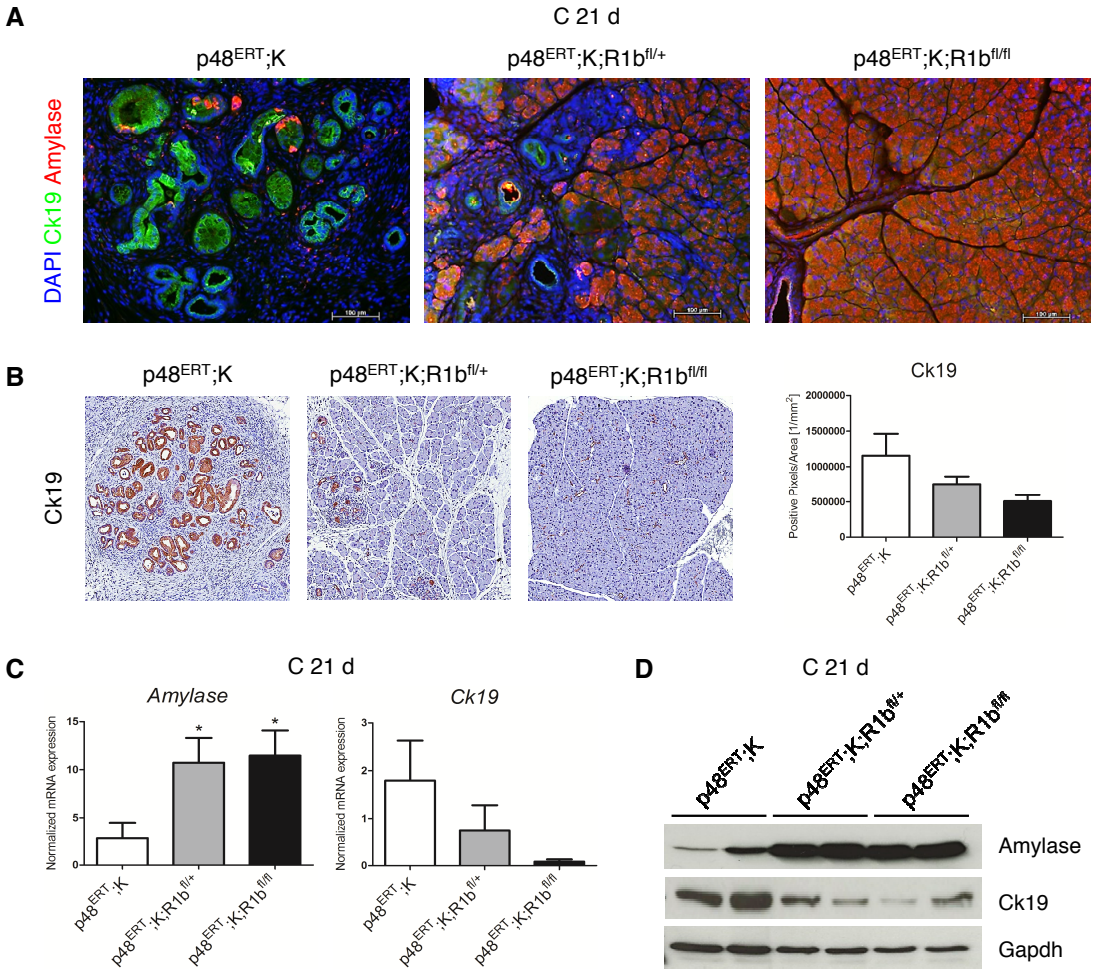

Figure 4.27: Number of ADM and PanIN lesions is reduced in Ring1b-deficient Kras^{G12D} mice. (**A**) Representative immunofluorescence staining of p48^{ERT};K, p48^{ERT};K;R1b$^{fl/+}$ and p48^{ERT};K;R1b$^{fl/fl}$ mice, 21 days after the last caerulein application (n=3). Detection of amylase (red), CK19 (green) and cell nuclei (DAPI, blue). Scale bars, 100 μm. (**B**) Immunohistochemistry staining of Ck19 was performed on tissue of caerulein-treated mice (C 21 d). Whole tissue slides were scanned and positive pixels were counted with the Aperio ImageScope software. Data were calculated as positive pixels per area [1/mm^2] and are shown as mean ± SEM (n=4-6). (**C**) qRT-PCR analysis reveals mRNA expression of *amylase* and *CK19*. mRNA was isolated from pancreatic bulk tissue from caerulein-treated p48^{ERT};K, p48^{ERT};K;R1b$^{fl/+}$ and p48^{ERT};K;R1b$^{fl/fl}$ mice (C 21 d). Data were normalized to p48^{ERT};K mice and are represented as mean ± SEM (n=4). * $P < 0.05$, ** $P < 0.01$ (two-tailed, unpaired *t*-test in relation to p48^{ERT};K mice).

However, limitations of this analysis have to be considered. Since Ck19 is also expressed by cells from the normal ductal lineage and normal tissue composition is greatly disrupted in p48^{ERT};K mice, high background staining was detected in p48^{ERT};K;R1b$^{fl/+}$ and in p48^{ERT};K;R1b$^{fl/fl}$ mice. Moreover, pancreatic tissue area appeared larger in p48^{ERT};K mice due

to fibrotic tissue reaction and immune cell infiltration. This could also influence the calculated ratios. In addition, mRNA and protein levels of amylase and Ck19 of pancreatic bulk tissue were measured with qRT-PCR and Western blot (Fig 4.27 C, 4.27 D). The results support the histological analyses, suggesting that ADM and formation of precancerous lesions is greatly impaired in p48^{ERT};K;R1b$^{fl/+}$ and in p48^{ERT};K;R1b$^{fl/fl}$ mice.

4.3.4.2 Reactivation of progenitor and repression of differentiation genes is impaired in p48^{ERT};K;R1b$^{fl/fl}$ mice

Strikingly, the formation of pancreatic precursor lesions is greatly abrogated in caerulein-treated p48^{ERT};K;R1b$^{fl/fl}$ mice. To assess if this could be due to an impaired establishment of a progenitor-like expression profile, mRNA expression of indicated differentiation and progenitor genes was analyzed (Figure 4.28).

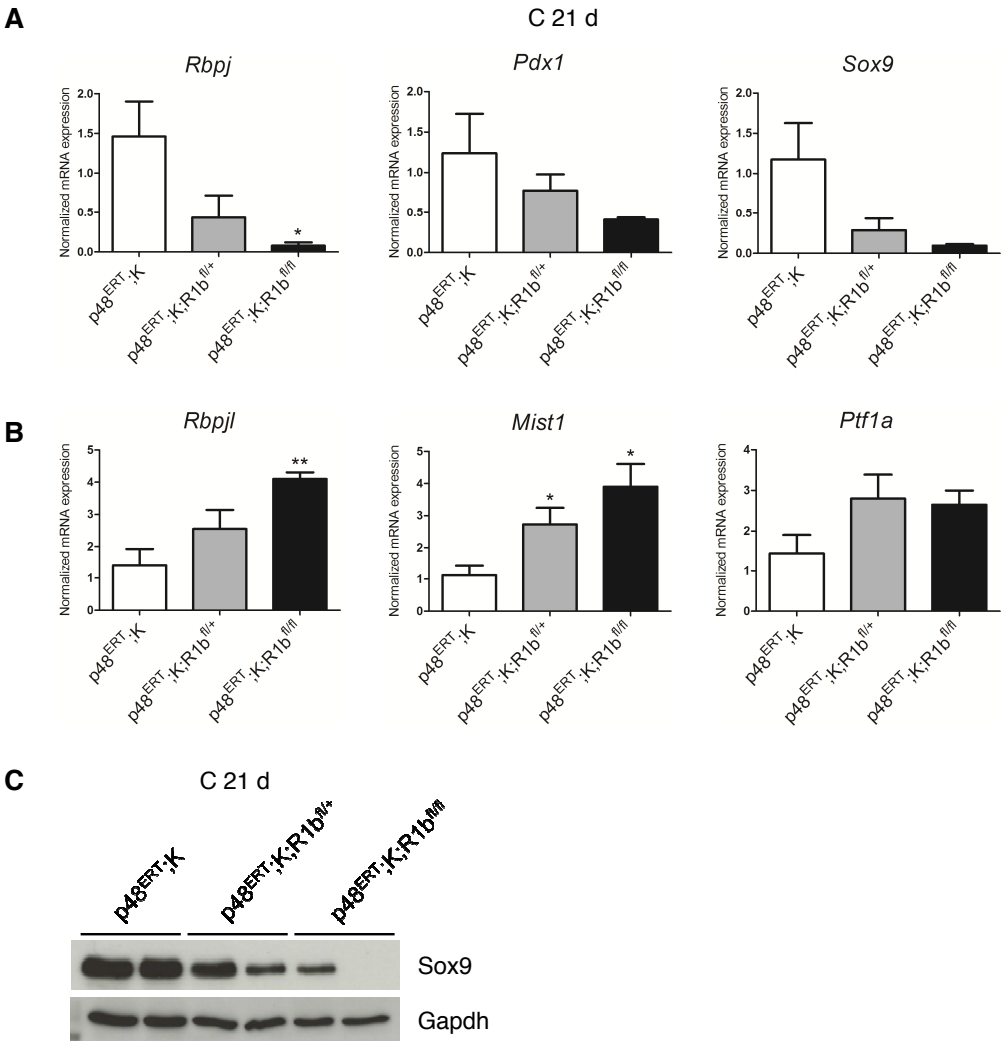

Figure 4.28: Loss of Ring1b compromises the establishment of a progenitor-like state and the repression of differentiation genes. qRT-PCR analysis reveals mRNA expression of pancreatic progenitor genes (**A**) and differentiation markers, such as *Rbpjl*, *Ptf1a* and *Mist1* (**B**). mRNA was extracted from pancreatic tissue of p48^{ERT};K,

p48^{ERT};K;R1b$^{fl/+}$ and p48^{ERT};K;R1b$^{fl/fl}$ mice, sacrificed 21 days after the last caerulein application. Data were normalized to p48^{ERT};K mice and are shown as mean ± SEM (n=4). * $P < 0.05$, ** $P < 0.01$ (two-tailed, unpaired *t*-test in relation to p48^{ERT};K mice).
(**C**) Protein levels of Sox9 in p48^{ERT};K, p48^{ERT};K;R1b$^{fl/+}$ and p48^{ERT};K;R1b$^{fl/fl}$ mice were determined by Western blot. Gapdh was used as a loading control.

Clearly, mRNA expression of the pancreatic progenitor markers, *Rbpj*, *Pdx1* and *Sox9* is less in mice deficient for Ring1b (C 21 d) (Figure 4.28 A). Moreover, protein levels of Sox9 are greatly diminished in these animals (Figure 4.28 C). In comparison to p48^{ERT};K mice, expression of the differentiation markers, *Rbpjl*, *Mist1* and *Ptf1a* is higher in p48^{ERT};K;R1b$^{fl/fl}$ mice (Figure 4.28 B). To analyze if repression of differentiation genes in p48^{ERT};K mice is triggered by H2AK119ub, tdTomato positive cells were sorted out from p48^{ERT};K and p48^{ERT};K;R1b$^{fl/fl}$ mice (C 21 d) (Figure 4.29 A) and ChIP analysis against H2AK119ub was performed. Thus, an enrichment of H2AK119ub can be detected at the promoter site of *Rbpjl* in cells of p48^{ERT};K mice, whereas no accumulation is apparent in p48^{ERT};K;R1b$^{fl/fl}$ mice (Figure 4.29 B). This suggests, that observed repression of *Rbpjl* in p48^{ERT};K mice, could be indeed triggered by H2AK119ub. On the other hand, this could implicate that upon loss of Ring1b, H2AK119ub is not enriched and expression of the differentiation marker *Rbpjl* is concomitantly not suppressed (Figure 4.28 B). Overall, the results implicate that Ring1b is crucial for inducing changes in the transcriptome, which themselves are an important prerequisite for the initiation of PDAC.

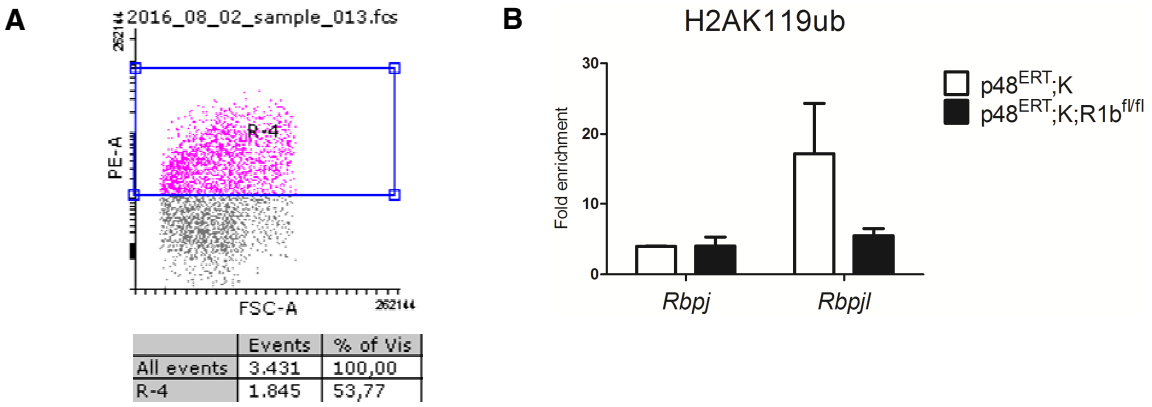

Figure 4.29: H2AK119ub is not enriched at the promoter site of the differentiation gene *Rbpjl* in Ring1b-depleted Kras^{G12D} mice. (**A**) tdTomato positive (recombined) cells were sorted out from caerulein-treated p48^{ERT};K and p48^{ERT};K;R1b$^{fl/fl}$ mice (C 21 d). Sorted cells were immediately transferred into ChIP lysing buffer and ChIP was performed (**B**). ChIP DNA was quantified with qRT-PCR and data are displayed as fold enrichment over IgG control. Data are represented as mean ± SEM (n=2). For every single analysis three mice were used (C 21 d).

In regard to this, it was found that in comparison to p48^{ERT};K mice, expression of further epigenetic remodelers, important in cancer development, such as *Dnmt3a* or the histone

demethylase *Kdm2b*, is not reactivated in Ring1b-deficient mice (C 21 d) (Figure 4.30 A, 4.30 B).

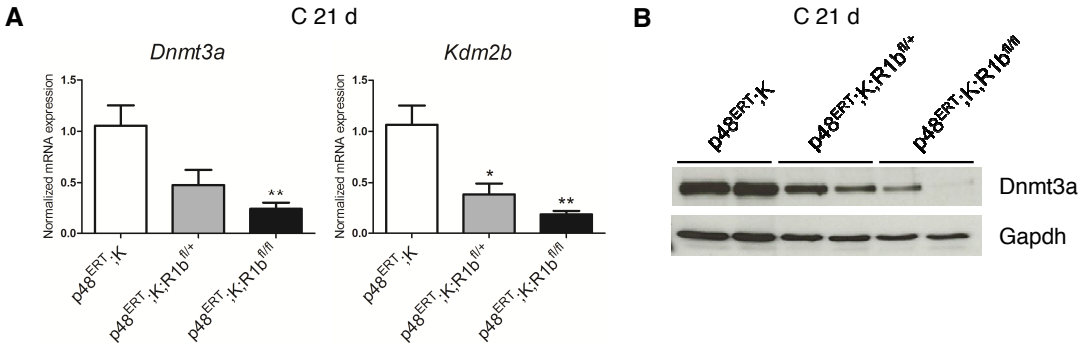

Figure 4.30: Other epigenetic remodelers are less reactivated in p48^{ERT};K;R1b$^{fl/fl}$ mice. (**A**) qRT-PCR analysis to detect mRNA expression of *Kdm2b* and *Dnmt3a* in caerulein-treated p48^{ERT};K, p48^{ERT};K;R1b$^{fl/+}$ and p48^{ERT};K;R1b$^{fl/fl}$ mice (C 21 d). mRNA was isolated from bulk tissue. Data were normalized to p48^{ERT};K mice and are represented as mean ± SEM (n=4). * $P < 0.05$, ** $P < 0.01$ (two-tailed, unpaired *t*-test in relation to p48^{ERT};K mice). (**B**) Western blot analysis of Dnmt3a in whole tissue protein lysates of caerulein-injected p48^{ERT};K, p48^{ERT};K;R1b$^{fl/+}$ and p48^{ERT};K;R1b$^{fl/fl}$ mice (C 21 d). As a loading control, Gapdh was used.

In summary, results indicate that Ring1b can be regarded as one key factor for driving the initiation of PDAC. Moreover, loss of Ring1b can overcome oncogenic Kras^{G12D}- and pancreatitis-induced neoplastic cell transformation.

4.4 Crispr/Cas9-mediated depletion of Ring1b in full-blown pancreatic cancer cells

So far, generated data reveals that re-activation of Ring1b in the setting of pancreatitis and pancreatic carcinogenesis promotes ADM and the establishment of a progenitor-like phenoytpe. Immunohistochemistry staining indicate that Ring1b is not only highly expressed in ADMs and PDAC precursor lesions but also in full-blown tumor cells (Figure 4.9, Figure 4.13). To investigate if the epigenetic remodeler is pivotal for sustaining cancer cells in a dedifferentiated state, Ring1b was knocked out in an isolated cancer cell line from a p48$^{Cre/+}$;LSL-Kras$^{G12D/+}$;Trp$^{53lox/+}$ mouse. For this, the genome editing system, CRISPR/Cas9, was used. Then, single, positively selected cell clones were picked, cultivated and gene knockout was confirmed by Western blot analysis (Ring1b KO no 8, no 17, no 35). In addition, levels of H2AK119ub were found to be reduced in Ring1b-depleted cell lines (Figure 4.31 A, 4.31 B), whereas those of H3K27me3 seem to be not influenced (Figure 4.31 A).

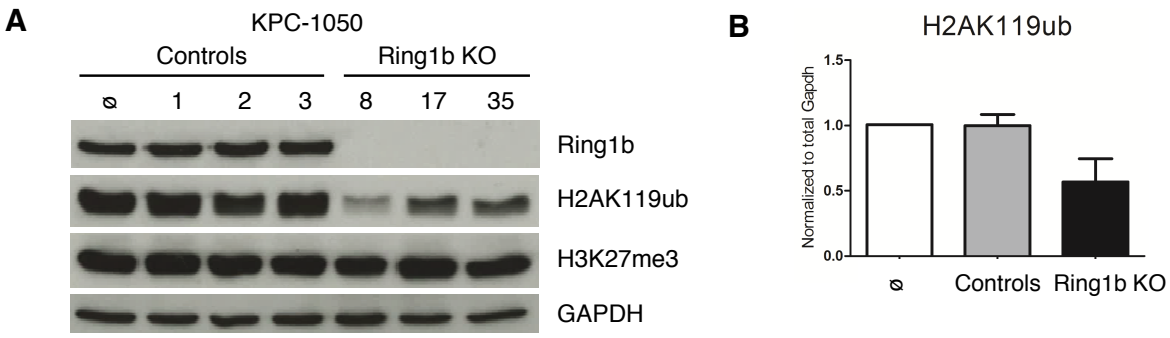

Figure 4.31: CRISPR/Cas9-mediated knockout of Ring1b in cancer cells. (**A**) Protein lysates of Ring1b KO and control clones (KPC-1050 cell line) were analyzed for the presence of indicated antigens by Western blot analysis. Gapdh was used as internal loading control. (**B**) Band intensity of H2AK119ub and Gapdh was determined with ImageJ. H2AK119ub levels were normalized to total Gapdh and are represented as mean ± SEM (n=3).

4.4.1 Large-scale gene expression analysis of Ring1b KO cancer cells

In a further approach, gene expression profiles of Ring1b KO clones and control clones were determined by mRNA microarray analysis. Genes, which showed a fold change of more than 1.5 in at least two Ring1b KO clones, were selected and functionally annotated through the generation of GO terms and KEGG pathway analysis. The majority of GO terms with genes up-regulated in Ring1b KO cells are associated with developmental processes (29 %), such as epithelium development (Figure 4.32 A). Interestingly, expression of the transcription factors *Klf4* or *Prrx1*, is elevated in Ring1b KO cells. In the *in vitro* carcinogenesis model, high mRNA levels of *Klf4* and *Prrx1* were detected in 3D-ADM, but not in cancer cells (Figure 4.3). Together with this observation and the increased expression of genes related to the epithelial cell lineage, data may indicate that Ring1b KO cells have a higher differentiation status. Moreover, amongst others, the GO term 'positive regulation of cell differentiation' was generated (Figure 4.32 A).

GO terms, assigned from genes down-regulated upon Ring1b knockout, are mainly linked to DNA organization (26 %) (Figure 4.32 B). Remarkably, a broad range of genes encode for histone proteins. Fifteen percent of GO terms, down-regulated in Ring1b KO cells are related to immune response (Figure 4.32 B). For instance, expression of the chemokines *Cxcl5* (C-X-C motif chemokine ligand 5) or *Cxcl3* was found to be decreased.

A GO Terms up-regulated in Ring1b KO cells

GO term	P-Value	Genes
Epithelium development	1.20E-04	***EGFR***, *BMP2, RET, PTGS1, JAG2, PTK7, GJA1, FZD3, FZD2, PAX3, SCEL, RGMA, IRF6, ALDH1A3, ZIC5, SIX1, SEMA3C, TWIST1*
Regulation of transcription from RNA polymerase II promoter	0.001	*E2F6, ONECUT3, CBX4,* ***PRRX1****, PAX3, TCF7L1, PLAGL1, GATA2, LBH, BCOR, PRL2C2, MAF, TXNIP, BMP2, SATB2, EPAS1, OTX1, TLE4, TEAD2, MED13L, SIRT1, DLX2, DLX1, NCOA1, SIX1, FOXC1,* ***KLF4***
Positive regulation of cell differentiation	0.016	*FGF18, WNT7B, BMP2, PLXNB1, TIAM1, EOMES, ITPKB, ADA, NGF, PRL2C2*

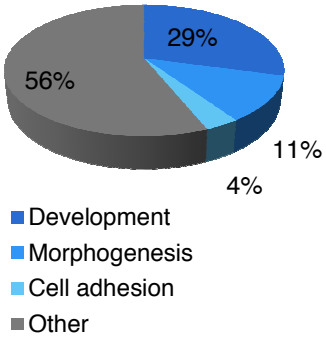

B GO Terms down-regulated in Ring1b KO cells

GO term	P-Value	Genes
Chromatin organization	0.003	*H1F0, ING4, HIST1H2BC, HIST1H2BG, HIST1H2BM, HIST2H2BE,* ***RNF2****, HIST1H2BJ, HIST1H3A, HIST1H2AI, HIST1H3B, HIST1H3C, HIST3H2A, HIST1H3D, HIST1H4D, HIST1H3E, HIST1H3G, HIST1H4H*
Immune response	0.003	*NLRC4, C4BP, NUPR1,* ***CXCL5****, CCL20, CFB,* ***CXCL3****, CFI, LBP, CD14*

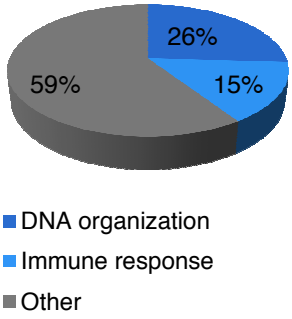

Figure 4.32: Functional annotation of genes, which are differentially expressed in Ring1b KO cells. (**A**) GO terms were generated for genes up-regulated (fold change of > 1.5) in Ring1b KO cells (3 different cell clones) in comparison to control cells (3 different cell clones) with DAVID 6.7. Percentage distribution of GO terms is visualized in the pie chart. (**B**) Selected GO terms down-regulated in Ring1b KO cells (fold change of > 1.5). Overall distribution was quantified in percent and is represented in the pie chart.

4.4.2 Ring1b supports chemoresistance of pancreatic cancer cells

Importantly, the KEGG pathways "metabolism of xenobiotics by cytochrome P450", "drug metabolism" or "glutathione metabolism" were annotated for genes, down-regulated in Ring1b KO cells. Here, the genes *Gstt1* (*Glutathione S-transferase theta 1*) and *Gsta4* (*Glutathione S-transferase alpha 4*) were assigned (Figure 4.33 A). Bai et al. previously published that expression of *Gstt1* in pancreatic cancer cells correlates a with chemoresistance to gemcitabine (Bai, Sata, and Nagai 2007). Therefore, sensitivity of Ring1b KO and control clones to gemcitabine was assessed using the MTT assay. As indicated by Figure 4.33 B, Ring1b KO cells are more sensitive towards gemcitabine, suggesting that Ring1b influences chemoresistance in pancreatic cancer cells (data were kindly provided by Sabrina Deubler) (Deubler 2016).

A

KEGG pathway	P-Value	Genes
Drug metabolism	2.06E-06	*GSTA1, CYP2C65, GSTA4, CYP3A13, UGT2B34, CYP2C68, GSTT1, CYP2D26, ALDH3A1, MGST2*
Glutathione metabolism	0.009	*GSTA1, GSTA4, GSTT1, IDH1, MGST2*

B

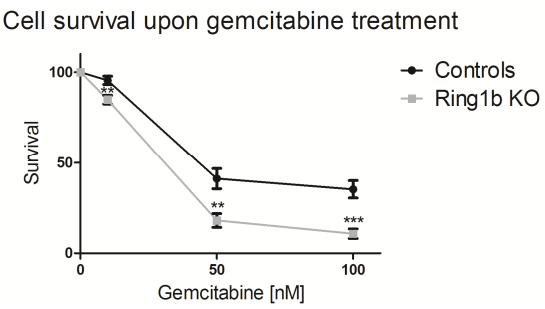

Figure 4.33: Ring1b contributes to the chemoresistance of pancreatic cancer cells. (**A**) Identified KEGG pathways of genes, down-regulated in Ring1b KO cells. (**B**) Sensitivity of control and Ring1b KO cell clones (n=3) to gemcitabine was determined with the MTT assay. For this, equal amount of cells were seeded and treated with 10, 50 and 100 nM of gemcitabine. MTT reagent was added after 72 hours. Experiments were performed and data were kindly provided by Sabrina Deubler. Data are represented as mean ± SEM (n=9). ** $P < 0.01$, *** $P < 0.001$ (two-tailed, unpaired *t*-test in relation to control clones).

4.4.3 Analysis of the tumor initiation capacity of Ring1b KO clones *in vivo*

To assess the tumor initiation capacity and growth of Ring1b KO cells *in vivo*, cells were orthotopically transplanted into the pancreata of WT mice. Transplantation of Ring1b KO cells leads to the formation of small tumors. Hence, slight differences are evident in the pancreas to body weight ratio (Figure 4.34 A). As an indicator of cancer cell metastasis, circulating epithelial cells were isolated from the blood and cultivated *in vitro* for six days. Representative images demonstrate that from mice, which received Ring1b KO cells, nearly no epithelial cells attached and grew *in vitro* (Figure 4.34 B).

A

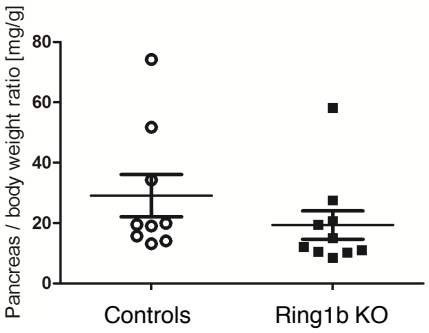

B

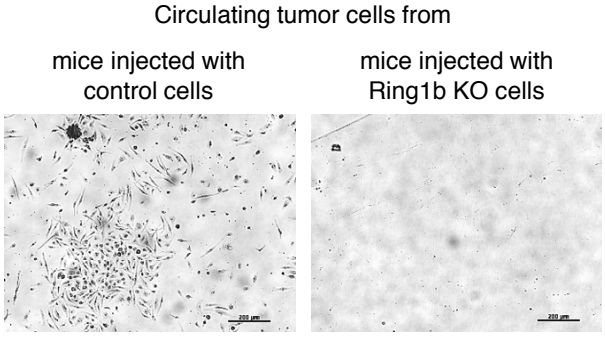

Figure 4.34: Ring1b KO cells initiate slightly smaller tumors. (**A**) Pancreas to body weight ratio was calculated for WT mice, which received orthotopic injection of Ring1b KO or control cells, respectively. Mice were sacrificed after 19 days. (**B**) Circulating epithelial cells were isolated from the blood of operated mice and cultivated for six days *in vitro*. Scale bars, 200 μm.

In summary, when Ring1b was knocked out in full-blown tumor cells, cancer cell dedifferentiation may be impaired. Moreover, tumorigenic characteristics, such as chemotherapeutic resistance or tumor initiation are slightly diminished in Ring1b KO cells.

4.5 PRC1 as a druggable target

Analysis of Ring1b knockout mice in the setting of pancreatitis and tumor development demonstrated that the epigenetic remodeler is crucial for the initiation of neoplastic tissue transformation and PDAC development. Moreover, when Ring1b was depleted in tumor cells, cells turned out to be more sensitive towards gemcitabine. Thus, Ring1b could be suited as a potential therapeutic target for PDAC. Fortunately, the compound 2-pyridine-3-yl-methylene-indan-1,3-dione (*PRT4165*) was previously identified as a potent inhibitor of PRC1 and of Ring1b mediated histone ubiquitination (Alchanati et al. 2009, Ismail et al. 2013).

4.5.1 PRT4165-mediated inhibition of PRC1 causes impaired ADM formation *in vitro*

To investigate if application of PRT4165 could impede ADM formation *in vitro*, collagen-embedded acinar cells were treated with the PRC1 inhibitor. Treatment was started on the first day of the 3D culture and was maintained until the last day. As illustrated by the immunofluorescence staining, ADM formation is not completely blocked upon treatment (Figure 4.35 A). However, the size of ADMs is significantly diminished (Figure 4.35 A, 4.35 E). Moreover, less nuclei positive for H2AK119ub (red) and especially for BrdU were detected in treated cultures (Figure 4.35 A, 4.35 C, 4.35 D). Interestingly, in control ADM cells, 80 % of cells which are positive for BrdU, are also co-stained for H2AK119ub (Figure 4.35 B). This suggests, that presence of H2AK119ub could positively influence the proliferative capacity of ADM cells.

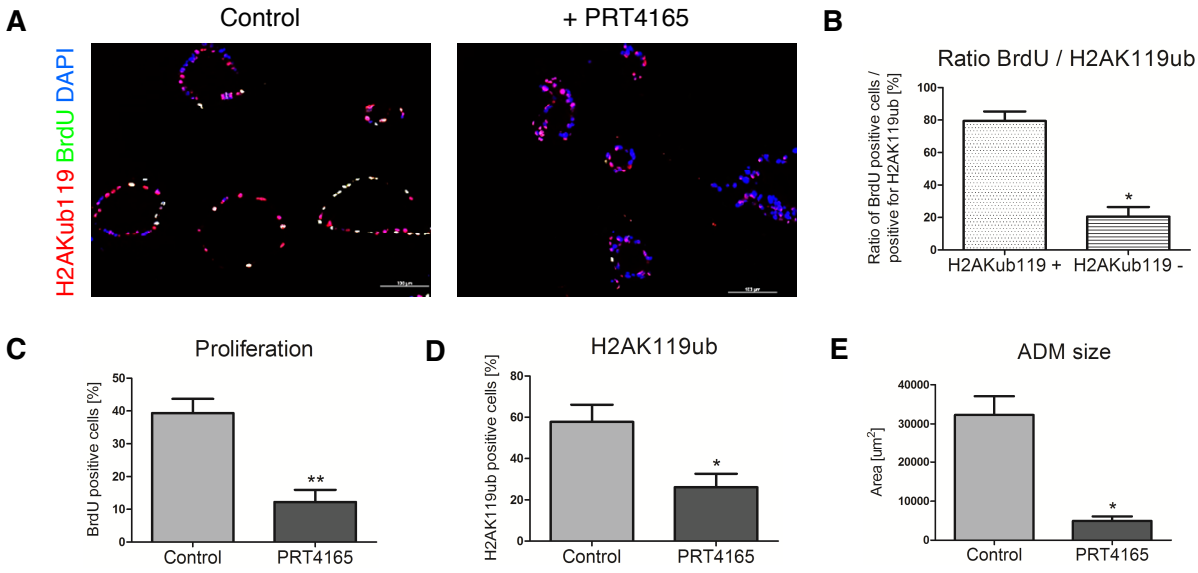

Figure 4.35: Application of the PRC1 inhibitor PRT4165 impairs ADM formation *in vitro*. (**A**) Representative images of immunofluorescence co-staining of H2AKub119 (red) and BrdU (green) of control and PRT4165 (100 μM) treated 3D-ADMs. Nuclei are stained with DAPI. Scale bar, 100 μm. To quantify the staining, five representative pictures were taken per sample and evaluated. (**B**) Quantification of BrdU positive cells and correlation to H2AK119ub status of control 3D-ADMs, as well as the assessment of BrdU (**C**) and H2AK119ub (**D**) positive cells in control 3D-ADMs compared to PRT4165 treated cultures. Data are represented as mean ± SEM (n=3). * $P < 0.05$, ** $P < 0.01$ (two-tailed, paired *t*-test). (**E**) Size of control and treated 3D-ADMs was determined by measuring the area with the ImageJ software. For this, five representative pictures of H&E staining were analyzed per sample. Data are represented as mean ± SEM (n=3). * $P < 0.05$ (two-tailed, paired *t*-test).

4.5.2 Short-term inhibition of PRC1 in cancer cells causes changes in gene expression

In a further approach, cancer cells were treated with PRT4165 to assess if this could lead to changes in the expression of acinar differentiation and progenitor markers. First, to identify the most appropriate treatment period, cells were lysed after different time points and the amount of H2AK119ub was assessed via Western blot. After six hours of treatment, H2AK119ub levels were found to be greatly reduced, identifying the most efficient time point (Figure 4.36 A).

Thus, PRT4165 was applied to KC as well as KPC cells (data not shown) for six hours and mRNA expression of differentiation and progenitor genes was measured. In comparison to control cells, treatment leads to an increased expression of the acinar-specific enzymes, such as *amylase* or *elastase1* or the differentiation marker *Mist1* (Figure 4.36 B). Here, only differentiation genes showing stable C_t expression values were considered. On the other

hand, expression of the progenitor genes, *Rbpj*, *Pdx1* and *Hes1* is decreased upon treatment (Figure 4.36 C).

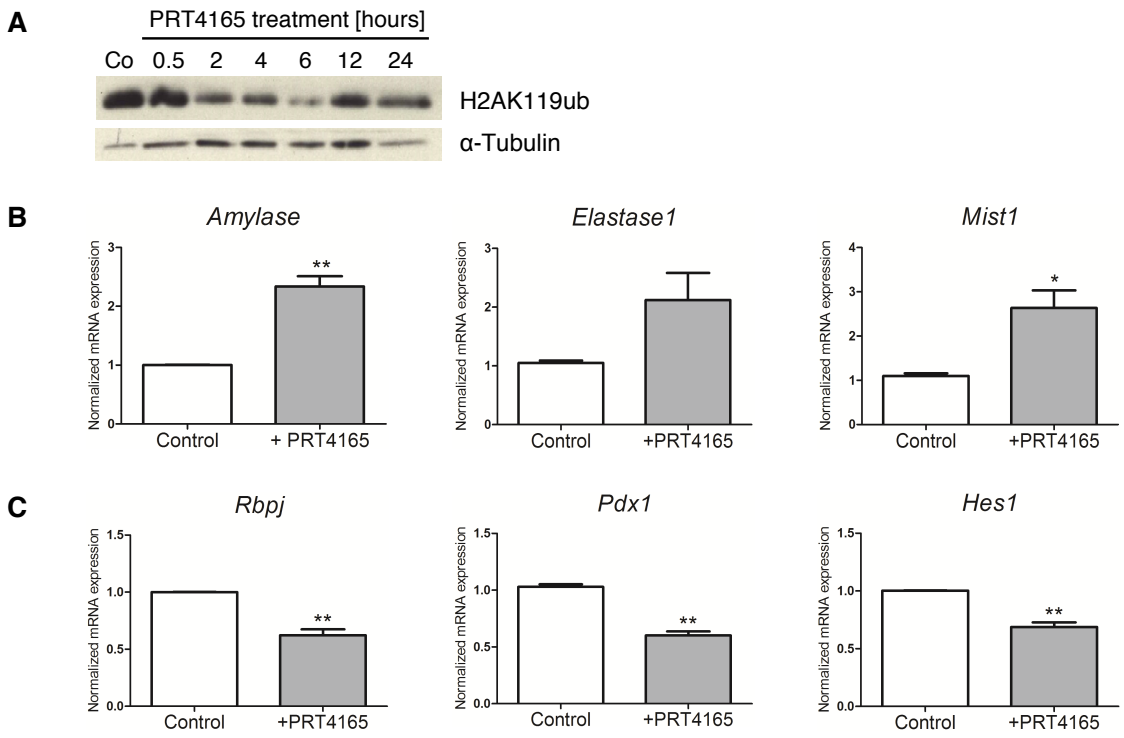

Figure 4.36: Treatment of pancreatic cancer cells with PRT4165 leads to transient changes in gene expression. (**A**) Immunoblots of H2AK119ub and the housekeeper α-Tubulin of protein lysates from cancer cells (KC-921). Cells were treated with 100 μM of PRT4165 and lysed at indicated time points. (**B, C**) qRT-PCR analysis of selected acinar differentiation (**B**) and progenitor genes (**C**) in control (DMSO) and PRT4165 (100 μM) treated KC cells. mRNA was isolated after 6 hours. Data were normalized to control group and are represented as mean ± SEM (n=4). * $P < 0.05$, ** $P < 0.01$ (two-tailed, paired *t*-test in relation to control groups).

In summary, inhibition of PRC1 with the chemical compound PRT4165 causes reduced ADM formation and to a slight reactivation of acinar differentiation genes *in vitro*. In the future, PDAC mouse models will be treated with the inhibitor to assess if inhibition of Ring1b has to the potential to decrease PDAC development *in vivo*. However, *in vitro* data indicate that inhibition of PRC1 could be beneficial for treating pancreatic cancer.

5 Discussion

By 2030, it is predicted that pancreatic cancer will be the second leading cause of cancer-related deaths in the US (Rahib et al. 2014). Thus, a great effort has to be made to improve diagnostic and therapeutic opportunities, as well as the research to define tumor-initiating events, risk factors and key drivers of pancreatic cancer.

The most prevalent malignancy of the exocrine pancreatic tissue is the pancreatic ductal adenocarcinoma (PDAC) (Becker et al. 2014). Previous studies suggest that initiation of PDAC is caused by a reprogramming of digestive enzyme-producing acinar cells into cells with a duct-like phenotype (Kopp et al. 2012, Strobel et al. 2007, Guerra et al. 2007), demonstrating the immense cellular plasticity of acinar cells. The process of acinar-to-ductal metaplasia (ADM) is believed to be an important prerequisite for the formation of pancreatic precursor lesions, such as pancreatic intraepithelial neoplasia, and PDAC (Guerra et al. 2007, Zhu et al. 2007). Amongst others, ADM occurs in the setting of pancreatitis, a major risk factor for PDAC (Lowenfels et al. 1993). Acinar-to-ductal reprogramming is accompanied by a reactivation of progenitor genes, and a concomitant down-regulation of acinar specific differentiation genes, such as *amylase* (Jensen et al. 2005). In the setting of inflammatory ADM, ADM and transcriptional changes are transiently induced (Jensen et al. 2005). Moreover, ADM can be stably generated upon oncogenic Kras expression in embryonic acinar cells or in combination with pancreatitis in adult acinar cells in mice (Guerra et al. 2007). Actually, activating genetic alterations of the *Kras* gene were identified as the main drivers for pancreatic carcinogenesis (Hingorani et al. 2003, Collins et al. 2012). Importantly, when oncogenic Kras is expressed in metaplastic cells, the process of ADM is not reversible and transcriptional changes are persistent (Guerra et al. 2007, Kopp et al. 2012). As a result, PDAC development is manifested. In pancreatic cancer, expression of progenitor genes, such as of *SOX9* (Shroff et al. 2014), and repression of acinar differentiation genes is maintained (Johnson et al. 2012, Torres et al. 2013). Since the initiation and progression of PDAC is characterized by broad changes in gene expression and the acquirement of progenitor-like transcriptional programs, the presented project investigates if in addition to genetic alterations, also epigenetic remodeling could contribute to the neoplastic reprogramming of acinar cells. Indeed, epigenetic silencing of the tumor suppressor gene *P16* through DNA methylation was already described in 1997 (Schutte et al. 1997), but until now, very few studies identifying an epigenetic deregulation in pancreatic cancer, have been published.

5.1 Characterization of transcriptional changes in pancreatic carcinogenesis

PDAC precursor lesions and ADM are hallmarked by their duct-like morphological appearance (Hruban, Maitra, and Goggins 2008, Means et al. 2005) and the concomitant expression of progenitor-like transcriptional programs (Kopp et al. 2012, Prevot et al. 2012, Jensen et al. 2005), which is also apparent in cancer cells (Shroff et al. 2014). In the literature, the first metaplastic event in the sequence of pancreatic carcinogenesis, ADM, has been defined either as cellular dedifferentiation (Jensen et al. 2005) or transdifferentiation (Means et al. 2005, Houbracken et al. 2011). Until now, the overall expression profile of ADM cells has not been characterized, thus, not completely ruling out that acinar cells undergo the one or the other process. Analyzing a multi-step *in vitro* PDAC carcinogenesis model, consisting of homogenous cell fractions of differentiated adult acinar cells, acinar-to-ductal metaplasia (3D culture) and cancer cells (isolated from a p48Cre;LSL-Kras^{G12D} mouse) reveals that expression of progenitor genes is reactivated in cancer cells, as well as in 3D-ADM cells. Concomitantly, expression of the acinar cell fate genes *Ptf1a*, *Mist1* and *Rbpjl* is repressed (Benitz et al. 2016). These results suggest that the acquisition of a progenitor-like expression program is already induced in ADM cells and maintained in pancreatic cancer cells. Hence, to identify if pancreatic cancer initiation is recapitulated by a reprogramming of acinar cells towards a progenitor-like state, mRNA microarray analysis of the *in vitro* model and of acinar progenitor cells (E18.5) was carried out. In regard to cellular heterogeneity of tissue samples (Kong et al. 2016), the analysis of the *in vitro* model allows the establishment of pure expression profiles.

Principle component analysis and annotation of differentially expressed genes demonstrates that the transcriptional program of embryonic acinar cells has great similarities to that of 3D-ADM cells. Here, the majority of up-regulated genes was grouped into GO terms associated with development and morphogenesis (47 %). For instance, expression of *Klf4*, a transcription factor crucial for ES cell pluripotency and terminal cell differentiation (Zhang et al. 2010, Katz et al. 2002), was found to be up-regulated. A recent study highlighted that over-expression of Klf4 induces the expression of Ck19 and thereby favors ADM and Kras^{G12D}-dependent tumor formation (Wei et al. 2016). Moreover, expression of *Gli3*, an important effector of the Sonic hedgehog signaling pathway mediating embryonic organogenesis and pattern formation (Coy et al. 2011), is reactivated in 3D-ADM cells. In addition, expression of *Hoxa5* is elevated. Amongst others, Hoxa5 is crucial for the development of axial structures (Jeannotte et al. 1993). This proposes, that 3D-ADM cells do not only reactivate transcription factors influencing acinar cell fate, but also those, which mediate early embryonic morphogenesis .

GO terms, solely up-regulated in 3D-ADM cells, are amongst others linked with developmental processes, such as gland and epithelium development, cell death and regulation of the MAP kinase signaling pathway. Interestingly, GO terms associated with the "negative regulation of cell death" were generated, claiming that overcoming cell death mechanisms could be regarded as an early event in PDAC development (Esposito et al. 2007). In accordance, up-regulation of anti-apoptotic genes in 3D-ADM cells has been previously described and is associated with stimulated NF-kB signaling (Liou et al. 2013). Positive regulation and stimulation of the Raf/Mek/Erk pathway is crucial for ADM formation (Shi et al. 2013). In this study, activation of the pathway was probably caused by the addition of TGF-α to the embedded wildtype acinar cells, which is indispensable for proper ADM formation (Shi et al. 2013). Interestingly, GO terms associated with phosphorylation are concomitantly elevated in 3D-ADM and cancer cells. Here, the MAP kinases Mapk3 (Erk1) and Mapk8 (Jnk1), as well as the Egf receptor were assigned. Moreover, the GO term "epidermal growth factor receptor signaling pathway" was annotated for genes up-regulated in 3D-ADM and cancer cells. Over-expression of Egfr was also identified in ADM and PanIN lesions of p48;$Kras^{G12D}$ mice *in vivo*. Moreover, collagen-embedded $Kras^{G12D}$;$Egfr^{KO}$ acinar cells do not undergo complete ADM (Ardito et al. 2012), highlighting the importance of Egfr signaling for pancreatic carcinogenesis. Interestingly, further similarities regarding over-expressed genes in 3D-ADM and cancer cells are amongst others related to the GO terms 'cell migration', 'cell motility' or 'blood vessel morphogenesis'.

Overall, genes up-regulated in 3D-ADMs were mostly assigned to embryonic development, morphogenesis, cell cycle progression, DNA organization and cell death. Since no GO terms were found, which are related to ductal cells, it has to be assumed that acinar cells do not trans-differentiate into the ductal cell lineage during ADM. On the one hand, qRT-PCR analysis show an elevated expression of progenitor markers, such as *Pdx1, Rbpj* or *Hes1*. On the other hand, expression of the ductal marker *Ck19* is highly increased in the ADM cells. Since transdifferentiation is defined as direct conversion of one cell lineage into another without the acquisition of an intermediate pluripotent state (Graf and Enver 2009), acinar-to-ductal metaplasia has to rather be regarded as cellular dedifferentiation into a progenitor-like cell with a duct-like appearance.

Remarkably, it was previously shown that embryonic acinar and ADM cells, but not adult acinar cells, are receptive to oncogenic $Kras^{G12D}$ transformation (Guerra et al. 2007). Thus, in the presented project it has been hypothesized that the existence of a progenitor-like transcriptome, a common factor between embryonic acinar and ADM cells, could be an

important prerequisite for oncogenic Kras-induced cellular transformation and pancreatic carcinogenesis.

Genes, solely up-regulated in pancreatic cancer cells (data not shown), were annotated to RNA processing (21 %), cell cycle processes (16 %) and DNA repair (3 %). Recently, over-expression of RNA processing and splicing components was detected in poorly differentiated NSCLC (non-small cell lung cancer) cells, associated with alternative splicing events favoring tumor progression (Geles et al. 2016). For instance, the genes *Dkc1* and *Npm1* (Geles et al. 2016) were also found to be increasingly expressed in pancreatic cancer cells, delineating a further possible mechanism for promoting PDAC.

Importantly, besides the reactivation of progenitor-like and cancer cell-specific genes, pancreatic carcinogenesis is accompanied by a down-regulation of acinar differentiation genes (Benitz et al. 2016, Krah et al. 2015). Here, GO terms associated with acinar enzymes, metabolic and catabolic processes were annotated. Moreover, expression of *Ptf1a* and *Rbpjl*, essential transcription factors for acinar cell maturation (Beres et al. 2006), is decreased in 3D-ADM and cancer cells (Benitz et al. 2016). Until now, responsible mechanisms for acinar reprogramming have remained largely elusive. Krah et al. revealed that the loss of the acinar cell fate determinant Ptf1a in an adult stage induces acinar-to-ductal metaplasia and potentiates $Kras^{G12D}$-mediated carcinogenesis (Krah et al. 2015). Moreover, $Kras^{G12D}$-dependent pancreatic tumor formation is accelerated in mice deficient for Mist1 (Shi et al. 2009). Thus, these studies demonstrate that the silencing of acinar cell fate genes promotes ADM and PDAC carcinogenesis. However, the mechanisms causing gene repression have not been unveiled.

5.2 Silencing of acinar differentiation genes in the sequence of pancreatic carcinogenesis is supported by epigenetic mechanisms

As indicated by the mRNA microarray data, expression of chromatin modifiers is elevated in acinar progenitor, 3D-ADM and cancer cells. Here, DNA methyltransferases, histone deacetylases and the catalytic subunits of the Polycomb repressive complexes (PRCs), all of them causing transcriptional repression, were annotated. For instance, in ES cells, PRCs are associated with ES cell self-renewal and pluripotency through the repression of genes, which are responsible for cell-fate commitment and differentiation (Lee et al. 2006, Boyer et al. 2006, van der Stoop et al. 2008). Moreover, Xie et al. demonstrated that pancreatic endocrine cell differentiation is driven by a dynamic and temporal remodeling of H3K27me3 levels at cell-fate determining genes (Xie et al. 2013). Since reactivated expression of Polycomb repressor complexes in 3D-ADM and cancer cells correlates with a repressed

expression of acinar cell fate genes, it was speculated whether acinar gene silencing is introduced through epigenetic mechanisms (Benitz et al. 2016).

In this project, increased expression levels of *Ezh2*, the catalytic subunit of PRC2, as well as of the PRC1 components *Ring1b* and *Bmi1*, were detected in 3D-ADM and cancer cells of the *in vitro* model. Moreover, H2AK119ub, the histone modification catalyzed by PRC1, is greatly enriched (Benitz et al. 2016). These results are in line with previous studies, which showed that Ring1b, H2AK119ub and Ezh2 are elevated in pancreatic precursor lesions and PDAC (Martinez-Romero et al. 2009, Chen, Chen, et al. 2014). However, for the PRC2-dependent modification, H3K27me3, no broad variations were identifed in the *in vitro* carcinogenesis model. However, this does not rule out the possibility that H3K27me3 could be remodeled dynamically at different gene loci (Benitz et al. 2016).
To assess, if remodeling of histone patterns occurs at the promoter sites of the acinar differentiation genes *Ptf1a* and *Rbpjl* during pancreatic carcinogenesis, chromatin immunoprecipitation against H2AK119ub, H3K27me3 and the activating histone mark H3K4me3 was performed. The repressive histone modifications H3K27me3 and H2AK119ub are greatly enriched at the promoter sites of *Rbpjl* and *Ptf1a* in cancer cells (Benitz et al. 2016). In 3D-ADM cells, only a slight accumulation of H2AK119ub was detected at the promoter of *Ptf1a*. However, these cells show bivalent levels of H3K27me3 and H3K4me3, which could explain their plasticity (Benitz et al. 2016). By losing H3K27me3 the cells could re-differentiate back into acinar cells, as it occurs during pancreatitis-driven regeneration. In the setting of oncogenic Kras-driven tumor initiation, persistent gene silencing could be achieved through an additional enrichment of H3K27me3 and H2AK119ub. Overall, these findings propose a mechanism for the repression of the acinar-specific genes *Rbpjl* and *Ptf1a* during pancreatic carcinogenesis, which is dependent on PRC-mediated histone remodeling (Benitz et al. 2016).

Western blot analysis indicate a great enrichment of H2AK119ub in 3D-ADM cells, which is however not so prominent at the promoter sites of *Rbpjl* and *Ptf1a* (Benitz et al. 2016). Thus, in the future, further PRC1 target genes have to be identified. For this, ChIP-sequencing (ChIP-Seq) has already been performed in this study. Unfortunately, the data processing and analysis is still in progress. With the ChIP-Seq approach, global distribution of H2AK119ub in progenitor and differentiated acinar cells, as well as in 3D-ADM and cancer cells, shall be mapped to elucidate epigenetically modified genes during pancreatic carcinogenesis.
In 3D-ADM and cancer cells, the most down-regulated genes (> 10 fold) are associated with proteolysis, metabolic and catabolic processes. Here, it needs to be determined if these genes could be silenced through de novo ubiquitination of H2AK119. In a previous study, it

was moreover proposed that Ring1b binding, without ubiquitination of H2AK119, can lead to chromatin compaction (Eskeland et al. 2010). Thus, it may be speculated if repressed expression of *Ptf1a* and *Rbpjl* in ADM cells, could be additionally caused by a binding of Ring1b to the gene loci.

In addition to histone remodeling of acinar cell fate genes, epigenetic regulation of the PRC1 component Bmi1 was identified. Strikingly, levels of H3K27me3 and H2AK119ub are accumulated at the *Bmi1* promoter in acinar cells, contributing to its transcriptional repression. In contrast, in 3D-ADM and tumor cells, levels of H2AK119ub are greatly decreased, supporting active gene transcription. Enrichment of H3K27me3 is still detectable in 3D-ADM cells, suggesting that expression could already be activated through a loss of H2AK119ub. An additional deprivation of H3K27me3, as apparent in cancer cells, could permit persistent expression (Benitz et al. 2016). Generally, it is remarkable that in spite of the reactivation of Ring1b in 3D-ADM and cancer cells, levels of H2AK119ub are lost at the promoter site of *Bmi1*, allowing its expression and the subsequent assembly of active PRC1. Here, reduction of H2AK119ub levels could have been catalyzed by deubiquitinases, such as the recently described H2A deubiquitinase Usp16 or the Polycomb repressive deubiquitinase complex (PR-DUB) (Yang et al. 2014, Scheuermann et al. 2010). Interestingly, in embryonic stem cells, Yang et al. demonstrated that the deubiquitinase Usp16 and Ring1b competitively remodel H2Aub levels; Usp16 bound genes were associated with active gene expression (Yang et al. 2014). This suggests, that in dependence of the gene loci, levels of H2AK119ub could be dynamically changed, influencing gene transcription. However, factors mediating the binding of Ring1b to distinct gene loci have been rarely identified, up to now.

5.3 The role of Ring1b in inflammatory acinar-to-ductal metaplasia

Reactivation of PRC1 components, in combination with a concomitant enrichment of the histone modification H2AK119ub, was identified in 3D-ADM cells (Benitz et al. 2016). To characterize the significance of PRC1 in ADM *in vivo*, pancreatitis was induced in wildtype mice and expression of Ring1b and Bmi1, as well as the presence of H2AK119ub, were determined (Benitz et al. 2016). In accordance with previous studies, adult acinar cells are barely positive for Ring1b and Bmi1 (Martinez-Romero et al. 2009, Fukuda, Morris, and Hebrok 2012). During acute pancreatitis, levels of Bmi1, Ring1b and H2AK119ub are greatly increased (Benitz et al. 2016, Martinez-Romero et al. 2009, Fukuda, Morris, and Hebrok 2012), which is morphologically associated with exocrine tissue damage, ADM formation and inflammation. Here, the majority of ADM complexes are positive for the PRC1 components, Bmi1 and Ring1b, and H2AK119ub (Benitz et al. 2016). This suggests that PRC1 is not only reactivated in ADM *in vitro*, but also in inflammatory acinar-to-ductal metaplasia *in vivo*.

Seven days after the last caerulein injection, pancreatic tissue is regenerated and consequently Ring1b and Bmi1 expression is decreased (Benitz et al. 2016). In parallel to elevated levels of Ring1b and Bmi1 during acute pancreatitis, activation of Akt and Erk was observed. It was previously reported, that the Akt kinase can directly phosphorylate Bmi1, leading to enhanced PRC1 activity (Nacerddine et al. 2012). Moreover, Qian et al. revealed that the transcription of *Bmi1* is induced by c-Myc (Qian et al. 2010), an important downstream effector of the MAP kinase pathway (Sears et al. 2000). Thus, it was speculated if reactivated expression of Ring1b in acinar cells could be stimulated by these pathways. To find answers to this, a PI3K or a Mek inhibitor was administered to acinar suspension cells. When acinar cells are kept in suspension for five days, they acquire a progenitor-like expression profile (Pinho et al. 2011). Concomitantly, expression of Ring1b is reactivated in cultured cells (120 hours), and upon inhibition of either the PI3 or the Mek/Erk kinase pathway, Ring1b protein levels are greatly reduced. However, future studies have to clarify whether diminished protein levels are due to decreased post-translational stability of the protein or if gene transcription is directly or indirectly compromised upon inhibition of PI3K or Mek/Erk.

Moreover, to assess the functional relevance of reactivated Ring1b in inflammatory ADM, conditional Ring1b knockout mice were generated and the animals were injected with caerulein to cause an acute pancreatitis. Since epigenetic modifications catalyzed by Ring1b are crucial for proper cell lineage decisions and developmental processes (van Arensbergen et al. 2013), Cre-mediated knockout of Ring1b in acinar cells was induced at an adult stage (5.5- to 6-week-old mice). Blood analyses of the acinar cell stress markers amylase and lipase (six hours after last caerulein administration) indicate that $p48^{ERT}$ and $p48^{ERT}$;$R1b^{fl/fl}$ mice are equally challenged. However, HE stainings of tissue, harvested 24 or 48 hours after the caerulein treatment, show that Ring1b knockout mice are largely protected from manifestations of pancreatitis. Precisely, 48 hours after the last caerulein administration, $p48^{ERT}$ mice exhibit numerous ADMs and a strong stromal response, indicated by immune cell infiltrations, edema and fibrotic areas. In contrast, pancreata of $p48^{ERT}$;$Ring1b^{flox/flox}$ mice appear to be already regenerated, whereas $p48^{ERT}$;$Ring1b^{flox/+}$ animals display an intermediate phenotype. Regeneration of pancreatic tissue of $p48^{ERT}$ animals is however not apparent until seven days after the caerulein treatment. These results suggest that upon a loss of Ring1b, acinar-to-ductal metaplasia is not adequately and persistently induced, and that the establishment of progenitor-like cell status could be impaired. Indeed, in comparison to caerulein-treated control mice, expression of progenitor markers, such as *Pdx1*, *Rbpj* and *Sox9* is not induced in Ring1b knockout mice 48 hours after the caerulein treatment.

Although expression of the ductal gene *Ck19* and repression of *amylase* is observed in Ring1b knockout mice, it was not as prominent as in caerulein-treated control mice. Despite expression of *Ck19*, duct-like structures are barely observed in Ring1b knockout mice, 48 hours after the last caerulein administration. This suggests that complete ductal reprogramming could be dependent on the reactivation of further genes, such as the ductal fate determinant *Sox9*.
In regard to the expression of the differentiation genes *Rbpjl*, *Ptf1a* and *Mist1* no differences were detected between caerulein-injected $p48^{ERT}$ and $p48^{ERT;}R1b^{fl/fl}$ mice (48-hour time point). Importantly, in comparison to NaCl-treated $p48^{ERT}$ control mice, also no distinctions were identified, claiming that a repression of these genes is not present 48 hours after the last caerulein administration. Here, the study of Kong et al. revealed that silencing of the differentiation genes *Rbpjl* and *Mist1* is more persistent in mice expressing oncogenic $Kras^{G12D}$ (Kong et al. 2016).

Overall, this study indicates that loss of the catalytic subunit of PRC1, Ring1b, reduces ADM and tissue damage in the setting of pancreatitis. In striking contrast, Fukuda et al. revealed that pancreatic regeneration is greatly impaired in Bmi1 KO mice, accompanied by a persistent expression of the progenitor markers *Sox9* and *Hes1* (Fukuda, Morris, and Hebrok 2012). However, it has to be considered that in this study, global, non-conditional Bmi1 KO mice were used (Fukuda, Morris, and Hebrok 2012) meaning that all cell lineages throughout all developmental stages harbored a Bmi1 depletion. Since epigenetic changes catalyzed by PRC1 are important for stem cell maintenance (van der Stoop et al. 2008), but also for further embryonic development (van Arensbergen et al. 2013), early depletion of Bmi1 could have caused deregulated expression of progenitor genes during embryonic development, which could explain the contradictory results.

Sustained expression of the progenitor gene *Pdx1* in mice (induced in an embryonic stage through the use of the Ptf1a-Cre) causes acinar-to-ductal transition (Miyatsuka et al. 2006). Moreover, a previous study highlighted that aberrant expression of Sox9 in the setting of acute pancreatitis promotes more persistent ADM (Kopp et al. 2012), explaining why ADM formation could be decreased or not so enduring in Ring1b-depleted mice. Since Ring1b is largely associated with gene repression (de Napoles et al. 2004, Eskeland et al. 2010), the mechanism of how progenitor genes are activated in the presence of PRC1 is not clear. It can be speculated that expression could be influenced through the remodeling of histone modifications, binding of distinct transcription factors or by the activation status of signaling pathways. During the development of the pancreatic endoderm, expression of *PDX1* and *SOX9* is induced through loss of H3K27me3 (Xie et al. 2013). Analysis of the *in vitro*

carcinogenesis model reveals up-regulated expression of Bmi1 in 3D-ADM and cancer cells. At the *Bmi1* promoter of these cells, H3K27me3 and H2AK119ub is lost, supporting gene expression, although Ring1b is also increasingly expressed (Benitz et al. 2016). Thus, in response to reactivated Ring1b, PRC-mediated gene repression could be displaced at distinct gene loci ensuring reactivation of these genes. Interestingly, Kondo et al. demonstrated that initial binding of Ring1b to the *Meis2* promoter is essential for the recruitment of a specific enhancer (Kondo et al. 2014). Upon binding of the enhancer, Ring1b dissociates and transcriptional activation of the *Meis2* gene is achieved (Kondo et al. 2014). However, molecular details of PRC1-dependent transcriptional activation remain elusive. Amongst others, it was suggested that initial binding of PRC1 to inactive promoters could cause an open chromatin conformation, facilitating the binding of enhancers (Cavalli 2014). In addition to the remodeling of histone patterns and interaction with other transcription factors, also deregulations of signaling pathways could contribute to transcriptional activation. Importantly, Chen et al. indicated that EGFR signaling promotes expression of Sox9 in ADM (Chen et al. 2015). Similar to Ring1b$^{fl/fl}$ mice, Egfr^{KO} mice barely exhibit ADM, tissue fibrosis and inflammation upon subjection to a chronic-like pancreatitis (Ardito et al. 2012). Thus, it can be speculated if Ring1b could also influence the activation status of signaling pathways, such as the Egf receptor signaling cascade, thereby indirectly mediating the expression of progenitor genes and ADM. However, in the future, further studies are needed to elucidate how PRC1-dependent epigenetic remodeling contributes to the activation of progenitor-like expression programs in ADM and pancreatic carcinogenesis.

Besides the impaired set-up of a progenitor-like expression profile, also decreased stimulation of the microenvironment could contribute to reduced pancreatitis in Ring1b$^{fl/fl}$ mice. Hence, knockdown of Ring1b in various cancer cells caused increased apoptosis through enhanced stabilization of p53. Precisely, it was shown that Ring1b stabilizes Mdm2, which ubiquitinates and marks p53 for protein degradation (Wen et al. 2014). Moreover, analysis of caerulein-treated Bmi1 KO acinar suspension cells revealed that pro-apoptotic genes, such as Noxa, are significantly up-regulated in comparison to control cells (Fukuda, Morris, and Hebrok 2012). These data suggest, that upon loss of the PRC1 components Ring1b or Bmi1, apoptosis could be rather induced. Therefore, decreased tissue damage and inflammation in Ring1b-deficient mice could be due to the fact, that damaged acinar cells rather undergo apoptosis than cell necrosis (nowadays also described as oncosis) (Miao, Rajan, and Aderem 2011). In contrast to apoptosis, oncosis is characterized as a lytic process, causing tissue inflammation and attracting immune cells (Miao, Rajan, and Aderem 2011). It was also reported that cytokines, released by macrophages, greatly promote ADM (Liou et al. 2013). Thus, it may be speculated whether reduced pancreatitis in Ring1b$^{fl/fl}$ mice could also be due to changes in the mode of cell death and/or inflammation. Future efforts

have to be made to quantify CD45-positive immune cells and cleaved Caspase3, an indicator for apoptosis, to verify these hypotheses.

5.4 The importance of Ring1b in pancreatic tumor development

Elevated expression of the epigenetic remodeler Ring1b was previously detected in PanIN lesions and PDAC (Martinez-Romero et al. 2009, Benitz et al. 2016). In human PDAC, high levels of H2AK119ub are associated with poor differentiation and increased tumor size (Chen, Chen, et al. 2014). Besides elevated expression in advanced tumor stages, the presented study should reveal if PRC1 is implicated in $Kras^{G12D}$-dependent pancreatic cancer initiation.

For this, the presence of Ring1b, Bmi1 and H2AK119ub was determined in three-, ten- and 20-week-old KPC mice. Expression of Ring1b and Bmi1 is already apparent in morphologically normal appearing acinar cells from three-week-old mice and can be detected in ADM and early pancreatic precursor lesions. PDAC cells are also greatly positive. These results suggest that reactivation of PRC1 already occurs during early pancreatic tumorigenesis (Benitz et al. 2016).

To explore if epigenetic changes mediated by Ring1b influence oncogenic Kras-driven cell transformation, $Kras^{G12D}$ was additionally expressed in the transgenic Ring1b knockout mouse model. Since adult acinar cells are refractory to mutant Kras (Guerra et al. 2007), mice were additionally treated according to the caerulein-based regeneration model. After 21 days, control mice have developed metaplastic ductal structures, such as ADM and PanIN-1, in combination with a strong stromal response, evident through pancreatic fibrosis and immune cell infiltration. In contrast, $Kras^{G12D}$-driven neoplastic tissue transformation is greatly abrogated in $Ring1b^{fl/fl}$ mice. Here, nearly no metaplastic ductal structures were detected and pancreatic tissue morphology appears almost normal. Six months after the caerulein application, focal areas of PDAC precursor lesions and PDAC were identified in $p48^{ERT}$;K mice, whereas $p48^{ERT}$;K;$R1b^{fl/fl}$ animals exhibit rare, rather low-grade PDAC lesions. Here, it needs to be determined if the transformed cells in the Ring1b-deficient mice are cells in which recombination of the Ring1b locus was not successful.

Generally, results are in accordance with a recent study of Bednar et al., which showed that knockout of Bmi1 in Pdx1-Cre;$Kras^{G12D}$ mice nearly completely abolishes the formation of pancreatic precancerous lesions (Bednar et al. 2015). Even in the context of pancreatitis-induced carcinogenesis, PanIN formation is blocked in Bmi1-deficient mice (Bednar et al. 2015). Functionally, Bednar et al. described that upon knockdown of Bmi1 in pancreatic cancer cells, levels of reactive oxygen species (ROS) are increased. Thus, it was suggested that elevated expression of Bmi1 in PDAC development protects the cells from oxidative stress and consequently favors carcinogenesis (Bednar et al. 2015). Hence, in the future,

tissue of Ring1b knockout mice shall be analyzed on the activation status of DNA damage response pathways and apopotosis.
However, in contrast to the results of the Bmi1 and Ring1b KO mice, deletion of the catalytic subunit of PRC2, Ezh2, accelerates pancreatic carcinogenesis in a $p48^{Cre}$;$Kras^{G12D}$ mouse model (Mallen-St Clair et al. 2012). This implies that epigenetic remodeling, catalyzed by PRC1 or PRC2, is quite distinct. Therefore, future studies are needed to unravel the PRC target genes.

Adult acinar cells are resistant to oncogenic Kras-dependent cell transformation (Guerra et al. 2007). However, only in combination with the induction of pancreatitis, acinar dedifferentiation and initiation of PDAC can be observed (Guerra et al. 2007). Thus, it was speculated if pancreatitis-induced acinar dedifferentiation and establishment of a progenitor-like expression profile is an important prerequisite for further $Kras^{G12D}$-driven cell transformation. Analyzing the functional role of Ring1b in pancreatitis (48-hour time point) revealed that the reactivation of progenitor genes is impaired in $Ring1b^{fl/fl}$ mice. This is also evident in $Kras^{G12D}$;$Ring1b^{fl/fl}$ mice, which were sacrificed 21 days after the caerulein treatment. For instance, expression of *Sox9* is significantly lower in Ring1b-deficient mice. Moreover, the differentiation genes *Rbpjl*, *Ptf1a* and *Mist1* remain more highly expressed in $Ring1b^{fl/fl}$ mice, whereas expression is repressed in caerulein-treated $p48^{ERT}$;$Kras^{G12D}$ mice. Thus, at the promoter site of the differentiation gene *Rbpjl*, an enrichment of H2AK119ub is apparent in $p48^{ERT}$;$Kras^{G12D}$ animals. This suggests, that in the setting of activated oncogenic $Kras^{G12D}$, Ring1b contributes to the silencing of the differentiation marker *Rbpjl*, favoring acinar cell dedifferentiation. This is in accordance with the results from the *in vitro* model, which shows enriched levels of H2AK119ub at the *Rbpjl* promoter in oncogenic $Kras^{G12D}$-expressing pancreatic cancer cells (Benitz et al. 2016).
In addition to the loss of Ring1b or Bmi1 (Bednar et al. 2015), $Kras^{G12D}$-dependent pancreatic carcinogenesis is abrogated upon deletion of the Egf receptor (Ardito et al. 2012) or Stat3 (signal transducer and activator of transcription 3), which is activated by growth-factor-dependent receptor tyrosine kinases (Corcoran et al. 2011). Thus, future studies shall reveal if there is a relation between PRC1 and the activation of these signaling pathways.
Overall, the loss of Ring1b seems to impair oncogenic Kras-driven neoplastic tissue transformation and initiation of PDAC. Hence, Ring1b can be regarded as an important oncogene supporting pancreatic carcinogenesis.

5.5 The role of Ring1b in pancreatic cancer cells

Loss of Ring1b greatly inhibits $Kras^{G12D}$-driven neoplastic cell transformation and prevents the activation of a progenitor-like expression program. Since murine, as well as human

PDAC are hallmarked by elevated expression of the epigenetic remodeler Ring1b (Benitz et al. 2016, Martinez-Romero et al. 2009, Chen, Chen, et al. 2014), its functional role was determined in pancreatic cancer cells. Here, with the aid of the CRISPR/Cas9 system, Ring1b was knocked out in an aggressive pancreatic cancer cell line, isolated from a p48Cre;LSL-Kras^{G12D};p53$^{fl/+}$ (KPC) mouse. Ring1b KO cells are characterized by a loss of H2AK119ub, whereas levels of H3K27me3 remain stable. This was also reported in another study, in which Ring1b was knocked down (Chen, Xu, et al. 2014).

mRNA microarray analysis reveal elevated expression of 474 genes (fold change > 1.5), which are mostly related to developmental, such as epithelium development, and morphogenetic processes. For instance, expression of *Klf4* or *Prrx1* was found to be increased upon loss of Ring1b. Remarkably, in the *in vitro* carcinogenesis model, high *Klf4* and *Prrx1* expression was detected in 3D-ADM cells but not in pancreatic cancer cells. Recently, *Klf4* was associated as an important mediator of ADM (Wei et al. 2016). Overall, since GO terms, related to epithelium development, as well as genes, solely up-regulated in 3D-ADM cells, were found to be increased in Ring1b KO cells, it may be speculated that Ring1b KO cells harbor a higher differentiation grade than the control cells. Diaferia et al. analyzed the transcriptome of low- and high-grade human pancreatic cancer lines and assessed that low-grade PDAC cells are associated with an increased expression of epithelial genes, whereas high-grade cells rather possess mesenchymale features (Diaferia et al. 2016). For genes, up-regulated in Ring1b KO cells, GO terms also related to mesenchyme development were assigned, but a higher number of genes was grouped into terms associated with the epithelium lineage. However, microarray data and expression analysis indicate no increased expression of the differentiation genes *Rbpjl* or *Ptf1a*. Although levels of H2AK119ub are greatly reduced at the indicated promoter sites, expression is not reactivated. At the *Ptf1a* promoter, hardly any levels of the activating mark H3K4me3 were detected, suggesting that gene expression is not epigenetically activated (data were kindly provided by Sabrina Deubler) (Deubler 2016). Western blot analyses reveal an elevated expression of the DNA methyltransferase Dnmt3a in Ring1b KO cells. This could be regarded as a compensatory mechanism, ensuring gene silencing of initially H2AK119ub-marked genes (data were kindly provided by Sabrina Deubler) (Deubler 2016).

In accordance with the results of this study, deletion of Ring1b in pancreatic progenitor cells leads to the de-repression of a small subset of genes, which are mostly associated with de-novo targeting of Ring1b (van Arensbergen et al. 2013). However, since most genes are not reactivated upon Ring1b loss, van Arensbergen et al. proposed that Ring1b bookmarks genes for transcriptional repression and additional mechanisms, such as DNA methylation, support persistent gene silencing (van Arensbergen et al. 2013). Knockdown of Ring1b and Ezh2 in pancreatic cancer cells, causes an increased de-repression of the *Hoxc10* gene,

whereas the loss of Ring1b alone just slightly induces gene expression (Chen, Chen, et al. 2014). Moreover, this demonstrates that additional epigenetic repressor complexes help to silence Ring1b target genes in cancer cells.

Interestingly, expression of *Dusp9* (dual specificity phosphatase 9), a negative regulator of the MAP kinase Erk2 (Muda et al. 1997), was found to be up-regulated in Ring1b KO cells. In human gastric cancer samples, it was shown that *Dusp9* is epigenetically silenced through DNA hypermethylation (Wu et al. 2015). Thus, further experiments should be performed to unveil if the *Dusp9* gene is a direct target of Ring1b. However, in Ring1bKO cells, also up-regulated expression of the *Egf* receptor was detected, which could present a compensatory mechanism for overcoming Dusp9-mediated repression of the MAP kinase pathway.

Chen et al. reported that shRNA-mediated Ring1b knockdown in human pancreatic cancer cells, significantly decreased tumor growth of subcutaneously implanted cancer cells in nude mice (Chen, Chen, et al. 2014). In this study, orthotopic injection of Ring1b KO cells into pancreata of wildtype mice shows that tumor formation, measured by tumor size, is slightly but not significantly decreased in comparison to control cells.

Importantly, nearly no epithelial cells were detected in the blood of mice, which were orthotopically transplanted with Ring1b KO cells. In contrast, great amounts were isolated and cultivated from the blood of mice, which were injected with control cells. In line with these observations, a recent study showed that depletion of Ring1b in breast cancer cells compromises cell migration and invasion due to a decreased expression of the focal adhesion kinase (Bosch et al. 2014).

Annotation of down-regulated genes generated the KEGG pathways "metabolism of xenobiotics by cytochrome P450" and "drug metabolism". Here, the genes *Gstt1* (*Glutathione S-transferase theta 1*) and *Gsta4* (*Glutathione S-transferase alpha 4*) were assigned. In this context, Ring1b KO cells were found to be more sensitive to gemcitabine (data were kindly provided by Sabrina Deubler) (Deubler 2016). Elevated expression of microsomal *GSTT1* was detected in gemcitabine-resistant human primary pancreatic cancer cells (Bai, Sata, and Nagai 2007). Over-expression of GSTs was described in a great variety of tumor entities (Townsend and Tew 2003). It is assumed that the enzymes contribute to the detoxification of drugs and alkylating agents through the conjugation of glutathione (Townsend and Tew 2003).

In summary, knockout of Ring1b in pancreatic cancer cells induces cellular reprogramming towards a chemosensitive phenotype and a reduced tumor formation capability.

5.6 PRC1 as a druggable target

Knockout of Ring1b in pancreatic tumor cells causes increased expression of a small subset of genes, associated with epithelium developmental processes, claiming that cells could

have adopted a more differentiated state. In addition, Ring1b KO cells display a greater sensitivity towards gemcitabine. Overall, this study indicates that Ring1b can be regarded as a potential oncogene, contributing especially to cancer initiation, but also favoring PDAC progression. Therefore, Ring1b and PRC1 could present a promising therapeutic target. Alchanti et al. identified the compound 2-pyridine-3-yl-methylene-indan-1,3-dione (*PRT4165*) as a potent inhibitor of PRC1 (Alchanati et al. 2009). Besides inhibition of protein ubiquitination (Alchanati et al. 2009), application of the inhibitor specifically decreases levels of H2AK119ub (Ismail et al. 2013).

PRT4165 treatment of 3D-ADM cell cultures leads to the formation of significantly smaller metaplastic ductal structures. Hence, a smaller number of proliferative, BrdU-positive cells was detected in PRT4165-treated cell cultures. In accordance, depletion of Ring1a and Ring1b in mouse embryonic fibroblasts causes impaired proliferation through the up-regulation of p21 and defects in replication (Bravo et al. 2015). Overall, the results indicate that application of PRT4165 can weaken the process of ADM formation *in vitro*. Short-time treatment of cancer cells (six hours) induces slight reprogramming of the transcriptional pattern. Thus, expression of acinar differentiation genes is slightly elevated, whereas expression of progenitor markers, such as *Rbpj*, is decreased. This suggests, that short-time inhibition of PRC1 positively influences the transcriptional activation of acinar cell fate genes. Here, it has to be evaluated if increased expression is due to decreased levels of H2AK119ub, reduced binding of Ring1b or influenced by indirect mechanisms. However, it has to be critically considered that a twofold increase in expression is not immense. In comparison to acinar cells, expression of these genes is strongly repressed in cancer cells and treatment with PRT4165 cannot restore complete expression. Hence, expression must be inhibited through other repressive mechanisms. In contrast to PRT4165-treated cells, no changes in the expression of acinar differentiation genes were detected in Ring1b KO cancer cells (data were kindly provided by Sabrina Deubler) (Deubler 2016). Here, it can be speculated that during several cell culture rounds, other compensatory gene repressive mechanisms are reactivated. For instance, levels of the DNA methyltransferase Dnmt3a are increased in Ring1b KO cells compared to controls (data were kindly provided by Sabrina Deubler) (Deubler 2016). From this point of view, it has to be validated if long-term application of PRT4165 can cause transcriptional reprogramming of cancer cells. Since Ring1b KO cancer cells are more sensitive to gemcitabine, it has to be determined if long-term application of PRT4165 could have the same effects. In regard to this, it should be established if combinatorial treatment with PRT4165 and gemcitabine could be beneficial for treating PDAC. However, future studies are needed to assess the therapeutical potential of PRT4165.

Until now, it remains largely elusive how PRT4165 exerts its PRC1 inhibiting effect. Alchanti et al. only showed that upon application, Bmi1 is no longer localized in the cell nuclei (Alchanati et al. 2009). In this study, PRT4165 was applied in high concentrations (100 μM) and a significant reduction of H2AKub119 levels are only apparent until 6 hours of treatment. Thus, more potent compounds have to be developed in the future. Since Ring1b seems to influence ADM and initiation of pancreatic carcinogenesis, it has to be analyzed if inhibition of PRC1 could be also applied as a preventive therapeutic approach for pancreatitis. A study by Kreso et al. highlighted that targeting PRC1 can also decrease the tumor burden (Kreso et al. 2014). Here, treatment of colon cancer xenografts in nude mice with the compound PTC-209, which reduces expression of *Bmi1*, greatly abrogated tumor growth (Kreso et al. 2014). Thus, future studies are implicitly needed to determine if targeting PRC1 in PDAC could be of therapeutic value.

5.7 Conclusions and outlook

Elevated expression of PRC1 components was described in various cancer entities, such as prostate cancer, ductal breast carcinoma and PDAC (Bosch et al. 2014, Lukacs et al. 2010, van Leenders et al. 2007) (Martinez-Romero et al. 2009). Over-expression of Ring1b in cancer cells is associated with cancer cell metastasis (Bosch et al. 2014, Chen, Xu, et al. 2014), reduced apoptosis (Wen et al. 2014) and tumor growth (Chen, Chen, et al. 2014). Importantly, the PRC1 component Bmi1, is moreover defined as a cancer stem cell marker (Proctor et al. 2013, Chiba et al. 2008, Kreso et al. 2014).

This study indicates that reactivation of Ring1b is crucial for the formation of ADM and pancreatic precancerous lesions. Besides its important role in the initiation of PDAC, the epigenetic remodeler accounts for the silencing of pancreatic differentiation genes in cancer cells, helping to establish a dedifferentiated, progenitor-like expression program (Benitz et al. 2016). With the aid of a ChIP-sequencing approach, it is expected to identify further Ring1b target genes, helping to fully comprehend how epigenetic changes mediated by PRC1 drive pancreatic carcinogenesis. Moreover, significance of identified genes will be validated in the conditional Ring1b knockout mouse model.

Administration of a PRC1 inhibitor *in vitro*, constrains ADM formation. In a future approach, effects of the inhibitor have to be studied *in vivo* to assess its therapeutic value. Since a knockout of Ring1b in pancreatic cancer cells leads to an enhanced sensitivity towards gemcitabine, it needs to be further evaluated if combinatorial treatment with a Ring1b inhibitor and gemcitabine could be beneficial.

Overall, this work presents that, in addition to well-defined genetic mutations, also epigenetic dysregulations are of major importance for the initiation and progression of PDAC. Thus, an integration of epigenetic drugs may provide a promising avenue for treating PDAC.

6 Summary

The process of acinar cell de- or transdifferentiation into cells with a duct-like character is defined as acinar-to-ductal metaplasia, which has been accepted as an important premise for PDAC initiation. However, ADM cell characteristics and key factors responsible for transcriptional reprogramming have been rarely described. In this study, gene expression profiling demonstrates that ADM cells possess a high degree of similarity to embryonic acinar cells. Precisely, numerous developmental processes are up-regulated in metaplastic cells, suggesting that ADM can be regarded as cellular dedifferentiation with the concomitant acquirement of a ductal phenotype. In addition to the reactivated expression of progenitor genes, ADM and pancreatic cancer cells are characterized by the down-regulation of acinar differentiation genes. In parallel, increased expression of epigenetic remodeling complexes, such as PRC1 and its catalytic subunit Ring1b, can be detected in these cells. A significant enrichment of the Ring1b-mediated repressive histone modification H2AK119ub exists at the promoter sites of the acinar cell fate genes *Rbpjl* and *Ptf1a* in pancreatic cancer cells. This highlights that epigenetic modifications catalyzed by PRC1 contribute to acinar gene silencing in PDAC (Benitz et al. 2016).

Elevated levels of the PRC1 components Bmi1 and Ring1b as well as of H2AK119ub can be determined in pancreatitis-triggered ADM cells in wildtype mice, as well as in precursor lesions and tumor cells in a mouse model of PDAC (Benitz et al. 2016). Importantly, mice, harboring a conditional Ring1b knockout in acinar cells, largely fail to develop ADM in the setting of acute pancreatitis. Moreover, the formation of precancerous lesions is greatly abrogated in pancreatitis-induced, Ring1b-depleted $Kras^{G12D}$ mice. Here, mRNA expression data confirm, that the establishment of a progenitor-like transcriptional profile is reduced in Ring1b knockout mice. Namely, differentiation genes remain expressed and activation of progenitor genes is suppressed, proposing that a loss of Ring1b impairs $Kras^{G12D}$-driven cell transformation. CRISPR/Cas9-mediated knockout of Ring1b in pancreatic cancer cells does not cause complete transcriptional reprogramming. The altered transcription profile correlates with an increased expression of genes associated with the epithelium cell lineage, indicating that upon loss of Ring1b tumor cells may become more differentiated. Functionally, Ring1b knockout cells display increased sensitivity towards gemcitabine and a slightly diminished tumor growth *in vivo*. Application of a PRC1 inhibitor impairs ADM formation *in vitro* and induces modest transcriptional reprogramming of pancreatic cancer cells.

Overall, this work suggests that the reactivation of the epigenetic regulator Ring1b is critical for ADM and pancreatic carcinogenesis. Specifically, epigenetic changes catalyzed by Ring1b contribute to the establishment of a progenitor-like expression profile, an important prerequisite for PDAC initiation and progression.

7 References

Abremski, K., A. Wierzbicki, B. Frommer, and R. H. Hoess. 1986. "Bacteriophage P1 Cre-loxP site-specific recombination. Site-specific DNA topoisomerase activity of the Cre recombination protein." *J Biol Chem* 261 (1): 391-396.

Abreu Velez, A. M., and M. S. Howard. 2015. "Tumor-suppressor Genes, Cell Cycle Regulatory Checkpoints, and the Skin." *N Am J Med Sci* 7 (5): 176-188. doi: 10.4103/1947-2714.157476.

Aghdassi, A., M. Sendler, A. Guenther, J. Mayerle, C. O. Behn, C. D. Heidecke, H. Friess, M. Buchler, M. Evert, M. M. Lerch, and F. U. Weiss. 2012. "Recruitment of histone deacetylases HDAC1 and HDAC2 by the transcriptional repressor ZEB1 downregulates E-cadherin expression in pancreatic cancer." *Gut* 61 (3): 439-448. doi: 10.1136/gutjnl-2011-300060.

Aichler, M., C. Seiler, M. Tost, J. Siveke, P. K. Mazur, P. Da Silva-Buttkus, D. K. Bartsch, P. Langer, S. Chiblak, A. Durr, H. Hofler, G. Kloppel, K. Muller-Decker, M. Brielmeier, and I. Esposito. 2012. "Origin of pancreatic ductal adenocarcinoma from atypical flat lesions: a comparative study in transgenic mice and human tissues." *J Pathol* 226 (5): 723-734. doi: 10.1002/path.3017.

Al Mofleh, I. A. 2008. "Severe acute pancreatitis: pathogenetic aspects and prognostic factors." *World J Gastroenterol* 14 (5): 675-684.

Alchanati, I., C. Teicher, G. Cohen, V. Shemesh, H. M. Barr, P. Nakache, D. Ben-Avraham, A. Idelevich, I. Angel, N. Livnah, S. Tuvia, Y. Reiss, D. Taglicht, and O. Erez. 2009. "The E3 ubiquitin-ligase Bmi1/Ring1A controls the proteasomal degradation of Top2alpha cleavage complex - a potentially new drug target." *PLoS One* 4 (12): e8104. doi: 10.1371/journal.pone.0008104.

Ammann, R. W., and B. Muellhaupt. 1994. "Progression of alcoholic acute to chronic pancreatitis." *Gut* 35 (4): 552-556.

Andea, A., F. Sarkar, and V. N. Adsay. 2003. "Clinicopathological correlates of pancreatic intraepithelial neoplasia: a comparative analysis of 82 cases with and 152 cases without pancreatic ductal adenocarcinoma." *Mod Pathol* 16 (10): 996-1006. doi: 10.1097/01.MP.0000087422.24733.62.

Ardito, C. M., B. M. Gruner, K. K. Takeuchi, C. Lubeseder-Martellato, N. Teichmann, P. K. Mazur, K. E. Delgiorno, E. S. Carpenter, C. J. Halbrook, J. C. Hall, D. Pal, T. Briel, A. Herner, M. Trajkovic-Arsic, B. Sipos, G. Y. Liou, P. Storz, N. R. Murray, D. W. Threadgill, M. Sibilia, M. K. Washington, C. L. Wilson, R. M. Schmid, E. W. Raines, H. C. Crawford, and J. T. Siveke. 2012. "EGF receptor is required for KRAS-induced pancreatic tumorigenesis." *Cancer Cell* 22 (3): 304-317. doi: 10.1016/j.ccr.2012.07.024.

Bai, C. B., D. Stephen, and A. L. Joyner. 2004. "All mouse ventral spinal cord patterning by hedgehog is Gli dependent and involves an activator function of Gli3." *Dev Cell* 6 (1): 103-115.

Bai, J., N. Sata, and H. Nagai. 2007. "Gene expression analysis for predicting gemcitabine sensitivity in pancreatic cancer patients." *HPB (Oxford)* 9 (2): 150-155. doi: 10.1080/13651820601175918.

Ballehaninna, U. K., and R. S. Chamberlain. 2011. "Serum CA 19-9 as a Biomarker for Pancreatic Cancer-A Comprehensive Review." *Indian J Surg Oncol* 2 (2): 88-100. doi: 10.1007/s13193-011-0042-1.

Bardeesy, N., A. J. Aguirre, G. C. Chu, K. H. Cheng, L. V. Lopez, A. F. Hezel, B. Feng, C. Brennan, R. Weissleder, U. Mahmood, D. Hanahan, M. S. Redston, L. Chin, and R. A. Depinho. 2006. "Both p16(Ink4a) and the p19(Arf)-p53 pathway constrain progression of pancreatic adenocarcinoma in the mouse." *Proc Natl Acad Sci U S A* 103 (15): 5947-5952. doi: 10.1073/pnas.0601273103.

Bardeesy, N., K. H. Cheng, J. H. Berger, G. C. Chu, J. Pahler, P. Olson, A. F. Hezel, J. Horner, G. Y. Lauwers, D. Hanahan, and R. A. DePinho. 2006. "Smad4 is dispensable for normal pancreas development yet critical in progression and tumor biology of pancreas cancer." *Genes Dev* 20 (22): 3130-3146. doi: 10.1101/gad.1478706.

Bardeesy, N., and R. A. DePinho. 2002. "Pancreatic cancer biology and genetics." *Nat Rev Cancer* 2 (12): 897-909. doi: 10.1038/nrc949.

Batchu, R. B., A. M. Qazi, O. V. Gruzdyn, A. Semaan, S. M. Seward, S. Chamala, V. B. Dhulipala, D. L. Bouwman, D. W. Weaver, and S. A. Gruber. 2013. "EZH2-shRNA-mediated upregulation of p21waf1/cip1 and its transcriptional enhancers with concomitant downmodulation of mutant p53 in pancreatic ductal adenocarcinoma." *Surgery* 154 (4): 739-746; discussion 746-737. doi: 10.1016/j.surg.2013.06.041.

Becker, A. E., Y. G. Hernandez, H. Frucht, and A. L. Lucas. 2014. "Pancreatic ductal adenocarcinoma: risk factors, screening, and early detection." *World J Gastroenterol* 20 (32): 11182-11198. doi: 10.3748/wjg.v20.i32.11182.

Bednar, F., H. K. Schofield, M. A. Collins, W. Yan, Y. Zhang, N. Shyam, J. A. Eberle, L. L. Almada, K. P. Olive, N. Bardeesy, M. E. Fernandez-Zapico, D. Nakada, D. M. Simeone, S. J. Morrison, and M. Pasca di Magliano. 2015. "Bmi1 is required for the initiation of pancreatic cancer through an Ink4a-independent mechanism." *Carcinogenesis* 36 (7): 730-738. doi: 10.1093/carcin/bgv058.

Behrens, C., L. M. Solis, H. Lin, P. Yuan, X. Tang, H. Kadara, E. Riquelme, H. Galindo, C. A. Moran, N. Kalhor, S. G. Swisher, G. R. Simon, D. J. Stewart, J. J. Lee, and Wistuba, II. 2013. "EZH2 protein expression associates with the early pathogenesis, tumor progression, and prognosis of non-small cell lung carcinoma." *Clin Cancer Res* 19 (23): 6556-6565. doi: 10.1158/1078-0432.CCR-12-3946.

Ben-Saadon, R., D. Zaaroor, T. Ziv, and A. Ciechanover. 2006. "The polycomb protein Ring1B generates self atypical mixed ubiquitin chains required for its in vitro histone H2A ligase activity." *Mol Cell* 24 (5): 701-711. doi: 10.1016/j.molcel.2006.10.022.

Benitez, C. M., W. R. Goodyer, and S. K. Kim. 2012. "Deconstructing pancreas developmental biology." *Cold Spring Harb Perspect Biol* 4 (6). doi: 10.1101/cshperspect.a012401.

Benitz, S., I. Regel, T. Reinhard, A. Popp, I. Schaffer, S. Raulefs, B. Kong, I. Esposito, C. W. Michalski, and J. Kleeff. 2016. "Polycomb repressor complex 1 promotes gene silencing through H2AK119 mono-ubiquitination in acinar-to-ductal metaplasia and pancreatic cancer cells." *Oncotarget* 7 (10): 11424-11433. doi: 10.18632/oncotarget.6717.

Beres, T. M., T. Masui, G. H. Swift, L. Shi, R. M. Henke, and R. J. MacDonald. 2006. "PTF1 is an organ-specific and Notch-independent basic helix-loop-helix complex containing the mammalian Suppressor of Hairless (RBP-J) or its paralogue, RBP-L." *Mol Cell Biol* 26 (1): 117-130. doi: 10.1128/MCB.26.1.117-130.2006.

Bernstein, B. E., T. S. Mikkelsen, X. Xie, M. Kamal, D. J. Huebert, J. Cuff, B. Fry, A. Meissner, M. Wernig, K. Plath, R. Jaenisch, A. Wagschal, R. Feil, S. L. Schreiber, and E. S. Lander. 2006. "A bivalent chromatin structure marks key developmental genes in embryonic stem cells." *Cell* 125 (2): 315-326. doi: 10.1016/j.cell.2006.02.041.

Bernstein, E., E. M. Duncan, O. Masui, J. Gil, E. Heard, and C. D. Allis. 2006. "Mouse polycomb proteins bind differentially to methylated histone H3 and RNA and are enriched in facultative heterochromatin." *Mol Cell Biol* 26 (7): 2560-2569. doi: 10.1128/MCB.26.7.2560-2569.2006.

Bird, A. 2002. "DNA methylation patterns and epigenetic memory." *Genes Dev* 16 (1): 6-21. doi: 10.1101/gad.947102.

Bosch, A., K. Panoutsopoulou, J. M. Corominas, R. Gimeno, G. Moreno-Bueno, J. Martin-Caballero, S. Morales, T. Lobato, C. Martinez-Romero, E. F. Farias, X. Mayol, A. Cano, and I. Hernandez-Munoz. 2014. "The Polycomb group protein RING1B is overexpressed in ductal breast carcinoma and is required to sustain FAK steady state levels in breast cancer epithelial cells." *Oncotarget* 5 (8): 2065-2076. doi: 10.18632/oncotarget.1779.

Boyer, L. A., K. Plath, J. Zeitlinger, T. Brambrink, L. A. Medeiros, T. I. Lee, S. S. Levine, M. Wernig, A. Tajonar, M. K. Ray, G. W. Bell, A. P. Otte, M. Vidal, D. K. Gifford, R. A. Young, and R. Jaenisch. 2006. "Polycomb complexes repress developmental regulators in murine embryonic stem cells." *Nature* 441 (7091): 349-353. doi: 10.1038/nature04733.

Bracken, A. P., D. Pasini, M. Capra, E. Prosperini, E. Colli, and K. Helin. 2003. "EZH2 is downstream of the pRB-E2F pathway, essential for proliferation and amplified in cancer." *EMBO J* 22 (20): 5323-5335. doi: 10.1093/emboj/cdg542.

Brady, M., M. Bhatia, S. Christmas, M. T. Boyd, J. P. Neoptolemos, and J. Slavin. 2002. "Expression of the chemokines MCP-1/JE and cytokine-induced neutrophil chemoattractant in early acute pancreatitis." *Pancreas* 25 (3): 260-269.

Brat, D. J., K. D. Lillemoe, C. J. Yeo, P. B. Warfield, and R. H. Hruban. 1998. "Progression of pancreatic intraductal neoplasias to infiltrating adenocarcinoma of the pancreas." *Am J Surg Pathol* 22 (2): 163-169.

Bravo, M., F. Nicolini, K. Starowicz, S. Barroso, C. Cales, A. Aguilera, and M. Vidal. 2015. "Polycomb RING1A- and RING1B-dependent histone H2A monoubiquitylation at pericentromeric regions promotes S-phase progression." *J Cell Sci* 128 (19): 3660-3671. doi: 10.1242/jcs.173021.

Brembeck, F. H., F. S. Schreiber, T. B. Deramaudt, L. Craig, B. Rhoades, G. Swain, P. Grippo, D. A. Stoffers, D. G. Silberg, and A. K. Rustgi. 2003. "The mutant K-ras oncogene causes pancreatic periductal lymphocytic infiltration and gastric mucous neck cell hyperplasia in transgenic mice." *Cancer Res* 63 (9): 2005-2009.

Brock, C., L. M. Nielsen, D. Lelic, and A. M. Drewes. 2013. "Pathophysiology of chronic pancreatitis." *World J Gastroenterol* 19 (42): 7231-7240. doi: 10.3748/wjg.v19.i42.7231.

Buchwald, G., P. van der Stoop, O. Weichenrieder, A. Perrakis, M. van Lohuizen, and T. K. Sixma. 2006. "Structure and E3-ligase activity of the Ring-Ring complex of polycomb proteins Bmi1 and Ring1b." *EMBO J* 25 (11): 2465-2474. doi: 10.1038/sj.emboj.7601144.

Bustin, M., F. Catez, and J. H. Lim. 2005. "The dynamics of histone H1 function in chromatin." *Mol Cell* 17 (5): 617-620. doi: 10.1016/j.molcel.2005.02.019.

Cales, C., M. Roman-Trufero, L. Pavon, I. Serrano, T. Melgar, M. Endoh, C. Perez, H. Koseki, and M. Vidal. 2008. "Inactivation of the polycomb group protein Ring1B unveils an antiproliferative role in hematopoietic cell expansion and cooperation with tumorigenesis associated with Ink4a deletion." *Mol Cell Biol* 28 (3): 1018-1028. doi: 10.1128/MCB.01136-07.

Cao, Q., X. Wang, M. Zhao, R. Yang, R. Malik, Y. Qiao, A. Poliakov, A. K. Yocum, Y. Li, W. Chen, X. Cao, X. Jiang, A. Dahiya, C. Harris, F. Y. Feng, S. Kalantry, Z. S. Qin, S. M. Dhanasekaran, and A. M. Chinnaiyan. 2014. "The central role of EED in the orchestration of polycomb group complexes." *Nat Commun* 5: 3127. doi: 10.1038/ncomms4127.

Cao, R., Y. Tsukada, and Y. Zhang. 2005. "Role of Bmi-1 and Ring1A in H2A ubiquitylation and Hox gene silencing." *Mol Cell* 20 (6): 845-854. doi: 10.1016/j.molcel.2005.12.002.

Cao, R., L. Wang, H. Wang, L. Xia, H. Erdjument-Bromage, P. Tempst, R. S. Jones, and Y. Zhang. 2002. "Role of histone H3 lysine 27 methylation in Polycomb-group silencing." *Science* 298 (5595): 1039-1043. doi: 10.1126/science.1076997.

Cao, R., and Y. Zhang. 2004. "SUZ12 is required for both the histone methyltransferase activity and the silencing function of the EED-EZH2 complex." *Mol Cell* 15 (1): 57-67. doi: 10.1016/j.molcel.2004.06.020.

Castellano-Megias, V. M., C. I. Andres, G. Lopez-Alonso, and F. Colina-Ruizdelgado. 2014. "Pathological features and diagnosis of intraductal papillary mucinous neoplasm of the pancreas." *World J Gastrointest Oncol* 6 (9): 311-324. doi: 10.4251/wjgo.v6.i9.311.

Cavalli, G. 2014. "A RING to rule them all: RING1 as silencer and activator." *Dev Cell* 28 (1): 1-2. doi: 10.1016/j.devcel.2013.12.015.

Chan, E., L. R. Arlinghaus, D. B. Cardin, L. Goff, J. D. Berlin, A. Parikh, R. G. Abramson, T. E. Yankeelov, S. Hiebert, N. Merchant, S. Bhaskara, and A. B. Chakravarthy. 2016. "Phase I trial of vorinostat added to chemoradiation with capecitabine in pancreatic cancer." *Radiother Oncol* 119 (2): 312-318. doi: 10.1016/j.radonc.2016.04.013.

Chen, J., F. M. Ghazawi, and Q. Li. 2010. "Interplay of bromodomain and histone acetylation in the regulation of p300-dependent genes." *Epigenetics* 5 (6): 509-515.

Chen, J., H. Xu, X. Zou, J. Wang, Y. Zhu, H. Chen, B. Shen, X. Deng, A. Zhou, Y. E. Chin, F. J. Rauscher, 3rd, C. Peng, and Z. Hou. 2014. "Snail recruits Ring1B to mediate transcriptional repression and cell migration in pancreatic cancer cells." *Cancer Res* 74 (16): 4353-4363. doi: 10.1158/0008-5472.CAN-14-0181.

Chen, N. M., G. Singh, A. Koenig, G. Y. Liou, P. Storz, J. S. Zhang, L. Regul, S. Nagarajan, B. Kuhnemuth, S. A. Johnsen, M. Hebrok, J. Siveke, D. D. Billadeau, V. Ellenrieder, and E. Hessmann. 2015. "NFATc1 Links EGFR Signaling to Induction of Sox9 Transcription and Acinar-Ductal Transdifferentiation in the Pancreas." *Gastroenterology* 148 (5): 1024-1034 e1029. doi: 10.1053/j.gastro.2015.01.033.

Chen, S., J. Chen, Q. Zhan, Y. Zhu, H. Chen, X. Deng, Z. Hou, B. Shen, Y. Chen, and C. Peng. 2014. "H2AK119Ub1 and H3K27Me3 in molecular staging for survival prediction of patients with pancreatic ductal adenocarcinoma." *Oncotarget* 5 (21): 10421-10433. doi: 10.18632/oncotarget.2126.

Chiba, T., S. Miyagi, A. Saraya, R. Aoki, A. Seki, Y. Morita, Y. Yonemitsu, O. Yokosuka, H. Taniguchi, H. Nakauchi, and A. Iwama. 2008. "The polycomb gene product BMI1 contributes to the maintenance of tumor-initiating side population cells in hepatocellular carcinoma." *Cancer Res* 68 (19): 7742-7749. doi: 10.1158/0008-5472.CAN-07-5882.

Choi, D., and S. Kang. 2011. "Identification and characterization of RNF2 response elements in human kidney cells." *Mol Cells* 31 (3): 247-253. doi: 10.1007/s10059-011-0033-7.

Choy, M. K., M. Movassagh, H. G. Goh, M. R. Bennett, T. A. Down, and R. S. Foo. 2010. "Genome-wide conserved consensus transcription factor binding motifs are hyper-methylated." *BMC Genomics* 11: 519. doi: 10.1186/1471-2164-11-519.

Collado, M., M. A. Blasco, and M. Serrano. 2007. "Cellular senescence in cancer and aging." *Cell* 130 (2): 223-233. doi: 10.1016/j.cell.2007.07.003.

Collins, M. A., F. Bednar, Y. Zhang, J. C. Brisset, S. Galban, C. J. Galban, S. Rakshit, K. S. Flannagan, N. V. Adsay, and M. Pasca di Magliano. 2012. "Oncogenic Kras is required for both the initiation and maintenance of pancreatic cancer in mice." *J Clin Invest* 122 (2): 639-653. doi: 10.1172/JCI59227.

Conroy, T., F. Desseigne, M. Ychou, O. Bouche, R. Guimbaud, Y. Becouarn, A. Adenis, J. L. Raoul, S. Gourgou-Bourgade, C. de la Fouchardiere, J. Bennouna, J. B. Bachet, F. Khemissa-Akouz, D.

Pere-Verge, C. Delbaldo, E. Assenat, B. Chauffert, P. Michel, C. Montoto-Grillot, M. Ducreux, Unicancer Groupe Tumeurs Digestives of, and Prodige Intergroup. 2011. "FOLFIRINOX versus gemcitabine for metastatic pancreatic cancer." *N Engl J Med* 364 (19): 1817-1825. doi: 10.1056/NEJMoa1011923.

Corcoran, R. B., G. Contino, V. Deshpande, A. Tzatsos, C. Conrad, C. H. Benes, D. E. Levy, J. Settleman, J. A. Engelman, and N. Bardeesy. 2011. "STAT3 plays a critical role in KRAS-induced pancreatic tumorigenesis." *Cancer Res* 71 (14): 5020-5029. doi: 10.1158/0008-5472.CAN-11-0908.

Coy, S., J. H. Caamano, J. Carvajal, M. L. Cleary, and A. G. Borycki. 2011. "A novel Gli3 enhancer controls the Gli3 spatiotemporal expression pattern through a TALE homeodomain protein binding site." *Mol Cell Biol* 31 (7): 1432-1443. doi: 10.1128/MCB.00451-10.

Croce, C. M. 2008. "Oncogenes and cancer." *N Engl J Med* 358 (5): 502-511. doi: 10.1056/NEJMra072367.

de Napoles, M., J. E. Mermoud, R. Wakao, Y. A. Tang, M. Endoh, R. Appanah, T. B. Nesterova, J. Silva, A. P. Otte, M. Vidal, H. Koseki, and N. Brockdorff. 2004. "Polycomb group proteins Ring1A/B link ubiquitylation of histone H2A to heritable gene silencing and X inactivation." *Dev Cell* 7 (5): 663-676. doi: 10.1016/j.devcel.2004.10.005.

del Mar Lorente, M., C. Marcos-Gutierrez, C. Perez, J. Schoorlemmer, A. Ramirez, T. Magin, and M. Vidal. 2000. "Loss- and gain-of-function mutations show a polycomb group function for Ring1A in mice." *Development* 127 (23): 5093-5100.

Deubler, S. 2016. "The role of the epigenetic remodeller RING1b in pancreatic carcinogenesis." Unpublished master's thesis, Fakultät für Chemie, Technische Universität München, Munich, Germany.

Diaferia, G. R., C. Balestrieri, E. Prosperini, P. Nicoli, P. Spaggiari, A. Zerbi, and G. Natoli. 2016. "Dissection of transcriptional and cis-regulatory control of differentiation in human pancreatic cancer." *EMBO J* 35 (6): 595-617. doi: 10.15252/embj.201592404.

Distler, M., D. Aust, J. Weitz, C. Pilarsky, and R. Grutzmann. 2014. "Precursor lesions for sporadic pancreatic cancer: PanIN, IPMN, and MCN." *Biomed Res Int* 2014: 474905. doi: 10.1155/2014/474905.

Dockray, G. J. 1972. "The action of scretin, cholecystokinin-pancreozymin and caerulein on pancreatic secretion in the rat." *J Physiol* 225 (3): 679-692.

Dow, L. E., J. Fisher, K. P. O'Rourke, A. Muley, E. R. Kastenhuber, G. Livshits, D. F. Tschaharganeh, N. D. Socci, and S. W. Lowe. 2015. "Inducible in vivo genome editing with CRISPR-Cas9." *Nat Biotechnol* 33 (4): 390-394. doi: 10.1038/nbt.3155.

Dutruel, C., F. Bergmann, I. Rooman, M. Zucknick, D. Weichenhan, L. Geiselhart, T. Kaffenberger, P. S. Rachakonda, A. Bauer, N. Giese, C. Hong, H. Xie, J. F. Costello, J. Hoheisel, R. Kumar, M. Rehli, P. Schirmacher, J. Werner, C. Plass, O. Popanda, and P. Schmezer. 2014. "Early epigenetic downregulation of WNK2 kinase during pancreatic ductal adenocarcinoma development." *Oncogene* 33 (26): 3401-3410. doi: 10.1038/onc.2013.312.

Endoh, M., T. A. Endo, T. Endoh, Y. Fujimura, O. Ohara, T. Toyoda, A. P. Otte, M. Okano, N. Brockdorff, M. Vidal, and H. Koseki. 2008. "Polycomb group proteins Ring1A/B are functionally linked to the core transcriptional regulatory circuitry to maintain ES cell identity." *Development* 135 (8): 1513-1524. doi: 10.1242/dev.014340.

Erkan, M., C. Reiser-Erkan, C. W. Michalski, and J. Kleeff. 2010. "Tumor microenvironment and progression of pancreatic cancer." *Exp Oncol* 32 (3): 128-131.

Ernst, J., and Z. Bar-Joseph. 2006. "STEM: a tool for the analysis of short time series gene expression data." *BMC Bioinformatics* 7: 191. doi: 10.1186/1471-2105-7-191.

Ernst, J., G. J. Nau, and Z. Bar-Joseph. 2005. "Clustering short time series gene expression data." *Bioinformatics* 21 Suppl 1: i159-168. doi: 10.1093/bioinformatics/bti1022.

Eser, S., A. Schnieke, G. Schneider, and D. Saur. 2014. "Oncogenic KRAS signalling in pancreatic cancer." *Br J Cancer* 111 (5): 817-822. doi: 10.1038/bjc.2014.215.

Eskeland, R., M. Leeb, G. R. Grimes, C. Kress, S. Boyle, D. Sproul, N. Gilbert, Y. Fan, A. I. Skoultchi, A. Wutz, and W. A. Bickmore. 2010. "Ring1B compacts chromatin structure and represses gene expression independent of histone ubiquitination." *Mol Cell* 38 (3): 452-464. doi: 10.1016/j.molcel.2010.02.032.

Esposito, I., J. Kleeff, I. Abiatari, X. Shi, N. Giese, F. Bergmann, W. Roth, H. Friess, and P. Schirmacher. 2007. "Overexpression of cellular inhibitor of apoptosis protein 2 is an early event in the progression of pancreatic cancer." *J Clin Pathol* 60 (8): 885-895. doi: 10.1136/jcp.2006.038257.

Esposito, I., B. Konukiewitz, A. M. Schlitter, and G. Kloppel. 2014. "Pathology of pancreatic ductal adenocarcinoma: facts, challenges and future developments." *World J Gastroenterol* 20 (38): 13833-13841. doi: 10.3748/wjg.v20.i38.13833.

Etemad, B., and D. C. Whitcomb. 2001. "Chronic pancreatitis: diagnosis, classification, and new genetic developments." *Gastroenterology* 120 (3): 682-707.
Ezhkova, E., H. A. Pasolli, J. S. Parker, N. Stokes, I. H. Su, G. Hannon, A. Tarakhovsky, and E. Fuchs. 2009. "Ezh2 orchestrates gene expression for the stepwise differentiation of tissue-specific stem cells." *Cell* 136 (6): 1122-1135. doi: 10.1016/j.cell.2008.12.043.
Feil, R., J. Brocard, B. Mascrez, M. LeMeur, D. Metzger, and P. Chambon. 1996. "Ligand-activated site-specific recombination in mice." *Proc Natl Acad Sci U S A* 93 (20): 10887-10890.
Feinberg, A. P., and B. Vogelstein. 1983. "Hypomethylation of ras oncogenes in primary human cancers." *Biochem Biophys Res Commun* 111 (1): 47-54.
Fendrich, V., F. Esni, M. V. Garay, G. Feldmann, N. Habbe, J. N. Jensen, Y. Dor, D. Stoffers, J. Jensen, S. D. Leach, and A. Maitra. 2008. "Hedgehog signaling is required for effective regeneration of exocrine pancreas." *Gastroenterology* 135 (2): 621-631. doi: 10.1053/j.gastro.2008.04.011.
Field, Andrew S., and Matthew A. Zarka. 2016. *Practical cytopathology : a diagnostic approach to fine-needle aspiration biopsy*. 1. ed. St. Louis: Elsevier. p.
Frossard, J. L., M. L. Steer, and C. M. Pastor. 2008. "Acute pancreatitis." *Lancet* 371 (9607): 143-152. doi: 10.1016/S0140-6736(08)60107-5.
Fu, C. Y., C. N. Yeh, J. T. Hsu, Y. Y. Jan, and T. L. Hwang. 2007. "Timing of mortality in severe acute pancreatitis: experience from 643 patients." *World J Gastroenterol* 13 (13): 1966-1969.
Fuks, F., P. J. Hurd, D. Wolf, X. Nan, A. P. Bird, and T. Kouzarides. 2003. "The methyl-CpG-binding protein MeCP2 links DNA methylation to histone methylation." *J Biol Chem* 278 (6): 4035-4040. doi: 10.1074/jbc.M210256200.
Fukuda, A., J. P. th Morris, and M. Hebrok. 2012. "Bmi1 is required for regeneration of the exocrine pancreas in mice." *Gastroenterology* 143 (3): 821-831 e821-822. doi: 10.1053/j.gastro.2012.05.009.
Geles, K. G., W. Zhong, S. K. O'Brien, M. Baxter, C. Loreth, D. Pallares, and M. Damelin. 2016. "Upregulation of RNA Processing Factors in Poorly Differentiated Lung Cancer Cells." *Transl Oncol* 9 (2): 89-98. doi: 10.1016/j.tranon.2016.01.006.
Geron, E., E. D. Schejter, and B. Z. Shilo. 2014. "Assessing the secretory capacity of pancreatic acinar cells." *J Vis Exp* (90). doi: 10.3791/51799.
Giardiello, F. M., J. D. Brensinger, A. C. Tersmette, S. N. Goodman, G. M. Petersen, S. V. Booker, M. Cruz-Correa, and J. A. Offerhaus. 2000. "Very high risk of cancer in familial Peutz-Jeghers syndrome." *Gastroenterology* 119 (6): 1447-1453.
Gittes, G. K. 2009. "Developmental biology of the pancreas: a comprehensive review." *Dev Biol* 326 (1): 4-35. doi: 10.1016/j.ydbio.2008.10.024.
Goke, J., Y. S. Chan, J. Yan, M. Vingron, and H. H. Ng. 2013. "Genome-wide kinase-chromatin interactions reveal the regulatory network of ERK signaling in human embryonic stem cells." *Mol Cell* 50 (6): 844-855. doi: 10.1016/j.molcel.2013.04.030.
Goldberg, A. D., C. D. Allis, and E. Bernstein. 2007. "Epigenetics: a landscape takes shape." *Cell* 128 (4): 635-638. doi: 10.1016/j.cell.2007.02.006.
Graf, T., and T. Enver. 2009. "Forcing cells to change lineages." *Nature* 462 (7273): 587-594. doi: 10.1038/nature08533.
Guerra, C., and M. Barbacid. 2013. "Genetically engineered mouse models of pancreatic adenocarcinoma." *Mol Oncol* 7 (2): 232-247. doi: 10.1016/j.molonc.2013.02.002.
Guerra, C., A. J. Schuhmacher, M. Canamero, P. J. Grippo, L. Verdaguer, L. Perez-Gallego, P. Dubus, E. P. Sandgren, and M. Barbacid. 2007. "Chronic pancreatitis is essential for induction of pancreatic ductal adenocarcinoma by K-Ras oncogenes in adult mice." *Cancer Cell* 11 (3): 291-302. doi: 10.1016/j.ccr.2007.01.012.
Gukovskaya, A. S., I. Gukovsky, V. Zaninovic, M. Song, D. Sandoval, S. Gukovsky, and S. J. Pandol. 1997. "Pancreatic acinar cells produce, release, and respond to tumor necrosis factor-alpha. Role in regulating cell death and pancreatitis." *J Clin Invest* 100 (7): 1853-1862. doi: 10.1172/JCI119714.
Habbe, N., G. Shi, R. A. Meguid, V. Fendrich, F. Esni, H. Chen, G. Feldmann, D. A. Stoffers, S. F. Konieczny, S. D. Leach, and A. Maitra. 2008. "Spontaneous induction of murine pancreatic intraepithelial neoplasia (mPanIN) by acinar cell targeting of oncogenic Kras in adult mice." *Proc Natl Acad Sci U S A* 105 (48): 18913-18918. doi: 10.1073/pnas.0810097105.
Halangk, W., M. M. Lerch, B. Brandt-Nedelev, W. Roth, M. Ruthenbuerger, T. Reinheckel, W. Domschke, H. Lippert, C. Peters, and J. Deussing. 2000. "Role of cathepsin B in intracellular trypsinogen activation and the onset of acute pancreatitis." *J Clin Invest* 106 (6): 773-781. doi: 10.1172/JCI9411.

Hald, J., J. P. Hjorth, M. S. German, O. D. Madsen, P. Serup, and J. Jensen. 2003. "Activated Notch1 prevents differentiation of pancreatic acinar cells and attenuate endocrine development." *Dev Biol* 260 (2): 426-437.

Hale, M. A., H. Kagami, L. Shi, A. M. Holland, H. P. Elsasser, R. E. Hammer, and R. J. MacDonald. 2005. "The homeodomain protein PDX1 is required at mid-pancreatic development for the formation of the exocrine pancreas." *Dev Biol* 286 (1): 225-237. doi: 10.1016/j.ydbio.2005.07.026.

Haring, M., S. Offermann, T. Danker, I. Horst, C. Peterhansel, and M. Stam. 2007. "Chromatin immunoprecipitation: optimization, quantitative analysis and data normalization." *Plant Methods* 3: 11. doi: 10.1186/1746-4811-3-11.

Hebrok, M., S. K. Kim, B. St Jacques, A. P. McMahon, and D. A. Melton. 2000. "Regulation of pancreas development by hedgehog signaling." *Development* 127 (22): 4905-4913.

Helm, O., R. Mennrich, D. Petrick, L. Goebel, S. Freitag-Wolf, C. Roder, H. Kalthoff, C. Rocken, B. Sipos, D. Kabelitz, H. Schafer, H. H. Oberg, D. Wesch, and S. Sebens. 2014. "Comparative characterization of stroma cells and ductal epithelium in chronic pancreatitis and pancreatic ductal adenocarcinoma." *PLoS One* 9 (5): e94357. doi: 10.1371/journal.pone.0094357.

Hendrich, B., and A. Bird. 1998. "Identification and characterization of a family of mammalian methyl-CpG binding proteins." *Mol Cell Biol* 18 (11): 6538-6547.

Herman, J. G., A. Merlo, L. Mao, R. G. Lapidus, J. P. Issa, N. E. Davidson, D. Sidransky, and S. B. Baylin. 1995. "Inactivation of the CDKN2/p16/MTS1 gene is frequently associated with aberrant DNA methylation in all common human cancers." *Cancer Res* 55 (20): 4525-4530.

Hezel, A. F., A. C. Kimmelman, B. Z. Stanger, N. Bardeesy, and R. A. Depinho. 2006. "Genetics and biology of pancreatic ductal adenocarcinoma." *Genes Dev* 20 (10): 1218-1249. doi: 10.1101/gad.1415606.

Hidalgo, M., F. Amant, A. V. Biankin, E. Budinska, A. T. Byrne, C. Caldas, R. B. Clarke, S. de Jong, J. Jonkers, G. M. Maelandsmo, S. Roman-Roman, J. Seoane, L. Trusolino, and A. Villanueva. 2014. "Patient-derived xenograft models: an emerging platform for translational cancer research." *Cancer Discov* 4 (9): 998-1013. doi: 10.1158/2159-8290.CD-14-0001.

Hidalgo, M., E. Bruckheimer, N. V. Rajeshkumar, I. Garrido-Laguna, E. De Oliveira, B. Rubio-Viqueira, S. Strawn, M. J. Wick, J. Martell, and D. Sidransky. 2011. "A pilot clinical study of treatment guided by personalized tumorgrafts in patients with advanced cancer." *Mol Cancer Ther* 10 (8): 1311-1316. doi: 10.1158/1535-7163.MCT-11-0233.

Hingorani, S. R., E. F. Petricoin, A. Maitra, V. Rajapakse, C. King, M. A. Jacobetz, S. Ross, T. P. Conrads, T. D. Veenstra, B. A. Hitt, Y. Kawaguchi, D. Johann, L. A. Liotta, H. C. Crawford, M. E. Putt, T. Jacks, C. V. Wright, R. H. Hruban, A. M. Lowy, and D. A. Tuveson. 2003. "Preinvasive and invasive ductal pancreatic cancer and its early detection in the mouse." *Cancer Cell* 4 (6): 437-450.

Hingorani, S. R., L. Wang, A. S. Multani, C. Combs, T. B. Deramaudt, R. H. Hruban, A. K. Rustgi, S. Chang, and D. A. Tuveson. 2005. "Trp53R172H and KrasG12D cooperate to promote chromosomal instability and widely metastatic pancreatic ductal adenocarcinoma in mice." *Cancer Cell* 7 (5): 469-483. doi: 10.1016/j.ccr.2005.04.023.

Hong, L., G. P. Schroth, H. R. Matthews, P. Yau, and E. M. Bradbury. 1993. "Studies of the DNA binding properties of histone H4 amino terminus. Thermal denaturation studies reveal that acetylation markedly reduces the binding constant of the H4 "tail" to DNA." *J Biol Chem* 268 (1): 305-314.

Houbracken, I., E. de Waele, J. Lardon, Z. Ling, H. Heimberg, I. Rooman, and L. Bouwens. 2011. "Lineage tracing evidence for transdifferentiation of acinar to duct cells and plasticity of human pancreas." *Gastroenterology* 141 (2): 731-741, 741 e731-734. doi: 10.1053/j.gastro.2011.04.050.

Hruban, R. H., N. V. Adsay, J. Albores-Saavedra, C. Compton, E. S. Garrett, S. N. Goodman, S. E. Kern, D. S. Klimstra, G. Kloppel, D. S. Longnecker, J. Luttges, and G. J. Offerhaus. 2001. "Pancreatic intraepithelial neoplasia: a new nomenclature and classification system for pancreatic duct lesions." *Am J Surg Pathol* 25 (5): 579-586.

Hruban, R. H., A. Maitra, and M. Goggins. 2008. "Update on pancreatic intraepithelial neoplasia." *Int J Clin Exp Pathol* 1 (4): 306-316.

Ismail, I. H., D. McDonald, H. Strickfaden, Z. Xu, and M. J. Hendzel. 2013. "A small molecule inhibitor of polycomb repressive complex 1 inhibits ubiquitin signaling at DNA double-strand breaks." *J Biol Chem* 288 (37): 26944-26954. doi: 10.1074/jbc.M113.461699.

Jackson, E. L., N. Willis, K. Mercer, R. T. Bronson, D. Crowley, R. Montoya, T. Jacks, and D. A. Tuveson. 2001. "Analysis of lung tumor initiation and progression using conditional expression of oncogenic K-ras." *Genes Dev* 15 (24): 3243-3248. doi: 10.1101/gad.943001.

Jeannotte, L., M. Lemieux, J. Charron, F. Poirier, and E. J. Robertson. 1993. "Specification of axial identity in the mouse: role of the Hoxa-5 (Hox1.3) gene." *Genes Dev* 7 (11): 2085-2096.

Jenne, D. E., H. Reimann, J. Nezu, W. Friedel, S. Loff, R. Jeschke, O. Muller, W. Back, and M. Zimmer. 1998. "Peutz-Jeghers syndrome is caused by mutations in a novel serine threonine kinase." *Nat Genet* 18 (1): 38-43. doi: 10.1038/ng0198-38.

Jensen, J. N., E. Cameron, M. V. Garay, T. W. Starkey, R. Gianani, and J. Jensen. 2005. "Recapitulation of elements of embryonic development in adult mouse pancreatic regeneration." *Gastroenterology* 128 (3): 728-741.

Jensen, R. T., S. A. Wank, W. H. Rowley, S. Sato, and J. D. Gardner. 1989. "Interaction of CCK with pancreatic acinar cells." *Trends Pharmacol Sci* 10 (10): 418-423.

Jimenez, R. E., A. L. Warshaw, K. Z'Graggen, W. Hartwig, D. Z. Taylor, C. C. Compton, and C. Fernandez-del Castillo. 1999. "Sequential accumulation of K-ras mutations and p53 overexpression in the progression of pancreatic mucinous cystic neoplasms to malignancy." *Ann Surg* 230 (4): 501-509; discussion 509-511.

Jin, B., J. Ernst, R. L. Tiedemann, H. Xu, S. Sureshchandra, M. Kellis, S. Dalton, C. Liu, J. H. Choi, and K. D. Robertson. 2012. "Linking DNA methyltransferases to epigenetic marks and nucleosome structure genome-wide in human tumor cells." *Cell Rep* 2 (5): 1411-1424. doi: 10.1016/j.celrep.2012.10.017.

Johnson, C. L., J. M. Peat, S. N. Volante, R. Wang, C. A. McLean, and C. L. Pin. 2012. "Activation of protein kinase Cdelta leads to increased pancreatic acinar cell dedifferentiation in the absence of MIST1." *J Pathol* 228 (3): 351-365. doi: 10.1002/path.4015.

Jonsson, J., L. Carlsson, T. Edlund, and H. Edlund. 1994. "Insulin-promoter-factor 1 is required for pancreas development in mice." *Nature* 371 (6498): 606-609. doi: 10.1038/371606a0.

Kalluri, R., and R. A. Weinberg. 2009. "The basics of epithelial-mesenchymal transition." *J Clin Invest* 119 (6): 1420-1428. doi: 10.1172/JCI39104.

Kanda, M., H. Matthaei, J. Wu, S. M. Hong, J. Yu, M. Borges, R. H. Hruban, A. Maitra, K. Kinzler, B. Vogelstein, and M. Goggins. 2012. "Presence of somatic mutations in most early-stage pancreatic intraepithelial neoplasia." *Gastroenterology* 142 (4): 730-733 e739. doi: 10.1053/j.gastro.2011.12.042.

Katz, J. P., N. Perreault, B. G. Goldstein, C. S. Lee, P. A. Labosky, V. W. Yang, and K. H. Kaestner. 2002. "The zinc-finger transcription factor Klf4 is required for terminal differentiation of goblet cells in the colon." *Development* 129 (11): 2619-2628.

Kawaguchi, Y., B. Cooper, M. Gannon, M. Ray, R. J. MacDonald, and C. V. Wright. 2002. "The role of the transcriptional regulator Ptf1a in converting intestinal to pancreatic progenitors." *Nat Genet* 32 (1): 128-134. doi: 10.1038/ng959.

Kim, C. A., M. Gingery, R. M. Pilpa, and J. U. Bowie. 2002. "The SAM domain of polyhomeotic forms a helical polymer." *Nat Struct Biol* 9 (6): 453-457. doi: 10.1038/nsb802.

Kim, W., G. H. Bird, T. Neff, G. Guo, M. A. Kerenyi, L. D. Walensky, and S. H. Orkin. 2013. "Targeted disruption of the EZH2-EED complex inhibits EZH2-dependent cancer." *Nat Chem Biol* 9 (10): 643-650. doi: 10.1038/nchembio.1331.

Kleer, C. G., Q. Cao, S. Varambally, R. Shen, I. Ota, S. A. Tomlins, D. Ghosh, R. G. Sewalt, A. P. Otte, D. F. Hayes, M. S. Sabel, D. Livant, S. J. Weiss, M. A. Rubin, and A. M. Chinnaiyan. 2003. "EZH2 is a marker of aggressive breast cancer and promotes neoplastic transformation of breast epithelial cells." *Proc Natl Acad Sci U S A* 100 (20): 11606-11611. doi: 10.1073/pnas.1933744100.

Knudson, A. G., Jr. 1971. "Mutation and cancer: statistical study of retinoblastoma." *Proc Natl Acad Sci U S A* 68 (4): 820-823.

Koch, C. M., R. M. Andrews, P. Flicek, S. C. Dillon, U. Karaoz, G. K. Clelland, S. Wilcox, D. M. Beare, J. C. Fowler, P. Couttet, K. D. James, G. C. Lefebvre, A. W. Bruce, O. M. Dovey, P. D. Ellis, P. Dhami, C. F. Langford, Z. Weng, E. Birney, N. P. Carter, D. Vetrie, and I. Dunham. 2007. "The landscape of histone modifications across 1% of the human genome in five human cell lines." *Genome Res* 17 (6): 691-707. doi: 10.1101/gr.5704207.

Kondo, T., K. Isono, K. Kondo, T. A. Endo, S. Itohara, M. Vidal, and H. Koseki. 2014. "Polycomb potentiates meis2 activation in midbrain by mediating interaction of the promoter with a tissue-specific enhancer." *Dev Cell* 28 (1): 94-101. doi: 10.1016/j.devcel.2013.11.021.

Kong, B., P. Bruns, N. A. Behler, L. Chang, A. M. Schlitter, J. Cao, A. Gewies, J. Ruland, S. Fritzsche, N. Valkovskaya, Z. Jian, I. Regel, S. Raulefs, M. Irmler, J. Beckers, H. Friess, M. Erkan, N. S. Mueller, S. Roth, T. Hackert, I. Esposito, F. J. Theis, J. Kleeff, and C. W. Michalski. 2016. "Dynamic landscape of pancreatic carcinogenesis reveals early molecular networks of malignancy." *Gut*. doi: 10.1136/gutjnl-2015-310913.

Kopinke, D., M. Brailsford, F. C. Pan, M. A. Magnuson, C. V. Wright, and L. C. Murtaugh. 2012. "Ongoing Notch signaling maintains phenotypic fidelity in the adult exocrine pancreas." *Dev Biol* 362 (1): 57-64. doi: 10.1016/j.ydbio.2011.11.010.

Kopp, J. L., C. L. Dubois, A. E. Schaffer, E. Hao, H. P. Shih, P. A. Seymour, J. Ma, and M. Sander. 2011. "Sox9+ ductal cells are multipotent progenitors throughout development but do not produce new endocrine cells in the normal or injured adult pancreas." *Development* 138 (4): 653-665. doi: 10.1242/dev.056499.

Kopp, J. L., G. von Figura, E. Mayes, F. F. Liu, C. L. Dubois, J. P. th Morris, F. C. Pan, H. Akiyama, C. V. Wright, K. Jensen, M. Hebrok, and M. Sander. 2012. "Identification of Sox9-dependent acinar-to-ductal reprogramming as the principal mechanism for initiation of pancreatic ductal adenocarcinoma." *Cancer Cell* 22 (6): 737-750. doi: 10.1016/j.ccr.2012.10.025.

Krah, N. M., O. Jp De La, G. H. Swift, C. Q. Hoang, S. G. Willet, F. Chen Pan, G. M. Cash, M. P. Bronner, C. V. Wright, R. J. MacDonald, and L. C. Murtaugh. 2015. "The acinar differentiation determinant PTF1A inhibits initiation of pancreatic ductal adenocarcinoma." *Elife* 4. doi: 10.7554/eLife.07125.

Krapp, A., M. Knofler, B. Ledermann, K. Burki, C. Berney, N. Zoerkler, O. Hagenbuchle, and P. K. Wellauer. 1998. "The bHLH protein PTF1-p48 is essential for the formation of the exocrine and the correct spatial organization of the endocrine pancreas." *Genes Dev* 12 (23): 3752-3763.

Kreso, A., P. van Galen, N. M. Pedley, E. Lima-Fernandes, C. Frelin, T. Davis, L. Cao, R. Baiazitov, W. Du, N. Sydorenko, Y. C. Moon, L. Gibson, Y. Wang, C. Leung, N. N. Iscove, C. H. Arrowsmith, E. Szentgyorgyi, S. Gallinger, J. E. Dick, and C. A. O'Brien. 2014. "Self-renewal as a therapeutic target in human colorectal cancer." *Nat Med* 20 (1): 29-36. doi: 10.1038/nm.3418.

Ku, M., R. P. Koche, E. Rheinbay, E. M. Mendenhall, M. Endoh, T. S. Mikkelsen, A. Presser, C. Nusbaum, X. Xie, A. S. Chi, M. Adli, S. Kasif, L. M. Ptaszek, C. A. Cowan, E. S. Lander, H. Koseki, and B. E. Bernstein. 2008. "Genomewide analysis of PRC1 and PRC2 occupancy identifies two classes of bivalent domains." *PLoS Genet* 4 (10): e1000242. doi: 10.1371/journal.pgen.1000242.

Larsen, F., G. Gundersen, R. Lopez, and H. Prydz. 1992. "CpG islands as gene markers in the human genome." *Genomics* 13 (4): 1095-1107.

Lau, P. P., M. A. Dubick, G. S. Yu, P. R. Morrill, and M. C. Geokas. 1990. "Dynamic changes of pancreatic structure and function in rats treated chronically with nicotine." *Toxicol Appl Pharmacol* 104 (3): 457-465.

Lee, T. I., R. G. Jenner, L. A. Boyer, M. G. Guenther, S. S. Levine, R. M. Kumar, B. Chevalier, S. E. Johnstone, M. F. Cole, K. Isono, H. Koseki, T. Fuchikami, K. Abe, H. L. Murray, J. P. Zucker, B. Yuan, G. W. Bell, E. Herbolsheimer, N. M. Hannett, K. Sun, D. T. Odom, A. P. Otte, T. L. Volkert, D. P. Bartel, D. A. Melton, D. K. Gifford, R. Jaenisch, and R. A. Young. 2006. "Control of developmental regulators by Polycomb in human embryonic stem cells." *Cell* 125 (2): 301-313. doi: 10.1016/j.cell.2006.02.043.

Legube, G., and D. Trouche. 2003. "Regulating histone acetyltransferases and deacetylases." *EMBO Rep* 4 (10): 944-947. doi: 10.1038/sj.embor.embor941.

Lehmann, L., R. Ferrari, A. A. Vashisht, J. A. Wohlschlegel, S. K. Kurdistani, and M. Carey. 2012. "Polycomb repressive complex 1 (PRC1) disassembles RNA polymerase II preinitiation complexes." *J Biol Chem* 287 (43): 35784-35794. doi: 10.1074/jbc.M112.397430.

Levine, A. J. 1997. "p53, the cellular gatekeeper for growth and division." *Cell* 88 (3): 323-331.

Li, Z., R. Cao, M. Wang, M. P. Myers, Y. Zhang, and R. M. Xu. 2006. "Structure of a Bmi-1-Ring1B polycomb group ubiquitin ligase complex." *J Biol Chem* 281 (29): 20643-20649. doi: 10.1074/jbc.M602461200.

Liou, G. Y., H. Doppler, B. Necela, M. Krishna, H. C. Crawford, M. Raimondo, and P. Storz. 2013. "Macrophage-secreted cytokines drive pancreatic acinar-to-ductal metaplasia through NF-kappaB and MMPs." *J Cell Biol* 202 (3): 563-577. doi: 10.1083/jcb.201301001.

Liu, T., S. M. Gou, C. Y. Wang, H. S. Wu, J. X. Xiong, and F. Zhou. 2007. "Pancreas duodenal homeobox-1 expression and significance in pancreatic cancer." *World J Gastroenterol* 13 (18): 2615-2618.

Livak, K. J., and T. D. Schmittgen. 2001. "Analysis of relative gene expression data using real-time quantitative PCR and the 2(-Delta Delta C(T)) Method." *Methods* 25 (4): 402-408. doi: 10.1006/meth.2001.1262.

Lovering, R., I. M. Hanson, K. L. Borden, S. Martin, N. J. O'Reilly, G. I. Evan, D. Rahman, D. J. Pappin, J. Trowsdale, and P. S. Freemont. 1993. "Identification and preliminary characterization of a protein motif related to the zinc finger." *Proc Natl Acad Sci U S A* 90 (6): 2112-2116.

Lowenfels, A. B., P. Maisonneuve, G. Cavallini, R. W. Ammann, P. G. Lankisch, J. R. Andersen, E. P. Dimagno, A. Andren-Sandberg, and L. Domellof. 1993. "Pancreatitis and the risk of pancreatic cancer. International Pancreatitis Study Group." *N Engl J Med* 328 (20): 1433-1437. doi: 10.1056/NEJM199305203282001.

Lowenfels, A. B., P. Maisonneuve, E. P. DiMagno, Y. Elitsur, L. K. Gates, Jr., J. Perrault, and D. C. Whitcomb. 1997. "Hereditary pancreatitis and the risk of pancreatic cancer. International Hereditary Pancreatitis Study Group." *J Natl Cancer Inst* 89 (6): 442-446.

Lowy, Andrew M., Steven D. Leach, and Philip A. Philip. 2008. *Pancreatic cancer*, *M D Anderson solid tumor oncology series*. New York ; London: Springer. p.

Luger, K., A. W. Mader, R. K. Richmond, D. F. Sargent, and T. J. Richmond. 1997. "Crystal structure of the nucleosome core particle at 2.8 A resolution." *Nature* 389 (6648): 251-260. doi: 10.1038/38444.

Lukacs, R. U., S. Memarzadeh, H. Wu, and O. N. Witte. 2010. "Bmi-1 is a crucial regulator of prostate stem cell self-renewal and malignant transformation." *Cell Stem Cell* 7 (6): 682-693. doi: 10.1016/j.stem.2010.11.013.

Ma, Y., L. Zhang, and X. Huang. 2014. "Genome modification by CRISPR/Cas9." *FEBS J* 281 (23): 5186-5193. doi: 10.1111/febs.13110.

Madisen, L., T. A. Zwingman, S. M. Sunkin, S. W. Oh, H. A. Zariwala, H. Gu, L. L. Ng, R. D. Palmiter, M. J. Hawrylycz, A. R. Jones, E. S. Lein, and H. Zeng. 2010. "A robust and high-throughput Cre reporting and characterization system for the whole mouse brain." *Nat Neurosci* 13 (1): 133-140. doi: 10.1038/nn.2467.

Mahajan, U. M., S. Teller, M. Sendler, R. Palankar, C. van den Brandt, T. Schwaiger, J. P. Kuhn, S. Ribback, G. Glockl, M. Evert, W. Weitschies, N. Hosten, F. Dombrowski, M. Delcea, F. U. Weiss, M. M. Lerch, and J. Mayerle. 2016. "Tumour-specific delivery of siRNA-coupled superparamagnetic iron oxide nanoparticles, targeted against PLK1, stops progression of pancreatic cancer." *Gut*. doi: 10.1136/gutjnl-2016-311393.

Maisonneuve, P., and A. B. Lowenfels. 2010. "Epidemiology of pancreatic cancer: an update." *Dig Dis* 28 (4-5): 645-656. doi: 10.1159/000320068.

Maitra, A., N. Fukushima, K. Takaori, and R. H. Hruban. 2005. "Precursors to invasive pancreatic cancer." *Adv Anat Pathol* 12 (2): 81-91.

Mallen-St Clair, J., R. Soydaner-Azeloglu, K. E. Lee, L. Taylor, A. Livanos, Y. Pylayeva-Gupta, G. Miller, R. Margueron, D. Reinberg, and D. Bar-Sagi. 2012. "EZH2 couples pancreatic regeneration to neoplastic progression." *Genes Dev* 26 (5): 439-444. doi: 10.1101/gad.181800.111.

Marchesi, F., L. Piemonti, A. Mantovani, and P. Allavena. 2010. "Molecular mechanisms of perineural invasion, a forgotten pathway of dissemination and metastasis." *Cytokine Growth Factor Rev* 21 (1): 77-82. doi: 10.1016/j.cytogfr.2009.11.001.

Margueron, R., and D. Reinberg. 2011. "The Polycomb complex PRC2 and its mark in life." *Nature* 469 (7330): 343-349. doi: 10.1038/nature09784.

Marino-Ramirez, L., M. G. Kann, B. A. Shoemaker, and D. Landsman. 2005. "Histone structure and nucleosome stability." *Expert Rev Proteomics* 2 (5): 719-729. doi: 10.1586/14789450.2.5.719.

Marino, S., M. Vooijs, H. van Der Gulden, J. Jonkers, and A. Berns. 2000. "Induction of medulloblastomas in p53-null mutant mice by somatic inactivation of Rb in the external granular layer cells of the cerebellum." *Genes Dev* 14 (8): 994-1004.

Martinez-Romero, C., I. Rooman, A. Skoudy, C. Guerra, X. Molero, A. Gonzalez, M. Iglesias, T. Lobato, A. Bosch, M. Barbacid, F. X. Real, and I. Hernandez-Munoz. 2009. "The epigenetic regulators Bmi1 and Ring1B are differentially regulated in pancreatitis and pancreatic ductal adenocarcinoma." *J Pathol* 219 (2): 205-213. doi: 10.1002/path.2585.

Masui, T., Q. Long, T. M. Beres, M. A. Magnuson, and R. J. MacDonald. 2007. "Early pancreatic development requires the vertebrate Suppressor of Hairless (RBPJ) in the PTF1 bHLH complex." *Genes Dev* 21 (20): 2629-2643. doi: 10.1101/gad.1575207.

Masui, T., G. H. Swift, T. Deering, C. Shen, W. S. Coats, Q. Long, H. P. Elsasser, M. A. Magnuson, and R. J. MacDonald. 2010. "Replacement of Rbpj with Rbpjl in the PTF1 complex controls the final maturation of pancreatic acinar cells." *Gastroenterology* 139 (1): 270-280. doi: 10.1053/j.gastro.2010.04.003.

Matull, W. R., S. P. Pereira, and J. W. O'Donohue. 2006. "Biochemical markers of acute pancreatitis." *J Clin Pathol* 59 (4): 340-344. doi: 10.1136/jcp.2002.002923.

McCleary-Wheeler, A. L., G. A. Lomberk, F. U. Weiss, G. Schneider, M. Fabbri, T. L. Poshusta, N. J. Dusetti, S. Baumgart, J. L. Iovanna, V. Ellenrieder, R. Urrutia, and M. E. Fernandez-Zapico. 2013. "Insights into the epigenetic mechanisms controlling pancreatic carcinogenesis." *Cancer Lett* 328 (2): 212-221. doi: 10.1016/j.canlet.2012.10.005.

Means, A. L., I. M. Meszoely, K. Suzuki, Y. Miyamoto, A. K. Rustgi, R. J. Coffey, Jr., C. V. Wright, D. A. Stoffers, and S. D. Leach. 2005. "Pancreatic epithelial plasticity mediated by acinar cell transdifferentiation and generation of nestin-positive intermediates." *Development* 132 (16): 3767-3776. doi: 10.1242/dev.01925.

Mendenhall, E. M., R. P. Koche, T. Truong, V. W. Zhou, B. Issac, A. S. Chi, M. Ku, and B. E. Bernstein. 2010. "GC-rich sequence elements recruit PRC2 in mammalian ES cells." *PLoS Genet* 6 (12): e1001244. doi: 10.1371/journal.pgen.1001244.

Miao, E. A., J. V. Rajan, and A. Aderem. 2011. "Caspase-1-induced pyroptotic cell death." *Immunol Rev* 243 (1): 206-214. doi: 10.1111/j.1600-065X.2011.01044.x.

Mikkelsen, T. S., M. Ku, D. B. Jaffe, B. Issac, E. Lieberman, G. Giannoukos, P. Alvarez, W. Brockman, T. K. Kim, R. P. Koche, W. Lee, E. Mendenhall, A. O'Donovan, A. Presser, C. Russ, X. Xie, A. Meissner, M. Wernig, R. Jaenisch, C. Nusbaum, E. S. Lander, and B. E. Bernstein. 2007. "Genome-wide maps of chromatin state in pluripotent and lineage-committed cells." *Nature* 448 (7153): 553-560. doi: 10.1038/nature06008.

Miyatsuka, T., H. Kaneto, T. Shiraiwa, T. A. Matsuoka, K. Yamamoto, K. Kato, Y. Nakamura, S. Akira, K. Takeda, Y. Kajimoto, Y. Yamasaki, E. P. Sandgren, Y. Kawaguchi, C. V. Wright, and Y. Fujitani. 2006. "Persistent expression of PDX-1 in the pancreas causes acinar-to-ductal metaplasia through Stat3 activation." *Genes Dev* 20 (11): 1435-1440. doi: 10.1101/gad.1412806.

Montgomery, N. D., D. Yee, A. Chen, S. Kalantry, S. J. Chamberlain, A. P. Otte, and T. Magnuson. 2005. "The murine polycomb group protein Eed is required for global histone H3 lysine-27 methylation." *Curr Biol* 15 (10): 942-947. doi: 10.1016/j.cub.2005.04.051.

Moore, M. J., D. Goldstein, J. Hamm, A. Figer, J. R. Hecht, S. Gallinger, H. J. Au, P. Murawa, D. Walde, R. A. Wolff, D. Campos, R. Lim, K. Ding, G. Clark, T. Voskoglou-Nomikos, M. Ptasynski, W. Parulekar, and Group National Cancer Institute of Canada Clinical Trials. 2007. "Erlotinib plus gemcitabine compared with gemcitabine alone in patients with advanced pancreatic cancer: a phase III trial of the National Cancer Institute of Canada Clinical Trials Group." *J Clin Oncol* 25 (15): 1960-1966. doi: 10.1200/JCO.2006.07.9525.

Morris, J. P. th, S. C. Wang, and M. Hebrok. 2010. "KRAS, Hedgehog, Wnt and the twisted developmental biology of pancreatic ductal adenocarcinoma." *Nat Rev Cancer* 10 (10): 683-695. doi: 10.1038/nrc2899.

Morton, J. P., P. Timpson, S. A. Karim, R. A. Ridgway, D. Athineos, B. Doyle, N. B. Jamieson, K. A. Oien, A. M. Lowy, V. G. Brunton, M. C. Frame, T. R. Evans, and O. J. Sansom. 2010. "Mutant p53 drives metastasis and overcomes growth arrest/senescence in pancreatic cancer." *Proc Natl Acad Sci U S A* 107 (1): 246-251. doi: 10.1073/pnas.0908428107.

Muda, M., U. Boschert, A. Smith, B. Antonsson, C. Gillieron, C. Chabert, M. Camps, I. Martinou, A. Ashworth, and S. Arkinstall. 1997. "Molecular cloning and functional characterization of a novel mitogen-activated protein kinase phosphatase, MKP-4." *J Biol Chem* 272 (8): 5141-5151.

Muff, R., P. Rath, R. M. Ram Kumar, K. Husmann, W. Born, M. Baudis, and B. Fuchs. 2015. "Genomic instability of osteosarcoma cell lines in culture: impact on the prediction of metastasis relevant genes." *PLoS One* 10 (5): e0125611. doi: 10.1371/journal.pone.0125611.

Nacerddine, K., J. B. Beaudry, V. Ginjala, B. Westerman, F. Mattiroli, J. Y. Song, H. van der Poel, O. B. Ponz, C. Pritchard, P. Cornelissen-Steijger, J. Zevenhoven, E. Tanger, T. K. Sixma, S. Ganesan, and M. van Lohuizen. 2012. "Akt-mediated phosphorylation of Bmi1 modulates its oncogenic potential, E3 ligase activity, and DNA damage repair activity in mouse prostate cancer." *J Clin Invest* 122 (5): 1920-1932. doi: 10.1172/JCI57477.

Nan, X., H. H. Ng, C. A. Johnson, C. D. Laherty, B. M. Turner, R. N. Eisenman, and A. Bird. 1998. "Transcriptional repression by the methyl-CpG-binding protein MeCP2 involves a histone deacetylase complex." *Nature* 393 (6683): 386-389. doi: 10.1038/30764.

Neoptolemos, J. P., D. D. Stocken, H. Friess, C. Bassi, J. A. Dunn, H. Hickey, H. Beger, L. Fernandez-Cruz, C. Dervenis, F. Lacaine, M. Falconi, P. Pederzoli, A. Pap, D. Spooner, D. J. Kerr, M. W. Buchler, and Cancer European Study Group for Pancreatic. 2004. "A randomized trial of chemoradiotherapy and chemotherapy after resection of pancreatic cancer." *N Engl J Med* 350 (12): 1200-1210. doi: 10.1056/NEJMoa032295.

Niederau, C., L. D. Ferrell, and J. H. Grendell. 1985. "Caerulein-induced acute necrotizing pancreatitis in mice: protective effects of proglumide, benzotript, and secretin." *Gastroenterology* 88 (5 Pt 1): 1192-1204.

Niessen, H. E., J. A. Demmers, and J. W. Voncken. 2009. "Talking to chromatin: post-translational modulation of polycomb group function." *Epigenetics Chromatin* 2 (1): 10. doi: 10.1186/1756-8935-2-10.

Oettle, H., S. Post, P. Neuhaus, K. Gellert, J. Langrehr, K. Ridwelski, H. Schramm, J. Fahlke, C. Zuelke, C. Burkart, K. Gutberlet, E. Kettner, H. Schmalenberg, K. Weigang-Koehler, W. O. Bechstein, M. Niedergethmann, I. Schmidt-Wolf, L. Roll, B. Doerken, and H. Riess. 2007. "Adjuvant chemotherapy with gemcitabine vs observation in patients undergoing curative-intent resection of pancreatic cancer: a randomized controlled trial." *JAMA* 297 (3): 267-277. doi: 10.1001/jama.297.3.267.

Omary, M. B., A. Lugea, A. W. Lowe, and S. J. Pandol. 2007. "The pancreatic stellate cell: a star on the rise in pancreatic diseases." *J Clin Invest* 117 (1): 50-59. doi: 10.1172/JCI30082.

Oshima, M., K. Okano, S. Muraki, R. Haba, T. Maeba, Y. Suzuki, and S. Yachida. 2013. "Immunohistochemically detected expression of 3 major genes (CDKN2A/p16, TP53, and SMAD4/DPC4) strongly predicts survival in patients with resectable pancreatic cancer." *Ann Surg* 258 (2): 336-346. doi: 10.1097/SLA.0b013e3182827a65.

Ougolkov, A. V., V. N. Bilim, and D. D. Billadeau. 2008. "Regulation of pancreatic tumor cell proliferation and chemoresistance by the histone methyltransferase enhancer of zeste homologue 2." *Clin Cancer Res* 14 (21): 6790-6796. doi: 10.1158/1078-0432.CCR-08-1013.

Pandol, S., M. Edderkaoui, I. Gukovsky, A. Lugea, and A. Gukovskaya. 2009. "Desmoplasia of pancreatic ductal adenocarcinoma." *Clin Gastroenterol Hepatol* 7 (11 Suppl): S44-47. doi: 10.1016/j.cgh.2009.07.039.

Pandol, S. J. 2010. "Gross Anatomic Considerations." In *The Exocrine Pancreas*. San Rafael (CA): Morgan & Claypool Life Sciences.

Pasini, D., P. A. Cloos, J. Walfridsson, L. Olsson, J. P. Bukowski, J. V. Johansen, M. Bak, N. Tommerup, J. Rappsilber, and K. Helin. 2010. "JARID2 regulates binding of the Polycomb repressive complex 2 to target genes in ES cells." *Nature* 464 (7286): 306-310. doi: 10.1038/nature08788.

Pierreux, C. E., A. V. Poll, C. R. Kemp, F. Clotman, M. A. Maestro, S. Cordi, J. Ferrer, L. Leyns, G. G. Rousseau, and F. P. Lemaigre. 2006. "The transcription factor hepatocyte nuclear factor-6 controls the development of pancreatic ducts in the mouse." *Gastroenterology* 130 (2): 532-541. doi: 10.1053/j.gastro.2005.12.005.

Pin, C. L., J. M. Rukstalis, C. Johnson, and S. F. Konieczny. 2001. "The bHLH transcription factor Mist1 is required to maintain exocrine pancreas cell organization and acinar cell identity." *J Cell Biol* 155 (4): 519-530. doi: 10.1083/jcb.200105060.

Pinho, A. V., I. Rooman, M. Reichert, N. De Medts, L. Bouwens, A. K. Rustgi, and F. X. Real. 2011. "Adult pancreatic acinar cells dedifferentiate to an embryonic progenitor phenotype with concomitant activation of a senescence programme that is present in chronic pancreatitis." *Gut* 60 (7): 958-966. doi: 10.1136/gut.2010.225920.

Piunti, A., A. Rossi, A. Cerutti, M. Albert, S. Jammula, A. Scelfo, L. Cedrone, G. Fragola, L. Olsson, H. Koseki, G. Testa, S. Casola, K. Helin, F. d'Adda di Fagagna, and D. Pasini. 2014. "Polycomb proteins control proliferation and transformation independently of cell cycle checkpoints by regulating DNA replication." *Nat Commun* 5: 3649. doi: 10.1038/ncomms4649.

Prevot, P. P., A. Simion, A. Grimont, M. Colletti, A. Khalaileh, G. Van den Steen, C. Sempoux, X. Xu, V. Roelants, J. Hald, L. Bertrand, H. Heimberg, S. F. Konieczny, Y. Dor, F. P. Lemaigre, and P. Jacquemin. 2012. "Role of the ductal transcription factors HNF6 and Sox9 in pancreatic acinar-to-ductal metaplasia." *Gut* 61 (12): 1723-1732. doi: 10.1136/gutjnl-2011-300266.

Proctor, E., M. Waghray, C. J. Lee, D. G. Heidt, M. Yalamanchili, C. Li, F. Bednar, and D. M. Simeone. 2013. "Bmi1 enhances tumorigenicity and cancer stem cell function in pancreatic adenocarcinoma." *PLoS One* 8 (2): e55820. doi: 10.1371/journal.pone.0055820.

Qian, T., J. Y. Lee, J. H. Park, H. J. Kim, and G. Kong. 2010. "Id1 enhances RING1b E3 ubiquitin ligase activity through the Mel-18/Bmi-1 polycomb group complex." *Oncogene* 29 (43): 5818-5827. doi: 10.1038/onc.2010.317.

Rahib, L., B. D. Smith, R. Aizenberg, A. B. Rosenzweig, J. M. Fleshman, and L. M. Matrisian. 2014. "Projecting cancer incidence and deaths to 2030: the unexpected burden of thyroid, liver, and pancreas cancers in the United States." *Cancer Res* 74 (11): 2913-2921. doi: 10.1158/0008-5472.CAN-14-0155.

Rayess, H., M. B. Wang, and E. S. Srivatsan. 2012. "Cellular senescence and tumor suppressor gene p16." *Int J Cancer* 130 (8): 1715-1725. doi: 10.1002/ijc.27316.

Reichert, M., and A. K. Rustgi. 2011. "Pancreatic ductal cells in development, regeneration, and neoplasia." *J Clin Invest* 121 (12): 4572-4578. doi: 10.1172/JCI57131.

Reznik, R., A. E. Hendifar, and R. Tuli. 2014. "Genetic determinants and potential therapeutic targets for pancreatic adenocarcinoma." *Front Physiol* 5: 87. doi: 10.3389/fphys.2014.00087.

Robertson, K. D., E. Uzvolgyi, G. Liang, C. Talmadge, J. Sumegi, F. A. Gonzales, and P. A. Jones. 1999. "The human DNA methyltransferases (DNMTs) 1, 3a and 3b: coordinate mRNA

expression in normal tissues and overexpression in tumors." *Nucleic Acids Res* 27 (11): 2291-2298.
Rodier, F., and J. Campisi. 2011. "Four faces of cellular senescence." *J Cell Biol* 192 (4): 547-556. doi: 10.1083/jcb.201009094.
Scarpa, A., P. Capelli, K. Mukai, G. Zamboni, T. Oda, C. Iacono, and S. Hirohashi. 1993. "Pancreatic adenocarcinomas frequently show p53 gene mutations." *Am J Pathol* 142 (5): 1534-1543.
Scheffzek, K., M. R. Ahmadian, W. Kabsch, L. Wiesmuller, A. Lautwein, F. Schmitz, and A. Wittinghofer. 1997. "The Ras-RasGAP complex: structural basis for GTPase activation and its loss in oncogenic Ras mutants." *Science* 277 (5324): 333-338.
Scheuermann, J. C., A. G. de Ayala Alonso, K. Oktaba, N. Ly-Hartig, R. K. McGinty, S. Fraterman, M. Wilm, T. W. Muir, and J. Muller. 2010. "Histone H2A deubiquitinase activity of the Polycomb repressive complex PR-DUB." *Nature* 465 (7295): 243-247. doi: 10.1038/nature08966.
Schlesinger, Y., R. Straussman, I. Keshet, S. Farkash, M. Hecht, J. Zimmerman, E. Eden, Z. Yakhini, E. Ben-Shushan, B. E. Reubinoff, Y. Bergman, I. Simon, and H. Cedar. 2007. "Polycomb-mediated methylation on Lys27 of histone H3 pre-marks genes for de novo methylation in cancer." *Nat Genet* 39 (2): 232-236. doi: 10.1038/ng1950.
Schneider, G., O. H. Kramer, R. M. Schmid, and D. Saur. 2011. "Acetylation as a transcriptional control mechanism-HDACs and HATs in pancreatic ductal adenocarcinoma." *J Gastrointest Cancer* 42 (2): 85-92. doi: 10.1007/s12029-011-9257-1.
Schonhuber, N., B. Seidler, K. Schuck, C. Veltkamp, C. Schachtler, M. Zukowska, S. Eser, T. B. Feyerabend, M. C. Paul, P. Eser, S. Klein, A. M. Lowy, R. Banerjee, F. Yang, C. L. Lee, E. J. Moding, D. G. Kirsch, A. Scheideler, D. R. Alessi, I. Varela, A. Bradley, A. Kind, A. E. Schnieke, H. R. Rodewald, R. Rad, R. M. Schmid, G. Schneider, and D. Saur. 2014. "A next-generation dual-recombinase system for time- and host-specific targeting of pancreatic cancer." *Nat Med* 20 (11): 1340-1347. doi: 10.1038/nm.3646.
Schuettengruber, B., D. Chourrout, M. Vervoort, B. Leblanc, and G. Cavalli. 2007. "Genome regulation by polycomb and trithorax proteins." *Cell* 128 (4): 735-745. doi: 10.1016/j.cell.2007.02.009.
Schutte, M., R. H. Hruban, J. Geradts, R. Maynard, W. Hilgers, S. K. Rabindran, C. A. Moskaluk, S. A. Hahn, I. Schwarte-Waldhoff, W. Schmiegel, S. B. Baylin, S. E. Kern, and J. G. Herman. 1997. "Abrogation of the Rb/p16 tumor-suppressive pathway in virtually all pancreatic carcinomas." *Cancer Res* 57 (15): 3126-3130.
Sears, R., F. Nuckolls, E. Haura, Y. Taya, K. Tamai, and J. R. Nevins. 2000. "Multiple Ras-dependent phosphorylation pathways regulate Myc protein stability." *Genes Dev* 14 (19): 2501-2514.
Serrano, M., G. J. Hannon, and D. Beach. 1993. "A new regulatory motif in cell-cycle control causing specific inhibition of cyclin D/CDK4." *Nature* 366 (6456): 704-707. doi: 10.1038/366704a0.
Seymour, P. A., K. K. Freude, M. N. Tran, E. E. Mayes, J. Jensen, R. Kist, G. Scherer, and M. Sander. 2007. "SOX9 is required for maintenance of the pancreatic progenitor cell pool." *Proc Natl Acad Sci U S A* 104 (6): 1865-1870. doi: 10.1073/pnas.0609217104.
Sharpless, N. E., N. Bardeesy, K. H. Lee, D. Carrasco, D. H. Castrillon, A. J. Aguirre, E. A. Wu, J. W. Horner, and R. A. DePinho. 2001. "Loss of p16Ink4a with retention of p19Arf predisposes mice to tumorigenesis." *Nature* 413 (6851): 86-91. doi: 10.1038/35092592.
Shi, G., D. DiRenzo, C. Qu, D. Barney, D. Miley, and S. F. Konieczny. 2013. "Maintenance of acinar cell organization is critical to preventing Kras-induced acinar-ductal metaplasia." *Oncogene* 32 (15): 1950-1958. doi: 10.1038/onc.2012.210.
Shi, G., L. Zhu, Y. Sun, R. Bettencourt, B. Damsz, R. H. Hruban, and S. F. Konieczny. 2009. "Loss of the acinar-restricted transcription factor Mist1 accelerates Kras-induced pancreatic intraepithelial neoplasia." *Gastroenterology* 136 (4): 1368-1378. doi: 10.1053/j.gastro.2008.12.066.
Shimizu, Y., K. Yasui, K. Matsueda, A. Yanagisawa, and K. Yamao. 2005. "Small carcinoma of the pancreas is curable: new computed tomography finding, pathological study and postoperative results from a single institute." *J Gastroenterol Hepatol* 20 (10): 1591-1594. doi: 10.1111/j.1440-1746.2005.03895.x.
Shroff, S., A. Rashid, H. Wang, M. H. Katz, J. L. Abbruzzese, J. B. Fleming, and H. Wang. 2014. "SOX9: a useful marker for pancreatic ductal lineage of pancreatic neoplasms." *Hum Pathol* 45 (3): 456-463. doi: 10.1016/j.humpath.2013.10.008.
Siegel, R. L., K. D. Miller, and A. Jemal. 2015. "Cancer statistics, 2015." *CA Cancer J Clin* 65 (1): 5-29. doi: 10.3322/caac.21254.
Simon, J. A., and R. E. Kingston. 2009. "Mechanisms of polycomb gene silencing: knowns and unknowns." *Nat Rev Mol Cell Biol* 10 (10): 697-708. doi: 10.1038/nrm2763.
Singh, P., R. Srinivasan, and J. D. Wig. 2012. "SMAD4 genetic alterations predict a worse prognosis in patients with pancreatic ductal adenocarcinoma." *Pancreas* 41 (4): 541-546. doi: 10.1097/MPA.0b013e318247d6af.

Smit, V. T., A. J. Boot, A. M. Smits, G. J. Fleuren, C. J. Cornelisse, and J. L. Bos. 1988. "KRAS codon 12 mutations occur very frequently in pancreatic adenocarcinomas." *Nucleic Acids Res* 16 (16): 7773-7782.

Song, J., M. Teplova, S. Ishibe-Murakami, and D. J. Patel. 2012. "Structure-based mechanistic insights into DNMT1-mediated maintenance DNA methylation." *Science* 335 (6069): 709-712. doi: 10.1126/science.1214453.

Stanger, B. Z., and M. Hebrok. 2013. "Control of cell identity in pancreas development and regeneration." *Gastroenterology* 144 (6): 1170-1179. doi: 10.1053/j.gastro.2013.01.074.

Stock, J. K., S. Giadrossi, M. Casanova, E. Brookes, M. Vidal, H. Koseki, N. Brockdorff, A. G. Fisher, and A. Pombo. 2007. "Ring1-mediated ubiquitination of H2A restrains poised RNA polymerase II at bivalent genes in mouse ES cells." *Nat Cell Biol* 9 (12): 1428-1435. doi: 10.1038/ncb1663.

Strahl, B. D., and C. D. Allis. 2000. "The language of covalent histone modifications." *Nature* 403 (6765): 41-45. doi: 10.1038/47412.

Strobel, O., Y. Dor, J. Alsina, A. Stirman, G. Lauwers, A. Trainor, C. F. Castillo, A. L. Warshaw, and S. P. Thayer. 2007. "In vivo lineage tracing defines the role of acinar-to-ductal transdifferentiation in inflammatory ductal metaplasia." *Gastroenterology* 133 (6): 1999-2009. doi: 10.1053/j.gastro.2007.09.009.

Szabo, A., and M. Sahin-Toth. 2012. "Increased activation of hereditary pancreatitis-associated human cationic trypsinogen mutants in presence of chymotrypsin C." *J Biol Chem* 287 (24): 20701-20710. doi: 10.1074/jbc.M112.360065.

Tanaka, M., S. Chari, V. Adsay, C. Fernandez-del Castillo, M. Falconi, M. Shimizu, K. Yamaguchi, K. Yamao, S. Matsuno, and Pancreatology International Association of. 2006. "International consensus guidelines for management of intraductal papillary mucinous neoplasms and mucinous cystic neoplasms of the pancreas." *Pancreatology* 6 (1-2): 17-32. doi: 10.1159/000090023.

Testini, M., A. Gurrado, G. Lissidini, P. Venezia, L. Greco, and G. Piccinni. 2010. "Management of mucinous cystic neoplasms of the pancreas." *World J Gastroenterol* 16 (45): 5682-5692.

Tiwari, V. K., K. M. McGarvey, J. D. Licchesi, J. E. Ohm, J. G. Herman, D. Schubeler, and S. B. Baylin. 2008. "PcG proteins, DNA methylation, and gene repression by chromatin looping." *PLoS Biol* 6 (12): 2911-2927. doi: 10.1371/journal.pbio.0060306.

Torre, L. A., F. Bray, R. L. Siegel, J. Ferlay, J. Lortet-Tieulent, and A. Jemal. 2015. "Global cancer statistics, 2012." *CA Cancer J Clin* 65 (2): 87-108. doi: 10.3322/caac.21262.

Torres, M. P., S. Rachagani, J. J. Souchek, K. Mallya, S. L. Johansson, and S. K. Batra. 2013. "Novel pancreatic cancer cell lines derived from genetically engineered mouse models of spontaneous pancreatic adenocarcinoma: applications in diagnosis and therapy." *PLoS One* 8 (11): e80580. doi: 10.1371/journal.pone.0080580.

Townsend, D. M., and K. D. Tew. 2003. "The role of glutathione-S-transferase in anti-cancer drug resistance." *Oncogene* 22 (47): 7369-7375. doi: 10.1038/sj.onc.1206940.

Tropberger, P., and R. Schneider. 2013. "Scratching the (lateral) surface of chromatin regulation by histone modifications." *Nat Struct Mol Biol* 20 (6): 657-661. doi: 10.1038/nsmb.2581.

Uomo, G., and P. G. Rabitti. 2000. "Chronic pancreatitis: relation to acute pancreatitis and pancreatic cancer." *Ann Ital Chir* 71 (1): 17-21.

van Arensbergen, J., J. Garcia-Hurtado, M. A. Maestro, M. Correa-Tapia, G. A. Rutter, M. Vidal, and J. Ferrer. 2013. "Ring1b bookmarks genes in pancreatic embryonic progenitors for repression in adult beta cells." *Genes Dev* 27 (1): 52-63. doi: 10.1101/gad.206094.112.

van der Stoop, P., E. A. Boutsma, D. Hulsman, S. Noback, M. Heimerikx, R. M. Kerkhoven, J. W. Voncken, L. F. Wessels, and M. van Lohuizen. 2008. "Ubiquitin E3 ligase Ring1b/Rnf2 of polycomb repressive complex 1 contributes to stable maintenance of mouse embryonic stem cells." *PLoS One* 3 (5): e2235. doi: 10.1371/journal.pone.0002235.

van der Vlag, J., and A. P. Otte. 1999. "Transcriptional repression mediated by the human polycomb-group protein EED involves histone deacetylation." *Nat Genet* 23 (4): 474-478. doi: 10.1038/70602.

van Leenders, G. J., D. Dukers, D. Hessels, S. W. van den Kieboom, C. A. Hulsbergen, J. A. Witjes, A. P. Otte, C. J. Meijer, and F. M. Raaphorst. 2007. "Polycomb-group oncogenes EZH2, BMI1, and RING1 are overexpressed in prostate cancer with adverse pathologic and clinical features." *Eur Urol* 52 (2): 455-463. doi: 10.1016/j.eururo.2006.11.020.

van Vlerken, L. E., C. M. Kiefer, C. Morehouse, Y. Li, C. Groves, S. D. Wilson, Y. Yao, R. E. Hollingsworth, and E. M. Hurt. 2013. "EZH2 is required for breast and pancreatic cancer stem cell maintenance and can be used as a functional cancer stem cell reporter." *Stem Cells Transl Med* 2 (1): 43-52. doi: 10.5966/sctm.2012-0036.

Varambally, S., S. M. Dhanasekaran, M. Zhou, T. R. Barrette, C. Kumar-Sinha, M. G. Sanda, D. Ghosh, K. J. Pienta, R. G. Sewalt, A. P. Otte, M. A. Rubin, and A. M. Chinnaiyan. 2002. "The polycomb group protein EZH2 is involved in progression of prostate cancer." *Nature* 419 (6907): 624-629. doi: 10.1038/nature01075.

Villasenor, A., D. C. Chong, M. Henkemeyer, and O. Cleaver. 2010. "Epithelial dynamics of pancreatic branching morphogenesis." *Development* 137 (24): 4295-4305. doi: 10.1242/dev.052993.

Vincenz, C., and T. K. Kerppola. 2008. "Different polycomb group CBX family proteins associate with distinct regions of chromatin using nonhomologous protein sequences." *Proc Natl Acad Sci U S A* 105 (43): 16572-16577. doi: 10.1073/pnas.0805317105.

Vire, E., C. Brenner, R. Deplus, L. Blanchon, M. Fraga, C. Didelot, L. Morey, A. Van Eynde, D. Bernard, J. M. Vanderwinden, M. Bollen, M. Esteller, L. Di Croce, Y. de Launoit, and F. Fuks. 2006. "The Polycomb group protein EZH2 directly controls DNA methylation." *Nature* 439 (7078): 871-874. doi: 10.1038/nature04431.

Voncken, J. W., B. A. Roelen, M. Roefs, S. de Vries, E. Verhoeven, S. Marino, J. Deschamps, and M. van Lohuizen. 2003. "Rnf2 (Ring1b) deficiency causes gastrulation arrest and cell cycle inhibition." *Proc Natl Acad Sci U S A* 100 (5): 2468-2473. doi: 10.1073/pnas.0434312100.

Wagner, M., H. Luhrs, G. Kloppel, G. Adler, and R. M. Schmid. 1998. "Malignant transformation of duct-like cells originating from acini in transforming growth factor transgenic mice." *Gastroenterology* 115 (5): 1254-1262.

Wang, G. J., C. F. Gao, D. Wei, C. Wang, and S. Q. Ding. 2009. "Acute pancreatitis: etiology and common pathogenesis." *World J Gastroenterol* 15 (12): 1427-1430.

Wang, H., L. Wang, H. Erdjument-Bromage, M. Vidal, P. Tempst, R. S. Jones, and Y. Zhang. 2004. "Role of histone H2A ubiquitination in Polycomb silencing." *Nature* 431 (7010): 873-878. doi: 10.1038/nature02985.

Wang, H., H. Yang, C. S. Shivalila, M. M. Dawlaty, A. W. Cheng, F. Zhang, and R. Jaenisch. 2013. "One-step generation of mice carrying mutations in multiple genes by CRISPR/Cas-mediated genome engineering." *Cell* 153 (4): 910-918. doi: 10.1016/j.cell.2013.04.025.

Wei, D., L. Wang, Y. Yan, Z. Jia, M. Gagea, Z. Li, X. Zuo, X. Kong, S. Huang, and K. Xie. 2016. "KLF4 Is Essential for Induction of Cellular Identity Change and Acinar-to-Ductal Reprogramming during Early Pancreatic Carcinogenesis." *Cancer Cell* 29 (3): 324-338. doi: 10.1016/j.ccell.2016.02.005.

Weinberg, Robert A. 2007. *The biology of cancer*. 1 vols. New York: Garland Science. p. 288-291, 313-320, G:17.

Wen, W., C. Peng, M. O. Kim, C. Ho Jeong, F. Zhu, K. Yao, T. Zykova, W. Ma, A. Carper, A. Langfald, A. M. Bode, and Z. Dong. 2014. "Knockdown of RNF2 induces apoptosis by regulating MDM2 and p53 stability." *Oncogene* 33 (4): 421-428. doi: 10.1038/onc.2012.605.

Wennerberg, K., K. L. Rossman, and C. J. Der. 2005. "The Ras superfamily at a glance." *J Cell Sci* 118 (Pt 5): 843-846. doi: 10.1242/jcs.01660.

Whitcomb, D. C., M. C. Gorry, R. A. Preston, W. Furey, M. J. Sossenheimer, C. D. Ulrich, S. P. Martin, L. K. Gates, Jr., S. T. Amann, P. P. Toskes, R. Liddle, K. McGrath, G. Uomo, J. C. Post, and G. D. Ehrlich. 1996. "Hereditary pancreatitis is caused by a mutation in the cationic trypsinogen gene." *Nat Genet* 14 (2): 141-145. doi: 10.1038/ng1096-141.

Wilentz, R. E., C. A. Iacobuzio-Donahue, P. Argani, D. M. McCarthy, J. L. Parsons, C. J. Yeo, S. E. Kern, and R. H. Hruban. 2000. "Loss of expression of Dpc4 in pancreatic intraepithelial neoplasia: evidence that DPC4 inactivation occurs late in neoplastic progression." *Cancer Res* 60 (7): 2002-2006.

Willemer, S., H. P. Elsasser, H. F. Kern, and G. Adler. 1987. "Tubular complexes in cerulein- and oleic acid-induced pancreatitis in rats: glycoconjugate pattern, immunocytochemical, and ultrastructural findings." *Pancreas* 2 (6): 669-675.

Wittel, U. A., K. K. Pandey, M. Andrianifahanana, S. L. Johansson, D. M. Cullen, M. P. Akhter, R. E. Brand, B. Prokopczyk, and S. K. Batra. 2006. "Chronic pancreatic inflammation induced by environmental tobacco smoke inhalation in rats." *Am J Gastroenterol* 101 (1): 148-159. doi: 10.1111/j.1572-0241.2006.00405.x.

Wu, F., T. Lv, G. Chen, H. Ye, W. Wu, G. Li, and F. C. Zhi. 2015. "Epigenetic silencing of DUSP9 induces the proliferation of human gastric cancer by activating JNK signaling." *Oncol Rep* 34 (1): 121-128. doi: 10.3892/or.2015.3998.

Wu, X., J. V. Johansen, and K. Helin. 2013. "Fbxl10/Kdm2b recruits polycomb repressive complex 1 to CpG islands and regulates H2A ubiquitylation." *Mol Cell* 49 (6): 1134-1146. doi: 10.1016/j.molcel.2013.01.016.

Xie, R., L. J. Everett, H. W. Lim, N. A. Patel, J. Schug, E. Kroon, O. G. Kelly, A. Wang, K. A. D'Amour, A. J. Robins, K. J. Won, K. H. Kaestner, and M. Sander. 2013. "Dynamic chromatin

remodeling mediated by polycomb proteins orchestrates pancreatic differentiation of human embryonic stem cells." *Cell Stem Cell* 12 (2): 224-237. doi: 10.1016/j.stem.2012.11.023.

Yadav, D., R. H. Hawes, R. E. Brand, M. A. Anderson, M. E. Money, P. A. Banks, M. D. Bishop, J. Baillie, S. Sherman, J. DiSario, F. R. Burton, T. B. Gardner, S. T. Amann, A. Gelrud, C. Lawrence, B. Elinoff, J. B. Greer, M. O'Connell, M. M. Barmada, A. Slivka, D. C. Whitcomb, and Group North American Pancreatic Study. 2009. "Alcohol consumption, cigarette smoking, and the risk of recurrent acute and chronic pancreatitis." *Arch Intern Med* 169 (11): 1035-1045. doi: 10.1001/archinternmed.2009.125.

Yang, W., Y. H. Lee, A. E. Jones, J. L. Woolnough, D. Zhou, Q. Dai, Q. Wu, K. E. Giles, T. M. Townes, and H. Wang. 2014. "The histone H2A deubiquitinase Usp16 regulates embryonic stem cell gene expression and lineage commitment." *Nat Commun* 5: 3818. doi: 10.1038/ncomms4818.

Young, M. D., T. A. Willson, M. J. Wakefield, E. Trounson, D. J. Hilton, M. E. Blewitt, A. Oshlack, and I. J. Majewski. 2011. "ChIP-seq analysis reveals distinct H3K27me3 profiles that correlate with transcriptional activity." *Nucleic Acids Res* 39 (17): 7415-7427. doi: 10.1093/nar/gkr416.

Zaaroor-Regev, D., P. de Bie, M. Scheffner, T. Noy, R. Shemer, M. Heled, I. Stein, E. Pikarsky, and A. Ciechanover. 2010. "Regulation of the polycomb protein Ring1B by self-ubiquitination or by E6-AP may have implications to the pathogenesis of Angelman syndrome." *Proc Natl Acad Sci U S A* 107 (15): 6788-6793. doi: 10.1073/pnas.1003108107.

Zhang, J. J., Y. Zhu, Y. Zhu, J. L. Wu, W. B. Liang, R. Zhu, Z. K. Xu, Q. Du, and Y. Miao. 2012. "Association of increased DNA methyltransferase expression with carcinogenesis and poor prognosis in pancreatic ductal adenocarcinoma." *Clin Transl Oncol* 14 (2): 116-124. doi: 10.1007/s12094-012-0770-x.

Zhang, P., R. Andrianakos, Y. Yang, C. Liu, and W. Lu. 2010. "Kruppel-like factor 4 (Klf4) prevents embryonic stem (ES) cell differentiation by regulating Nanog gene expression." *J Biol Chem* 285 (12): 9180-9189. doi: 10.1074/jbc.M109.077958.

Zhang, X., H. Wen, and X. Shi. 2012. "Lysine methylation: beyond histones." *Acta Biochim Biophys Sin (Shanghai)* 44 (1): 14-27. doi: 10.1093/abbs/gmr100.

Zhu, L., G. Shi, C. M. Schmidt, R. H. Hruban, and S. F. Konieczny. 2007. "Acinar cells contribute to the molecular heterogeneity of pancreatic intraepithelial neoplasia." *Am J Pathol* 171 (1): 263-273. doi: 10.2353/ajpath.2007.061176.

8 Appendix

8.1 List of tables

8.2 List of figures

9 Acknowledgements

First of all, I would like to express my deep gratitude to my mentor **Dr. Ivonne Regel** for providing me with this interesting and promising dissertation project. Her fantastic support, inimitable motivation and pleasure for discussion enormously helped me in conducting my PhD research. I would also like to thank her for her great trust and the freedom, she gave me for realizing my own concepts. Her knowledge and guidance immensely contributed to my personal and professional development.

My sincere thanks go to **Dr. Güralp Ceyhan** for his comprehensive support. Without any reservation, he agreed on taking over the function as my first advisor.

I am very grateful to **Prof. Dr. Gabriele Multhoff** for being my second advisor and for the insightful comments and feedback, she gave in the thesis committee meetings.

A big thanks goes to **Prof. Dr. Jörg Kleeff** for his constructive suggestions and questions, which greatly helped me to improve my scientific work and knowledge.

I thank **Dr. Katja Steiger** for her help in the histological evaluation of tissue sections.

Especially, I would like to thank all my **colleagues** for the pleasant working atmosphere. I owe it to you, that I enjoyed going to work every day, also in difficult times.
My special thanks go to **Dr. Susanne Raulefs** for her fantastic support and always having an open ear for my worries. **Tao** for performing the orthotopic injections. **Anna**, **Jessica** and **Sabrina** for their great help in the lab and the enjoyable time. **Nadja** and **Isabell** for their excellent technical support and their immense help with the animals. Thank you for reminding me that life consists of much more than lab work.

I would like to express my deep gratitude to my **parents** for everything they have done for me. Without their continuous encouragement and trust I would not have come so far.
I am very grateful to my brother **Timo**, who has never stopped believing in me. And, thanks for bringing so much joy into my life.

Finally, I would like to thank **Robert**. In the past four years, he shared all my worries and concerns. With his moral support and through the things we experienced together, I gained new strength and motivation for my work. Thank you for always being there for me.